

**SYNTHESIS AND CHARACTERISATION OF ALKALI METAL
TUNGSTEN BRONZES, Li_xWO_3 AND $\text{M}_x\text{M}'_y\text{W}_{1-y}\text{O}_3$ (M = Li, Na, Cs and
M' = Nb, Mo) SYSTEMS**

**Vom Fachbereich Geowissenschaften und Geographie
der Universität Hannover**

zur Erlangung des Grades

Doktor der Naturwissenschaften

Dr. rer. nat

genehmigte Dissertation

von:

Kalpana Rani Dey

Geboren am 17. Januar 1971 in Dhaka, Bangladesh

Dezember, 2004

Referent:

PD Dr. C. H. Rücher

Korreferent:

**Prof. Dr. J. –Ch. Buhl
Prof. Dr. Margareta Sundberg**

Tag der Promotion:

26.11.2004

Datum der Veröffentlichung:

Dezember, 2004

ABSTRACT

Keywords: Tungsten bronze systems: Li-Nb-PTB/Cs-Nb-HTB, optical properties, Phase stability range

Synthesis and characterisation of Li_xWO_3 ($x = 0.03 - 0.7$), $\text{Li}_x\text{Nb}_y\text{W}_{1-y}\text{O}_3$ ($x = 0.1, 0.4$; $y = 0.00 - 0.4$), $\text{Li}_x\text{Mo}_y\text{W}_{1-y}\text{O}_3$ ($x = 0.1, 0.4$; $y = 0.00 - 0.3$), $\text{Na}_{0.6}\text{Mo}_y\text{W}_{1-y}\text{O}_3$ ($y = 0.00 - 0.25$) and $\text{Cs}_x\text{Nb}_y\text{W}_{1-y}\text{O}_3$ ($x = 0.25, 0.3$; $y = 0.00 - 0.2$) systems have been studied. Powder samples were prepared by solid state method at 700°C for 7 days. Single crystals of Li_xWO_3 ($x = 0.1 - 0.45$) system were grown by chemical vapour transport method using HgCl_2 transporting agent in a temperature gradient $T_1 / T_2 = 700^\circ\text{C} / 800^\circ\text{C}$. The samples were characterized by using X-ray powder diffraction (Guinier, Philips diffractometer and Stoe Stadi P diffractometer), infrared investigation (KBr-method, Bruker IFS66) as well as by optical spectroscopy (Bruker IFS88 with attached microscope A590 and Zeiss-Specord S10 spectrometer). Some samples were also characterized by selected area electron diffraction, scanning electron microscopy (SEM) in combination with microanalysis and by high resolution electron microscopy (HREM).

From the powder samples of Li_xWO_3 , single phase $\text{PTB}_{\text{cubic}}$ (PTB = perovskite tungsten bronze) is observed for $0.3 \leq x \leq 0.5$, PTB_{tet} for $x = 0.1$, $\text{PTB}_{\text{cubic}}$ and PTB_{tet} mixed phase for $0.1 < x < 0.3$, PTB_{tet} and PTB_{orth} mixed phase for $x = 0.03, 0.05$. For $x > 0.5$ samples, Li_2WO_4 and WO_2 reactants appear along with $\text{PTB}_{\text{cubic}}$ phase. Single crystals of Li_xWO_3 show $\text{PTB}_{\text{cubic}}$ for $x = 0.45$ and 0.4 , mixed phase of $\text{PTB}_{\text{cubic}}$ and PTB_{tet} for $x = 0.35, 0.3$ and 0.25 and of PTB_{tet} and PTB_{orth} for $x = 0.1$. The cubic lattice parameter of Li_xWO_3 system tends to increase with decreasing x into the two phase region due to a strain minimising interaction between the tetragonal and cubic phases. The infrared absorption spectra also indicate the phase coexistence in the same range. Single crystal optical properties on polished crystals of the $x = 0.45$ sample show Drude free carrier type isotropic reflectivity with a minimum at about 14800 cm^{-1} . Crystals of $x = 0.4$ differ slightly indicating a superimposition of an additional spectral contribution in the range of the minimum. This contribution is related to the influence of the tetragonal phase due to submicroscopical exsolution phenomena. For $x < 0.4$ crystals, there are brighter lamellars separated by sharp interfaces due to the separation into PTB_{cub} and PTB_{tet} . The data imply that the properties in the tetragonal part of the crystals are dominated by electron localisation effects whereas the cubic parts are dominated by the free electron gas effect.

An interesting optical property is the gradual change in color of lithium tungsten bronzes, Li_xWO_3 at atmospheric condition. This effect is explained by the high mobility of Li, which is attracted by oxygen at the surface to form Li_2O , followed by a reaction with atmospheric H_2O and CO_2 to form $\text{Li}(\text{OH})$ and Li_2CO_3 . Therefore, Li_xWO_3 is transformed to WO_3 as indicated by the color change from blue or dark blue to greenish. The color change phenomena and all the atmospheric effects are mostly reversible when the sample is heated in evacuated tubes above 500°C .

The system $\text{Li}_{0.4}\text{Nb}_y\text{W}_{1-y}\text{O}_3$ shows that in presence of even small contents of Nb ($y = 0.04$), trace amount of LiNbWO_6 type phase comes as impurity along with $\text{PTB}_{\text{cubic}}$ phase. The intensity of $\text{PTB}_{\text{cubic}}$ phase reduces and the intensity of LiNbWO_6 trirutile type phase increases with increasing Nb content. For $x = y = 0.4$ the structure shows mainly the LiNbWO_6 trirutile. The system $\text{Li}_{0.4}\text{Mo}_y\text{W}_{1-y}\text{O}_3$ shows that $\text{Li}_2\text{W}_2\text{O}_7$ type impure phase comes out along with $\text{PTB}_{\text{cubic}}$ phase in presence of small amount of Mo contents. For samples with $y > 0.15$, the $\text{PTB}_{\text{cubic}}$ phase totally disappears and $\text{Li}_2\text{W}_2\text{O}_7$ type phase is mainly identified. The variations in the X-ray pattern compared to the $\text{Li}_2\text{W}_2\text{O}_7$ pure phase indicate the formation of $\text{Li}_2\text{W}_{2-x}\text{Mo}_x\text{O}_7$ of variable compositions. $\text{Li}_{0.1}\text{Nb}_y\text{W}_{1-y}\text{O}_3$ and $\text{Li}_{0.1}\text{Mo}_y\text{W}_{1-y}\text{O}_3$ systems show that with increasing Nb and Mo content, the Li content of the PTB phase decreases with increasing y . In the system $\text{Na}_{0.6}\text{Mo}_y\text{W}_{1-y}\text{O}_3$ significant amount of W can be substituted by Mo in the $\text{PTB}_{\text{cubic}}$ phase.

For the hexagonal tungsten bronzes (HTB) Cs_xWO_3 , it is observed that under the present preparation conditions a Nb/W substitution according to $\text{Cs}_x\text{Nb}_y\text{W}_{1-y}\text{O}_3$ is only possible for $x = 0.25, 0.3$ and $y < 0.1$. For sample with $y \geq 0.1$, along with main HTB type bronze phase a significant amount of oxidised HTB-II type phase is also observed. Similar results are obtained in the system $\text{Rb}_x\text{Nb}_y\text{W}_{1-y}\text{O}_3$.

Zusammenfassung

Schlagwörter: Wolframbronzen-Systeme: Li-Nb-PTB/Cs-Nb-HTB, Optische Eigenschaften Phasenstabilitätsbereiche

Es wurden Synthesen und Charakterisierungen an den Systemen Li_xWO_3 ($x = 0.03 - 0.7$), $\text{Li}_x\text{Nb}_y\text{W}_{1-y}\text{O}_3$ ($x = 0.1, 0.4$; $y = 0.00 - 0.4$), $\text{Li}_x\text{Mo}_y\text{W}_{1-y}\text{O}_3$ ($x = 0.1, 0.4$; $y = 0.00 - 0.3$), $\text{Na}_{0.6}\text{Mo}_y\text{W}_{1-y}\text{O}_3$ ($y = 0.00 - 0.25$) und $\text{Cs}_x\text{Nb}_y\text{W}_{1-y}\text{O}_3$ ($x = 0.25, 0.3$; $y = 0.00 - 0.2$) durchgeführt. Polykristallines Material wurde durch Festkörperreaktionen bei 700°C (Reaktionszeiten 7 Tage) erhalten. Größere Kristallkörper (bis 0.5 mm im Durchmesser) konnten im System Li_xWO_3 ($x = 0.1 - 0.45$) durch chemischen Transport mit HgCl_2 in einem Temperaturgradienten $T_1 / T_2 = 700^\circ\text{C} / 800^\circ\text{C}$ erhalten werden. Die Proben wurden durch Röntgenpulveruntersuchungen (Guinier Methode, Philips und Stoe Stadi P Diffraktometer), infrarot Absorptionsspektren (KBr-Methode, Bruker IFS66) und optischer Reflexionsspektroskopie (Bruker IFS88 mit Mikroskopzusatz A590 und Zeiss-Specord S10 Spektrometer) charakterisiert. Einige Proben wurden zudem durch elektronenmikroskopische Verfahren (HRTEM, SEM, EDX-Analysen) analysiert.

Die polykristallinen Proben im System Li_xWO_3 zeigen nach Röntgenuntersuchungen eine kubische Modifikation $\text{PTB}_{\text{cubic}}$ ($\text{PTB} = \text{„perovskite tungsten bronze“}$) für $0.3 \leq x \leq 0.5$, eine tetragonale Form PTB_{tet} für $x = 0.1$, sowie Mischphasen von $\text{PTB}_{\text{cubic}}$ und PTB_{tet} für $0.1 < x < 0.3$, PTB_{tet} und PTB_{orth} ($\text{orth} = \text{orthorhombisch}$) für $x = 0.03, 0.05$. Für $x > 0.5$ werden Li_2WO_4 and WO_2 neben $\text{PTB}_{\text{cubic}}$ beobachtet. Die Versuche zur Zucht größerer Kristalle im System Li_xWO_3 zeigen $\text{PTB}_{\text{cubic}}$ für $x = 0.45$ und 0.4 , Mischphasen von $\text{PTB}_{\text{cubic}}$ und PTB_{tet} für $x = 0.35, 0.3$ und 0.25 , sowie von PTB_{tet} und PTB_{orth} für $x = 0.1$. Der kubische Gitterparameter steigt mit abnehmenden x in das Zweiphasenfeld, was durch eine Minimierung des „strains“ erklärt wird. Die infrarot Absorptionsspektren ergeben analoge Phasenkoexistenzen von $\text{PTB}_{\text{cubic}}$ und PTB_{tet} wie sie auch in den Röntgenbeugungsdiagrammen beobachtet werden. Mikroreflexionsuntersuchungen an den polierten Kristallkörpern der $x = 0.45$ Proben zeigen ein „Drude freies Ladungsträger Verhalten“ mit einer isotropen Reflektivität mit einem Minimum bei ca. 14800 cm^{-1} . Kristalle der $x = 0.4$ Proben zeigen hiervon geringe Abweichungen, die auf eine Überlagerung eines zusätzlichen Effektes im Bereich des Minimums hindeuten. Dieser Beitrag deutet auf den Einfluß einer submikroskopischen Entmischung hin. Für Kristalle der Proben mit $x < 0.4$ werden durch die Entmischung in PTB_{tet} und $\text{PTB}_{\text{cubic}}$ hellere und dunklere Lamellen

beobachtet, die durch scharfe Grenzlinien voneinander getrennt erscheinen. Die Ergebnisse reflexionmikroskopischer Untersuchungen zeigen den Effekt von Elektronenlokalisierungen für die PTB_{tet} Bereiche, wohingegen die kubischen Bereiche durch den Effekt freier Ladungsträger dominiert werden.

Eine interessante optische Eigenschaft ist die allmähliche Farbänderung der polykristallinen Li_xWO_3 Proben unter atmosphärischen Bedingungen. Dieser Effekt wird durch die hohe Mobilität des Li erklärt, welches durch den Luftsauerstoff oberflächlich zu Li_2O oxidiert wird und im folgenden mit atmosphärischen H_2O und CO_2 zu $Li(OH)$ und Li_2CO_3 reagiert. Daher wird Li_xWO_3 an Li abgereichert und zu WO_3 , was eine Farbänderung von blau nach grün bewirkt. Die Farbänderung durch die atmosphärischen Effekte können durch eine nachfolgende Wärmebehandlung bei 500°C unter evakuierten Bedingungen zurückgeführt werden.

Im System $Li_{0.4}Nb_yW_{1-y}O_3$ werden schon durch die Gegenwart kleiner Anteile von Nb ($y = 0.04$) neben der Hauptphase PTB_{cubic} die Spuren einer $LiNbWO_6$ Typ Phase beobachtet. Bei einer weiteren Erhöhung von y verringert sich der Anteil der PTB_{cubic} Phase während der Anteil der „Trirutil-Typ“ Phase $LiNbWO_6$ zunimmt. Für $x = y = 0.4$ wird im wesentlichen nur $LiNbWO_6$ beobachtet. Im System $Li_{0.4}Mo_yW_{1-y}O_3$ wird bereits für kleine Mo-Anteile ein geringer Anteil einer $Li_2W_2O_7$ Typ Phase neben PTB_{cubic} als Hauptphase beobachtet. Für Proben mit $y > 0.15$ wird im wesentlichen nur noch eine $Li_2W_2O_7$ Typ Phase beobachtet und PTB_{cubic} Anteile sind vollkommen verschwunden. Die Veränderungen in den Röntgendiffraktogrammen deuten dabei auf die Bildung eines $Li_2W_{2-x}Mo_xO_7$ Mischkristallsystems hin. Die Systeme $Li_{0.1}Nb_yW_{1-y}O_3$ und $Li_{0.1}Mo_yW_{1-y}O_3$ zeigen, dass mit steigenden Nb bzw. Mo Anteilen offensichtlich der Li-Anteil der PTB Phase abnimmt. Im System $Na_{0.6}Mo_yW_{1-y}O_3$ können deutliche W Anteile durch Mo innerhalb der PTB_{cubic} ersetzt werden.

Im HTB (= “hexagonal tungsten bronzes”) System Cs_xWO_3 , wird eine geringe Nb/W – Substitution entsprechend der Zusammensetzungen $Cs_xNb_yW_{1-y}O_3$ mit $x = 0.25, 0.3$ und $y < 0.1$ beobachtet. Für Proben mit $y \geq 0.1$ wird eine Koexistenz mit einer sogenannten mehr oxidierten HTB-II Typ Phase beobachtet. Analoge Ergebnisse werden für das $Rb_xNb_yW_{1-y}O_3$ System erhalten.

LIST OF CONTENTS	P
ABSTRACT	i
1. INTRODUCTION	01
2. EXPERIMENTAL	13
2.1 Methods of preparation	13
2.2 Characterisation	16
3. RESULTS	19
3.1 Li_xWO₃ system (x = 0.03 –0.7)	19
3.1.1 Characterisation of solid state synthesis products	19
3.1.2 Characterisation of single crystal synthesis products	28
3.1.3 Color of Li_xWO₃ and its change at atmospheric condition	39
3.2 Characterisation of Li_{0.4}Nb_yW_{1-y}O₃ system (y = 0.00 – 0.4)	47
3.2.1 As prepared sample	47
3.2.2 Atmospheric effect on Li_{0.4}Nb_yW_{1-y}O₃ system	53
3.3 Characterisation of Li_{0.1}Nb_yW_{1-y}O₃ system (y = 0.00 – 0.1)	54
3.4 Characterisation of Li_{0.4}Mo_yW_{1-y}O₃ system (y = 0.00 – 0.3)	59
3.5 Characterisation of Li_{0.1}Mo_yW_{1-y}O₃ system (y = 0.00 – 0.1)	64
3.6 Characterisation of Na_{0.6}Mo_yW_{1-y}O₃ system (y = 0.00 – 0.25)	66
3.7 Characterisation of Cs_xNb_yW_{1-y}O₃ system (x = 0.25, 0.3 and y = 0.00 – 0.2) and Rb_{0.3}Nb_yW_{1-y}O₃ system (y = 0.0 – 0.175)	75
4. DISCUSSION	94
4.1 Li_xWO₃ system (x = 0.03 –0.7)	94
4.1.1 Phase stabilities in the Li_xWO₃ system and relation to the	94
4.1.2 Electronic properties and color of Li_xWO₃	100
4.2 Li_{0.4}Nb_yW_{1-y}O₃ and Li_{0.1}Nb_yW_{1-y}O₃ system	103
4.3 Li_{0.4}Mo_yW_{1-y}O₃ and Li_{0.1}Mo_yW_{1-y}O₃ system	106
4.4 Na_{0.6}Mo_yW_{1-y}O₃ system	106
4.5 Cs_xNb_yW_{1-y}O₃ and Rb_{0.3}Nb_yW_{1-y}O₃ system	107
5. ACKNOWLEDGEMENTS	111
6. REFERENCES	112

LIST OF TABLES**P**

1a. Results of X-ray powder analysis of different samples of lithium tungsten bronzes, Li_xWO_3 ($x = 0.03 - 0.7$) of series 1 and series 2	20
1b. Results of the X-ray powder analysis of some previous samples of Li_xWO_3 ($x = 0.1 - 0.7$) prepared at 600°C, 700°C and 800°C	21
2. X-ray results of single crystals of Li_xWO_3 prepared by chemical vapour transport method with a temperature gradient, $T = 100^\circ\text{C}$ ($T_2 = 800^\circ\text{C}$; $T_1 = 700^\circ\text{C}$)	29
3. Results of the X-ray powder analysis of different samples $\text{Li}_{0.4}\text{Nb}_y\text{W}_{1-y}\text{O}_3$ ($y = 0.00 - 0.4$) system of series 4, series 5 and some previous results	49
4. Results of the X-ray powder analysis of different samples of $\text{Li}_{0.1}\text{Nb}_y\text{W}_{1-y}\text{O}_3$ ($y = 0.020 - 0.1$) system of series 6 and some previous results	56
5. Phase observed from different samples of $\text{Li}_{0.4}\text{Mo}_y\text{W}_{1-y}\text{O}_3$ ($y = 0.02 - 0.4$) system and compared with some previous results of $\text{Li}_{0.3}\text{Mo}_y\text{W}_{1-y}\text{O}_3$	59
6. X- ray and electron microscopy results of the system $\text{Cs}_x\text{Nb}_y\text{W}_{1-y}\text{O}_3$ ($x = 0.25, 0.3$ and $y = 0.05 - 0.2$)	79

LIST OF FIGURES	P
Fig. 1. The structure of WO_3	04
Fig. 2. The structure of perovskite tungsten bronzes, PTB	05
Fig. 3. The structure of tetragonal tungsten bronze, TTB	06
Fig. 4. The structure of hexagonal tungsten bronze, HTB	07
Fig. 5. The structure of intergrowth tungsten bronze, ITB	08
Fig. 6. Examples of X-ray powder patterns taken immediately after opening the reaction tubes of Li_xWO_3 with $x = 0.1 - 0.7$ as denoted	22
Fig. 7. Examples of X-ray powder patterns taken immediately after opening the reaction tubes of Li_xWO_3 with $x = 0.03 - 0.1$ as denoted	24
Fig. 8. IR absorption spectra (KBr-method) of Li_xWO_3 (series 1) as measured directly after opening the reaction tubes	25
Fig. 9. Temperature dependent (in situ measurements) IR spectra of WO_3 (KBr-method)	26
Fig. 10. As measured UV-VIS spectra of Li_xWO_3 (series 1)	27
Fig. 11. UV-VIS spectra of Li_xWO_3 (series 1) in KM units.....	27
Fig. 12a. SEM image and polished single crystal of Li_xWO_3	30
Fig. 12b. SEM image and polished single crystal of Li_xWO_3 with	31
Fig. 13. IR absorption spectra (KBr-method) of crushed crystals of Li_xWO_3 as measured directly after opening the reaction tubes	32

Fig. 14a. Polarized reflectivity spectra of Li_xWO_3 crystals	33
Fig. 14b. Polarized reflectivity spectra of dark and white area of Li_xWO_3 crystals where $x = 0.25$ and 0.3	34
Fig. 14c. Polarized reflectivity spectra of Li_xWO_3 crystals where $x = 0.1$	35
Fig. 15a. HRTEM image of single crystal of $\text{Li}_{0.45}\text{WO}_3$ fragment with corresponding ED pattern	36
Fig. 15b. HRTEM image of a thin crystallite from $\text{Li}_{0.35}\text{WO}_3$ single crystal with corresponding ED pattern	37
Fig. 15c. HRTEM image of a thin crystallite from $\text{Li}_{0.25}\text{WO}_3$ single crystal with corresponding ED pattern	38
Fig. 16. The color of the sample Li_xWO_3 prepared at 600°C, 700°C and 800°C from old reactant before and after 60 days exposed in atmospheric condition	39
Fig. 17a. UV-VIS spectra of Li_xWO_3 (series 2) as measured after opening	40
Fig. 17b. UV-VIS spectra of Li_xWO_3 of series 2 as measured after 30 days (left) and after 90 days (right) exposed in atmospheric condition	41
Fig. 18. IR absorption spectra (KBr-method) of some samples of Li_xWO_3 of series 2 as measured directly after opening the reaction tubes and after 90 days	42
Fig. 19. IR absorption spectra (KBr-method) of $\text{Li}_{0.4}\text{WO}_3$ before exposed in atmospheric condition and after 5 months exposed in atmospheric condition	43
Fig. 20. The peak intensity of H_2O, CO_3^- and OH^- for the sample $\text{Li}_{0.4}\text{WO}_3$ after exposed in atmospheric condition	44

-
- Fig. 21. Typical X-ray diffraction pattern of Li_xWO_3 of series 1 with $x = 0.3$ and $x = 0.4$ after open the reaction tubes and after 60 days exposed in atmospheric45**
- Fig. 22. Typical IR-spectra of sample $\text{Li}_{0.35}\text{WO}_3$ showing the change in atmospheric condition46**
- Fig. 23. X-ray powder patterns of $\text{Li}_{0.4}\text{Nb}_y\text{W}_{1-y}\text{O}_3$ system taken immediately after opening the reaction tube48**
- Fig. 24a. SEM-image and SEM/EDX analysis results of $\text{Li}_{0.4}\text{Nb}_{0.15}\text{W}_{0.85}\text{O}_3$ 50**
- Fig. 24b. SEM-image and SEM/EDX analysis results of $\text{Li}_{0.4}\text{Nb}_{0.2}\text{W}_{0.8}\text{O}_3$ 50**
- Fig. 25. IR absorption spectra (KBr-method) of $\text{Li}_{0.4}\text{Nb}_y\text{W}_{1-y}\text{O}_3$ (series 5) system as measured directly after opening the reaction tubes51**
- Fig. 26. NIR spectra of $\text{Li}_{0.4}\text{Nb}_y\text{W}_{1-y}\text{O}_3$ (series 5) system as measured after opening ...52**
- Fig. 27. UV-VIS spectra of $\text{Li}_{0.4}\text{Nb}_y\text{W}_{1-y}\text{O}_3$ (series 4) system as measured after opening the reaction tubes and after 90 days exposed in atmospheric condition53**
- Fig. 28. X-ray powder pattern of $\text{Li}_{0.1}\text{Nb}_y\text{W}_{1-y}\text{O}_3$ (series 6) system taken immediately after open the reaction tubes55**
- Fig. 29. IR absorption spectra (KBr-method) of $\text{Li}_{0.1}\text{Nb}_y\text{W}_{1-y}\text{O}_3$ (series 6) system as measured after opening the reaction tubes57**
- Fig. 30. UV-VIS spectra (left) and NIR spectra (right) of $\text{Li}_{0.1}\text{Nb}_y\text{W}_{1-y}\text{O}_3$ (series 6) system as measured after opening the reaction tubes58**
- Fig. 31. X-ray powder diffraction patterns of $\text{Li}_{0.4}\text{Mo}_y\text{W}_{1-y}\text{O}_3$ (series 7) system and also a X-ray powder pattern of pure nominal $\text{Li}_2\text{W}_2\text{O}_7$ sample60**

-
- Fig. 32. SEM image and SEM/EDX analysis results of nominal $\text{Li}_{0.4}\text{Mo}_{0.15}\text{W}_{0.85}\text{O}_3$ and $\text{Li}_{0.4}\text{Mo}_{0.2}\text{W}_{0.8}\text{O}_3$ sample61**
- Fig. 33. IR absorption spectra (KBr-method) of $\text{Li}_{0.4}\text{Mo}_y\text{W}_{1-y}\text{O}_3$ (series 7) system as measured immediately after opening the reaction tubes62**
- Fig. 34. As measured UV-VIS spectra of $\text{Li}_{0.4}\text{Mo}_y\text{W}_{1-y}\text{O}_3$ (series 7) system after opening the reaction tubes63**
- Fig. 35. X-ray powder patterns of $\text{Li}_{0.1}\text{Mo}_y\text{W}_{1-y}\text{O}_3$ system taken immediately after opening the reaction tubes64**
- Fig. 36. IR absorption spectra (KBr-method) of $\text{Li}_{0.1}\text{Mo}_y\text{W}_{1-y}\text{O}_3$ system as measured immediately after opening the reaction tubes65**
- Fig. 37. X-ray powder diffraction patterns of $\text{Na}_{0.6}\text{Mo}_y\text{W}_{1-y}\text{O}_3$ system with $y = 0.0 - 0.25$ prepared at 600°C 67**
- Fig. 38. X-ray powder diffraction patterns of $\text{Na}_{0.6}\text{Mo}_y\text{W}_{1-y}\text{O}_3$ system with $y = 0.0 - 0.2$ prepared at 700°C 68**
- Fig. 39. IR absorption spectra (KBr-method) of $\text{Na}_{0.6}\text{Mo}_y\text{W}_{1-y}\text{O}_3$ system prepared at 600°C (left) and 700°C 69**
- Fig. 40a. Systematic SEM-image of $\text{Na}_{0.6}\text{Mo}_y\text{W}_{1-y}\text{O}_3$ system prepared at 600°C with increasing Mo content70**
- Fig. 40b. Systematic SEM-image of $\text{Na}_{0.6}\text{Mo}_y\text{W}_{1-y}\text{O}_3$ system prepared at 700°C with increasing Mo content71**
- Fig. 41a. Typical EDX spectra of $\text{Na}_{0.6}\text{Mo}_{0.2}\text{W}_{0.8}\text{O}_3$ system72**
- Fig. 41b. SEM-image and TEM/EDX analysis results of nominal $\text{Na}_{0.6}\text{Mo}_{0.2}\text{W}_{0.8}\text{O}_3$ 72**

Fig. 42. UV-VIS spectra of $\text{Na}_{0.6}\text{Mo}_y\text{W}_{1-y}\text{O}_3$ system	73
Fig. 43. HRTEM image of a thin crystallite from $\text{Na}_{0.6}\text{Mo}_{0.2}\text{W}_{0.8}\text{O}_3$ powder sample with corresponding ED pattern	74
Fig. 44. X-ray powder diffraction patterns of $\text{Cs}_{0.25}\text{Nb}_y\text{W}_{1-y}\text{O}_3$ system	76
Fig. 45. X-ray powder diffraction patterns of $\text{Cs}_{0.3}\text{Nb}_y\text{W}_{1-y}\text{O}_3$ system	77
Fig. 46a. SEM-image and EDX analysis results of nominal $\text{Cs}_{0.25}\text{WO}_3$	80
Fig. 46b. SEM-image and EDX analysis results of nominal $\text{Cs}_{0.25}\text{Nb}_{0.05}\text{W}_{0.95}\text{O}_3$ and $\text{Cs}_{0.25}\text{Nb}_{0.1}\text{W}_{0.9}\text{O}_3$ sample	81
Fig. 46c. SEM-image and EDX analysis results of nominal $\text{Cs}_{0.25}\text{Nb}_{0.15}\text{W}_{0.85}\text{O}_3$ and $\text{Cs}_{0.25}\text{Nb}_{0.2}\text{W}_{0.8}\text{O}_3$ sample	82
Fig. 47. SEM-image and EDX analysis results of $\text{Cs}_{0.3}\text{Nb}_y\text{W}_{1-y}\text{O}_3$ system	84
Fig. 48a. Typical EDX spectra of $\text{Cs}_{0.3}\text{Nb}_y\text{W}_{1-y}\text{O}_3$ system	85
Fig. 48b. Typical EDX spectra of $\text{Cs}_{0.25}\text{Nb}_y\text{W}_{1-y}\text{O}_3$ system	86
Fig. 49. IR absorption spectra (KBr-method) of $\text{Cs}_{0.25}\text{Nb}_y\text{W}_{1-y}\text{O}_3$ (left) and $\text{Cs}_{0.3}\text{Nb}_y\text{W}_{1-y}\text{O}_3$ (right) system	87
Fig. 50. Reflection spectra of powder samples of $\text{Cs}_{0.25}\text{Nb}_y\text{W}_{1-y}\text{O}_3$ (left) and $\text{Cs}_{0.3}\text{Nb}_y\text{W}_{1-y}\text{O}_3$ (right) system	88
Fig. 51. HRTEM image of a thin crystallite from $\text{Cs}_{0.25}\text{Nb}_{0.1}\text{W}_{0.9}\text{O}_3$ sample with corresponding ED pattern	89
Fig. 52. X-ray powder diffraction patterns of $\text{Rb}_{0.3}\text{Nb}_y\text{W}_{1-y}\text{O}_3$ system	90

Fig. 53. SEM image and SEM/EDX analysis results of $\text{Rb}_{0.3}\text{Nb}_y\text{W}_{1-y}\text{O}_3$ system92
Fig. 54. Phase diagram of lithium tungsten bronzes, Li_xWO_394
Fig. 55. Lattice parameters versus composition of cubic lithium tungsten bronzes, Li_xWO_3 of series 1, series 2 and series 3 together with some literature data95
Fig. 56. The phonon intensity at peak maximum relative to the minimum absorption intensities as a function of x in Li_xWO_3 (series 1)97
Fig. 57. Lattice parameter versus concentration of x in Li_xWO_3 of series 1, series 2, series 3 and a previous data98
Fig. 58. Lattice parameters versus concentration of y in $\text{Li}_{0.4}\text{Nb}_y\text{W}_{1-y}\text{O}_3$104
Fig. 59. Reflection spectra of $\text{Cs}_{0.3}\text{WO}_3$ for polarization parallel and perpendicular to the c-axis using the Drude model109

1. INTRODUCTION

Tungsten trioxide, WO_3 which is the host structure of alkali metal tungsten bronzes, is a transparent semiconductor with an indirect band gap of about 2.6 eV between the mostly oxygen 2p dominated filled valence band and the tungsten 3d dominated empty conduction band. WO_3 has a perovskite-like ABO_3 type structure with empty A sites. In the WO_3 structure the tungsten atoms are surrounded by six oxygen atoms, forming WO_6 octahedra, which are linked by corner sharing in three-dimensional network. The displacement of the tungsten atoms from the centre of the octahedra changes with the temperature, causing the symmetry of the structure to alter [1]. WO_3 thus exists in several polymorphic forms, which are stable within well-defined temperature regions and transform into each other reversibly. The tetragonal, orthorhombic, monoclinic and triclinic WO_3 modifications are observed in the temperature region -180° to 900°C [2]. A hexagonal form of WO_3 has also been prepared by soft chemistry methods [3].

During last 25 years it has become increasingly apparent that WO_3 , modified by ion incorporation or substoichiometry, can exhibit many technologically important properties. First and foremost one can achieve electrochromism, i.e., optical properties that can be modified reversibly and persistently by electrical pulses [4, 5]. Electrochromic WO_3 -based devices [4, 5] are currently being developed for "smart windows" with variable throughput of visible light and solar energy, high contrast system for passive and active information display, variable-reflectance mirrors, and variable emittance surfaces for controlled thermal emission.

The interest in the physical and chemical properties of WO_3 is also renewed for many reasons, such as, because of observing recently of novel crystal structure types in conjunction with sheet type superconductivity along twin boundaries in WO_{3-x} [6, 7], or because of reports on high temperature ($T_c = 91\text{k}$) superconductivity in Na_xWO_3 [8]. However, reconfirmation of such a high T_c in this systems is still required, or even because of the wish of a basic understanding of the insulator to metal transition in the field of d-metal oxides.

In the present work investigations were carried out on tungsten bronzes, M_xWO_3 and $\text{M}_x\text{M}'_y\text{W}_{1-y}\text{O}_3$ systems. The tungsten bronzes are ternary metal oxides of general formula, M_xWO_3 , where M is an electropositive metal, typically alkali and $0 < x < 1$. These non-stoichiometric compounds have been known since 1823 when Wöhler obtained a colored sodium tungsten bronze while he was trying to prepare metallic tungsten from a molten

mixture of Na_2WO_4 and WO_3 by hydrogen reduction [9]. Same type of compounds was observed by Laurent [10] a few years later with potassium. The reddish violet needles obtained were given formulas like $\text{K}_2\text{W}_3\text{O}_9$ [11], $\text{K}_2\text{W}_4\text{O}_{12}$ [12-14] and $\text{K}_2\text{W}_5\text{O}_{15}$ [11] or considered to be mixtures of several stoichiometric phases [10, 15]. Hallopeau [11] reported first the lithium tungsten bronzes in the beginning of 19th century. Later Brunner [15] submitted his dissertation on lithium tungsten bronzes. Schäfer [14] synthesized a corresponding rubidium compound and described it as an octatungstate.

The tungsten bronzes, however, regarded as stoichiometric compounds until 1935 when Hägg [16] showed that the sodium bronzes of cubic symmetry belong to a continuous series of solid solutions, Na_xWO_3 of variable composition within an extended homogeneity range $0.32 \leq x \leq 0.93$. Magnéli and Blomberg [17] reported the presence of such solid solution in other alkali metal tungsten bronzes and also prepared the corresponding cesium compounds.

As a general class bronzes of high-valency metals such as tungsten, vanadium, molybdenum, tantalum, and titanium accommodate the guest ions such as alkalis, alkaline earths, rare earths, copper, silver, uranium, hydrogen, and ammonium. There are a high number of publications on this field, which has been reviewed from time to time during the last 50 years by the authors Hägg and Magnéli (1954) [18], Sienko (1963) [19], Shanks et al. (1963) [20], Ribnick et al. (1963) [21], Wadsley (1964) [22], Dickens and Whittingham (1968) [23], Galasso (1969) [24], Hagenmuller (1971) [25], Bevan and Hagenmuller (1975) [26], Gamble and Geballe (1976) [27], T. Ekstrom (1980) [1], M. M. Dobson (1987) [28] and recently by Ph. Labbe (1992) [29].

The tungsten bronze comprises the metal – oxide lattice as the host matrix, the positive ions as the interstitial guests, resulting an equivalent number of quasi free electrons. The general formula M_xWO_3 can be written as $(\text{M}_x^+ \text{W}_x^{5+} \text{W}_{1-x}^{6+})\text{O}_3$, which formally indicate the presence of pentavalent tungsten in the bronzes. W atom can be replaced by other pentavalent metals of suitable atomic size such as V, Nb or Ta; the phase thus can become fully oxidised. Sabatier and Baud [30] reported that not only pentavalent but lower valent metals can also partly replace tungsten such as monovalent (Li), divalent (Mg), trivalent (Cr) and tetravalent (Ti) in appropriate amount so that the resultant compounds are completely oxidized. The oxidized analogues of bronzes have been called bronzoids [31]. Magnéli described the bronzoid in the 12th European Crystallographic meeting [32] by the following way ‘‘a number of compounds

and solid solutions crystallize with a structure of tungsten bronze-type''. Among them, niobates and tantalates take an important part and have been the most studied. The main feature of the substitution of Nb or Ta for W pertains to the fact that the resulting products are bronze-like from the compositional and structural points of view, but contrary to the bronzes are insulating phases owing to the d^0 character of Nb (v) and Ta (v). For this reason they have been called ''bronzoids''.

Such compounds of bronze, M_xWO_3 or bronzoid have properties which sensibly depend not only on the environment, temperature and pressure, but also on the ratio of the components in the solid, and notably on the nature and the rate of inserted ions. Thus, an original aspect of most of these phases is to possess composition-altering features which are function of a variable x fixing the atoms proportion. Thus by a variation of x the properties (color, conductivity, magnetic properties etc.) can change dramatically involving certain type of phase transitions of the WO_3 host.

Tungsten Bronzes have intense color (some are black), metallic lustre (hence their name), metallic or semi-metallic conductivity, inertness to attack by strong acids. The large interest in the tungsten bronzes is based on the fact that they exhibit interesting electric and magnetic properties. Except for tungsten bronzes with the lowest alkali content, they are all good electronic conductors with metallic character, which is due to that the M-atoms donate their valence electrons to a conduction band of the W-O framework [33]. Wanlass and Sienko [34] have shown that the rubidium tungsten bronzes, Rb_xWO_3 with $x = 0.2$ and 0.30 , are superconducting with critical temperature up to 4.35 °K and 2.90 °K, respectively.

Technological applications of the bronzes appear very promising. Because of the high electrical conductivity (comparable to graphite) and inertness to acid media, bronze can be an economical substitute for noble metals, particularly as electrode materials in acidic environments. Extensive studies have hence been pursued on the bronze electrodes in a wide range of electrochemical systems. Typical applications are indicating electrodes in analytical and synthetic reactions for acid-base, oxidation-reduction, metal-complexing, metal-chelating etc [35-50]. In some application, the bronze and the reference electrodes in water generate an electric potential which is a sensitive function of the dissolved oxygen; this assembly can be conveniently used for monitoring the oxygen level in water which is important for pollution control [51].

The bronzes are also invaluable in catalysis and related applications. The bronzes can catalyze the ortho–para conversion of hydrogen and the hydrogen–deuterium exchange reaction in the gas phase [52]. The bronze doped with platinum is as effective an electrocatalyst as the best known catalyst, platinum, in the electrochemical reduction of oxygen to water in acidic media [35, 53-57]. However, some platinum doped bronzes showed weak activity [58-60]. The bronze containing a trace of platinum enhances the catalytic oxidation of hydrogen, hydrocarbons, carbon monoxide and reformer gas in fuel cells [61-63]. The surface characteristics play a vital role in these catalytic reactions.

Tungsten bronzes adopt four different types of structures. In general, their structures consist of networks of corner-sharing WO_6 octahedra [Fig. 1], forming various kinds of cages or tunnels that are at least partly occupied by alkali metal atoms. These are, in stable form,

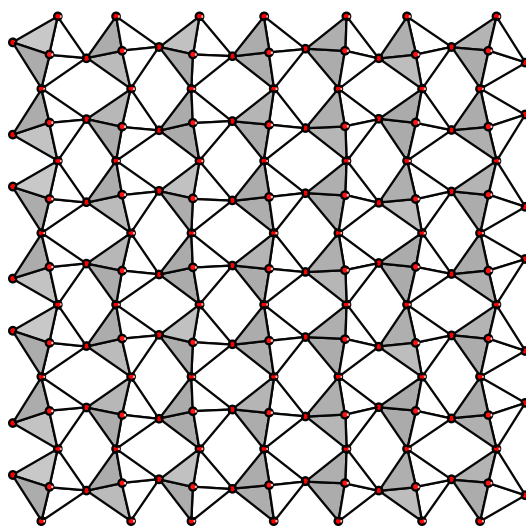


Fig. 1. The structure of WO_3

perovskite tungsten bronze (PTB), formed by Li, Na, rare earth, Zr, Al, Sb etc; tetragonal tungsten bronze (TTB), formed by Na, K, Sn, Pb etc; hexagonal tungsten bronze (HTB) formed by K, Rb, Cs, In and Tl often ions of large size; intergrowth tungsten bronze (ITB) formed with numerous cations. Some metals other than alkali are also known to form ITB bronzes, namely Sn, Ba, Sb, Pb and Bi. The present study is mainly focused on PTB and HTB structure.

The perovskite tungsten bronze (PTB), which is formed with lithium and sodium, has quadratic tunnels, or rather 12-coordinated cages, in which the smaller atoms of lithium and

sodium can be accommodated [16, 64] [Fig. 2]. The value of x varies from 0.028 to 0.50 for Li-PTB, whereas the Na-PTB forms within two composition ranges: $x = 0.01 - 0.11$ and $0.32 - 0.93$ [66]. The structure of the cubic sodium tungsten bronzes, Na_xWO_3 , is analogous to that of perovskite, CaTiO_3 (ABX_3), but with the A positions only partially occupied by Na. The

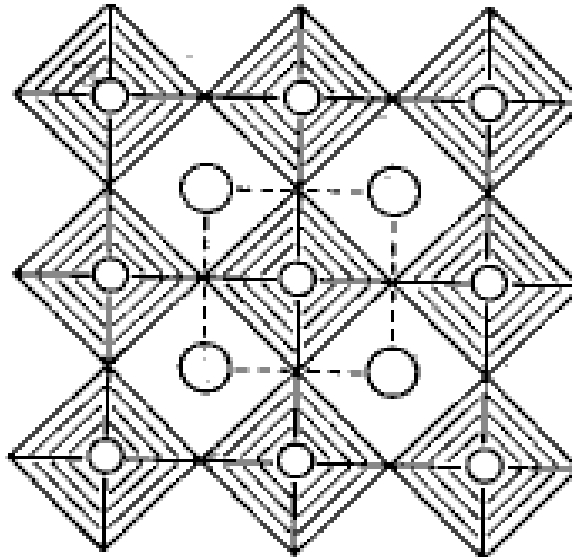


Fig. 2. The structure of perovskite tungsten bronzes, PTB. The large circles indicate metal atoms and the small circles tungsten atoms.

PTB structure permits only atoms with a maximum radius of 1.3 \AA at atmospheric pressure. Thus of the alkali metals only Li and Na are permitted [65]. The structure of the cubic sodium tungsten bronzes was determined by Hägg [16]. The structure of $\text{Na}_{0.1}\text{WO}_3$ reported by Magnéli [66], is closely related to the cubic perovskite tungsten bronzes, but the tungsten atoms are slightly displaced from the centre of the WO_6 octahedra along the c -axis, thus forming puckered layers. Due to this puckering the unit cell becomes tetragonal rather than cubic and the cell volume is doubled. This structure is thus designed as PTB_{tet} [65]. The PTB structure of lithium tungsten bronzes, Li_xWO_3 , was reported by Magnéli [67] and Straumanis and Hsu [68].

The second type, tetragonal tungsten bronze (TTB) structure determined by Magneli [69], has three type of tunnels, namely trigonal, tetragonal and pentagonal [Fig. 3]. The pentagonal and at least partially the tetragonal tunnels are occupied by alkali atoms [70, 71]. The occupancy of the alkali positions in the tunnels has been investigated for both K and Na – TTB. Kihlborg and Klug [70] showed that a crystal of composition $\text{K}_{0.37}\text{WO}_3$ has about 88% of the

pentagonal tunnel sites and about 10% of the tetragonal tunnel positions occupied by potassium. Takusagawa and Jacobsson [71] used Na as interstitial atoms in the TTB structure and found that for a sample of composition $\text{Na}_{0.48}\text{WO}_3$ the pentagonal tunnels were filled to 100% and the tetragonal tunnels to about 40%. However, in a sample of composition Na_xWO_3 ($x \approx 0.33$) only the pentagonal tunnels were occupied. From these results they concluded that

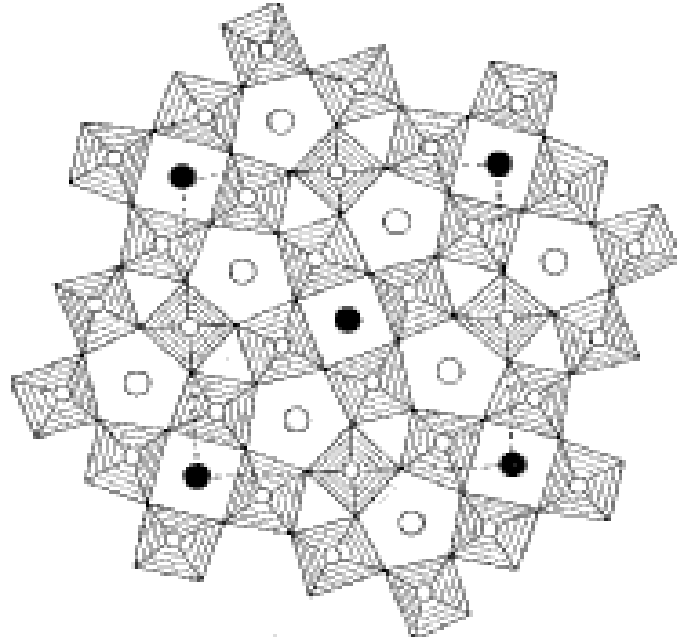


Fig. 3. The structure of tetragonal tungsten bronze, TTB, projected onto the xy plane. The large open and filled circles indicate the alkali metal atoms, located in pentagonal and tetragonal tunnels respectively. The WO_6 octahedra shown by shaded.

with increasing alkali content the pentagonal tunnels are first completely filled before the tetragonal tunnel positions are occupied ($x \geq 0.4$). This is probably due to that the pentagonal tunnels have more space available for the Na atoms.

In 1953, Magneli [72] reported the third type structure, hexagonal tungsten bronze (HTB), for $\text{Rb}_{0.29}\text{WO}_3$. This structure contains hexagonal and trigonal tunnels along the c -axis, formed by a network of corner-sharing tungsten-oxygen octahedra [Fig. 4]. The alkali atoms occupy the hexagonal tunnels in the structure. Since the A-ion site is larger in HTB than in PTB and TTB, the HTB phase is stabilized by large ions such as K^+ , Rb^+ and Cs^+ . Recent high pressure experiments [73, 74] have produced HTB phases containing Nd and Ca. Complete filling of all the hexagonal tunnel sites gives $x_{\text{max}} = 0.33$. A number of elements other than alkali metals are known to form the same structure. The heavy alkali metals also form HTB-type phases

with niobium oxide fluoride ($A_x\text{NbO}_{2+x}\text{F}_{1-x}$) [75] and vanadium fluoride ($A_x\text{VF}_3$) [76], with niobium and vanadium replacing tungsten in the structure. Gerand et al. [77, 78], using a special low-temperature synthesis technique, have succeeded in preparation of a hexagonal modification of WO_3 with the same structure as HTB but without alkali content.

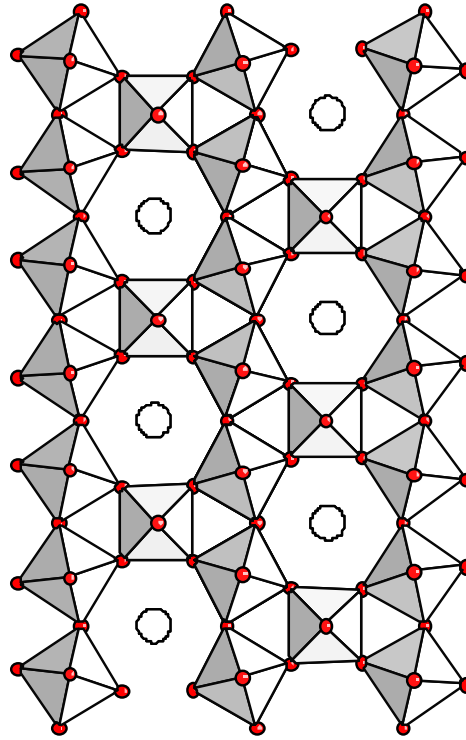


Fig. 4. The structure of hexagonal tungsten bronze, HTB, projected along the c -axis. The WO_6 octahedra form a network with three and six membered rings. The large open circles in the hexagonal tunnels are the alkali metal atoms.

This form of WO_3 transforms irreversibly to the normal ReO_3 -type modification at 400-500°C. Alkali metal atoms, even Li and Na which normally do not form an HTB phase, can be inserted into the tunnels by reacting hexagonal WO_3 with alkali vapour or organometallics [79].

In 1975, Hussain and Kihlberg [80] reported the fourth type structure, intergrowth tungsten bronze, (ITB), for $M_x\text{WO}_3$ ($M = \text{K, Rb, Cs, Tl}$ and $0.01 \leq x \leq 0.12$). This structure can be considered as an intergrowth of the HTB and WO_3 structure type at the unit cell level [Fig. 5], and it thus also contains hexagonal tunnels in which K, Rb and Cs can be accommodated. Here in this structure the alkali metal atoms are located in the hexagonal tunnels in the HTB slab, and the octahedra in the WO_3 slabs are tilted by about 15° in an alternating sequence, to allow the two slabs to fit together. The simplest series, in ITB is called (n)-ITB which consists of single hexagonal tunnel rows separated by n chains of WO_6 octahedra, $n = 2, 3, 4$ etc. A

second type, called (1,n)-ITB, has two hexagonal tunnels connected by one row of WO_6 octahedra, and these double rows are in turn separated by n layers of octahedra as in (n)-ITB [80].

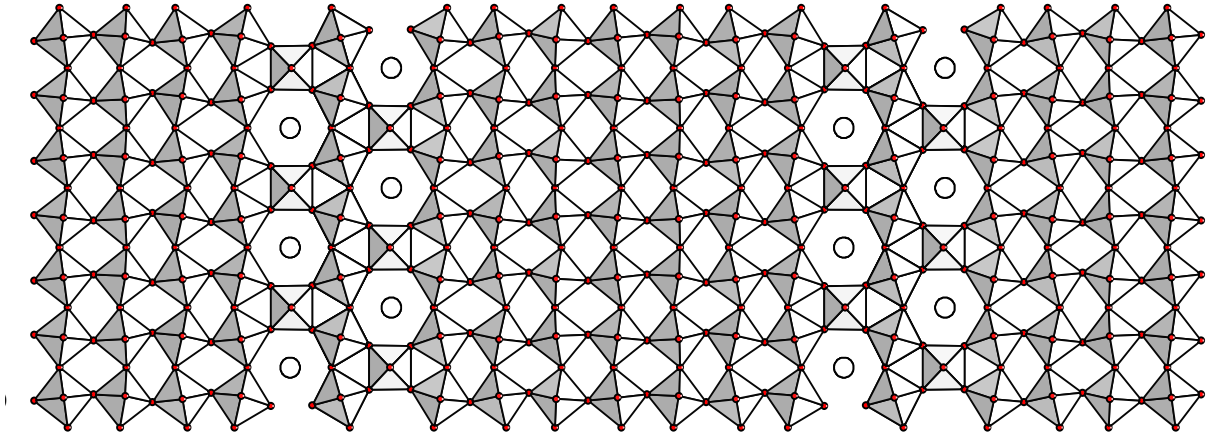


Fig. 5. The structure of intergrowth tungsten bronze, ITB, projected along the c-axis. The (1,7) member is shown. The large circles in the hexagonal tunnels indicate the positions of the heavy alkali metal atoms.

Several different methods have been used to synthesize bronzes and bronzoids. The most common method is conventional solid-state synthesis, which involves mixing appropriate amounts of the starting materials and heating the resulting powders in air or in an evacuated silica tube under ambient pressure conditions. In general, the fully oxidized phases are heat-treated in Al_2O_3 or Pt crucibles in air, whereas the reduced tungsten bronzes are heated in evacuated ampoules. Single crystal of tungsten bronzes can also be synthesized by chemical vapour transport method. Recently, alkali metal HTB and ITB [81] crystals of bronze and bronzoids were also prepared by chemical vapour transport method from a mixture of appropriate amount of oxides using transporting agents. Electrolytic reduction was also used to grow large single crystal of tungsten bronzes. Molten mixture of metal tungstate and tungstic acids were electrolytically reduced to grow big crystal of sodium tungsten bronzes.

Solid state synthesis can also be performed at high pressure and high temperatures, using the same starting materials as at ambient pressure, but the heating times are much shorter. Bither et al. [82] prepared the alkali and alkaline earth metal tungsten bronzes at high pressure, and the results obtained differ substantially from those at ambient pressure. Both sodium and calcium normally form compounds with PTB-type structures, but at high pressure phases with HTB-type structures are formed instead. Zakharov et al. [73] have performed high-pressure

synthesis at 50kbar in the $\text{Nd}_2\text{O}_3\text{-WO}_3$ system and obtained crystals with HTB and ITB related structure. Again this is an interesting difference from the same system at ambient pressure, for which only PTB-type RE_xWO_3 bronzes have been reported.

There are some alternative methods to solid state synthesis which include several fairly new techniques like soft chemistry or chemical intercalation reactions [83]. Shorter reaction times or lower synthesis temperature is the advantage of these two method. Preparation by intercalation chemistry in h.WO_3 , has recently given some spectacular compounds of HTB type [83]: H_xWO_3 , Li_xWO_3 , Na_xWO_3 , K_xWO_3 , Rb_xWO_3 and Cs_xWO_3 . Many research group use the film method for the synthesis of the tungsten bronzes. In the present investigation, solid state reaction method and chemical vapour transport method are used for powder sample and single crystal preparation, respectively.

Hydrothermal synthesis offers an alternative to the usually high temperature of conventional solid-state synthesis, and this method has been used to obtain both reduced and fully oxidized phases in the RE-W-O system. Kletsov et al. [84] prepared and studied $\text{RE}_2\text{W}_2\text{O}_9$ crystals with RE = Ce, Pr and Nd, and Reis et al. [85] synthesized alkali metal tungsten bronzes of both the pyrochlore and hexagonal structure types. Single HTB crystals were prepared hydrothermally under a pressure of 3000 atm [86]. The hexagonal symmetry, compatible with the space group P63/mcm is verified by precession photographs for $\text{Li}_{0.3}\text{WO}_3$ and $(\text{NH}_4)_{0.33}\text{WO}_3$.

The most extensively studied inorganic bronzes are sodium tungsten bronzes, Na_xWO_3 with $0.45 < x < 1$, which are metallic and exhibit perovskite structure. The electronic transport properties of the bronzes were interpreted based on various clustering models regarding the sodium distribution: a linear-polymer-like clustering [87], a randomly linked clustering [88] and NaWO_3 globules surrounded by WO_3 [89-91]. However, these clustering models ascribing microscopic inhomogeneity have been rejected by Tunstall [92], Crandall and Faughnan [93] and Weinberger [94]. According to these authors this perplexity is largely attributed to macroscopic inhomogeneity in the bronze specimen.

The optical reflectance spectra of sodium tungsten bronzes have been measured repeatedly to obtain congruous electronic energy values [23, 95-98]. There are still vital inconsistencies among these measurements. Inhomogeneities in the surface structure should be largely responsible for this.

Explanation of the electronic and optical properties of all the WO_3 based system are however, still somewhat controversial, in particular for the technically interesting compositions to the limit beyond the metal insulator transition, e.g. for the bronzes M_xWO_3 with x below about 0.4. It has often been ignored in theoretical considerations of the electronic properties of these systems, e.g. for the PTB containing H, Li and Na [99] that there occurs phase transitions together with the appearance of two phase fields [100]. These fact could of course produce largely inhomogeneous samples with metallic and insulating areas within one grain or even within one crystal. In this respect Zhong et al. [101] have shown in situ measurements using electrolytic cells of $\text{Li}/\text{Li}_x\text{WO}_3$ (films and powders) the coexistence ranges of monoclinic and tetragonal phases at about $0.01 < x < 0.082$ and between tetragonal and cubic phases at about $0.13 < x < 0.36$. Or with other words Li_xWO_3 is cubic for $0.36 < x < 0.5$ and tetragonal for $0.083 < x < 0.13$ during intercalation of Li. During deintercalation the lower stability limit of the cubic phase becomes $x = 0.21$ and the tetragonal phase was observed for $0.078 < x < 0.12$.

It seems to be well known that electrons introduced in WO_3 , either by oxygen deficiency WO_{3-x} or by intercalation with hydrogen are affected by strong electron phonon coupling. Therefore, these electrons are self trapped forming polarons rather than being free electron like [102-105]. These polarons are characterized by their strong absorption feature in the near infrared spectral range tailing into the visible, which is with increasing polaron concentration x responsible for the change to dark blue color in WO_{3-x} powders [104]. The ‘blue effect’ is also seen e. g. by H intercalation into WO_3 crystals [102] or Li into WO_3 films [106]. As discussed in ref [104] for WO_{3-x} with increasing x there occurs a metal/insulator transition at about $x = 0.1$, which has been explained by the saturation in polaron concentration, thus producing free carriers for further enhanced x . The spectral changes are dominated by the appearance of a Drude free carrier plasma frequency. In this respect the often cited visual appearance in Na_xWO_3 from greenish (for WO_3 according to the band to band transition) through gray to blue might be explained by the increase in polaron concentration from zero to above the metal insulator transition. On the other hand the change to purple, red, orange and yellow as x is further increased to one is well explained by a further increase in the carrier concentration due to a gradual shift in the plasma frequency through the visible part of the spectrum [107]. Thus an important question here is how the plasma frequency will break down, or with other words how the spectral properties will change on crossing from the metal to the insulating material in these systems or going through the two phase fields. It is interesting to note that recently Likalter [108] suggested on theoretical reasons a percolation

threshold value for x of about 0.1 for M_xWO_3 with $M = Li, Na$, i.e. there should be a first infinite metallic path through insulating islands for x about 0.1. This author ruled out also that any polaron formation suggesting the intercalated alkali atoms in the low concentration limit are only weakly ionized and that the binding energy to the alkali ions is of the order of 1eV. For comparison the polaron stabilisation energy is of the order of 0.5eV. Therefore, the near infrared absorption peak with maximum at about 1eV is explained by Likalter by the photo ionization of the intercalated atoms rather than by the polaron effect in strict contradiction to earlier assumption about polaron formation.

Thus, there are reasons to reinvestigate the PTB systems. Therefore, the main part of this thesis are focused on the synthesis and characterization of Li_xWO_3 system in order to explore the stability field in the solid state synthesis technique and to investigate in particular their spectral properties. The absorption spectra which are related on powder sample of strongly absorbing materials possessing strong anisotropic effects are often hard to interpret. Therefore, beside the investigation of powder samples of Li_xWO_3 and the crystal growth conditions of the nonstoichiometric Li_xWO_3 compounds, another aim was to obtain the crystals within the system Li_xWO_3 is sufficiently large for studying their single crystal optical properties. For this polarised micro reflectivity, crystal of Li_xWO_3 were also prepared with different composition by chemical vapour transport method.

Lithium ionic conductors have been a subject of interest not only because of their application to solid lithium batteries and chemical sensors, but also from a fundamental point of view in relation to ionic transportation inside of the solid state. Among many lithium ionic conductors, $(La_{2/3-x}Li_{3x})TiO_3$ has been especially interesting because of its high ionic conductivity as much as 10^{-3} S/cm at room temperature [109]. The structure of this compound and its modified materials are perovskite-type, in which lithium ion and its vacancy are located at its A-site, and the mechanism of ionic transportation is considered as hopping of lithium via vacancy. Li_xWO_3 itself cannot be a pure solid electrolyte, because it has high electronic conductivity. On the other hand, it has been reported that partial substitution of tungsten by niobium or tantalum reduces the electronic conductivity of sodium tungsten bronzes. The published bronzoid phases are mainly of the intergrowth tungsten bronze (ITB), hexagonal tungsten bronze (HTB) and tetragonal tungsten bronze (TTB) type compounds. There are very few reports on substitution of tungsten atom by other metal atoms in the PTB type bronzes. All these has incited us to investigate $Li_xM_yW_{1-y}O_3$ ($x = 0.1$ and 0.4 , $M = Nb$

and Mo) and $\text{Na}_x\text{Mo}_y\text{W}_{1-y}\text{O}_3$ ($x = 0.6$) system and determine their spectral and structural properties. The results of the study in these systems are reported in this thesis.

Recently there is a report about the synthesis and characterization of niobium substituted HTB phases, $\text{M}_x\text{Nb}_y\text{W}_{1-y}\text{O}_3$ with $\text{M} = \text{K}, \text{Rb}$; $x = 0.2, 0.25, 0.3$ and $0.0 \leq y \leq 0.2$ where the number of electrons introduced by alkali metal atoms are only partly compensated by pentavalent niobium [110]. There are no reports on substitution of tungsten atom by other metal atoms in the Cs-HTB type bronze phase. This has also incited us to investigate Nb substituted Cesium tungsten bronze system. The results of this study are reported in this thesis. Moreover, the reproducibility of Nb substituted rubidium system reported by Hussain et al. [110], was rechecked and the results obtained are also given in the present thesis.

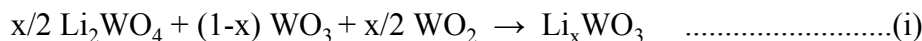
It is also interesting to note that Drude free carrier plasma frequencies have been detected in so far for all HTB type compounds, M_xWO_3 with $\text{M} = \text{K}, \text{Cs}, \text{Rb}$ and $0.2 < x < 0.3$ with a splitting in their position according to the strong anisotropic effect related on their hexagonal symmetry [81]. Here it was the main aim to see how far the stability limit of fully reduced forms of HTB could be extended to lower electron concentration according to a suggested equation $\text{M}_x(\text{W}_{x-y}^{5+}\text{Nb}_y^{5+}\text{W}_{1-x}^{6+})\text{O}_3$ with increasing y .

2. EXPERIMENTAL

2.1 Methods Of Preparation

Li_xWO_3

Series of Li_xWO_3 were prepared according to the following reaction :



Polycrystalline powder samples of Li_xWO_3 were prepared by solid state synthesis method and single crystals of Li_xWO_3 were prepared by chemical vapour transport method.

Two series of polycrystalline powder samples (series 1 and series 2) of lithium tungsten bronzes, Li_xWO_3 were prepared with various x running from x = 0.03 to x = 0.7.

The following procedure was followed for the polycrystalline sample [series 1, series 2, series 4 to series 10] preparation. Appropriate amount of the reactants were mixed in an agate mortar and transferred into clean dried silica tubes. The silica tubes were evacuated at room temperature for 1 - 2 hours, sealed and then heated in a Muffle Furnace at temperature 700°C for 7 days. In all cases the samples were quenched to room temperature within minutes by taking the reaction tubes out of the furnace.

Series 1: The preparation were carried out with the reactant Lithium tungsten oxide, Li_2WO_4 (99.9%), Tungsten (iv) oxide, WO_2 (99.9%) and Tungsten (vi) oxide, WO_3 (99.998%) all from Alfa Aesar.

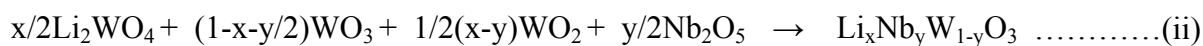
Series 2: Lithium tungsten oxide, Li_2WO_4 of ICN pharmaceuticals , Tungsten (iv) oxide, WO_2 (99%) of Alfa product of ventron Division, and Tungsten (vi) oxide, WO_3 (99.7%) of Ventron GMBH, were used as reactant.

Series 3: For the single crystal preparation chemical vapour transport method was carried out by using the same reactants as used for series 1. After many unsuccessful experiments the optimum condition was found out for single crystal preparation. From all of these experiments, it is observed that for the preparation of single crystal of Li_xWO_3 , the amount of reactant mixture, the amount of transport agent, the tube diameter and also the temperature gradients played important rule. Finally, the appropriate amount of reactants according to the

equation 1 were mixed thoroughly in an agate mortar, transferred into clean dried 10 mm diameter silica tubes, the silica tubes were then evacuated at room temperature for 2-3 hours and sealed. The transport agent mercury (ii) chloride, HgCl_2 of Alfa Aesar 99.9995% was loaded in the silica tubes before evacuation. The reaction tubes were then heated in a double-zone furnace for different periods of time with a temperature gradient between 700°C for the sink and 800°C for the source side.

$\text{Li}_x\text{Nb}_y\text{W}_{1-y}\text{O}_3$

Attempts were made to prepare niobium doped lithium tungsten bronzes according to the following reaction :



Series 4: For $\text{Li}_{0.4}\text{Nb}_y\text{WO}_3$ system with $y = 0.00 - 0.35$, the reactions were carried out at 700°C for 7 days with the same reactants as used for series 2 and for niobium source, Niobium (v) oxide, Nb_2O_5 (99.9%) of Fluka AG was used.

Series 5: Samples of nominal composition of $\text{Li}_{0.4}\text{Nb}_y\text{WO}_3$ with $y = 0.00 - 0.35$ were prepared at 700°C for 7 days from the same reactants as used for series 1 and for niobium source, Niobium (v) oxide, Nb_2O_5 of Alfa Aesar (99.9985%) was used. A sample with nominal composition $x = y$ (i.e fully oxidised) was prepared by sealing the silica tube without vacuum and then heated at 700°C for 7 days in a furnace.

Series 6: Attempts were also made to dope niobium in the $\text{Li}_{0.1}\text{WO}_3$ PTB_{tetr} system. Samples of nominal composition of $\text{Li}_{0.1}\text{Nb}_y\text{W}_{1-y}\text{O}_3$ with $y = 0.00 - 0.08$ were prepared at 700°C for 7 days from the appropriate amounts of reactants as used for series 5 according to the equation (ii). A sample with $x = y$ (i.e fully oxidised) for nominal composition was prepared by the same way as described in series 5.

$\text{Li}_x\text{Mo}_y\text{W}_{1-y}\text{O}_3$

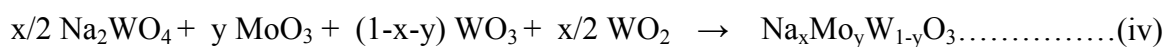
Series 7 and 8: In series 7 samples of various compositions of $\text{Li}_{0.4}\text{Mo}_y\text{W}_{1-y}\text{O}_3$ with $y = 0.00 - 0.3$ and in series 8 samples of various compositions of $\text{Li}_{0.1}\text{Mo}_y\text{W}_{1-y}\text{O}_3$ with $y = 0.00 - 0.1$ have been prepared at 700°C for 7 days according to the following reaction :



For these preparation reactants were used as for series 1 and MoO₃ (Alfa Aesar, 99.9985%). In series 7, a sample with y = 0.05 was unsuccessful because of the leakage of the tube on sealing in vacuum which could be identified from the color of the sample after completing the reaction.

Na_{0.6}Mo_yW_{1-y}O₃

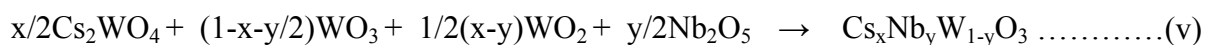
Series 9: Samples of various compositions of Na_{0.6}Mo_yW_{1-y}O₃ system with y = 0.00 – 0.2 have been prepared according to the following equation :



at 600°C and 700°C for 7 days by the same procedure as described for Li_xWO₃ powder sample in series 1. In this series Na₂WO₄ of ICN, Tungsten (iv) oxide, WO₂ of Alfa product of ventron Division, Tungsten (vi) oxide, WO₃ of Ventron GMBH and molybdenum (vi) oxide, MoO₃ of BDH were used as reactants.

Cs_xNb_yW_{1-y}O₃

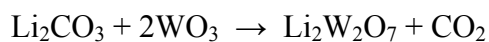
Series 10: Samples of various compositions of Cs_xNb_yW_{1-y}O₃ with x = 0.25 and 0.3; y = 0.00 – 0.2 have been prepared at 800°C for 7 days by the same procedure as described for series 1. Appropriate amounts of reactants were calculated and used according to the following reaction -



Cesium tungsten oxide, Cs₂WO₄ of BDH laboratory supplies, Tungsten (iv) oxide, WO₂ of Alfa product of ventron Division (99%), Tungsten (vi) oxide, WO₃ of Ventron GMBH (99.7%) and Nb₂O₅ of Fluka AG (99.9%) were used as reactant.

Li₂W₂O₇

Samples of Li₂W₂O₇ were prepared at atmospheric conditions to compare some results according to the following reaction :



2.2 Characterisation

X-ray diffraction

All the samples were characterised by X-ray powder diffraction using a Guinier camera with monochromatized $\text{CuK}\alpha_1$ radiation ($\lambda = 1.540598\text{\AA}$). Silicon was added as an internal standard and the positions of the silicon lines were used to correct shrinkage of the film. The 2θ peak position were measured manually by using a film reader. These parameters were indexed and used to refine the cell parameters with the programs Korguis, Korguisp, Lqrf and Asin [111].

Powder diffraction data for direct comparison between the samples were also collected from PW1800 Philips diffractometer with graphite monochromator and $\text{CuK}\alpha_1$ radiation. For some samples X-ray data were also collected in a Stoe Stadi P diffractometer in a 0.02 mm capillary tube by using $\text{MoK}\alpha_1$ radiation together with a focusing Ge (iii) monochromator.

Infrared absorption

All samples were investigated by infrared spectroscopy in the range $375 - 4000\text{ cm}^{-1}$ using a Bruker IFS66 FTIR-spectrometer. For the transmission (T) measurements, the powder samples were diluted by KBr (1 mg sample in 200 mg KBr) and pressed into pellets. The spectra are given in absorption units with $\text{Abs} = \log(I_0 / I)$, where I_0 and I are transmitted intensities through the reference pellet (KBr) and sample pellet diluted with KBr, respectively.

Powder Reflectivity

The optical reflectivity were measured in the range of $3000 - 24000\text{ cm}^{-1}$ from the undiluted powders against a suitable reference by using Bruker IFS88 FTIR spectrometer. In the present investigation KBr, MgO and mirror were used as a reference. The optical reflectivity of the series of powder samples were also measured in the range $10,000$ to $40,000\text{ cm}^{-1}$ against MgO as a reference by using a Zeiss-Specord S10 spectrometer. The relative intensities $R_d = I / I_0$ were plotted as well as recalculated to Kubelka Munk (KM) units according to :

$$F(R_d) = (1 - R_d)^2 / 2R_d$$

Single Crystal Reflectivity

For the single crystal reflectivity measurements crystals from different batches as obtained by transport reactions were glued to plane sample holder (ordinary glass). They were then mechanically abraded and finally polished (0.2 μm diamond paste) to show optically high quality surfaces. The reflectivity measurements were carried out between 600 and 20000 cm^{-1} using a spot size of 80 μm in diameter. All these single crystal reflection experiments were carried out using polarized light (Glan Thompson polarizer) at nearly normal incidence onto the surfaces. For the measurements, a FTIR equipment (Bruker IFS88) with an attached microscope (Bruker A590) were used. Al-mirror were used for reference measurements.

Electron Microscopy

A number of samples from different series have been investigated by electron microscopy methods, including microanalysis. The scanning electron microscopy (SEM) studies gave information about the variation in crystal size and shape, and energy-dispersive X-ray (EDX analysis) provided an indication of the compositions of the various crystals. Different SEM microscopes were used in the present investigation. For SEM-image and quantitative distribution of elements JEOL 820 SEM was used which is equipped with a LINK AN10000 EDX microanalysis system. For collecting the spectrum and to see the quantitative distribution of elements of some selective $\text{Na}_{0.6}\text{Mo}_y\text{W}_{1-y}\text{O}_3$ sample JEOL 880 SEM was also used which is equipped with a LINK ISIS EDX microanalysis system (GEM detector). HITACHI S-530 SEM was used for a large number of sample mainly for collecting the spectra. However, EDX analysis with HITACHI S-530 SEM shows lower local resolution comparing to that with JEOL 820 SEM. For JEOL 820 SEM and HITACHI S-530 microscope studies, the powders were smeared on adhesive carbon films and mounted on aluminium plates whereas for JEOL 880 SEM copper plate was used. The EDX analysis in the SEM microscope were taken from at least 2-3 different parts of each crystals in the JEOL 820 SEM.

For further information about phase and crystal composition the TEM microscope was used specially for the $\text{Cs}_x\text{Nb}_y\text{W}_{1-y}\text{O}_3$ and $\text{Na}_{0.6}\text{Mo}_y\text{W}_{1-y}\text{O}_3$ systems, where electron diffraction (ED) and microanalysis studies of individual crystal fragments were combined. A JEOL 2000FXII transmission electron microscope, equipped with a LINK AN10000EDS microanalysis system was used. For these studies, specimens were prepared by crushing a small amount of

the sample in an agate mortar, dispersing the fine powder in n-butanol and finally putting a drop of the suspension on a holey carbon film supported by a Cu grid.

High-resolution electron microscopy (HRTEM) was used for few samples to get information about the ordered and defect structures of crystals. The HRTEM images were taken in a JEOL 3010JEM, operated at an accelerating voltage of 300kV. The radius of the objective aperture used corresponded to 0.68 \AA^{-1} in reciprocal space, and the image were taken close to Scherzer focus conditions, which means that the projected metal atoms appear as dark spots in the HRTEM images.

Thermal analysis

Thermogravimetric analysis (TG) for the weight change of a sample as a function of temperature was measured by SETARAM Scientific and industrial equipment.

3. RESULTS

3.1 Li_xWO_3 system

3.1.1 Characterisation of solid state synthesis products

X-ray investigation

The results of the X-ray powder (Guinier method) analysis of all lithium tungsten bronzes, Li_xWO_3 of series 1 and series 2 are collected in table 1a. Results obtained previously [112] from samples of Li_xWO_3 which were prepared at 600°C, 700°C and 800°C by the same way and from the same reactants as described for series 2 are also given in table 1b. In series 1 single phase of $\text{PTB}_{\text{cubic}}$ is observed for $0.3 \leq x \leq 0.5$ whereas for series 2 it is observed for $0.4 \leq x \leq 0.5$. The $\text{PTB}_{\text{cubic}}$ phase field for series 2 is in good agreement with the data obtained previously [112] at 600°C, 700°C and 800°C indicating that the temperature conditions are not important for the resultant product. However, these samples show different color changes at atmospheric condition depending on preparation temperature (see below). On the other hand the differences between series 1 and series 2 can be explained by a different quality of WO_2 . IR spectra and X-ray pattern obtained a significant deviation from pure WO_2 for Alfa product of ventron Division as used in series 2 compared to WO_2 as used in series 1.

The typical deviation obtained by several time reading the same X-ray film is about ± 0.003 . Furthermore, the deviation in the results from some samples, in particular five times preparation of same nominal composition of $\text{Li}_{0.4}\text{WO}_3$, but prepared individually is ± 0.005 . In all cases the estimated standard deviation of the refinement was smaller, which is therefore not given in table 1a.

For cubic phase the refinement was done in all cases using a primitive cell (Pm3m) containing 1 formula unit of Li_xWO_3 . Some weak additional reflections are observed which are related to a unit cell parameter doubling, i.e. according to a body centred cell (Im3) containing 8 formula units. Doubling of unit cell has been reported first, using neutron diffraction data [113]. There are also some few reports about doubling of unit cell of cubic Li_xWO_3 [114, 115]. For comparison, refinements of unit cell parameter were carried out by using the 8 fold cell for series 1. The unit cell parameter are given in Table 1a as $a/2$. It can be seen that the change from the primitive to the body centre cubic phase does not have any significant change in the absolute value and general trend of lattice parameters on x .

Table 1a: Results of the X-ray powder analysis of different samples of lithium tungsten bronzes, Li_xWO_3 ($x = 0.03- 0.7$) of series 1 and series 2

Nominal composition	Li_xWO_3 Prepared at 700°C (series 1)			Li_xWO_3 Prepared at 700°C (series 2)	
	Phase observed 3 h X-ray	Cell parameters (Guinier method)		Phase observed 40 min X-ray	Cell parameters (Guinier method) (Å)
		(Å)	a / 2 (Å)		
$\text{Li}_{0.03}\text{WO}_3$	PTB _O +PTB _T	-	-	-	-
$\text{Li}_{0.05}\text{WO}_3$	PTB _O +PTB _T	a = 7.3114 b = 7.4654 c = 7.7901 a = 5.2106 c = 3.8558	-	PTB _O +PTB _T +●	a = 7.3254 b = 7.5250 c = 7.7306 a = 5.1906 c = 3.8453
$\text{Li}_{0.1}\text{WO}_3$	PTB _T	a = 5.2113 c = 3.8422	-	PTB _T +●	a = 5.2089 c = 3.8518
$\text{Li}_{0.15}\text{WO}_3$	-	-	-	PTB _C +PTB _T +●	a = 3.7400 a = 5.2027 c = 3.8457
$\text{Li}_{0.2}\text{WO}_3$	PTB _C +PTB _T	a = 3.7353 a = 5.2015 c = 3.8379	3.7376	PTB _C +PTB _T +●	a = 3.7381 a = 5.1886 c = 3.8324
$\text{Li}_{0.25}\text{WO}_3$	-	-	-	PTB _C +PTB _T +●	a = 3.7324
$\text{Li}_{0.3}\text{WO}_3$	PTB _C	a = 3.7394	3.7360	PTB _C +●	a = 3.7256
$\text{Li}_{0.35}\text{WO}_3$	PTB _C	a = 3.7383	3.7382	PTB _C +●	a = 3.7258
$\text{Li}_{0.4}\text{WO}_3$	PTB _C	a = 3.7237	3.7260	PTB _C	a = 3.7245
$\text{Li}_{0.45}\text{WO}_3$	PTB _C	a = 3.7177	3.7212	-	-
$\text{Li}_{0.5}\text{WO}_3$	PTB _C	a = 3.7181	3.7182	PTB _C	a = 3.7209
$\text{Li}_{0.55}\text{WO}_3$	PTB _C + traces of Li_2WO_4	a = 3.7170	3.7178	PTB _C +traces of Li_2WO_4	a = 3.7222
$\text{Li}_{0.6}\text{WO}_3$	PTB _C + Li_2WO_4 + WO_2	a = 3.7233	3.7238	PTB _C + Li_2WO_4 + WO_2	a = 3.7246
$\text{Li}_{0.7}\text{WO}_3$	PTB _C + Li_2WO_4 + WO_2	a = 3.7232	3.7247	PTB _C + Li_2WO_4 + WO_2	a = 3.7210

● = 2-8 extra lines

Table 1b: Results of the X-ray powder analysis of some previous samples [112] of Li_xWO_3 ($x = 0.1- 0.7$) prepared from old reactants at 600°C, 700°C and 800°C.

Nominal composition	Li_xWO_3 Prepared at 600°C		Li_xWO_3 Prepared at 700°C		Li_xWO_3 Prepared at 800°C	
	Phase observed (30 min X-ray)	Cell parameters (Guinier – Hägg method) (Å)	Phase observed (30 min X-ray)	Cell parameters (Guinier – Hägg method) (Å)	Phase observed (30 min X-ray)	Cell parameters (Guinier – Hägg method) (Å)
$\text{Li}_{0.1}\text{WO}_3$	PTB _T +●	a = 5.2034(12) c = 3.8441(18)	PTB _T +●	a = 5.2034(12) c = 3.8441(18)	PTB _T +●	-
$\text{Li}_{0.2}\text{WO}_3$	PTB _C +PTB _T +●	a = 3.7366(58) a = 5.2078(96) c = 3.8392(12)	PTB _C +PTB _T +●	a = 3.7378(33) a=5.2064(115) c=3.8420(136)	PTB _C +PTB _T +●	-
$\text{Li}_{0.3}\text{WO}_3$	PTB _C +PTB _T +●	a = 3.7268(45) a = 5.1974(744) c = 3.8379(293)	PTB _C +PTB _T +●	a = 3.7259(45) a=5.2029(217) c=3.8351(131)	PTB _C +●	-
$\text{Li}_{0.35}\text{WO}_3$	PTB _C +●	a = 3.7338(55)	PTB _C +●	a = 3.7261(47)	PTB _C +●	a = 3.7237(51)
$\text{Li}_{0.4}\text{WO}_3$	PTB _C	a = 3.7233(27)	PTB _C	a = 3.7238(21)	PTB _C	a = 3.7231(30)
$\text{Li}_{0.5}\text{WO}_3$	PTB _C	a = 3.7225(43)	PTB _C	a = 3.7209(40)	PTB _C	a = 3.7213(58)
$\text{Li}_{0.6}\text{WO}_3$	PTB _C +●	a = 3.7233(35)	PTB _C +●	-	PTB _C +●	-
$\text{Li}_{0.7}\text{WO}_3$	PTB _C +●	a = 3.7221(55)	PTB _C +●	-	PTB _C +●	-

● = 2-8 very weak extra lines.

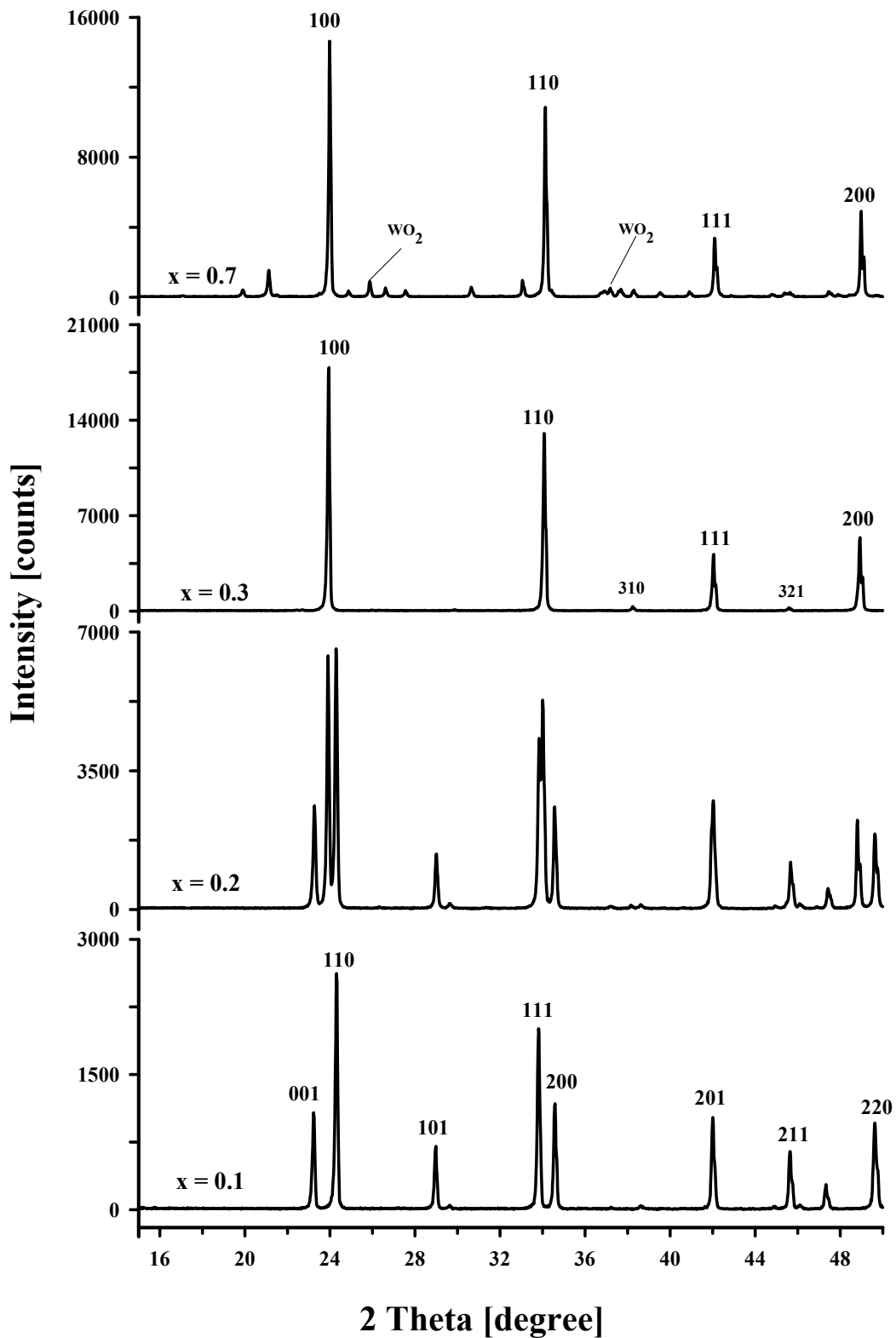


Fig.6. Examples of X-ray powder diffraction patterns taken immediately after opening the reaction tubes of Li_xWO_3 (series 1) with $x = 0.1 - 0.7$ as denoted. For $x = 0.1$ and 0.3 pure PTB_{tet} and $\text{PTB}_{\text{cubic}}$ is seen respectively. For sample with $x = 0.7$ along with main $\text{PTB}_{\text{cubic}}$ phase some weak additional lines observed which belongs to WO_2 reactant as denoted and the rest lines without any notation are belongs to Li_2WO_4 reactant. For $x = 0.2$ mixed phase of $\text{PTB}_{\text{cubic}}$ and PTB_{tet} is seen. (further explanation see text)

Selected X-ray diffraction patterns (Philips Diffractometer) of series 1 are given in Fig. 6 and Fig. 7. Fig. 6 gives a typical example of pure $\text{PTB}_{\text{cubic}}$ phase, $\text{PTB}_{\text{cubic}}$ phase in combination with non-bronze phases, $\text{PTB}_{\text{cubic}}$ phase coexisting with PTB_{tet} and pure PTB_{tet} . In Fig. 6 for $x = 0.3$ the bronze is typically identified as $\text{PTB}_{\text{cubic}}$ by the peaks 100 ($2\theta^\circ$ at about 24.02), 110 ($2\theta^\circ$ at about 34.13), 111 ($2\theta^\circ$ at about 42.07) and 200 ($2\theta^\circ$ at about 48.93). The two weak peaks at 38.0 and 45.32 2-theta position are identified as 310 and 321 respectively, indicating doubling of the unit cell as also used in the refinement in table 1a (series 1, column 3). In this case the peaks of 100, 110 become 200, 220 etc. The splitting of the peaks at higher 2-theta angle, is due to the effect of $\text{CuK}\alpha_2$ radiation in addition to $\text{CuK}\alpha_1$, indicating a misalignment of the graphite monocromator. When $x > 0.5$ some additional lines appear along with $\text{PTB}_{\text{cubic}}$ in the powder pattern which are identified as Li_2WO_4 and WO_2 as shown for the $\text{Li}_{0.7}\text{WO}_3$ sample in Fig. 6.

For $x = 0.1$ the PTB_{tet} bronze is identified by the peaks 001 ($2\theta^\circ$ at about 23.24), 110 ($2\theta^\circ$ at about 24.31), 101 ($2\theta^\circ$ at about 28.97), 111 ($2\theta^\circ$ at about 33.81), 200 ($2\theta^\circ$ at about 34.58), 201 ($2\theta^\circ$ at about 42.01), 211 ($2\theta^\circ$ at about 45.64) and 220 ($2\theta^\circ$ at about 49.63). For $x = 0.2$ the pattern is explained by a combination of $\text{PTB}_{\text{cubic}}$ and PTB_{tet} . The lattice parameter for both phases was obtained separately within the mixture as given in Table 1a. The same holds for the lower $x = 0.05$ and 0.03 composition which were PTB_{tet} together with PTB_{orth} is observed [Fig. 7]. The PTB_{orth} phase is identified by their diffraction peaks 001, 200, 020, 210, 111 etc. at about 2-theta 23.18, 23.67, 24.25, 26.67 and 28.89 positions as indicated for the $x = 0.03$ sample in Fig. 7. The reactant WO_3 is identified as monoclinic by the peaks 002 ($2\theta^\circ$ at about 23.19), 020 ($2\theta^\circ$ at about 23.67), 200 ($2\theta^\circ$ at about 24.42), 012 ($2\theta^\circ$ at about 26.07), 120 ($2\theta^\circ$ at about 26.66), 112 ($2\theta^\circ$ at about 28.69) and 121 ($2\theta^\circ$ at about 29.21). Thus the X-ray powder patterns of the samples of series 1 reveal that the single phase of perovskite tungsten bronze tetragonal type, PTB_{tet} can be prepared with nominal composition $\text{Li}_{0.1}\text{WO}_3$. For $x = 0.03$ and $x = 0.05$ mixed phase of PTB_{orth} and PTB_{tet} is obtained. A distinction between PTB_{orth} and monoclinic will be discussed further below.

Phonon absorption characteristics

In Fig. 8, all IR absorption spectra as obtained for series 1 samples are shown between 375 cm^{-1} and 1600 cm^{-1} . Above 1600 cm^{-1} all spectra appear featureless, which are not shown, therefore. For monoclinic WO_3 typical peaks with maxima at about 773 cm^{-1} and 825 cm^{-1} are present. There is a considerable change in the spectra with increasing the nominal Li content.

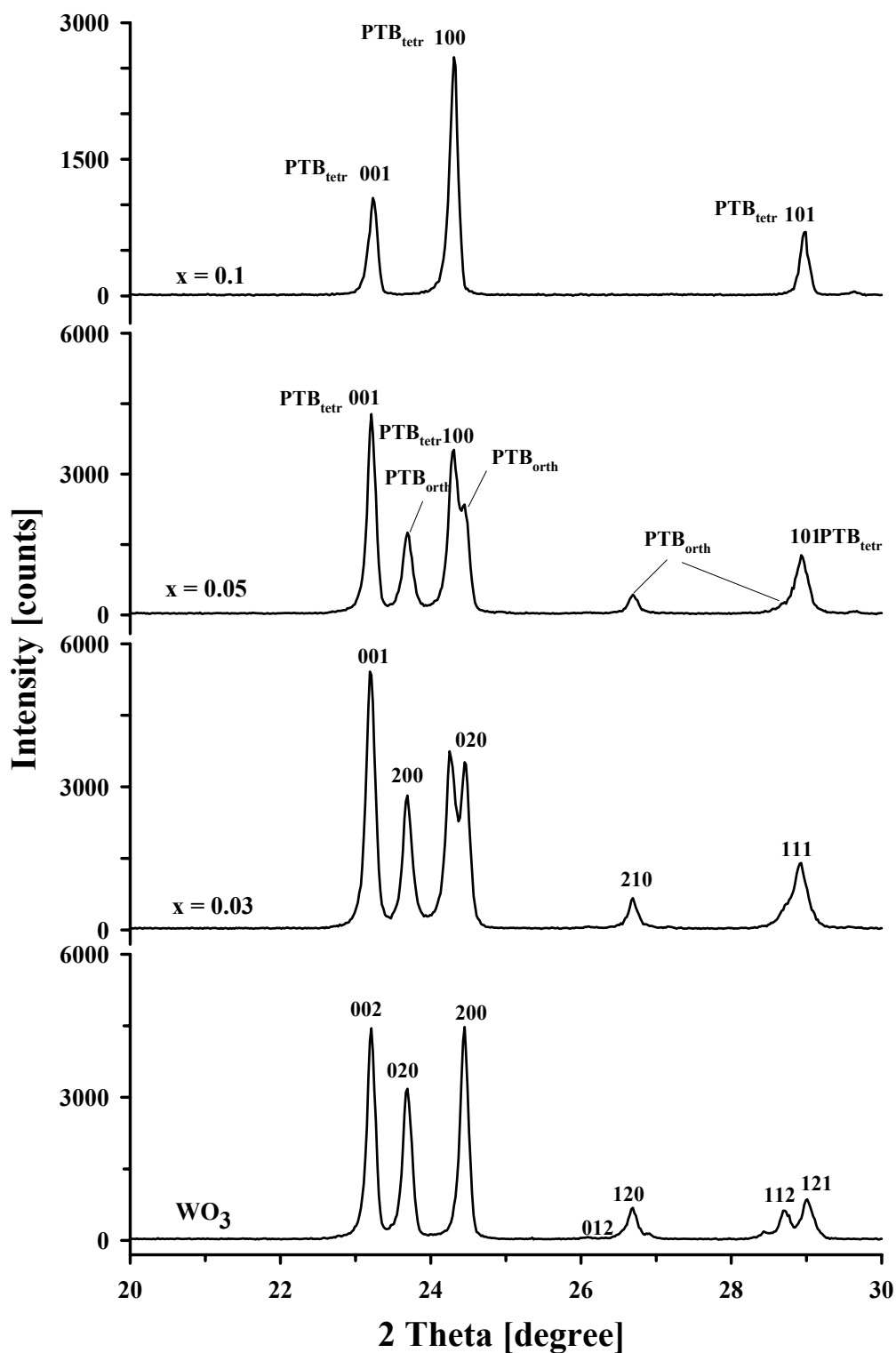


Fig. 7. Examples of X-ray powder diffraction patterns taken immediately after opening the reaction tubes of Li_xWO_3 (series1) with $x = 0.0 - 0.1$ as denoted. For $x = 0.0$ the monoclinic phase and for $x = 0.1$ PTB_{tetr} is seen, whereas for $x = 0.03$ and 0.05 mixed phase of PTB_{tetr} and PTB_{orth} are seen. (further explanation see text)

For $\text{Li}_{0.03}\text{WO}_3$ the maximum absorption becomes more pronounced compared to the peak on the low frequency side. The maxima is shifted to about 860 cm^{-1} . There is a further shift to

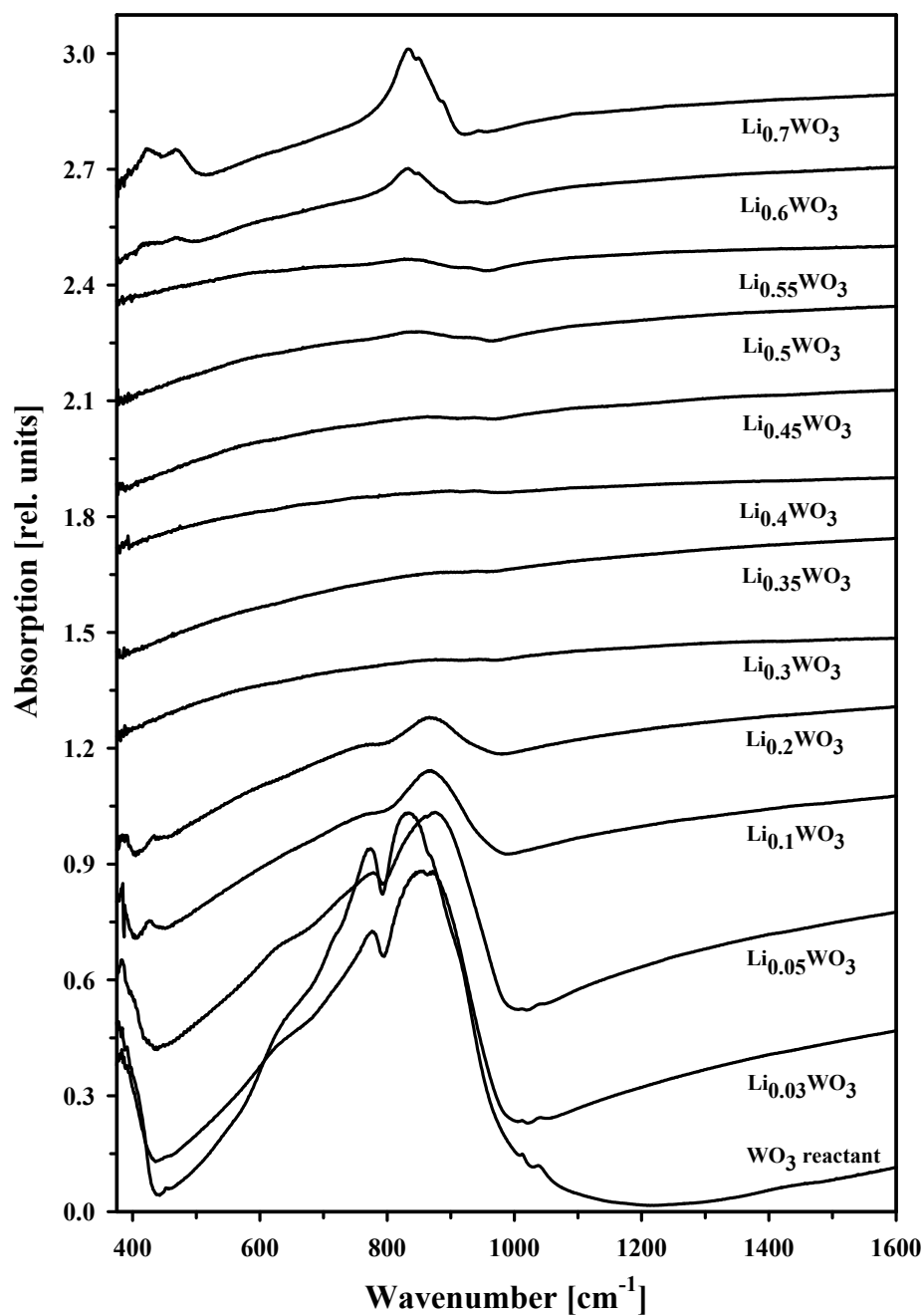


Fig. 8. IR absorption spectra (KBr-method) of Li_xWO_3 ($x = 0.0 - 0.7$) of series 1 as measured directly after opening the reaction tubes.

about 870 cm^{-1} for $\text{Li}_{0.05}\text{WO}_3$ but turns somehow back to 850 cm^{-1} for $\text{Li}_{0.1}\text{WO}_3$ and $\text{Li}_{0.2}\text{WO}_3$. Going from WO_3 to $\text{Li}_{0.1}\text{WO}_3$ and $\text{Li}_{0.2}\text{WO}_3$, the minimum structure observed at about 800 cm^{-1} tends to disappear. A new absorption feature is seen at about 430 cm^{-1} . The samples $\text{Li}_{0.3}\text{WO}_3$ to $\text{Li}_{0.5}\text{WO}_3$ do not show any phonon absorption signature. This can be

explained by the free electron metallic behaviour of the samples (see below). The systematic decrease in phonon absorption with increasing x may be noted. Phonon signature appear for $\text{Li}_{0.55}\text{WO}_3$ to $\text{Li}_{0.7}\text{WO}_3$ indicating typically Li_2WO_4 . From the X-ray result, $\text{Li}_{0.1}\text{WO}_3$ shows rather pure PTB_{tet} type. Therefore, the absorption spectra with $x = 0.1$ can clearly be related to this phase. The lower phonon absorption intensity for $\text{Li}_{0.2}\text{WO}_3$ can be explained by an increase of $\text{PTB}_{\text{cubic}}$ contribution with respect to PTB_{tet} . On the other hand towards lower x more PTB_{orth} has to be taken into account.

For a better comparison, the temperature dependent changes in the IR spectra of WO_3 was

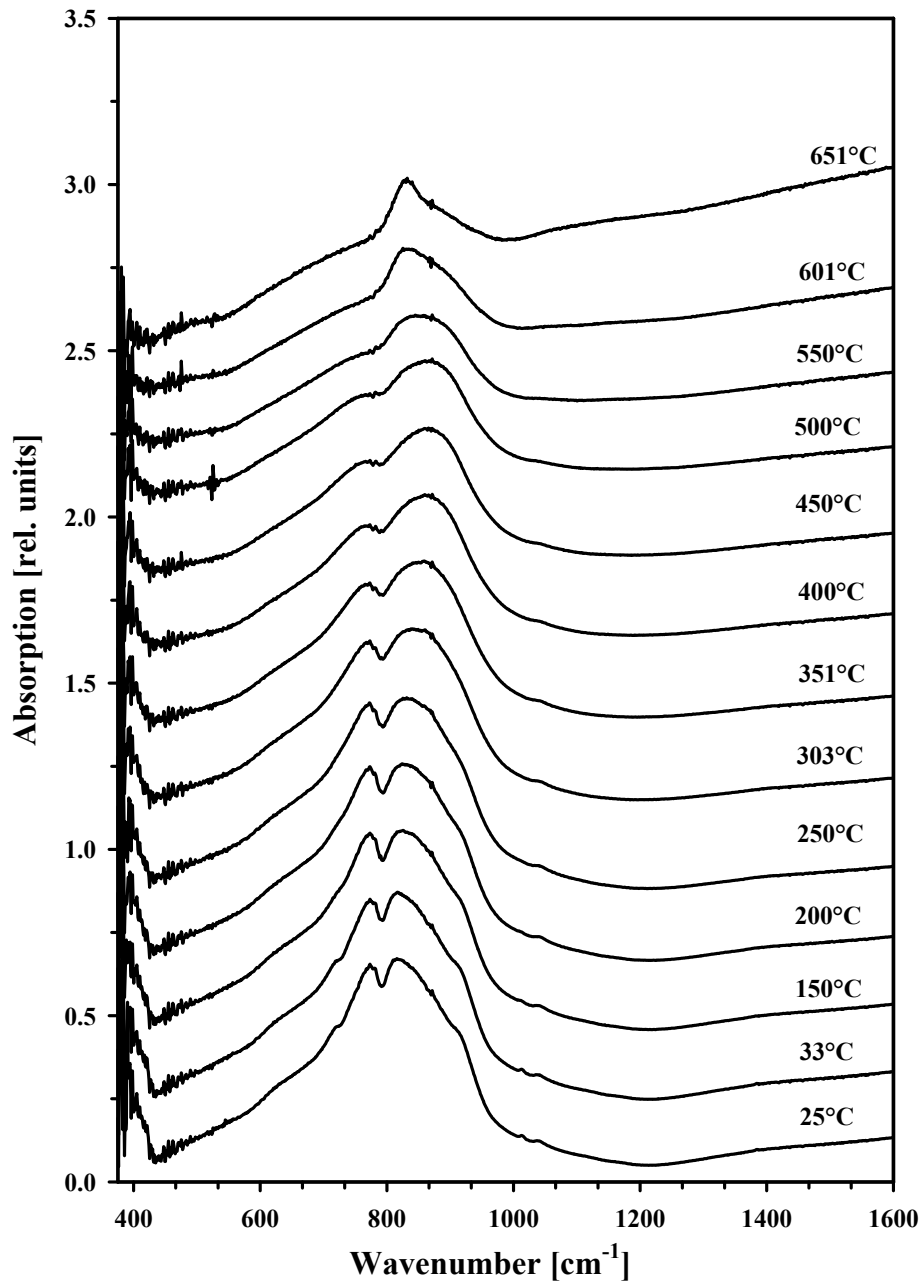


Fig.9. Temperature dependent (in situ measurement) IR absorption spectra (KBr-method) of WO_3 .

measured on heating the sample from 25°C to 651°C [Fig.9]. It is observed that the peak maximum at about 820 cm^{-1} at 25°C shifts to 860 cm^{-1} above 350°C. A further increase in temperature leads to a gradual disappearance of the peak at about 790 cm^{-1} and the minimum at about 800 cm^{-1} . Additionally the main peak position shifts towards lower wavenumber. This effect can be explained by the decreasing order parameter of the orthorhombic phase. The tetragonal phase has still not been reached here up to 651°C for experimental reasons. However, the peak form is almost indicative for the tetragonal phase of WO_3 . These interpretations become available on comparing the spectral changes with the results of temperature dependent X-ray diffraction studies [116] which will be further discussed below.

UV-VIS spectra

The reflectivity spectra of the powder samples of series 1 is given in Fig.10 in percent ($R = 100I/I_0$). The reflectivity of WO_3 is about 55% at 15000 cm^{-1} , increases to 65% at 21000 cm^{-1}

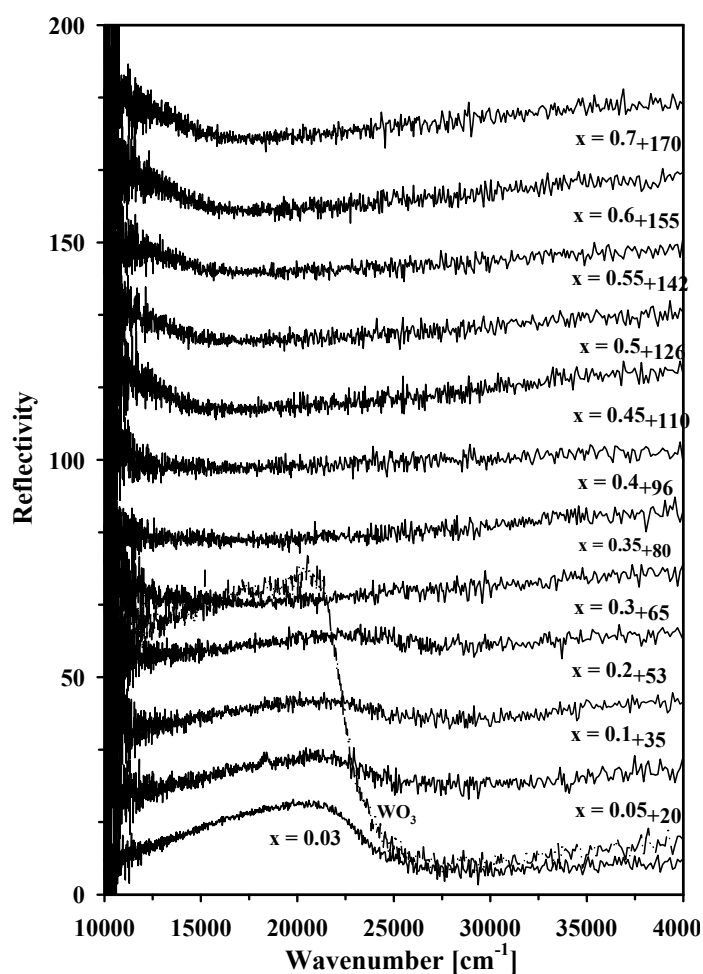


Fig.10. As measured UV- VIS spectra of Li_xWO_3 (series 1).

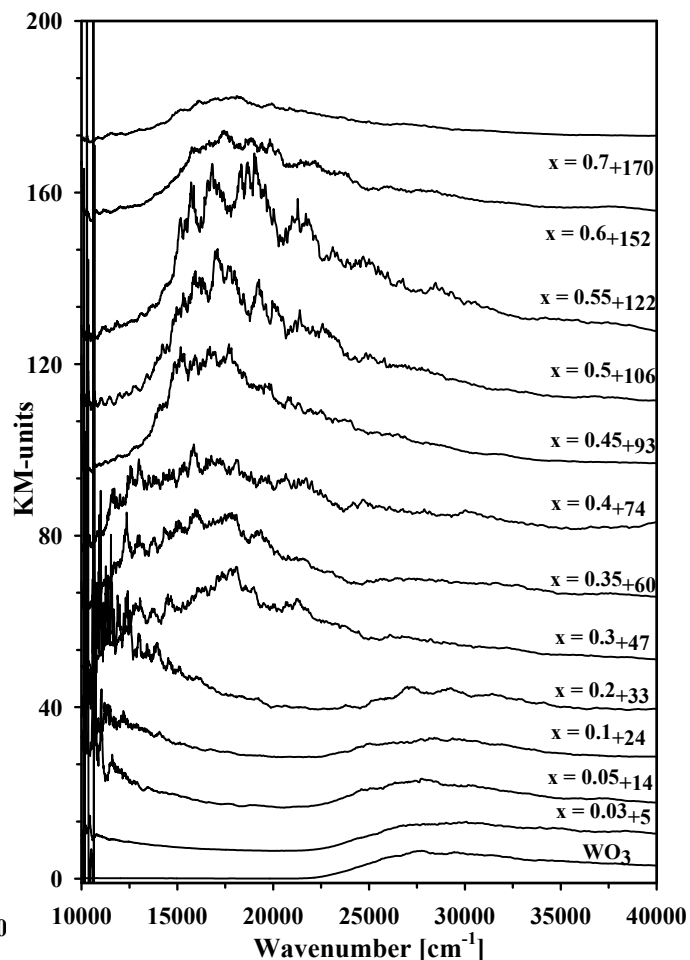


Fig.11. UV- VIS spectra of Li_xWO_3 (series 1) in KM units.

and sharply drop down above 22500 cm^{-1} to nearly 5-10% above 25000 cm^{-1} . For $x = 0.03$, the maximum reflectivity has reduced to about 20% and for $x = 0.05$, only 5% reflectivity is observed. For WO_3 and $x = 0.03$ the as measured spectra are shown whereas the spectra of the other samples are shifted as denoted. With increasing lithium concentration the reflectivity decreases in the range 10000 to 25000 cm^{-1} becoming rather flat for $x = 0.3$ to 0.4 samples. For $x = 0.45$ to 0.7 , the samples show a minimum in the reflectivity spectrum at around 15000 cm^{-1} to 18000 cm^{-1} respectively, increasing significantly towards lower wavenumber.

The reflectivity spectra were recalculated using the Kubalka Munk formula [Fig. 11]. The important observation is the strong increase in intensity of a broad peak between 15000 cm^{-1} and 18000 cm^{-1} for the Li_xWO_3 with $x = 0.3$ - 0.55 which corresponds to a minima in reflectivity [Fig. 10]. The peak shows the highest intensity for the $x = 0.5$ and strongly decreases in intensity towards $x = 0.7$. There is an evidence of decreasing intensity with decreasing effective Li-content, which thus shows the less contribution of the $\text{PTB}_{\text{cubic}}$ phase. On the other hand a shoulder towards lower wavenumbers corresponds to the absorption property of PTB_{tet} which becomes dominant for the sample with a nominal Li content of $x = 0.1$. In further experiments in the spectral range 2000 cm^{-1} to 12000 cm^{-1} a broad peak observed around 8000 cm^{-1} for $x = 0.05$ and at about 10000 cm^{-1} for the sample $x = 0.1$ [not shown]. These corresponds in principle with the reflectivity measurement for single crystals. However, it was difficult to reproduce the reflectivity spectra in the spectral range 2000 cm^{-1} to 12000 cm^{-1} on powder samples, probably due to the effect of superimposition of regular and diffuse reflectivity.

3.1.2 Characterisation of single crystal synthesis products

The SEM image and the photos of the abraded and polished crystals of $x = 0.1$ to 0.45 as obtained in the optical microscope (reflection mode) are given in Fig. 12a and 12b showing their typical shapes and sizes. For nominal composition of $\text{Li}_{0.45}\text{WO}_3$ and $\text{Li}_{0.4}\text{WO}_3$ the crystals appear homogeneous in the microscope. However, for further decreasing nominal Li content the crystals become optically inhomogeneous. For $\text{Li}_{0.35}\text{WO}_3$ crystals some regularly formed thin lighter slabs are observed, which become more expressed for $\text{Li}_{0.3}\text{WO}_3$ and probably dominant for $\text{Li}_{0.25}\text{WO}_3$. The $\text{Li}_{0.1}\text{WO}_3$ crystals show plat like shapes.

For characterisation, crystals were selected from the batches and crushed for X-ray and IR powder investigation. The phase observed and the refined lattice parameter are given in Table

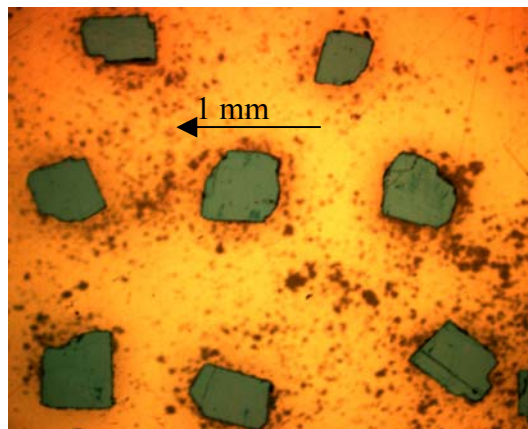
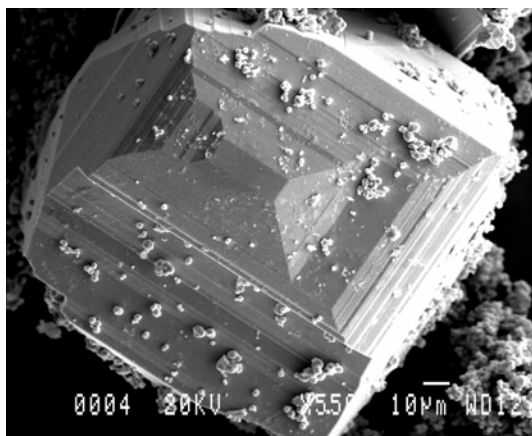
2. The samples with nominal composition $\text{Li}_{0.1}\text{WO}_3$ show $\text{PTB}_{\text{tetra}}$ with 3-5 weak lines of $\text{PTB}_{\text{ortho}}$ in the powder diffraction pattern. The sample $\text{Li}_{0.25}\text{WO}_3$ and $\text{Li}_{0.3}\text{WO}_3$ indexed as superimposition of $\text{PTB}_{\text{tetra}}$ plus $\text{PTB}_{\text{cubic}}$ and the lattice parameters were refined. For $\text{Li}_{0.35}\text{WO}_3$ there are also 2-3 weak lines of $\text{PTB}_{\text{tetra}}$ beside the phase $\text{PTB}_{\text{cubic}}$ which are, however, too weak for any refinement. $\text{Li}_{0.4}\text{WO}_3$ and $\text{Li}_{0.45}\text{WO}_3$ are single phase $\text{PTB}_{\text{cubic}}$ according to X-ray pattern refinement. The IR results of crushed crystals [KBr-method, Fig. 13] also support these X-ray results, although for $\text{Li}_{0.1}\text{WO}_3$ absorption is more indicative for $\text{PTB}_{\text{ortho}}$.

Table 2: X-ray results (Guinier) of single crystals of Li_xWO_3 prepared by chemical vapour transport method with a temperature Gradient, $T = 100^\circ\text{C}$ ($T_2 = 800^\circ\text{C}$; $T_1 = 700^\circ\text{C}$); HgCl_2 was used as a transporting agent. Crystals obtained by 100% transport .

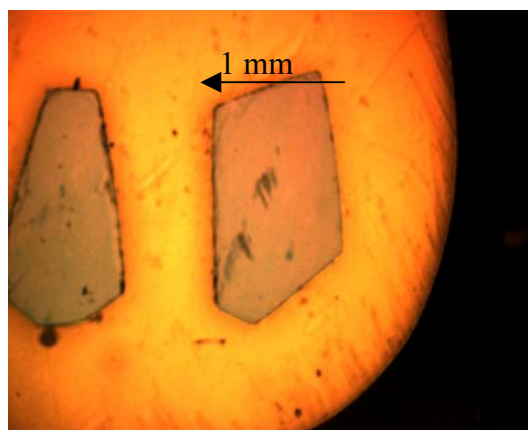
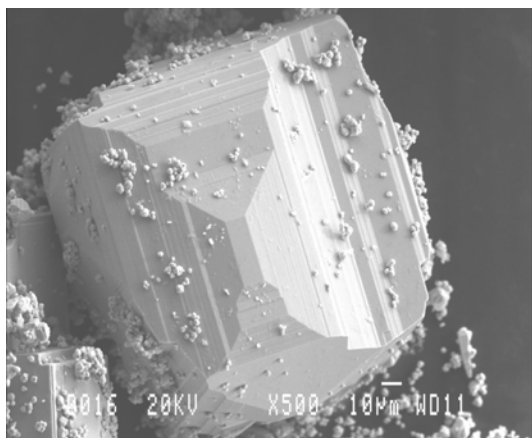
Experimental no.	Nominal composition	Heating period (days)	Phase observed in X-ray for transported crystals	Cell parameter obtained from crystals (Guinier method)
1	$\text{Li}_{0.1}\text{WO}_3$	5 days	$\text{PTB}_{\text{tetra}} + \blacksquare$	a = 5.2051(11) c = 3.8447(13)
2	$\text{Li}_{0.1}\text{WO}_3$	7 days	$\text{PTB}_{\text{tetra}} + \blacksquare$	a = 5.2015(12) c = 3.8448(12)
3	$\text{Li}_{0.25}\text{WO}_3$	7 days	$\text{PTB}_{\text{cubic}}$ + $\text{PTB}_{\text{tetra}}$.	a = 3.7325(13) a = 5.1997(09) c = 3.8381(11)
4	$\text{Li}_{0.3}\text{WO}_3$	7 days	$\text{PTB}_{\text{cubic}}$ + $\text{PTB}_{\text{tetra}}$.	a = 3.7322(12) a = 5.2029(11) c = 3.8379(01)
5	$\text{Li}_{0.35}\text{WO}_3$	7 days	$\text{PTB}_{\text{cubic}} + \bullet$	a = 3.7313(15)
6	$\text{Li}_{0.4}\text{WO}_3$	5 days	$\text{PTB}_{\text{cubic}}$	a = 3.7301(07)
7	$\text{Li}_{0.45}\text{WO}_3$	7 days	$\text{PTB}_{\text{cubic}}$	a = 3.7204(15)

● = 2-3 very weak extra lines of $\text{PTB}_{\text{tetra}}$.

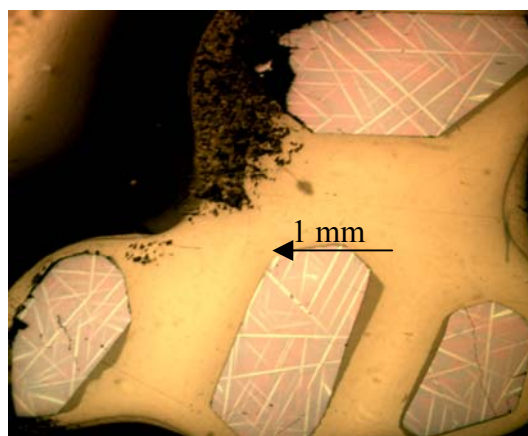
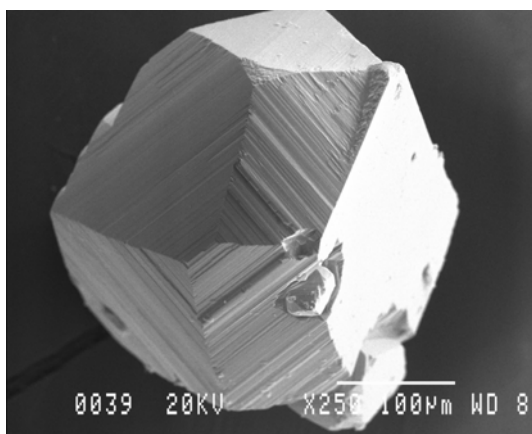
■ = 3-5 weak extra lines of $\text{PTB}_{\text{ortho}}$.



SEM image and the polished single crystal of $\text{Li}_{0.45}\text{WO}_3$

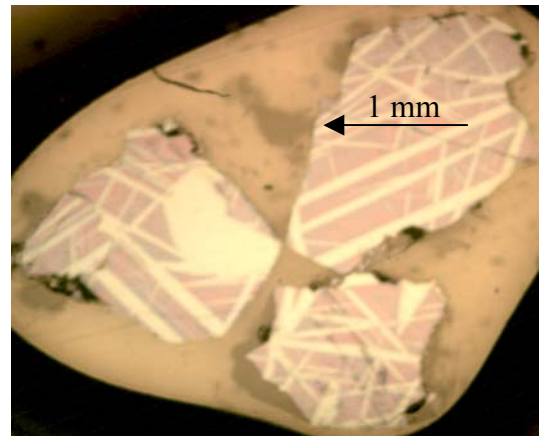
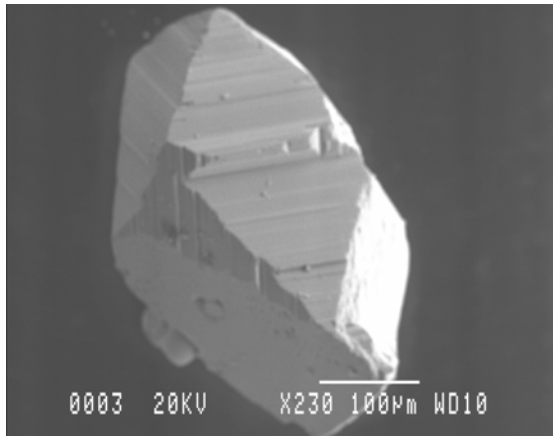


SEM image and the polished single crystal of $\text{Li}_{0.4}\text{WO}_3$

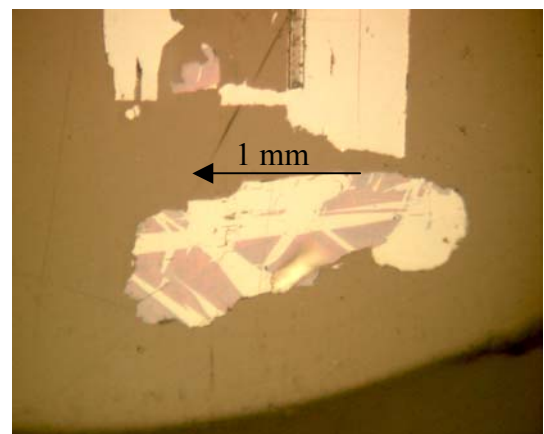
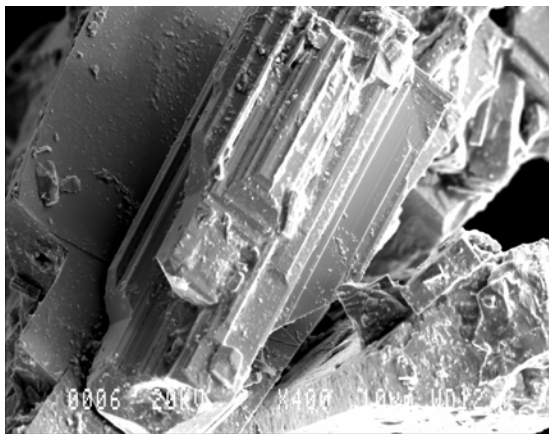


SEM image and the polished single crystal of $\text{Li}_{0.35}\text{WO}_3$

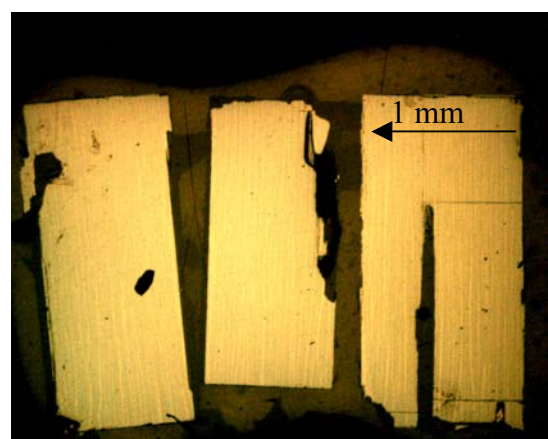
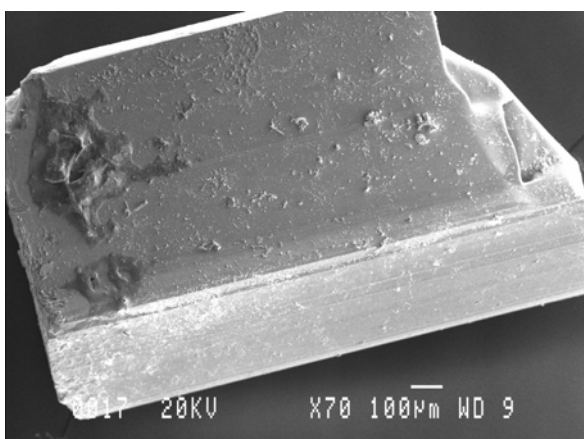
Fig. 12a. SEM image and polished single crystal of Li_xWO_3 with $x = 0.35 - 0.45$ as denoted.



SEM image and the polished single crystal of $\text{Li}_{0.3}\text{WO}_3$



SEM image and the polished single crystal of $\text{Li}_{0.25}\text{WO}_3$



SEM image and the polished single crystal of $\text{Li}_{0.1}\text{WO}_3$

Fig.12b. SEM image and polished single crystal of Li_xWO_3 with $x = 0.1- 0.3$ as denoted.

Polarized micro reflectivity measurements between 600 cm^{-1} to 18000 cm^{-1} were carried out on selected polished crystal slices using a spot size diameter of $80\text{ }\mu\text{m}$. The typical reflectivity spectra of Li_xWO_3 with nominal $x = 0.45, 0.4$ and 0.35 are shown in Fig. 14a. All the crystals

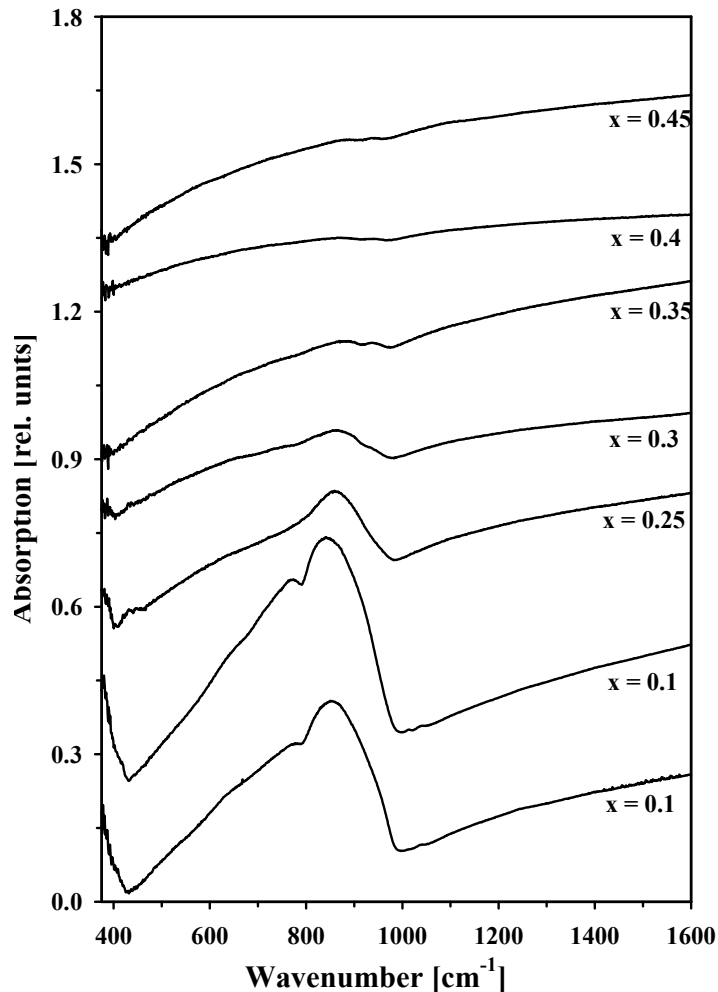


Fig. 13. IR absorption spectra (KBr-method) of crushed single crystals of Li_xWO_3 ($x = 0.1 - 0.45$) as measured immediately after opening the reaction tubes.

from the batches of $x = 0.45$ show the same Drude free carrier type isotropic reflectivity with a minimum between 14000 and 15000 cm^{-1} . Crystals from the batches with $x = 0.4$ and 0.35 all slightly differ indicating a superimposition of an additional spectral contribution in the range of the minimum. This contribution is related to the influence of submicroscopical exsolution of the tetragonal phase, since this effect becomes increasingly significant for crystals from the $x = 0.35$ batch. For these crystals, there are brighter lamellars which are separated by sharp interfaces [Fig. 12a], due to the phase separation. For $x = 0.35$, measurement spot sizes were only on the dark part avoiding any contribution of the white lamellars. However, already in the darker part deviation from isotropic reflectivity can be related to submicroscopical exsolution phenomena into $\text{PTB}_{\text{cubic}}$ and PTB_{tetr} .

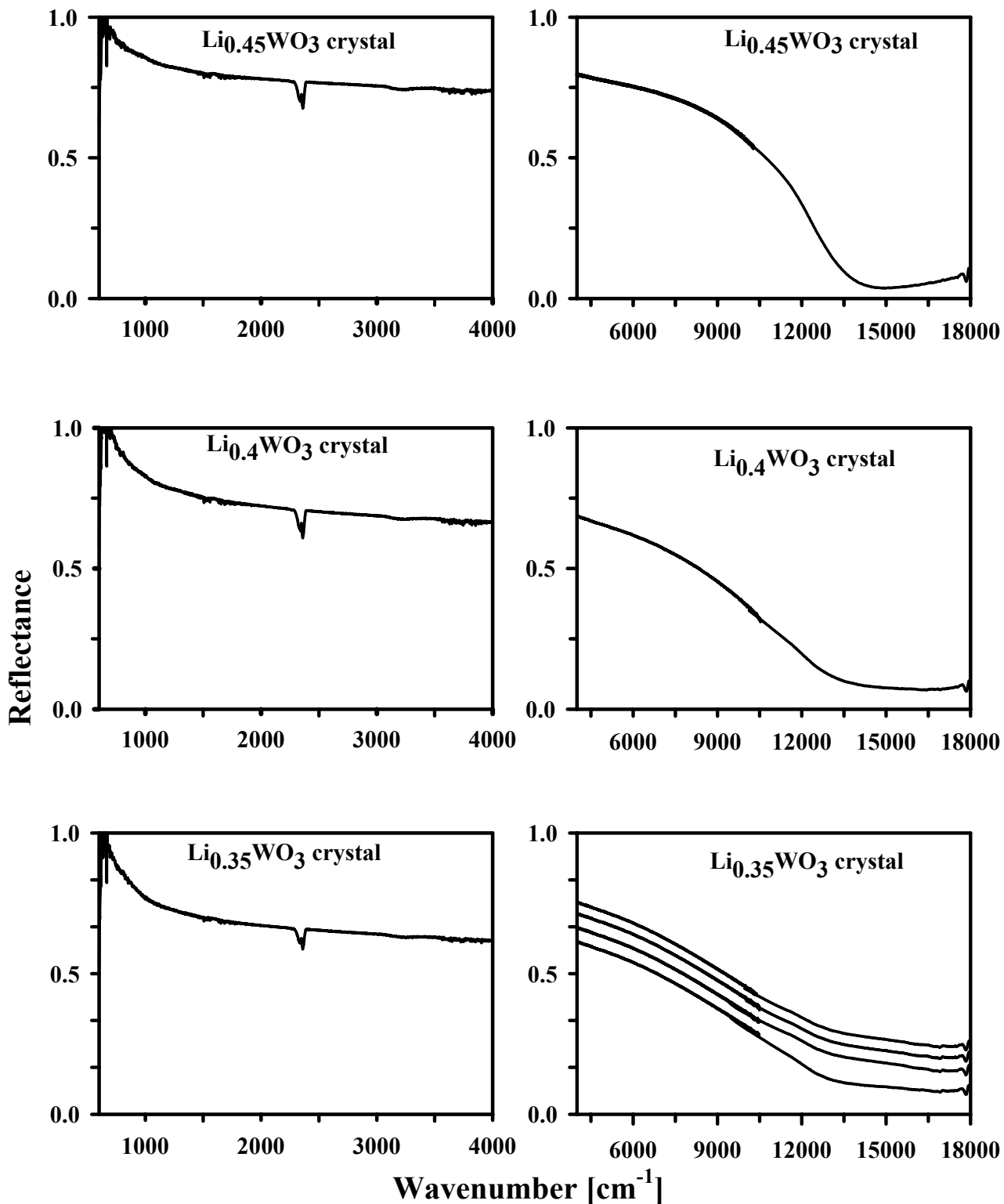


Fig. 14a. Polarized reflectivity spectra of Li_xWO_3 crystals where $x = 0.35, 0.4$ and 0.45 . For $x = 0.45$ and 0.4 isotropic behaviour is observed. For $x = 0.35$ there are angle dependencies between 8000 and 14000 cm^{-1} as shown by the spectra $R_\theta = 0^\circ, 30^\circ, 60^\circ$ and 90° (spectra are shifted upwards relative to each other).

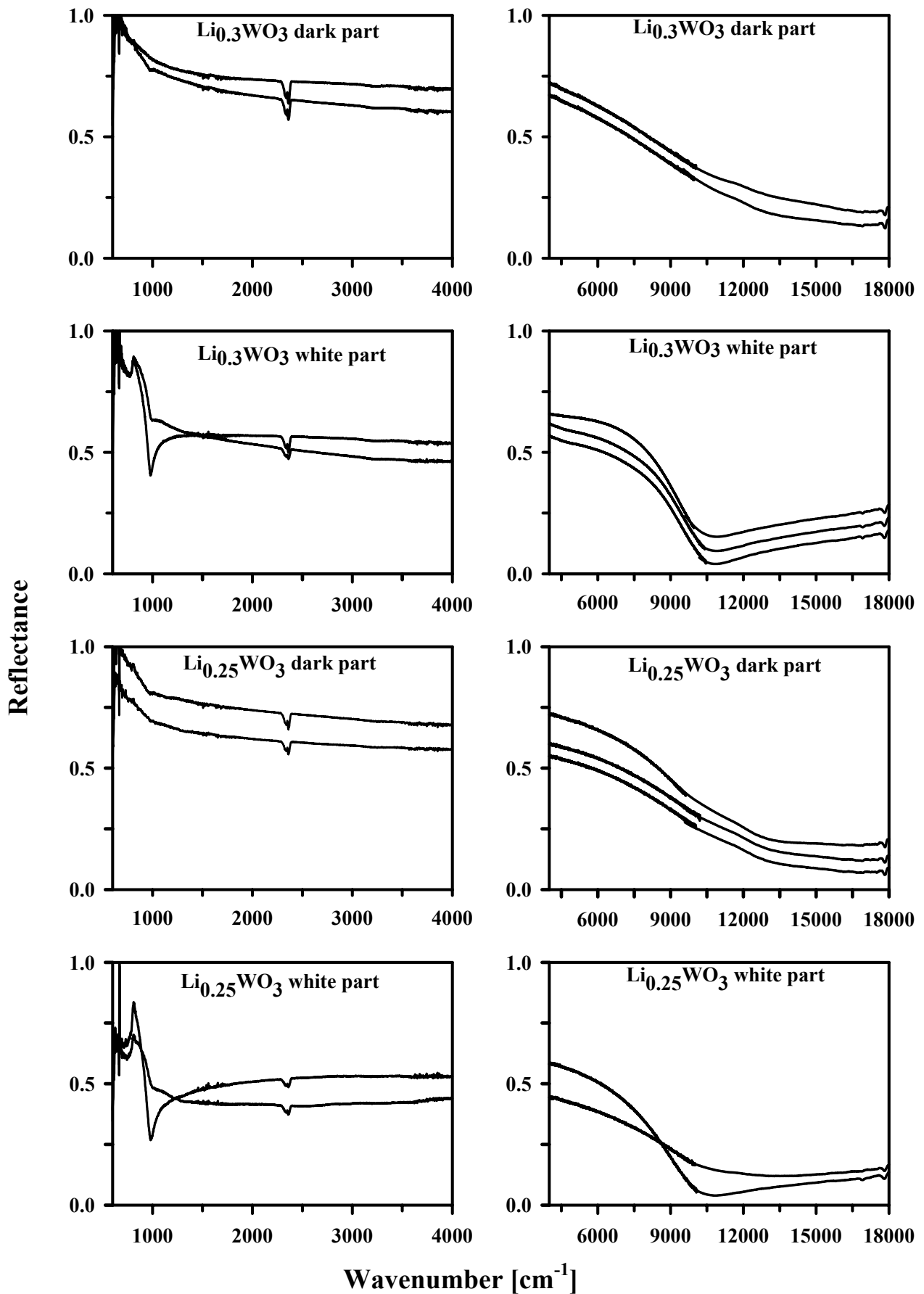


Fig. 14b. Polarized reflectivity spectra of dark and white area of Li_xWO_3 where $x = 0.25$ and 0.3 . For $x = 0.3$ (white part) and $x = 0.25$ (dark part) $R_\theta = 45^\circ$ also shown. (spectra are shifted upwards relative to each other)

The brighter lamellars become more significant in area for crystals from the batches $x = 0.3$ and 0.25 and their optical properties were measured separately as shown in fig. 14b. The dark parts show significant deviations from isotropy down from 14000 cm^{-1} extending into the mid infrared. For the white part a reflectivity minimum typically appear at about 10000 cm^{-1} . The spectra appear to be strongly anisotropic. The appearance of phonon effects indicate the disappearance of the free carrier plasma effect. Moreover, a systematic decrease in the NIR reflection intensity of the $\text{PTB}_{\text{cubic}}$ dark parts with decreasing x in Li_xWO_3 is also observed together with increasing anisotropy. The typical reflectivity spectra of $\text{Li}_{0.1}\text{WO}_3$ crystals show the strong anisotropic reflectivities, observing significant phonon contributions as shown in Fig. 14c. The minimum reflectivity occurs here at about 8000 cm^{-1} and 10000 cm^{-1} etc.

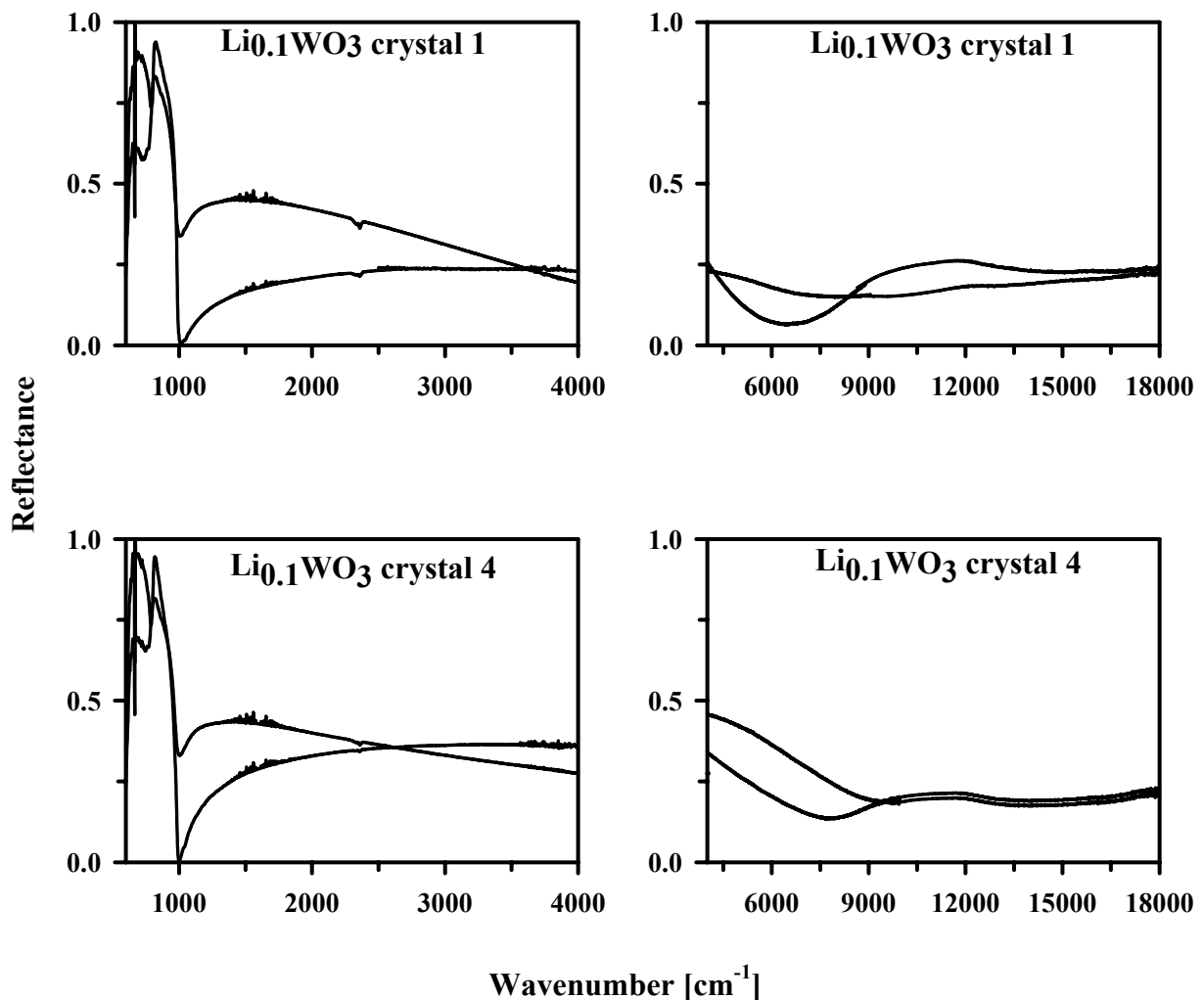


Fig. 14c. Polarized reflectivity spectra of examples of $\text{Li}_{0.1}\text{WO}_3$ crystals considering their main directions of polarisation $R_\theta = 0^\circ, 90^\circ$.

Some HRTEM images of $\text{Li}_{0.45}\text{WO}_3$, $\text{Li}_{0.35}\text{WO}_3$ and $\text{Li}_{0.25}\text{WO}_3$ single crystals are given in Fig. 15a, 15b and 15c respectively. Fig. 15a shows a well ordered crystal fragment of $\text{Li}_{0.45}\text{WO}_3$ single crystal sample with corresponding ED-pattern. Fig. 15b shows a defect in the image of a thin crystallite from $\text{Li}_{0.35}\text{WO}_3$ single crystal sample with corresponding ED pattern. However in Fig. 15c the image of a thin crystallite from $\text{Li}_{0.25}\text{WO}_3$ single crystal shows different atomic arrangements with different diffraction patterns which might indicate the transformation of phases.

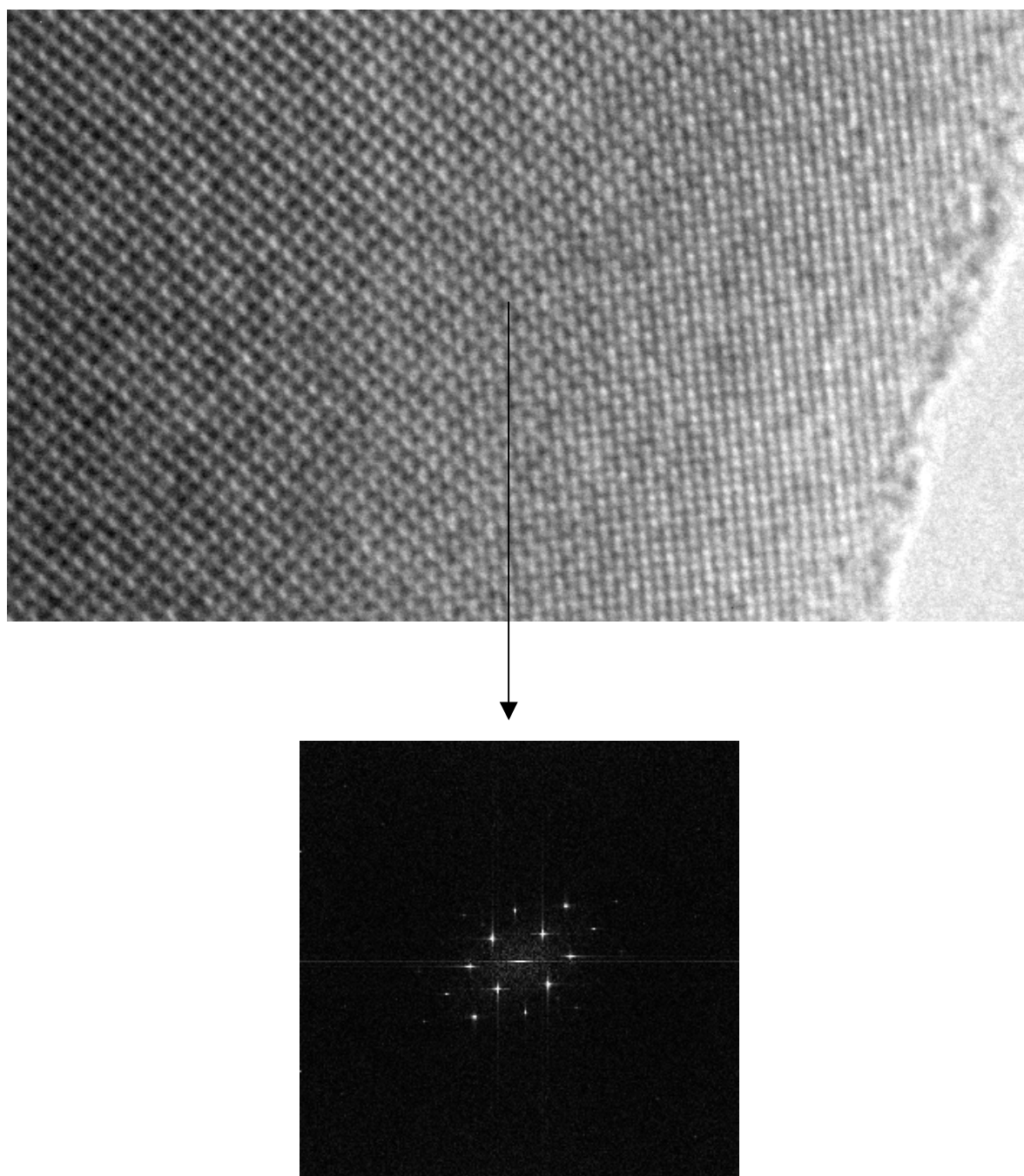


Fig. 15a. HRTEM image of a single crystal of $\text{Li}_{0.45}\text{WO}_3$ fragment with corresponding DP pattern processed with the CRISP program

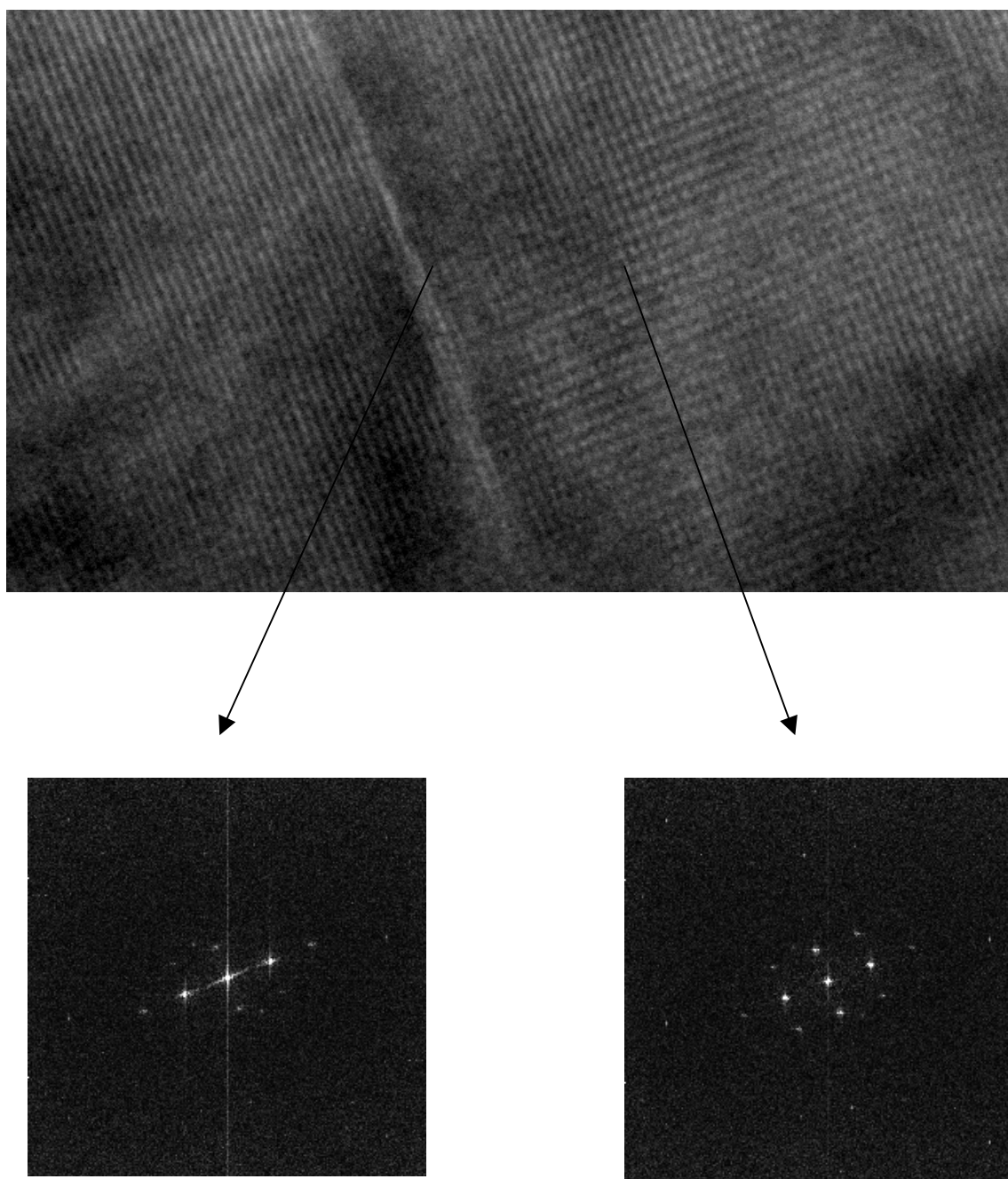


Fig. 15b. HRTEM image of a thin crystallite from $\text{Li}_{0.35}\text{WO}_3$ single crystal with corresponding DP patterns processed with the CRISP program.

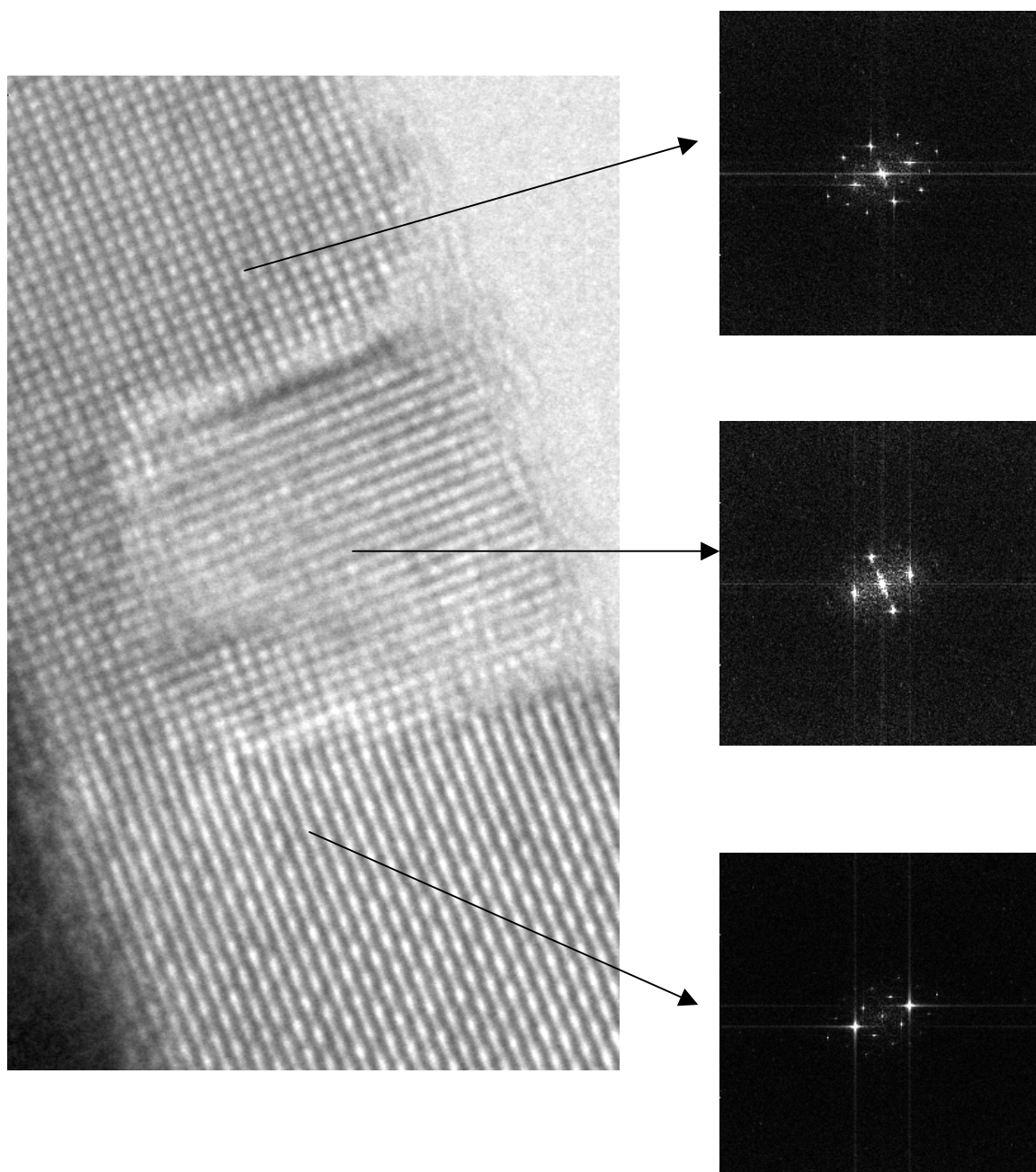


Fig. 15c. HRTEM image of a thin crystallite from $\text{Li}_{0.25}\text{WO}_3$ single crystal with corresponding DP patterns processed with the CRISP program.

3.1.3 Color of Li_xWO_3 and its change at atmospheric condition

The color of the samples of Li_xWO_3 changes systematically with increasing x from gray to blue, deep blue to violet blue as shown in Fig. 16 for series of sample prepared at 600, 700

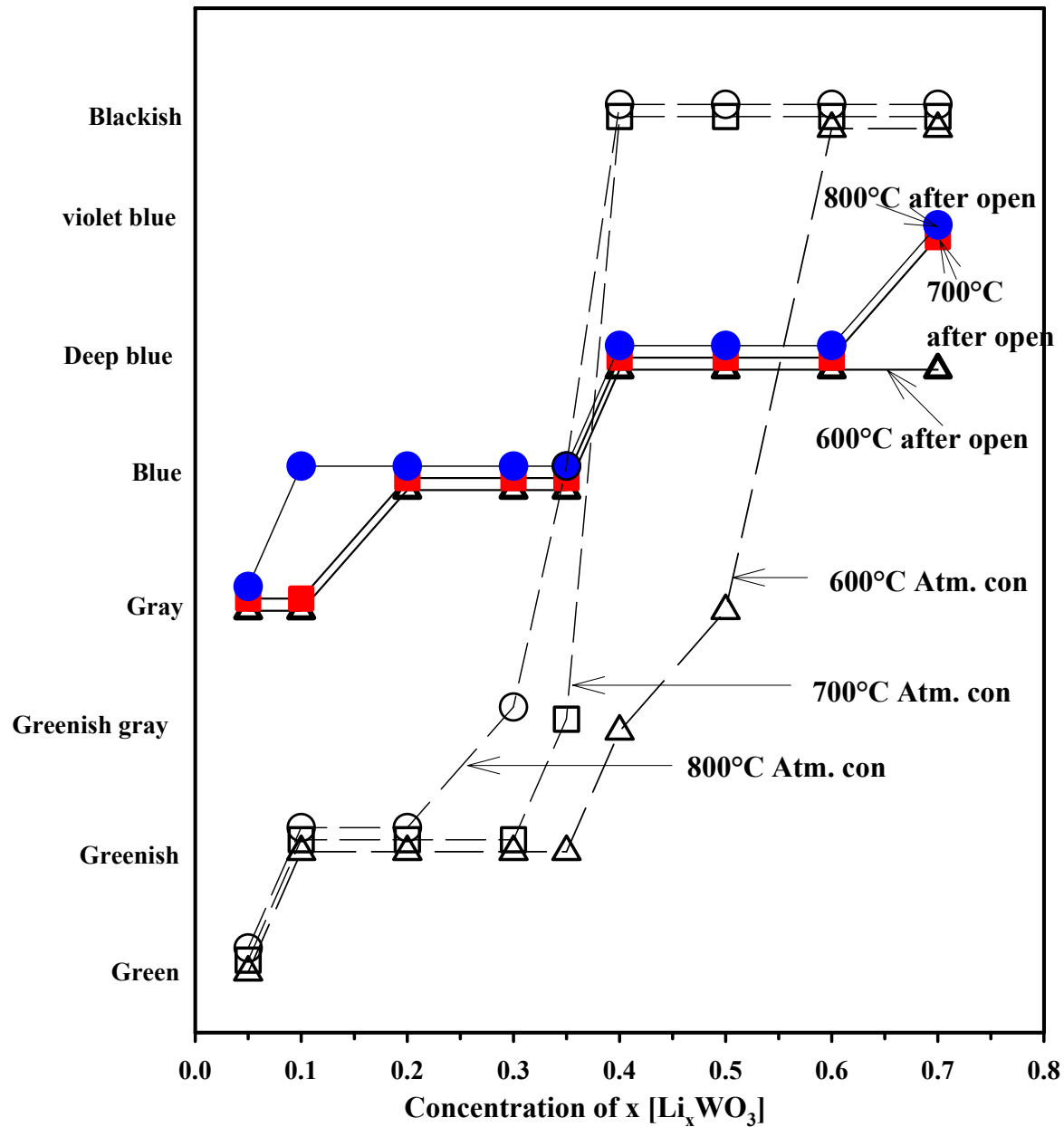


Fig. 16. The color of the sample Li_xWO_3 prepared at 600°C, 700°C and 800°C from old reactant before exposed in atmospheric condition and after 60 days exposed in atmospheric condition.

and 800°C [112]. The color changes significantly for samples exposed at atmospheric condition. After 60 days exposed in atmospheric condition, the samples with $x \geq 0.4$ change to blackish, excluding the samples prepared at 600°C with $x = 0.4$ which become greenish grey and with $x = 0.5$ which becomes grey [Fig.16]. There are also systematic changes in

color for sample with lower x . All samples with $0.2 \leq x \leq 0.35$ appear blue in color as prepared. The sample with $x = 0.1$ prepared at 800°C appeared also blue whereas the samples prepared with same composition at 600°C and 700°C are grey. The samples with $0.1 \leq x \leq 0.3$ prepared at 600°C and 700°C , with $x = 0.35$ prepared at 600°C and $x = 0.1$ and 0.2 at 800°C when exposed at atmospheric conditions become greenish. A change to greenish grey at atmospheric condition is also observed for samples with $x = 0.3$ when they were prepared at 800°C and for sample with $x = 0.35$ when prepared at 700°C . In contrast the sample with $x = 0.35$ prepared at 800°C has changed its colour to blackish. The sample with $x = 0.05$ prepared at 600°C , 700°C and 800°C appear gray in colour as prepared, whereas at atmospheric condition became green.

It can be suggested that the change in color here is related to change in absorption effects. Therefore the diffuse reflectivity of the samples of series 2 has been measured systematically directly after opening the reaction tube, after 30 days and 90 days of exposed at atmospheric

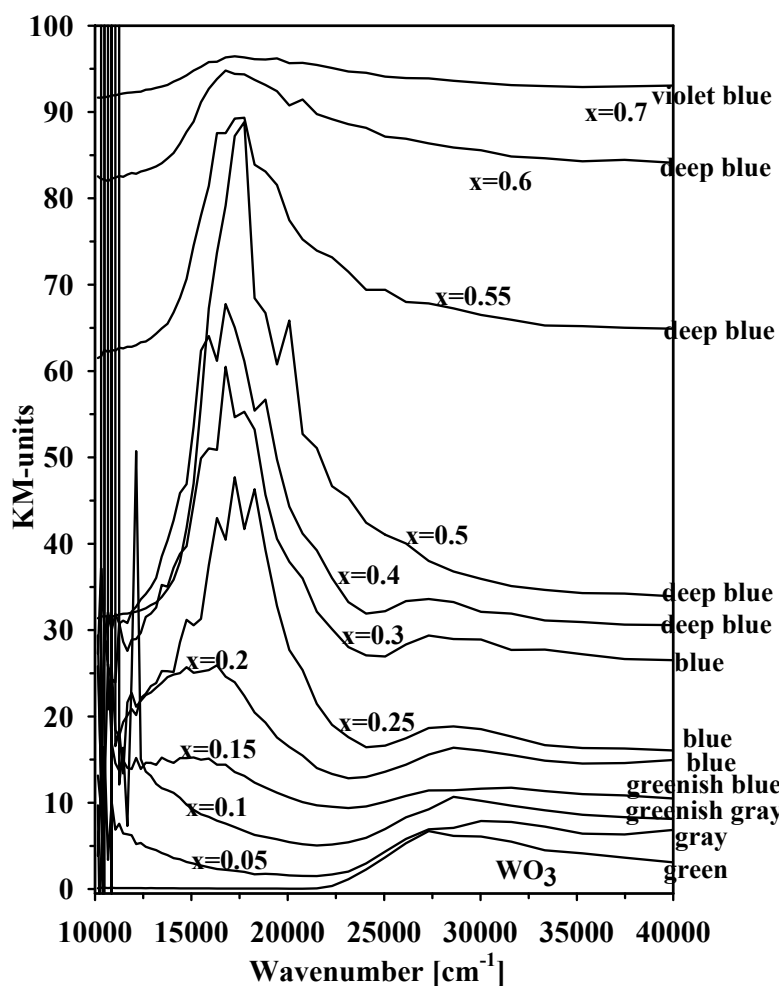


Fig. 17a. UV-VIS spectra of Li_xWO_3 ($x = 0.0 - 0.7$) of series 2 in KM-units as measured immediately after opening the reaction tubes.

conditions. The spectra are given in KM-units in Fig. 17a and 17b. It appears that the greenish color is related to strong increase in absorption above about 22500 cm^{-1} (absorption in the blue) and the slight increase in absorption with decreasing wave number (absorption in the red). The strong increase of absorption in the red around 16000 cm^{-1} changes the color

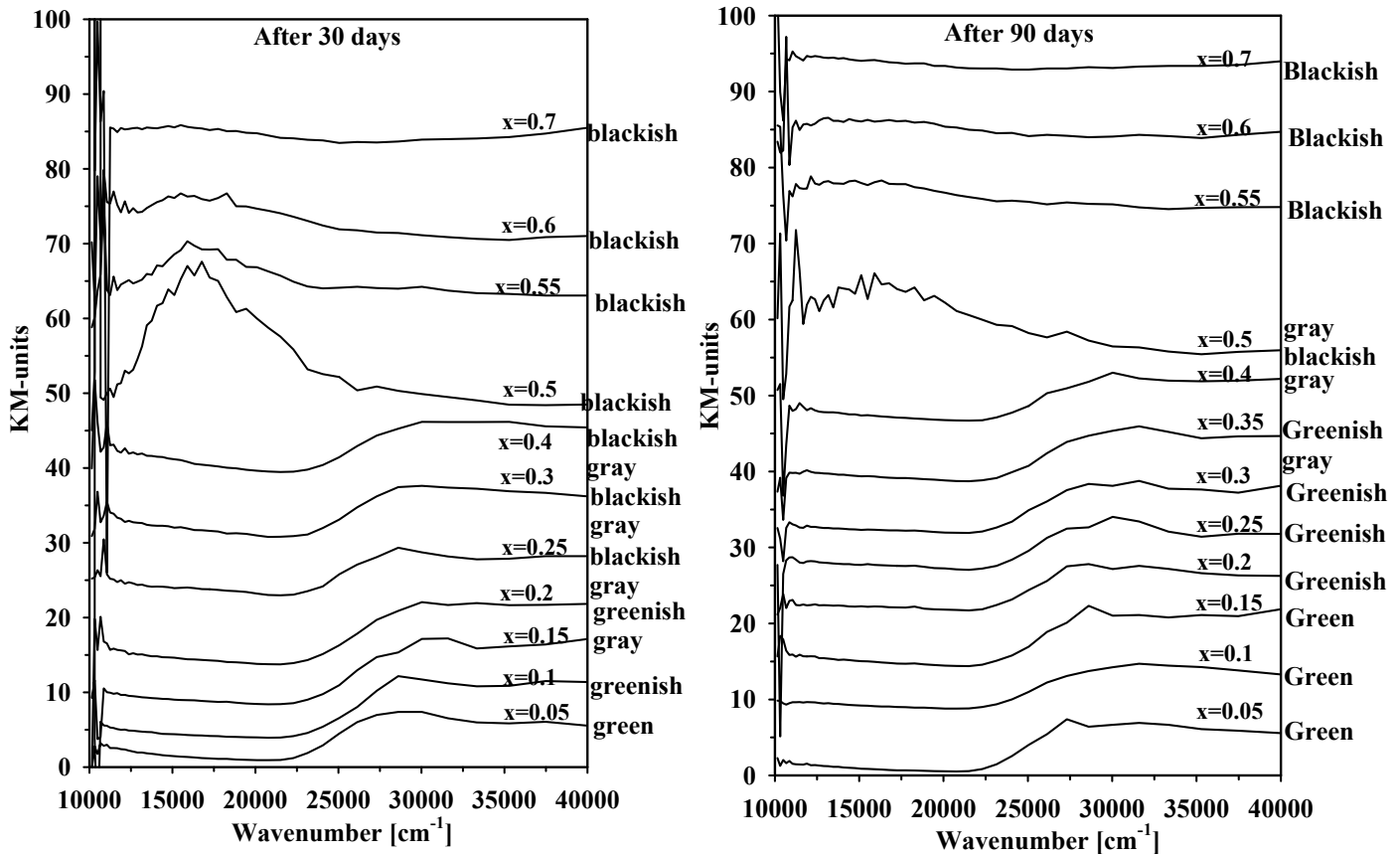


Fig. 17b. UV-VIS spectra of Li_xWO_3 ($x = 0.05 - 0.7$) of series 2 in KM-units as measured after 30 days (left) and after 90 days (right) exposed in atmospheric condition .

towards blue and dark blue [Fig. 17a]. However, there are considerable changes in the spectra of the samples after 30 days and even after 90 days exposed in atmospheric condition [Fig. 17b]. The strong peak completely disappears at about 16000 cm^{-1} for $x \leq 0.4$ samples. All of the spectra of the sample of $x \leq 0.4$ becomes similar to WO_3 like spectra. Only for $x = 0.5$ the sample has still a strong absorption effect which becomes less after 90 days exposure time and somehow shifted to lower wavenumber, similar to the peak that also observed in the sample with $x = 0.2$ after open. For $x > 0.5$, all the spectra after 90 days show a flat like behaviour which is related to strong absorption of blackish color of the sample. The spectra indicate a decrease in effective lithium content in Li_xWO_3 with increasing exposure time in atmospheric condition.

The IR spectra of the samples, Li_xWO_3 of series 2 together with the samples exposed to atmospheric condition for 90 days from the same series are given in Fig. 18. A gradual exsolution of Li from Li_xWO_3 with the appearance of $\text{Li}_{x'}\text{WO}_3$ forms occur indicating $x' < x$.

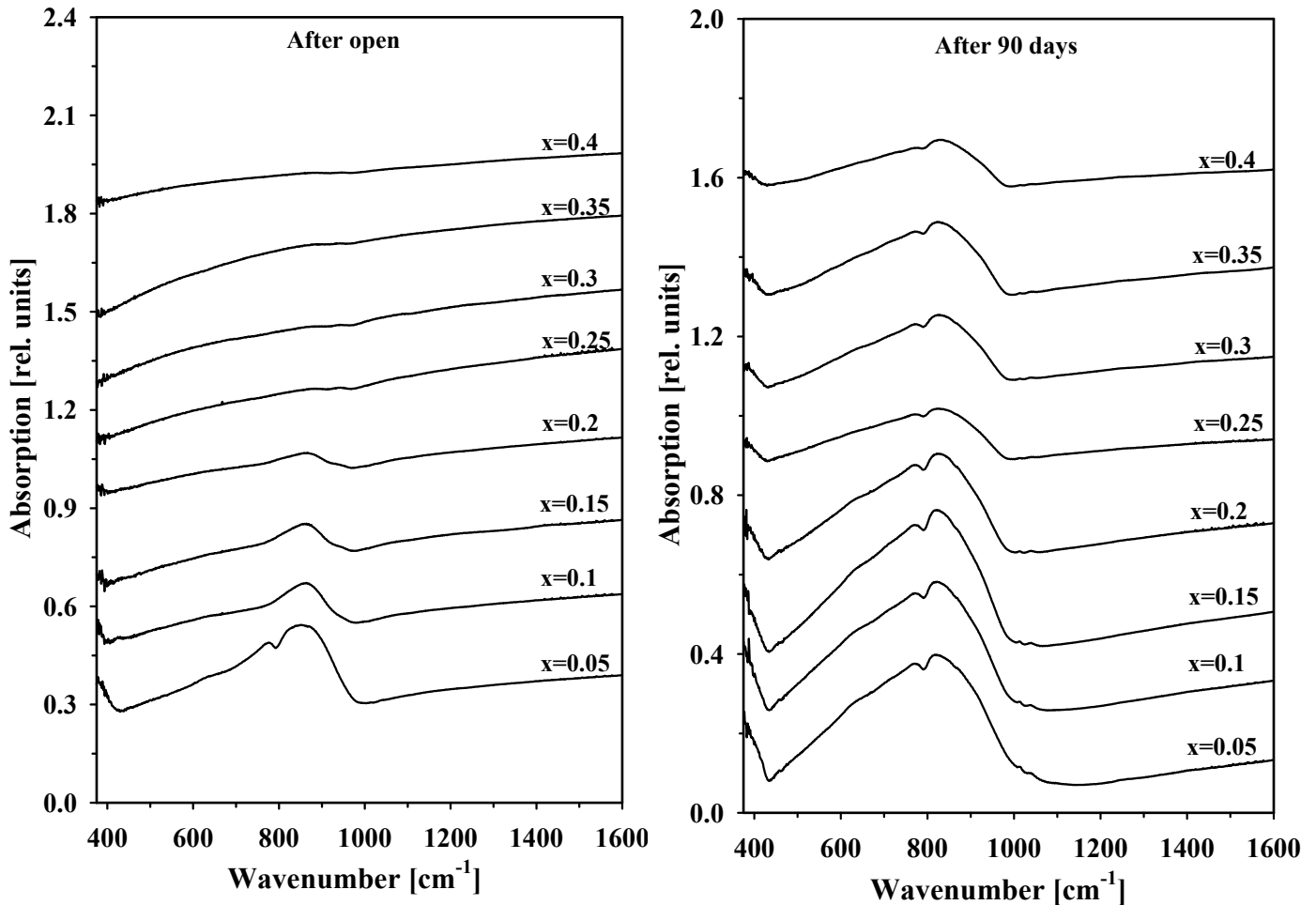


Fig. 18. IR absorption spectra (KBr-method) of some samples of Li_xWO_3 ($x = 0.05 - 0.4$) of series 2 as measured immediately after opening the reaction tubes (left) and after 90 days exposed in atmospheric condition (right).

After 90 days exposed in atmospheric condition the spectra for $x < 0.25$ look like the monoclinic form of WO_3 whereas for $0.25 \leq x \leq 0.5$ the IR spectra show a clear signature of PTB_{tet} which is superimposed to featureless absorption of $\text{PTB}_{\text{cubic}}$. It can be suggested that in all cases, Li_xWO_3 for $x < 0.5$ will become Li-free at the surface thus obtaining the monoclinic phase of WO_3 at room temperature depending on time, i.e the Li exsolution is kinetically controlled here. The question arises where the Li goes. Typical IR spectra in the range 1200 to 4000 cm^{-1} show clearly the presence of CO_3^{2-} , H_2O and OH^- peaks as shown in Fig. 19. And Fig. 20 shows clearly that with increasing the amount of weight of exposed sample, the intensity of the peak of CO_3^{2-} , H_2O and OH^- increases, which proves a contamination of

Li_xWO_3 samples at atmospheric condition. Therefore, as a main sink the formation of Li_2CO_3 and $\text{Li}(\text{OH})$ type phases could be suggested.

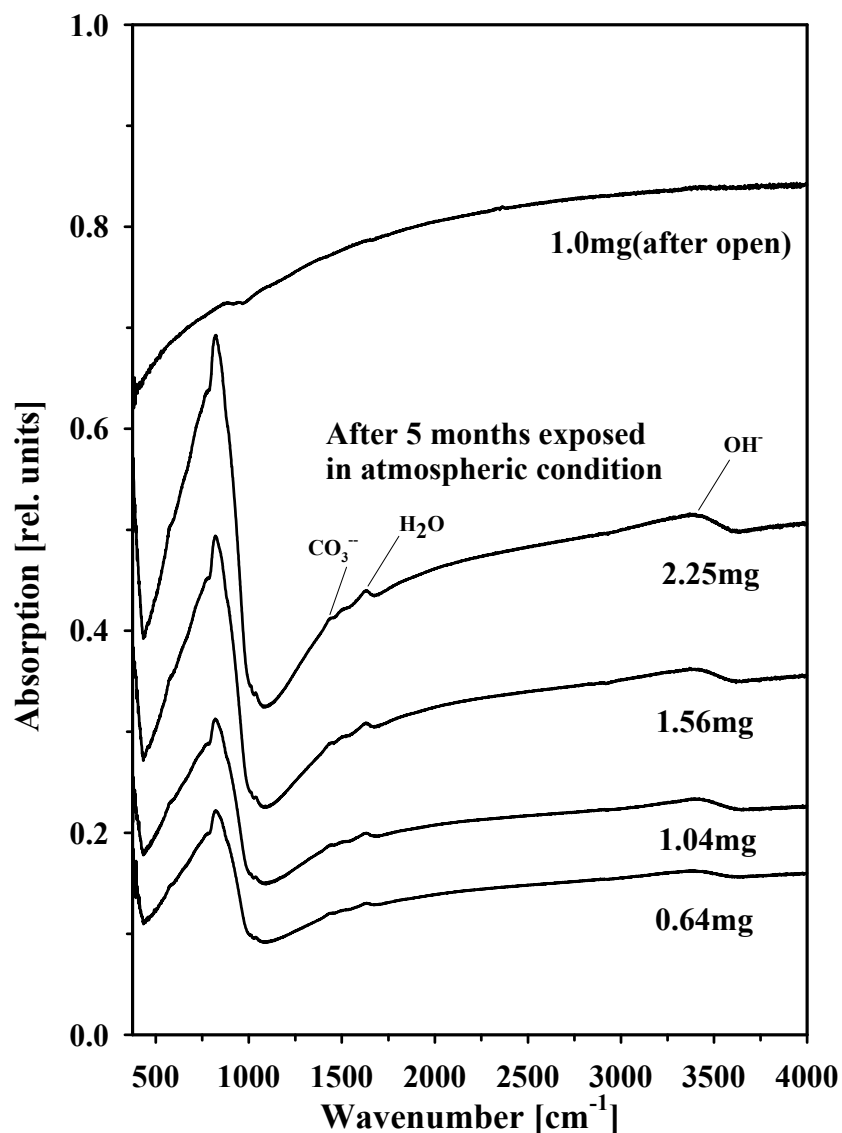


Fig. 19. IR absorption spectra (KBr-method) of $\text{Li}_{0.4}\text{WO}_3$, before exposed in atmospheric condition showing the typical $\text{PTB}_{\text{cubic}}$ spectra. Whereas after 5 month exposed in atmospheric condition the sample shows a spectra like the orthorhombic form of WO_3 and with increasing the weight of exposed sample, the intensity of the peak of OH^- , CO_3^{2-} and H_2O increases.

The X-ray powder diffraction patterns of some samples of Li_xWO_3 , before and after exposed in atmospheric condition, were collected from Guinier and also from Philips diffractometer [Fig. 21]. From these X-ray pattern, it can be seen that the exposed samples with nominal $x < 0.3$ are mainly converted to monoclinic WO_3 . But the exposed samples for $x \geq 0.3$ are partly converted to the tetragonal bronze first. With increasing exposure time these samples are further converted to monoclinic WO_3 . As for example, for $x \geq 0.3$ the sample shows a combined form of $\text{PTB}_{\text{cubic}}$ and PTB_{tet} in atmospheric condition even after 6 months.

However, the intensity of $\text{PTB}_{\text{cubic}}$ phase inside the sample reduces with increasing exposure time in atmospheric condition. In some cases, for the samples with $x \geq 0.5$ the WO_2 and Li_2WO_4 reactants are also observed along with $\text{PTB}_{\text{cubic}}$ and PTB_{tet} as they were present

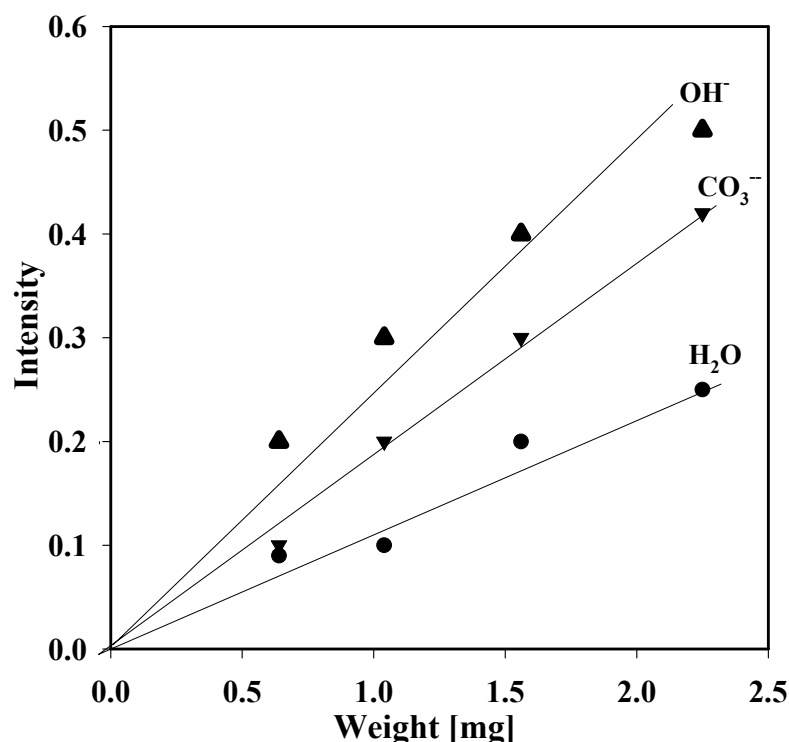


Fig. 20. Showing the peak intensity of H_2O , CO_3^- and OH^- increases with increasing the amount of weight of sample $\text{Li}_{0.4}\text{WO}_3$ after exposed in atmospheric condition.

before exposed in atmospheric condition. The X-ray diffraction patterns of some samples of Li_xWO_3 from series 1 with nominal $x = 0.3$ and 0.4 before and after 60 days exposed in atmospheric condition are given in Fig. 21 as representative spectra for whole series.

It may be noted that the color change phenomena and all this atmospheric effects are mostly reversible when the sample is heated in evacuated tubes above 500°C . It was also observed that a gradual mass loss of about 1 wt% occurs up to 500°C in TG experiments. The IR spectra and X-ray results from the samples after heat treatment, indicate the formation of $\text{Li}_2\text{W}_2\text{O}_7$ with main $\text{PTB}_{\text{cubic}}$ phase which is contrary to our first assumption [117] of a 100% reversible process. In the X-ray pattern (Guinier) even after 3 hour exposure of the film it was not possible to identify the $\text{Li}_2\text{W}_2\text{O}_7$ phase along with main $\text{PTB}_{\text{cubic}}$ phase. However, by the IR method it was easy to detect the identity of $\text{Li}_2\text{W}_2\text{O}_7$ after preparing a pure phase of $\text{Li}_2\text{W}_2\text{O}_7$ [see below, Fig. 22]. As for example the X-ray powder pattern of a reheated sample $\text{Li}_{0.4}\text{WO}_3$ is also given in Fig. 21, showing the $\text{PTB}_{\text{cubic}}$ pattern in presence of very small amount of $\text{Li}_2\text{W}_2\text{O}_7$, which is difficult to identify even after 3 hour X-ray. However, the

disappearance of PTB_{tetr} phase after being reheated the sample can clearly be seen in X-ray pattern. The IR spectra of the reheated sample $\text{Li}_{0.4}\text{WO}_3$ with many phonon lines is similar

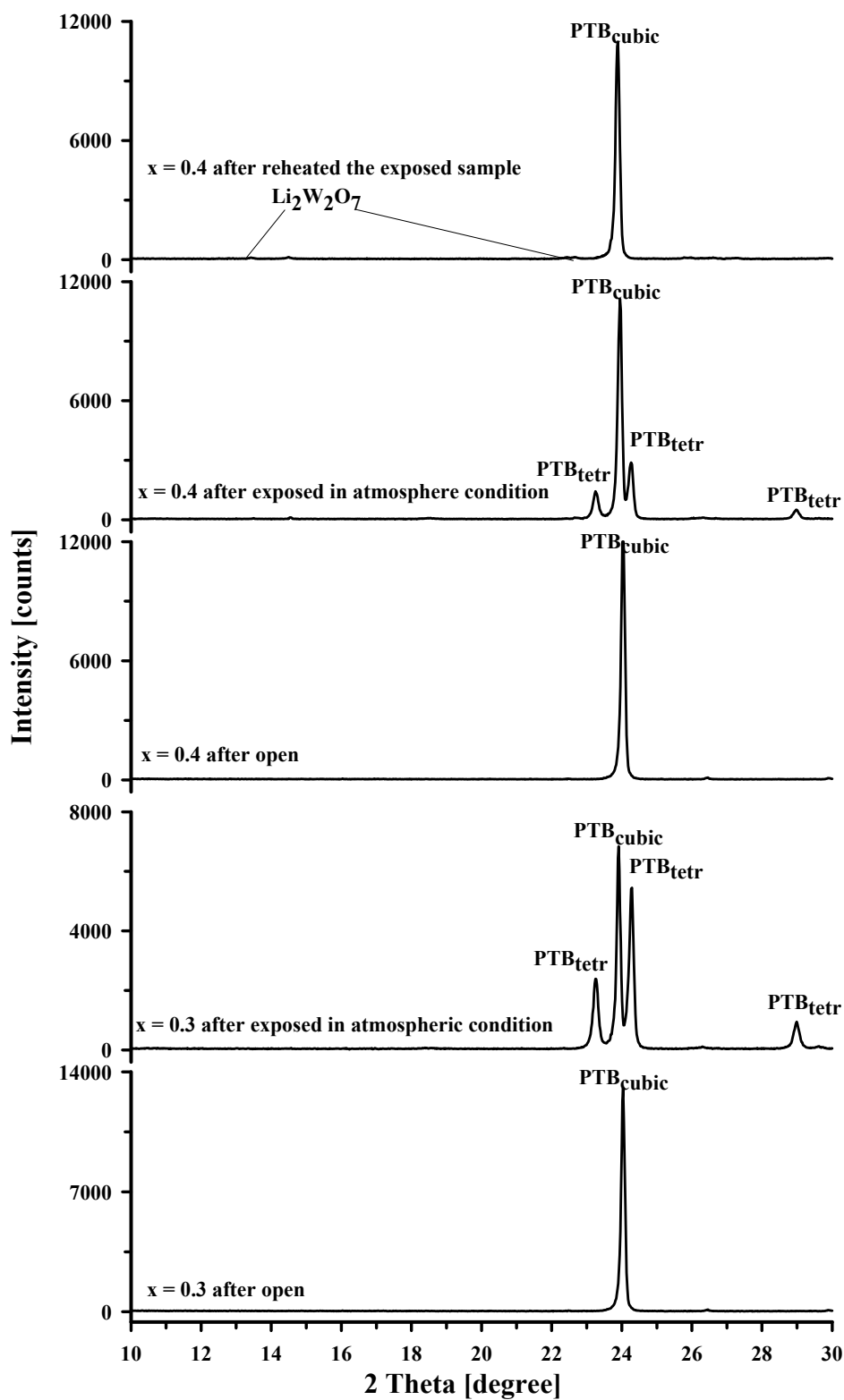


Fig. 21. Typical X-ray powder patterns of Li_xWO_3 of series 1 with $x = 0.3$ and 0.4 , taken immediately after opening the reaction tubes and after 60 days exposed in atmospheric condition. The X-ray powder pattern of $\text{Li}_{0.4}\text{WO}_3$ reheated sample also given as a representative pattern of reheated sample of $\text{PTB}_{\text{cubic}}$.

with the IR spectra of $\text{Li}_{0.35}\text{WO}_3$ after TG. Fig. 22 shows the IR-spectra of pure $\text{Li}_2\text{W}_2\text{O}_7$ with many phonon lines for comparing the IR spectra of $\text{Li}_{0.35}\text{WO}_3$ sample after TG treatment. In Fig. 22 the IR spectra of $\text{Li}_{0.35}\text{WO}_3$ before and after exposed in atmospheric condition are also given. Before and after exposed in atmospheric condition the IR spectra show $\text{PTB}_{\text{cubic}}$ form without any phonon lines and the WO_3 form with a peak maximum at about 820 cm^{-1} respectively. However, the IR-spectra of $\text{Li}_{0.35}\text{WO}_3$ sample after TG treatment shows a clear signature of $\text{Li}_2\text{W}_2\text{O}_7$ phase with many phonon lines which is superimposed to featureless absorption of $\text{PTB}_{\text{cubic}}$. Both exposed sample $\text{Li}_{0.4}\text{WO}_3$ and $\text{Li}_{0.35}\text{WO}_3$ regain their blue colour after being reheated or after TG treatment.

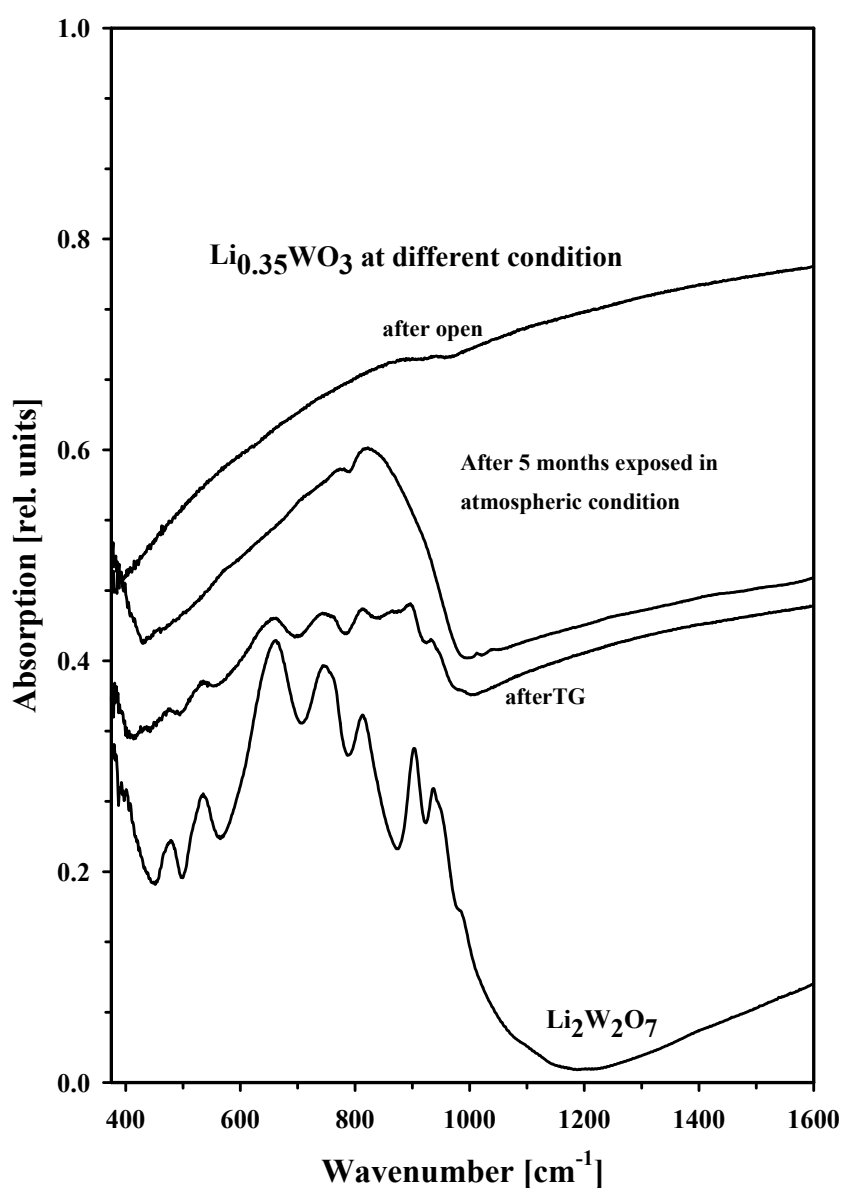


Fig. 22. Typical IR-spectra of sample $\text{Li}_{0.35}\text{WO}_3$ showing the change in atmospheric condition and also how it comes with an extra phase ($\text{Li}_2\text{W}_2\text{O}_7$) after TG or reheated on vacuum. IR absorption spectra of pure nominal $\text{Li}_2\text{W}_2\text{O}_7$ sample also given for comparing the IR spectra of $\text{Li}_{0.35}\text{WO}_3$ after TG treatment.

3.2. Characterisation of $\text{Li}_{0.4}\text{Nb}_y\text{W}_{1-y}\text{O}_3$ system where $y = 0.00 - 0.4$

3.2.1 As prepared samples

The X-ray powder diffraction patterns of $\text{Li}_{0.4}\text{Nb}_y\text{W}_{1-y}\text{O}_3$ system of series 5 samples with $y = 0.04 - 0.4$ are given in Fig. 23. For $y = 0.04$ the X-ray pattern can be identified mainly as $\text{PTB}_{\text{cubic}}$ with the peaks 100 at about 23.8 2-theta, 110 at about 34.0 2-theta positions in presence of two weak lines at about 26.95 and 34.76 2-theta positions. These 2 weak lines is due to the presence of LiNbWO_6 trirutile type structure. Untill $y < 0.1$ only this 2 extra lines of LiNbWO_6 along with $\text{PTB}_{\text{cubic}}$ are observed. The intensity of this extra lines become more significant and the intensity of the lines of $\text{PTB}_{\text{cubic}}$ phase decreases with increasing niobium content. For $0.1 \leq y < 0.4$ samples show the combination of $\text{PTB}_{\text{cubic}}$ phase, LiNbWO_6 type non-bronze oxidised phase and some very weak reflections of $\text{Nb}_2\text{W}_3\text{O}_{14}$ and LiNb_3O_8 phase in the X-ray diffraction patterns. For $y = 0.4$ the X-ray powder pattern shows mainly LiNbWO_6 type phase with some weak lines of $\text{Nb}_2\text{W}_3\text{O}_{14}$ and LiNb_3O_8 phases as impurity. LiNbWO_6 is a derivative of rutile structure except that the cations assume ordered positions resulting in a tripling of the C-axis. The weak reflections which correspond to the $\text{Nb}_2\text{W}_3\text{O}_{14}$ and LiNb_3O_8 phases listed in the JCPDS index are marked in the figure of diffraction patterns.

The results of the X-ray powder analysis of (Guinier method) all niobium doped lithium tungsten bronzes, $\text{Li}_{0.4}\text{Nb}_y\text{W}_{1-y}\text{O}_3$ of series 4 and series 5 are given in table 3. In a previous investigation [112], samples of $\text{Li}_{0.4}\text{Nb}_y\text{W}_{1-y}\text{O}_3$ were prepared at 600°C for 7 days by the same method using the same reactants as described for series 4. The X-ray results and the cell parameters obtained from previous investigation [112] are given in table 3. It can be seen from table 3 that the phase observed for series 4 are in good agreement with the results obtained previously at 600°C. However, in previous investigations, since the X-ray exposure time was only 30 minute for all samples prepared at 600°C, the extra phase had not been seen untill $y \leq 0.15$. The lattice parameters [table 3] show that with increasing Nb content the a $\text{PTB}_{\text{cubic}}$ cell parameter increases. In the present investigation in series 4 and 5 pure $\text{PTB}_{\text{cubic}}$ phase is only possible for $y = 0.0$ i.e for pure $\text{Li}_{0.4}\text{WO}_3$ bronze. In presence of very low amount of niobium as for example $y = 0.04$, a trace amount of LiNbWO_6 type extra phase is formed along with $\text{PTB}_{\text{cubic}}$ phase. However, for $y < 0.15$ the extra phase of LiNbWO_6 is observed after long time X-ray exposure (3h). For sample with $y > 0.15$, the extra phase is detected already in 30 min X-ray exposure time.

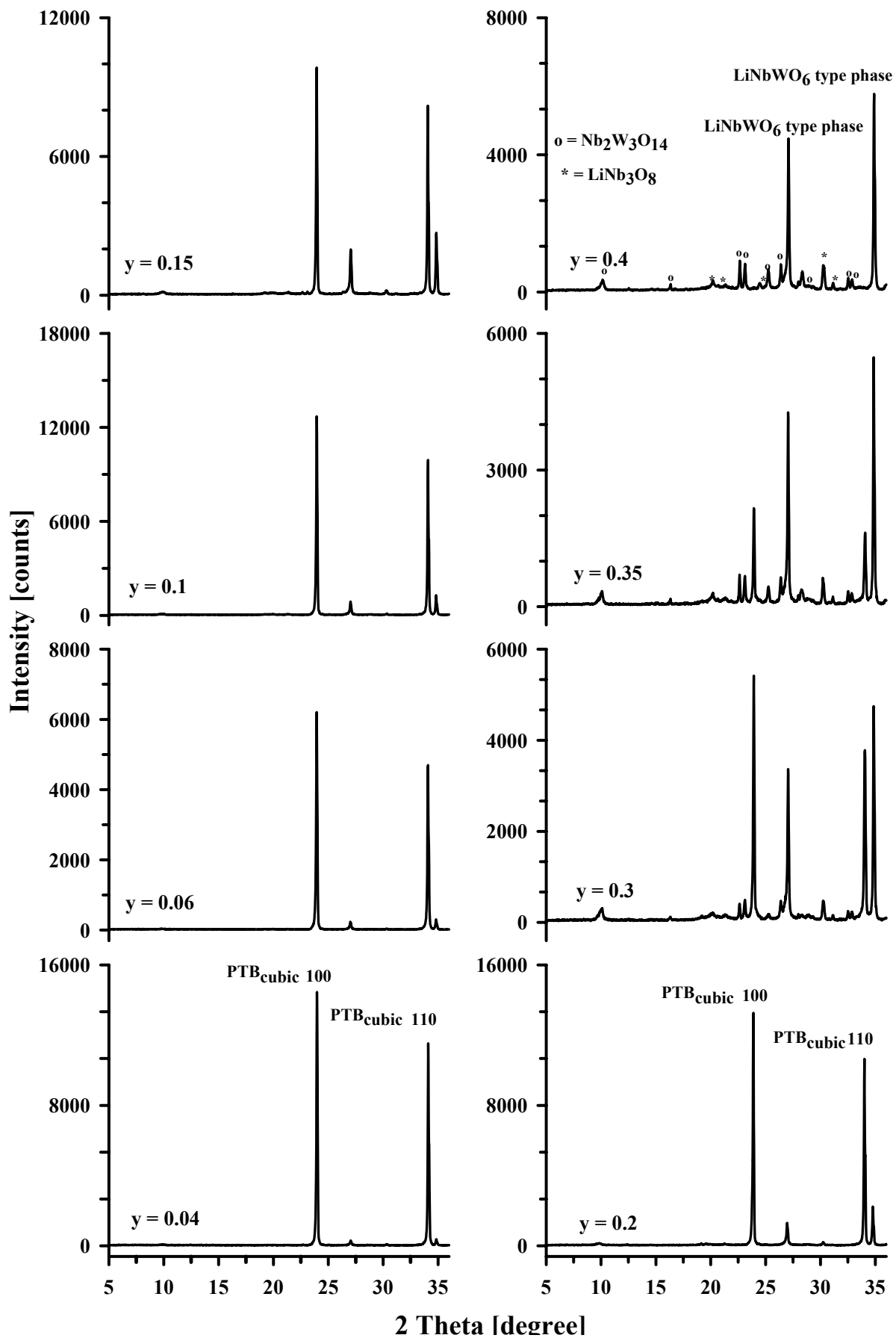


Fig. 23. X-ray powder patterns of $Li_{0.4}Nb_yW_{1-y}O_3$ system taken immediately after opening the reaction tubes with $y = 0.04 - 0.4$ as denoted.

Table 3: Results of the X-ray powder analysis of different samples of $\text{Li}_{0.4}\text{Nb}_y\text{W}_{1-y}\text{O}_3$ ($y = 0.04 - 0.4$) system of series 4, series 5 and some previous results [112] of the same system prepared at 600°C for 7 days.

Nominal composition	$\text{Li}_{0.4}\text{Nb}_y\text{W}_{1-y}\text{O}_3$ prepared at 700°C for 7 days (Series 4)	$\text{Li}_{0.4}\text{Nb}_y\text{W}_{1-y}\text{O}_3$ prepared at 700°C for 7 days (Series 5)		$\text{Li}_{0.4}\text{Nb}_y\text{W}_{1-y}\text{O}_3$ prepared at 600°C for 7 days	
	Phase observed (3h X-ray)	Phase observed (3h X-ray)	Cell parameters (Guinier method) (Å)	Phase observed (40min X-ray)	Cell parameters (Guinier Hägg-method) (Å)
$\text{Li}_{0.4}\text{WO}_3$	PTB_C	PTB_C	a = 3.7237(02)	PTB_C	a = 3.7232
$\text{Li}_{0.4}\text{Nb}_{0.02}\text{W}_{0.98}\text{O}_3$	-	-	-	PTB_C	a = 3.7231
$\text{Li}_{0.4}\text{Nb}_{0.04}\text{W}_{0.96}\text{O}_3$	PTB_C + traces of ●	PTB_C + traces of ●	a = 3.7247(08)	PTB_C	a = 3.7245
$\text{Li}_{0.4}\text{Nb}_{0.06}\text{W}_{0.94}\text{O}_3$	PTB_C + traces of ●	PTB_C + traces of ●	a = 3.7238(15)	PTB_C	a = 3.7240
$\text{Li}_{0.4}\text{Nb}_{0.08}\text{W}_{0.92}\text{O}_3$	-	-	-	PTB_C	a = 3.7239
$\text{Li}_{0.4}\text{Nb}_{0.1}\text{W}_{0.9}\text{O}_3$	PTB_C + traces of ●	PTB_C + traces of ●	a = 3.7257(19)	PTB_C	a = 3.7239
$\text{Li}_{0.4}\text{Nb}_{0.15}\text{W}_{0.85}\text{O}_3$	PTB_C + traces of ●	PTB_C + traces of ●	a = 3.7307(16)	PTB_C	a = 3.7242
$\text{Li}_{0.4}\text{Nb}_{0.2}\text{W}_{0.8}\text{O}_3$	PTB_C + traces of ●	PTB_C + traces of ●	a = 3.7316(15)	PTB_C +▲	a = 3.7252
$\text{Li}_{0.4}\text{Nb}_{0.3}\text{W}_{0.7}\text{O}_3$	PTB_C ●+■+□	PTB_C ●+■+□	a = 3.7315(23)	PTB_C +▲	a = 3.7332
$\text{Li}_{0.4}\text{Nb}_{0.35}\text{W}_{0.65}\text{O}_3$	PTB_C ●+■+□	PTB_C ●+■+□	a = 3.7316(20)	PTB_C +▲	a = 3.7357
$\text{Li}_{0.4}\text{Nb}_{0.4}\text{W}_{0.6}\text{O}_3$	-	LiNbWO_6 type(trirutile structure) +■+□	a = 4.6804(70) c = 9.2756(155)	-	-

● = LiNbWO_6

■ = $\text{Nb}_2\text{W}_3\text{O}_{14}$

□ = LiNb_3O_8 and ▲ = unknown phase.

Samples for nominal $y = 0.15$ and 0.2 were examined in the JEOL-820 SEM microscope. The EDX analysis on about 20 crystals also indicates the two phase coexistence. One phase is with the crystals of about $y = 0.03 - 0.08$ which belongs to PTB_{cubic} . The other phase is formed with the crystals containing about $y = 0.39$ which may belong to non-bronze oxidised phase or

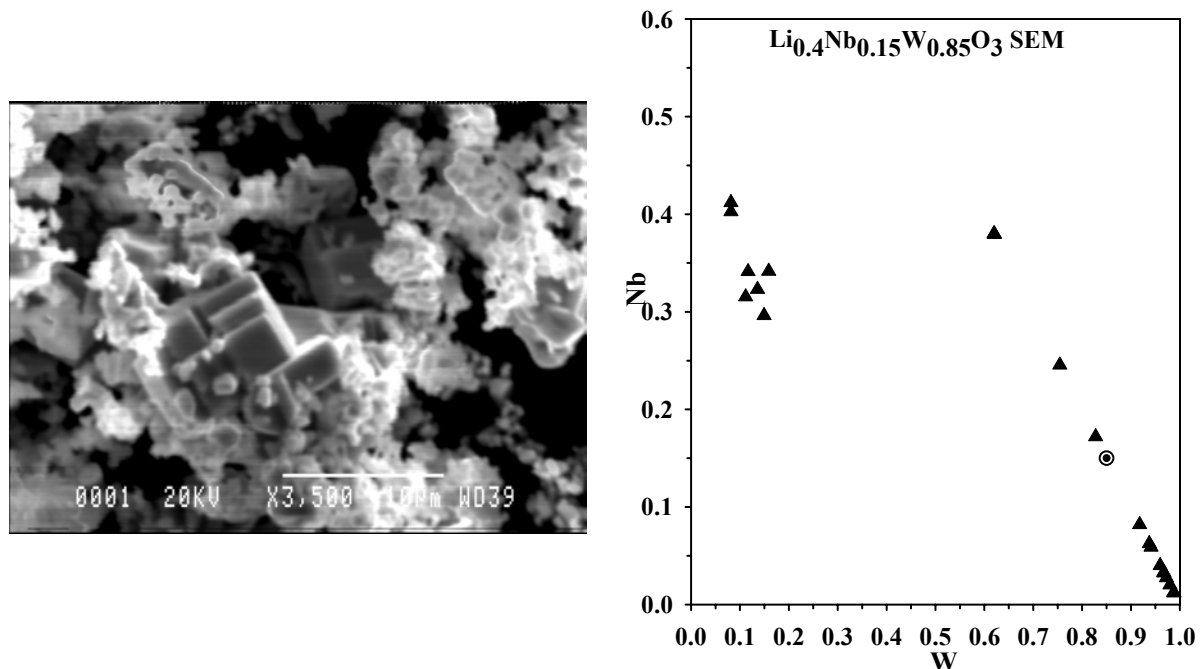


Fig. 24a. Li_{0.4}Nb_{0.15}W_{0.85}O₃

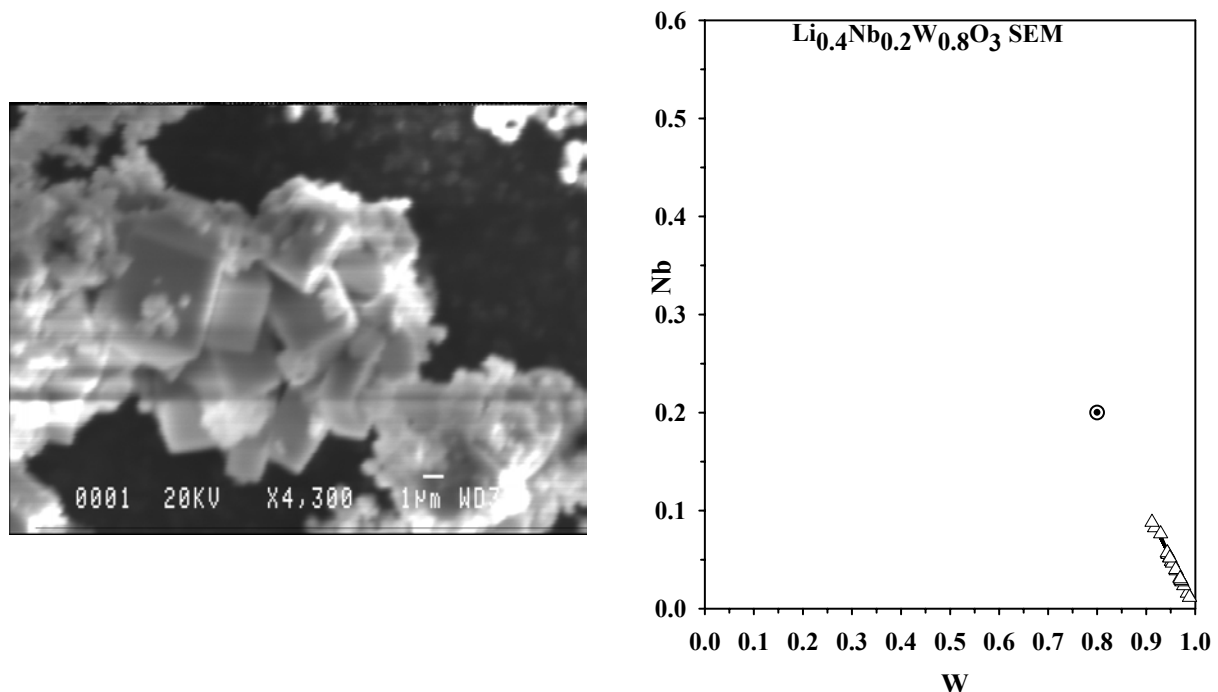


Fig. 24b. Li_{0.4}Nb_{0.2}W_{0.8}O₃

Fig. 24a and 24b. SEM-image of nominal $\text{Li}_{0.4}\text{Nb}_{0.15}\text{W}_{0.85}\text{O}_3$ and $\text{Li}_{0.4}\text{Nb}_{0.2}\text{W}_{0.8}\text{O}_3$ showing some cubic crystals together with polycrystalline powder. SEM/EDX analysis results of these samples are also given where the values of W and Nb are calculated as $W = W / (Nb+W)$ and $Nb = Nb / (Nb+W)$.

other impurity phases of LiNb_3O_8 or $\text{Nb}_2\text{W}_3\text{O}_{14}$. Fig. 24 shows the SEM image and the distribution of the SEM/EDX analysis made on crystals taken from nominal $\text{Li}_{0.4}\text{Nb}_{0.15}\text{W}_{0.85}\text{O}_3$ and $\text{Li}_{0.4}\text{Nb}_{0.2}\text{W}_{0.8}\text{O}_3$ samples. In most cases the impure phase was not easy to detect for the analysis because of the percentage of impure phase is very small in amount comparing to the main $\text{PTB}_{\text{cubic}}$ phase [for example Fig. 24b]. From this analysis it can be suggested that about 5-8 atom % niobium can be doped in the system $\text{Li}_{0.4}\text{Nb}_y\text{W}_{1-y}\text{O}_3$.

The IR absorption spectra between 375 cm^{-1} and 1600 cm^{-1} as obtained for $\text{Li}_{0.4}\text{Nb}_y\text{W}_{1-y}\text{O}_3$

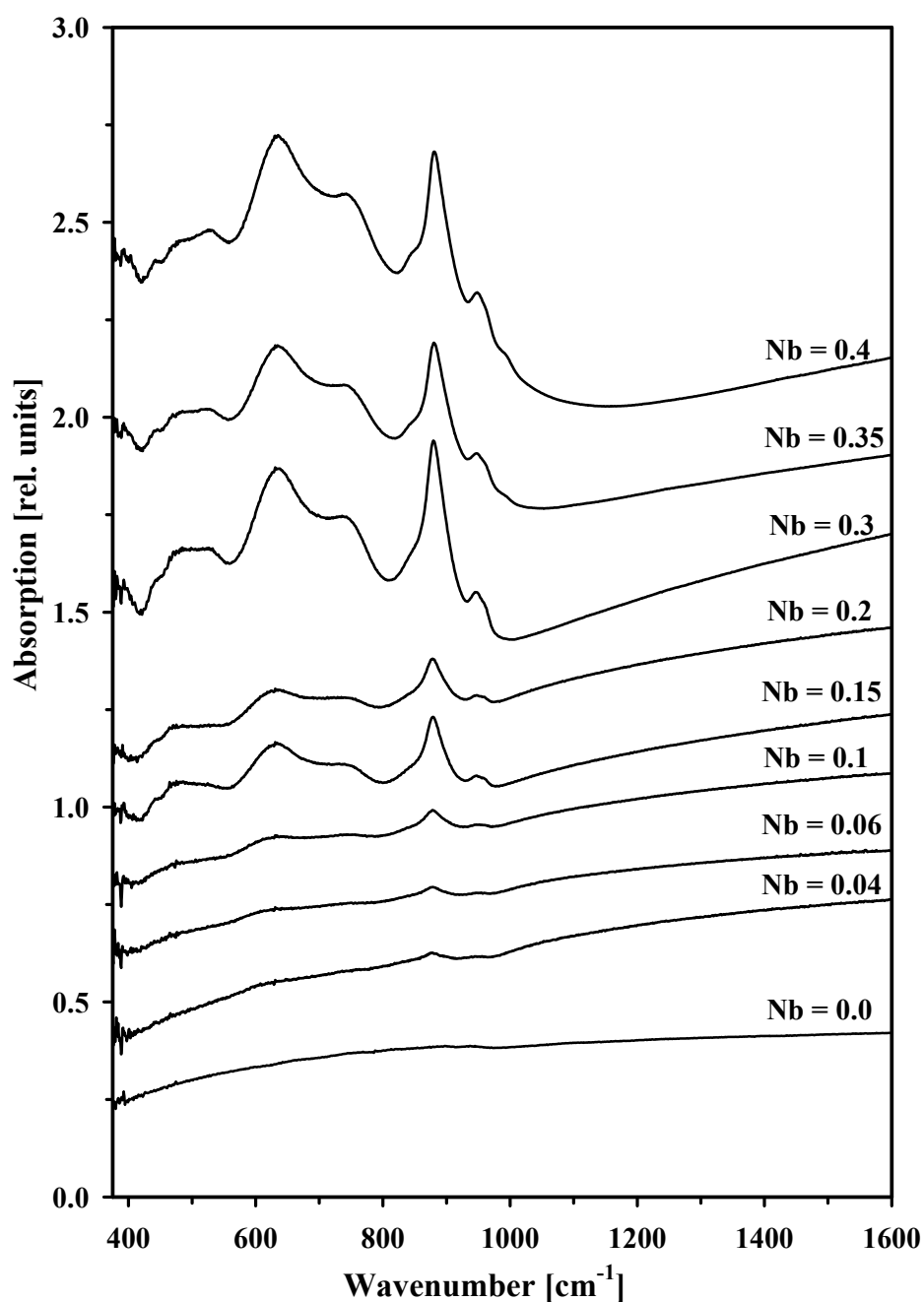


Fig. 25. IR absorption spectra (KBr-method) of $\text{Li}_{0.4}\text{Nb}_y\text{W}_{1-y}\text{O}_3$ ($y = 0.0 - 0.4$) as measured immediately after opening the reaction tubes.

system of series 5 samples are shown in Fig. 25. For the $y = 0.4$ sample the IR spectra show several peak at about 950 cm^{-1} , 875 cm^{-1} , 750 cm^{-1} , 628 cm^{-1} and 2-3 weak peaks below 600 cm^{-1} . These absorption characteristics are assigned to the LiNbWO_6 type phase. For $y = 0.0$ i.e for the pure $\text{Li}_{0.4}\text{WO}_3$ bronze, the typical $\text{PTB}_{\text{cubic}}$ spectra without any phonon signature are observed. For $y \leq 0.06$ a peak signature at 875 cm^{-1} is noted which is the most intense peak of the LiNbWO_6 type phase. The increase in intensity of the peak at 875 cm^{-1} with increasing niobium content is related to the increasing contribution of the LiNbWO_6 type phase.

The reflectivity of the powder samples of series 5 in the range 10000 cm^{-1} to 18000 cm^{-1} are given in Fig. 26. For $y = 0.0$ the spectra show a minimum at about 14000 cm^{-1} .

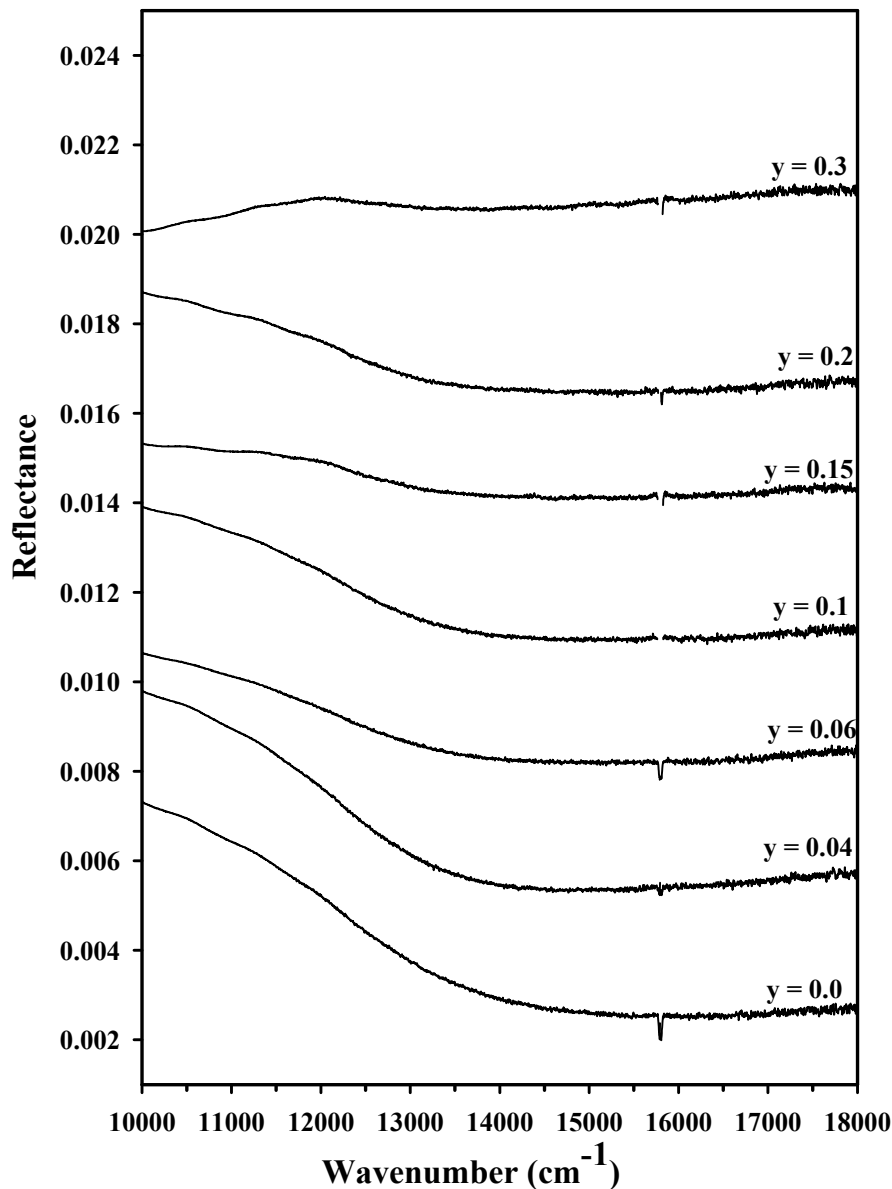


Fig. 26. Reflection spectra of powder samples of $\text{Li}_{0.4}\text{Nb}_y\text{W}_{1-y}\text{O}_3$ (series 5) system where $y = 0.0 - 0.3$ as denoted. All the spectra measured immediately after opening the reaction tubes.

When $0.0 < y < 0.1$, sample shows a small shift of minimum reflectivity to the lower wavenumber, which indicates a small amount of niobium doping in the system $\text{Li}_{0.4}\text{Nb}_y\text{W}_{1-y}\text{O}_3$. However, for $y > 0.1$ the minimum reflectivity feature nearly disappear due to the dilution by the LiNbWO_6 type phase.

3.2.2 Atmospheric effect on samples of $\text{Li}_{0.4}\text{Nb}_y\text{W}_{1-y}\text{O}_3$ system

The diffuse reflectivity of the samples of series 4 were measured systematically directly after opening the reaction tubes and after 90 days of exposed in atmospheric condition [Fig. 27].

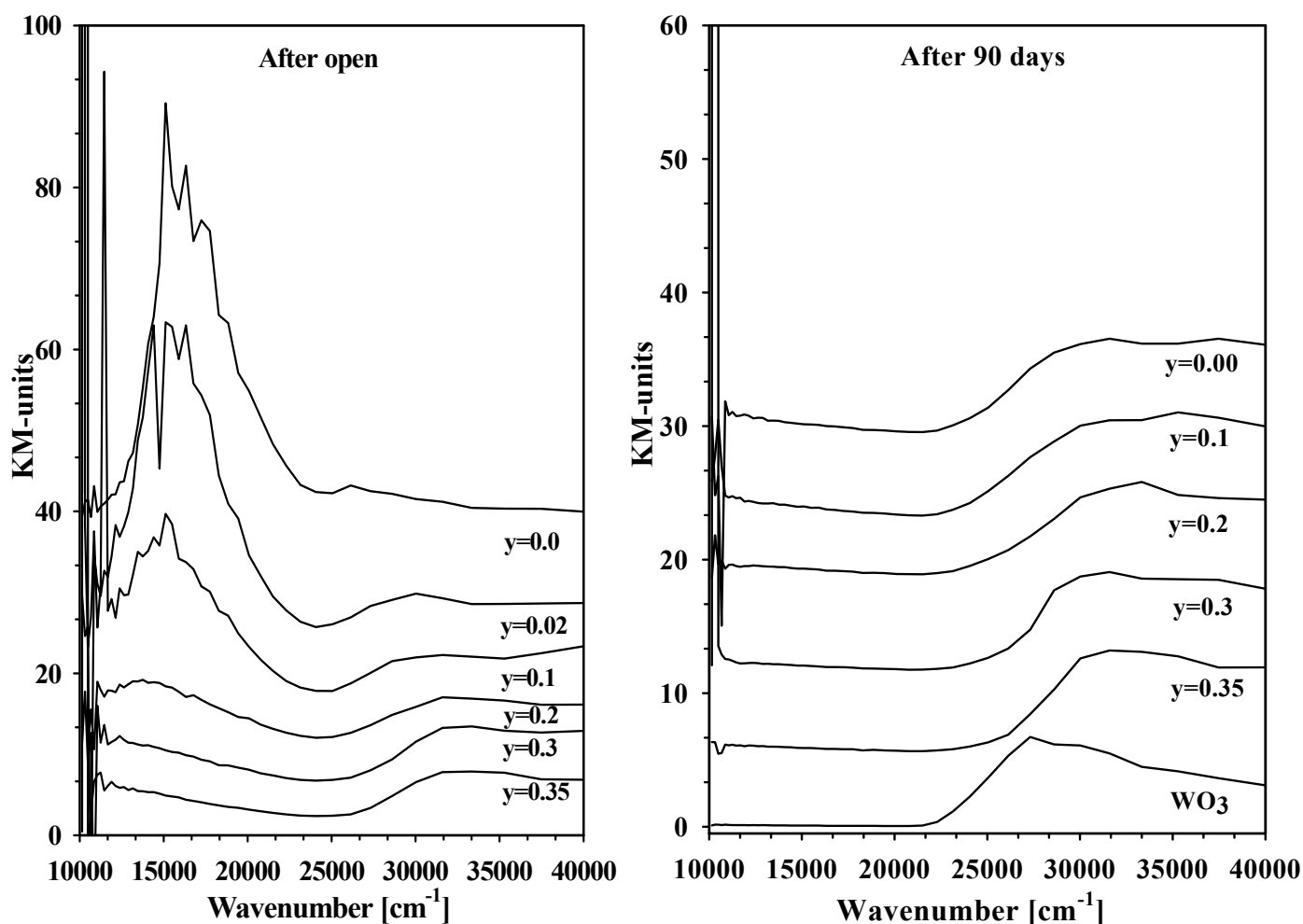


Fig. 27. UV-VIS spectra of $\text{Li}_{0.4}\text{Nb}_y\text{W}_{1-y}\text{O}_3$ ($y = 0.0 - 0.35$) system of series 4 as measured immediately after opening the reaction tubes (left) and after 90 days exposed in atmospheric condition (right).

The important observation in the UV-VIS spectra of series 4 before exposed at atmospheric condition is the strong decrease in intensity with increasing y of the broad peak between 15000 cm^{-1} and 18000 cm^{-1} . The peak shows highest intensity for the pure $\text{Li}_{0.4}\text{WO}_3$ and becomes shifted somewhat to lower wavenumber for $y = 0.02$ and 0.1 . The decreasing

intensity with increasing niobium content shows the less contribution of PTB_{cubic} phase. The minimum in the absorption observed for $y = 0.02$ at about 23000 cm^{-1} becomes shifted to about 26000 cm^{-1} for $y = 0.35$. This effect can be explained by the increasing contribution of the LiNbWO₆ type phase.

The spectra of series 4 samples after exposed 90 days at atmospheric conditions indicate a gradual loss of just that spectral feature which is related with decreasing the Li-content in the PTB_{cubic} phase. The change in the spectral feature before and after exposed in atmospheric condition is not so significant for $y > 0.15$ samples. This can be related to the high amount LiNbWO₆ type phase compared to Li_{0.4}WO₃. The effect that at atmospheric conditions the Li_{0.4}WO₃ phase contribution is affected, i.e as gradually transferred to WO₃ type contribution is also observed in IR-spectra and X-ray pattern (not shown).

3.3 Characterisation of Li_{0.1}Nb_yW_{1-y}O₃ system where $y = 0.00 - 0.1$

X-ray powder diffraction patterns of series 6 with $y = 0.00 - 0.1$ are given in Fig. 28. For $y = 0.02$ the X-ray patterns show mainly a PTB_{tetr} phase with the peaks 001 (2-theta 23.24), 110 (2theta 24.31), 101 (2-theta 28.97), 111 (2-theta 33.81) and 200 (2theta 34.58) in presence of traces amount of Nb₂O₅ at 2-theta 22.64, 24.89 and 28.3 positions. For $y = 0.04$ the X-ray pattern shows mainly the PTB_{tetr} phase and a small amount of Nb₂O₅ with the peaks as observed for $y = 0.02$ sample. However, $y = 0.04$ sample also indicates the presence of PTB_{orth} phase with the extra peaks at about 23.7, 26.69, 33.35 and 34.23 2-theta and a trace amount of LiNb₃O₈ at 30.21 2-theta position. Up to $y = 0.08$ all these peaks of PTB_{tetr} are present strongly and the intensity of the impure phase of PTB_{orth}, Nb₂O₅ and LiNb₃O₈ increases with increasing Nb content. For $y = 0.1$ all these peaks for PTB_{tetr} could identified but in low intensity along with Nb₂O₅ impurity and PTB_{orth} main phase. For $y = 0.1$ sample the impure phase Nb₂O₅ was identified at about 22.64, 24.89, 26.35 and 28.30 2-theta positions and also a small amount of LiNb₃O₈ type phase was present as impurity at about 2-theta 29.39, 30.21, 30.70, 31.06 etc.

The results obtained from series 6 by using Guinier method are collected in table 4. In a previous investigation [112] samples of Li_{0.1}Nb_yW_{1-y}O₃ with $y = 0.00 - 0.08$ were prepared at 600°C for 7 days by the same way and from the same reactants as described for series 4. The X-ray results which are observed and the cell parameters obtained from previous investigation

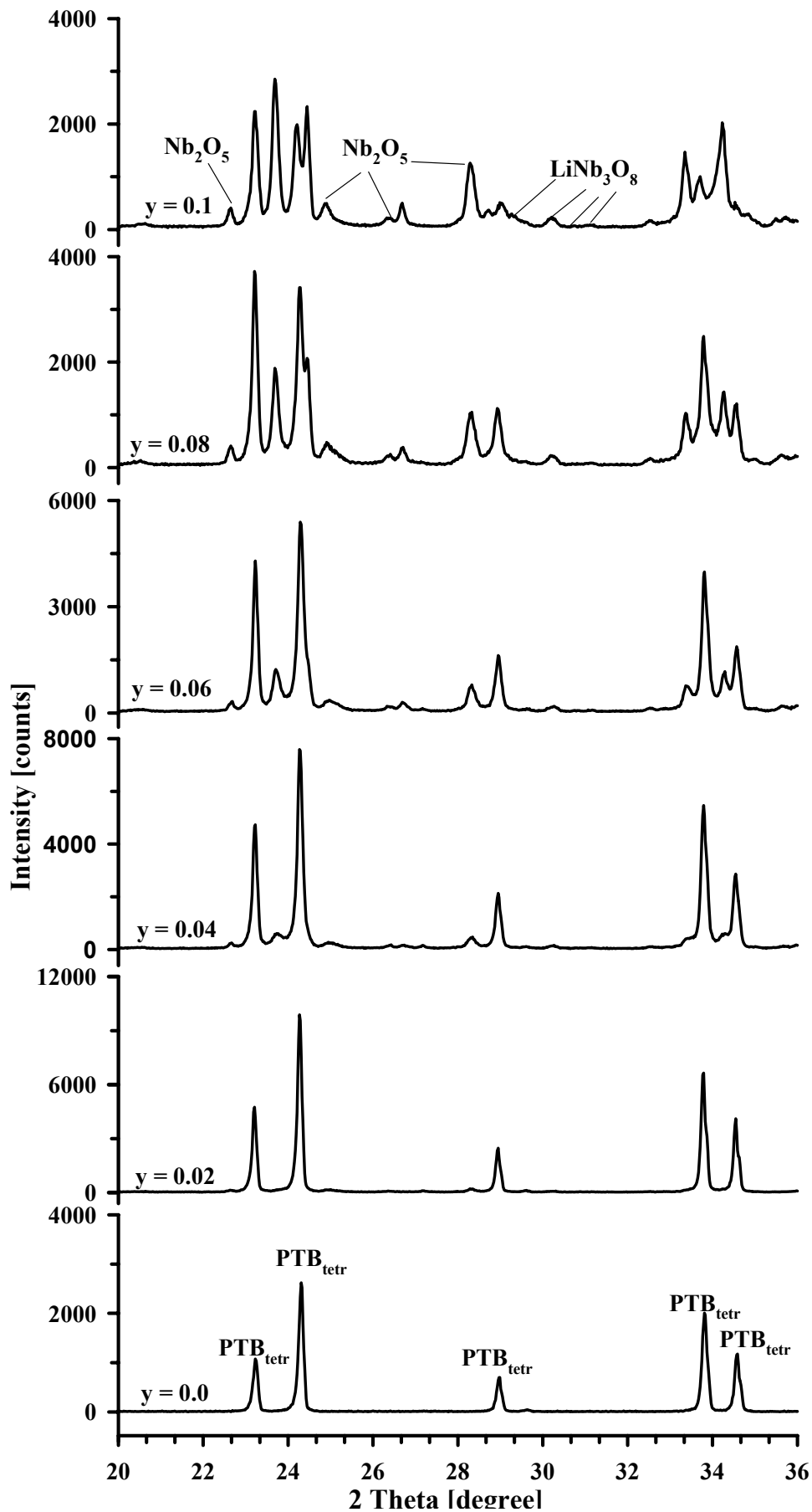


Fig. 28. X-ray powder pattern of $\text{Li}_{0.1}\text{Nb}_y\text{W}_{1-y}\text{O}_3$ ($y = 0.0 - 0.1$) system of series 6 taken immediately after opening the reaction tubes. For sample with $y = 0.1$, Nb_2O_5 and LiNb_3O_8 impure phase are denoted and the rest lines belongs to PTB_{orth} and PTB_{tetr} .

are also given in table 4. The data obtained from previous investigation well coincide with the present results obtained from series 6. In series 6, PTB_{tet} is only possible for $y = 0.02$. However, the samples with $0.02 < y < 0.1$ show the presence of PTB_{orth} , Nb_2O_5 and $LiNb_3O_8$ as impurity along with PTB_{tet} phase. For $x = y = 0.1$ the sample shows mainly the PTB_{orth} phase in presence of small amount of PTB_{tet} , Nb_2O_5 and $LiNb_3O_8$ as impurity.

Table 4: Results of the X-ray powder analysis of different samples of $Li_{0.1}Nb_yW_{1-y}O_3$ ($y = 0.02- 0.1$) system of series 6 and some previous results [112] of the same system prepared at 600°C for 7 days.

Nominal composition	$Li_{0.1}Nb_yW_{1-y}O_3$ prepared at 700°C for 7 days (Series 6)		$Li_{0.1}Nb_yW_{1-y}O_3$ prepared at 600°C for 7 days heated	
	Phase observed (4h X-ray)	Cell parameters (\AA) (Guinier method)	Phase observed (40 min X-ray)	Cell parameters (\AA) (Guinier-Hägg)
$Li_{0.1}WO_3$	PTB_T	$a = 5.2113(11)$ $c = 3.8424(12)$	PTB_T	$a = 5.2058(32)$ $c = 3.8498(43)$
$Li_{0.1}Nb_{0.02}W_{0.98}O_3$	PTB_T	$a = 5.1966(10)$ $c = 3.8435(13)$	PTB_T	$a = 5.2068(75)$ $c = 3.8485(88)$
$Li_{0.1}Nb_{0.04}W_{0.96}O_3$	PTB_T + traces of PTB_O +traces of Nb_2O_5 +traces of $LiNb_3O_8$	$a = 5.1983(15)$ $c = 3.8396(14)$	PTB_T	$a = 5.2084(54)$ $c = 3.8520(82)$
$Li_{0.1}Nb_{0.06}W_{0.94}O_3$	$PTB_T + PTB_O$ + traces of Nb_2O_5 + traces of $LiNb_3O_8$	$a = 5.2036(11)$ $c = 3.8474(15)$	PTB_T + \blacktriangle	$a = 5.2037(54)$ $c = 3.8474(52)$
$Li_{0.1}Nb_{0.08}W_{0.92}O_3$	$PTB_T + PTB_O$ + Nb_2O_5 + traces of $LiNb_3O_8$	$a = 5.2020(15)$ $c = 3.8482(15)$	PTB_T + \blacktriangle	$a = 5.2024(32)$ $c = 3.8469(34)$
$Li_{0.1}Nb_{0.1}W_{0.9}O_3$	$PTB_T + PTB_O$ + Nb_2O_5 + traces of $LiNb_3O_8$	$a = 5.1655(45)$ $c = 3.8404(45)$ $a = 7.3098(60)$ $c = 7.5164(30)$ $c = 7.8373(58)$	-	-

\blacktriangle = 2 - 5 weak lines of unknown phase.

The IR absorption spectra between 375 cm^{-1} and 1600 cm^{-1} of the sample of $\text{Li}_{0.1}\text{Nb}_y\text{W}_{1-y}\text{O}_3$ system of series 6 are given in Fig. 29. For $y = 0.00$ and 0.02 the spectra show a typical PTB_{tet} structure with a peak maximum at about 850 and 874 cm^{-1} respectively. The absorption feature at 423 cm^{-1} also can be seen only for $y = 0.00$ and 0.02 . For $y = 0.04$ the sample shows a peak maximum at about 871 cm^{-1} . Two peak maximum at about 867 cm^{-1} and 769 cm^{-1} and a minimum at about 800 cm^{-1} observed for sample with $y = 0.06$. For the sample with $y = 0.08$ two peak maximum at about 852 cm^{-1} and 773 cm^{-1} and a minimum at about 800 cm^{-1} also observed.

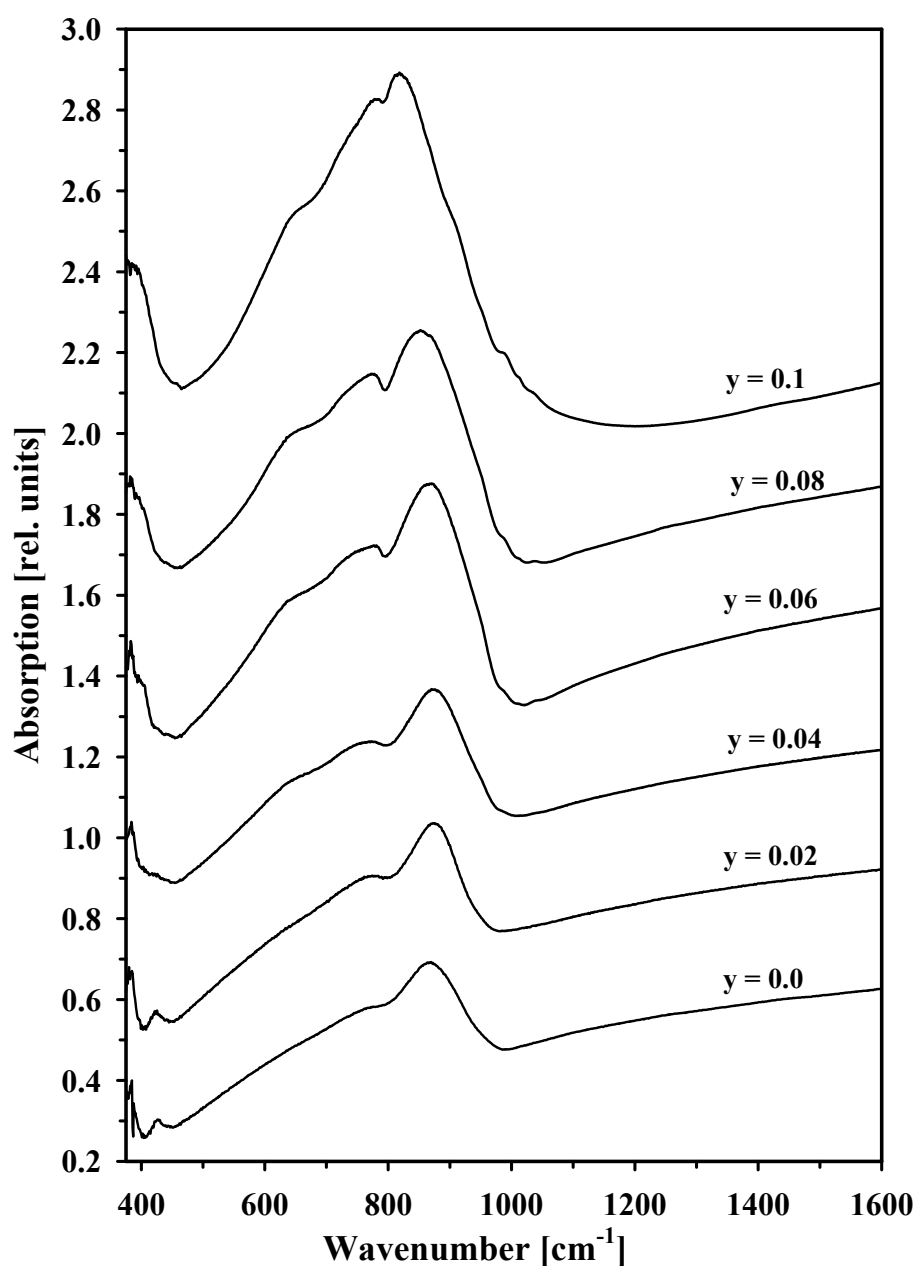


Fig. 29. IR absorption spectra (KBr-method) of $\text{Li}_{0.1}\text{Nb}_y\text{W}_{1-y}\text{O}_3$ ($y = 0.0 - 0.1$) system of series 6 as measured immediately after opening the reaction tubes.

However for $y = 0.1$ sample two peak maximum are observed at about 817 cm^{-1} and 778 cm^{-1} and the minimum at about 800 cm^{-1} indicating the monoclinic form of WO_3 .

The as measured reflectivity spectra of series 6 are given in Fig. 30. The color of the sample changes from grey greenish to greenish with increasing niobium content as prepared. It can be seen that with increasing niobium concentration the reflectivity increases below 25000 cm^{-1} .

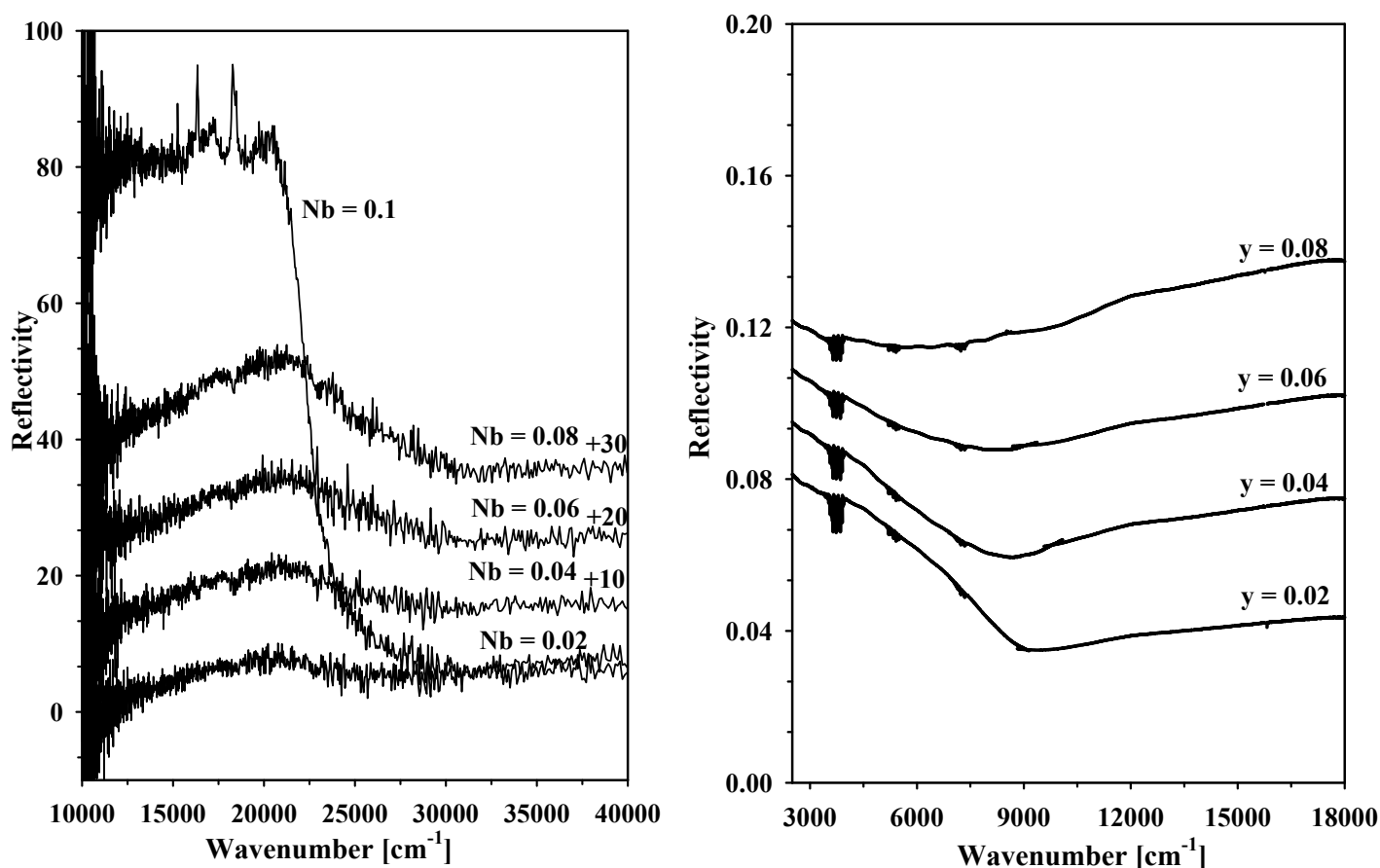


Fig. 30. UV-VIS spectra (left) and NIR spectra (right) of $\text{Li}_{0.1}\text{Nb}_y\text{W}_{1-y}\text{O}_3$ ($y = 0.02 - 0.1$) system of series 6 as measured after opening the reaction tubes.

For example, with $y = 0.02$, sample shows about 12% reflectivity whereas the sample with $y = 0.08$ shows 30% reflectivity at about 21000 cm^{-1} . In further experiments in the spectral range 2000 cm^{-1} to 18000 cm^{-1} a reflection minimum is observed at about 9000 cm^{-1} for sample with $y = 0.02$ [Fig. 30]. This minimum feature in the reflectivity becomes weaker and shifted to lower wavenumber with increasing niobium content. For $y \geq 0.08$, the minimum structure becomes less significant and there is nearly no shift in position, which could indicate the niobium doping in the system $\text{Li}_{0.1}\text{Nb}_y\text{W}_{1-y}\text{O}_3$. However, the whole effect can also be related to a decreasing amount of Li in Li_xWO_3 , which is supported by IR and X-ray data.

3.4 Characterisation of $\text{Li}_{0.4}\text{Mo}_y\text{W}_{1-y}\text{O}_3$ system where $y = 0.00 - 0.3$

The X-ray diffraction patterns of all samples of $\text{Li}_{0.4}\text{Mo}_y\text{W}_{1-y}\text{O}_3$ with $y = 0.00 - 0.3$ as collected by philips diffractometer are given in Fig. 31. For $y = 0.08$, the X-ray powder pattern can be identified mainly as $\text{PTB}_{\text{cubic}}$ phase in presence of some weak additional lines. These weak lines are due to the presence of $\text{Li}_2\text{W}_2\text{O}_7$ type phase as impurity as is seen by comparison to the $\text{Li}_2\text{W}_2\text{O}_7$ pattern also shown in Fig. 31. For $y = 0.1$ and 0.15 the samples show the same diffraction patterns as obtained for $y = 0.08$. With increasing molybdenum content the intensity of the $\text{Li}_2\text{W}_2\text{O}_7$ impure phase increases. For $y > 0.15$ there is a considerable change in the X-ray diffraction patterns. The $\text{PTB}_{\text{cubic}}$ phase has totally disappeared and $\text{Li}_2\text{W}_2\text{O}_7$ type phase is mainly identified in presence of small amount of $\text{Li}_2\text{Mo}_2\text{O}_7$ phase. Variation in the X-ray pattern compared to the $\text{Li}_2\text{W}_2\text{O}_7$ pure phase could indicate the formation of $\text{Li}_2\text{W}_{2-x}\text{Mo}_x\text{O}_7$ of variable composition.

The X-ray results of series 7 of system $\text{Li}_{0.4}\text{Mo}_y\text{W}_{1-y}\text{O}_3$ are given in table 5. In a previous investigation [118] samples of $\text{Li}_{0.3}\text{Mo}_y\text{W}_{1-y}\text{O}_3$ were prepared at 800°C for 7 days by the same

Table 5: Phase observed from different sample of $\text{Li}_{0.4}\text{Mo}_y\text{W}_{1-y}\text{O}_3$ ($y = 0.00 - 0.3$) system prepared at 700°C for 7 days and compared with some previous results [118] of $\text{Li}_{0.3}\text{Mo}_y\text{W}_{1-y}\text{O}_3$ ($y = 0.0 - 0.25$) system prepared at 800°C for 7 days.

$\text{Li}_{0.4}\text{Mo}_y\text{W}_{1-y}\text{O}_3$ prepared at 700°C for 7 days (Series 6) (6 h X-ray by philips diffractometer)		$\text{Li}_{0.3}\text{Mo}_y\text{W}_{1-y}\text{O}_3$ prepared at 800°C for 7 days (40 min Guinier- Hägg)	
Nominal composition	Phase observed	Nominal composition	Phase observed
$\text{Li}_{0.4}\text{WO}_3$	PTB_C	$\text{Li}_{0.3}\text{WO}_3$	$\text{PTB}_C + \bullet$
$\text{Li}_{0.4}\text{Mo}_{0.08}\text{W}_{0.92}\text{O}_3$	$\text{PTB}_C + \text{traces of } \text{Li}_2\text{W}_2\text{O}_7$	$\text{Li}_{0.3}\text{Mo}_{0.05}\text{W}_{0.95}\text{O}_3$	$\text{PTB}_C + \text{PTB}_T + \bullet$
$\text{Li}_{0.4}\text{Mo}_{0.1}\text{W}_{0.9}\text{O}_3$	$\text{PTB}_C + \text{traces of } \text{Li}_2\text{W}_2\text{O}_7$	$\text{Li}_{0.3}\text{Mo}_{0.1}\text{W}_{0.9}\text{O}_3$	$\text{PTB}_C + \text{PTB}_T + \bullet$
$\text{Li}_{0.4}\text{Mo}_{0.15}\text{W}_{0.85}\text{O}_3$	$\text{PTB}_C + \text{Li}_2\text{W}_2\text{O}_7 + \text{traces of } \text{Li}_2\text{Mo}_2\text{O}_7$	$\text{Li}_{0.3}\text{Mo}_{0.15}\text{W}_{0.85}\text{O}_3$	$\text{PTB}_C + \text{PTB}_T + \bullet$
$\text{Li}_{0.4}\text{Mo}_{0.2}\text{W}_{0.8}\text{O}_3$	$\text{Li}_2\text{W}_2\text{O}_7 + \text{Li}_2\text{Mo}_2\text{O}_7$	$\text{Li}_{0.3}\text{Mo}_{0.2}\text{W}_{0.8}\text{O}_3$	$\text{PTB}_T + \bullet$
$\text{Li}_{0.4}\text{Mo}_{0.3}\text{W}_{0.7}\text{O}_3$	$\text{Li}_2\text{W}_2\text{O}_7 + \text{Li}_2\text{Mo}_2\text{O}_7$	$\text{Li}_{0.3}\text{Mo}_{0.25}\text{W}_{0.75}\text{O}_3$	$\text{PTB}_T + \bullet$

$\bullet = 2 - 6$ weak lines of unknown phase.

way and from the same reactants as described for series 4 and molybdenum from BDH. The phase observed from this previous investigation are also given in table 5. From this table it

can be seen that $\text{PTB}_{\text{cubic}}$ phase is only possible up to $y = 0.15$. When $y > 0.15$ in the previous investigation the sample was identified as PTB_{tet} . However, in the present investigation for $y > 0.15$, the sample is mainly identified as $\text{Li}_2\text{W}_2\text{O}_7$ and $\text{Li}_2\text{Mo}_2\text{O}_7$ phase.

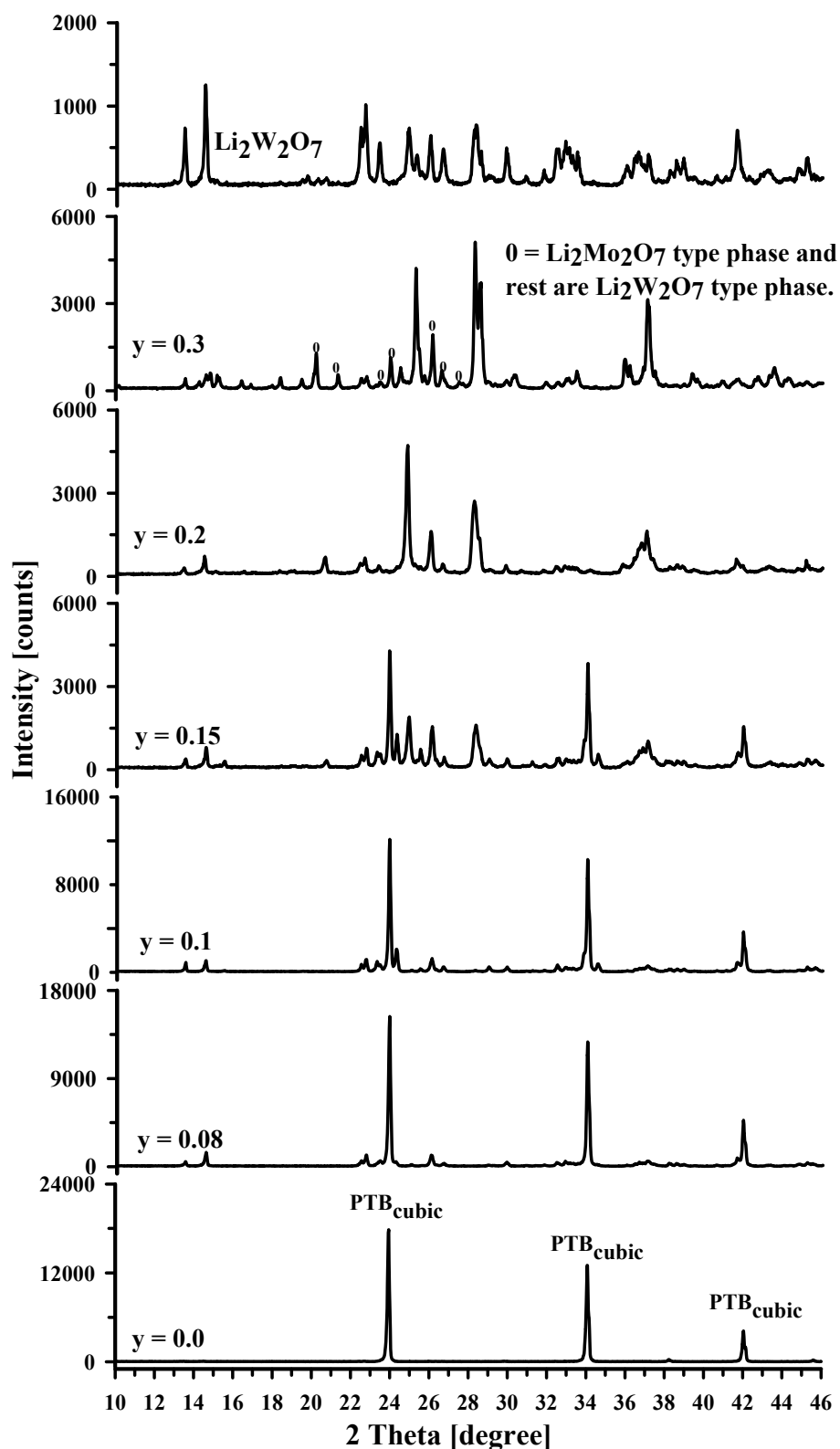
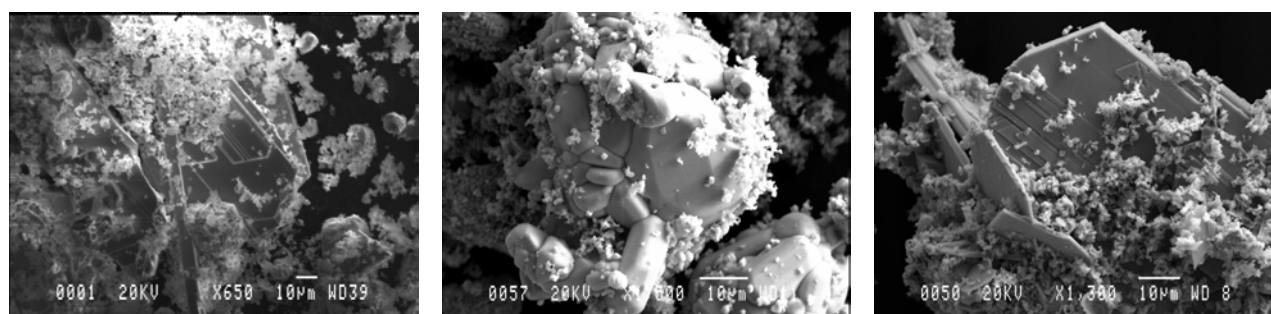


Fig.31. X-ray powder patterns of $\text{Li}_{0.4}\text{Mo}_y\text{W}_{1-y}\text{O}_3$ ($y = 0.0 - 0.3$) system of series 7 taken immediately after opening the reaction tubes. The X-ray powder pattern of pure nominal $\text{Li}_2\text{W}_2\text{O}_7$ sample also given for comparing the extra phase which formed with Mo content.

Samples for nominal composition $\text{Li}_{0.4}\text{Mo}_{0.15}\text{W}_{0.85}\text{O}_3$ and $\text{Li}_{0.4}\text{Mo}_{0.2}\text{W}_{0.8}\text{O}_3$ were examined in the JEOL-820 SEM microscope. The EDX analysis on about 10 crystals also indicates the formation of variable $\text{Li}_2\text{W}_{2-x}\text{Mo}_x\text{O}_7$ type phases which belong to high Mo content. There are also some crystals containing low Mo which belong to $\text{PTB}_{\text{cubic}}$. Fig. 32 shows the SEM image and the distribution of the SEM/EDX analysis made on crystals taken from nominal $\text{Li}_{0.4}\text{Mo}_{0.15}\text{W}_{0.85}\text{O}_3$ and $\text{Li}_{0.4}\text{Mo}_{0.2}\text{W}_{0.8}\text{O}_3$ samples. The SEM image of $\text{Li}_{0.4}\text{Mo}_{0.15}\text{W}_{0.85}\text{O}_3$ sample shows some cubic shape crystals together with some ‘‘flake-crystals’’ and powder. However, the SEM image of $\text{Li}_{0.4}\text{Mo}_{0.2}\text{W}_{0.8}\text{O}_3$ sample shows, only some ‘‘flake-crystals’’ and powder.



$\text{Li}_{0.4}\text{Mo}_{0.15}\text{W}_{0.85}\text{O}_3$ (a)

$\text{Li}_{0.4}\text{Mo}_{0.15}\text{W}_{0.85}\text{O}_3$ (b)

$\text{Li}_{0.4}\text{Mo}_{0.2}\text{W}_{0.8}\text{O}_3$

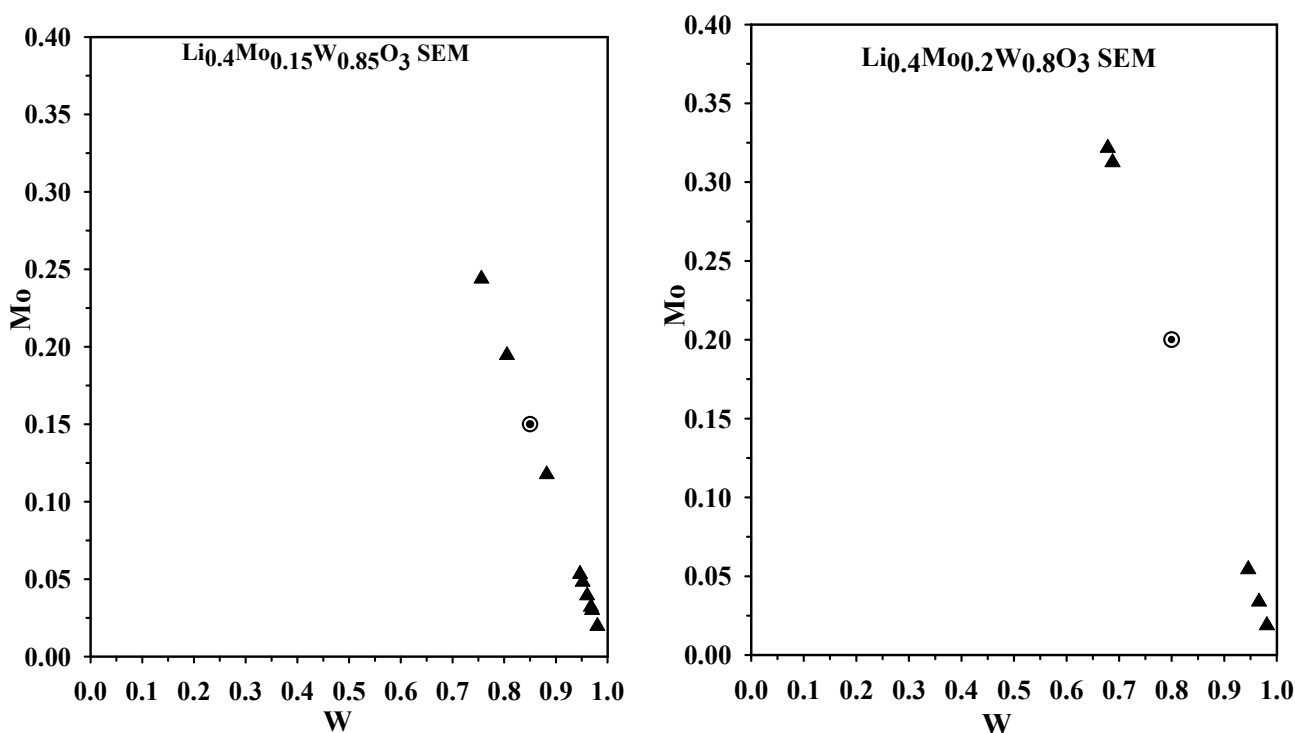


Fig. 32. SEM image of nominal $\text{Li}_{0.4}\text{Mo}_{0.15}\text{W}_{0.85}\text{O}_3$ sample shows few larger ‘flake-crystal’ (a) together with polycrystalline powder and some cubic crystals (b) with some powder. Whereas the SEM image of nominal $\text{Li}_{0.4}\text{Mo}_{0.2}\text{W}_{0.8}\text{O}_3$ sample shows only few larger ‘flake-crystal’ together with polycrystalline powder. SEM/EDX analysis results of these two samples also given where the values of W and Mo are calculated as $W = W / (\text{Mo} + W)$ and $\text{Mo} = \text{Mo} / (\text{Mo} + W)$.

The IR-absorption spectra of series 7 between 375 cm^{-1} and 1600 cm^{-1} are given in Fig. 33. For $y = 0.0$, the IR-spectra show the typical $\text{PTB}_{\text{cubic}}$ structure without any phonon signature. For $y = 0.08$, the IR-spectra show many phonon lines which are related to the $\text{Li}_2\text{W}_2\text{O}_7$ type

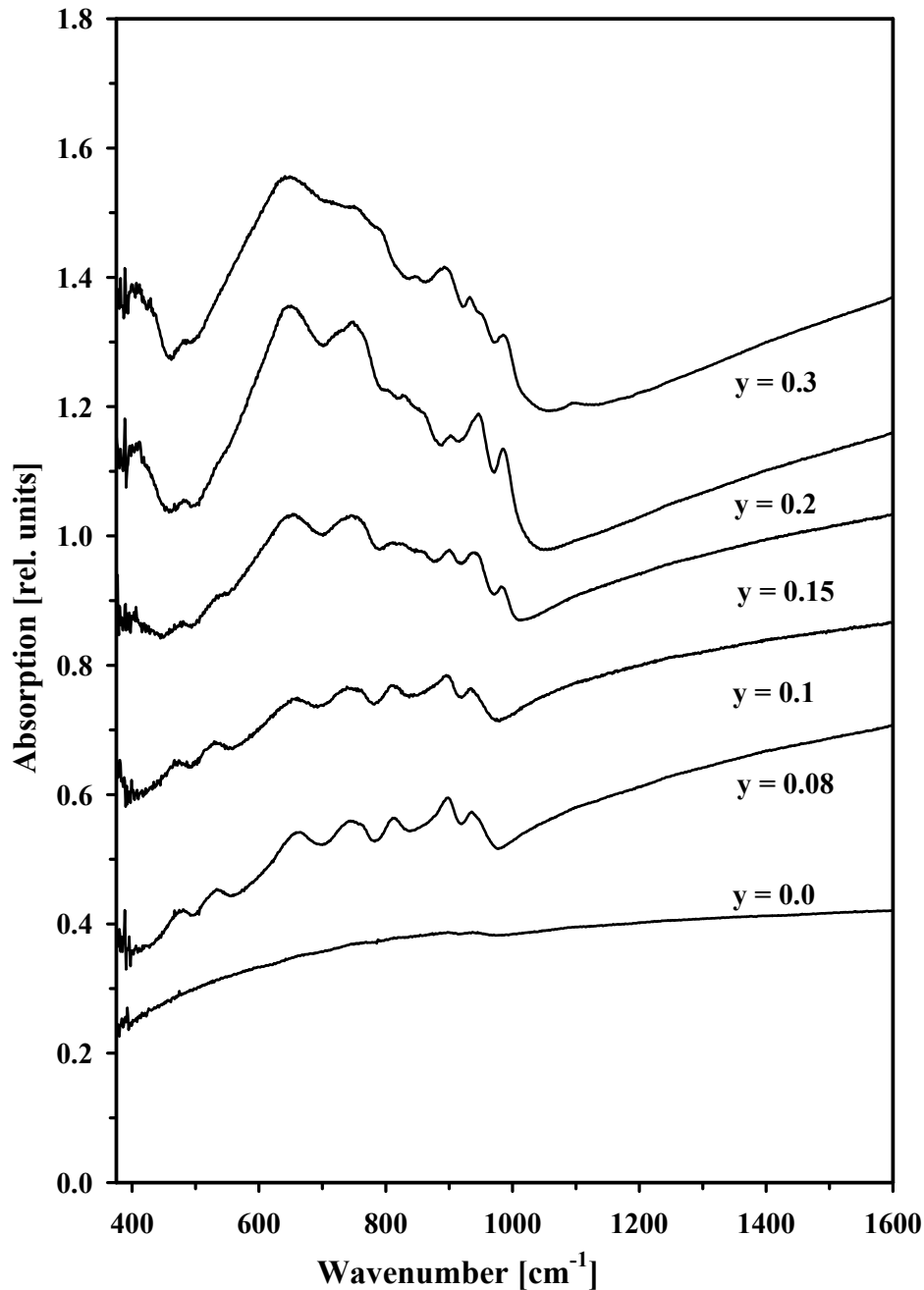


Fig. 33. IR absorption spectra (KBr-method) of $\text{Li}_{0.4}\text{Mo}_y\text{W}_{1-y}\text{O}_3$ ($y = 0.0 - 0.3$) system of series 7 as measured immediately after opening the reaction tubes.

phase. For $0.08 \leq y \leq 0.15$, the X-ray results shows a mixed phase of $\text{PTB}_{\text{cubic}}$ and $\text{Li}_2\text{W}_2\text{O}_7$. Therefore, for the samples with $0.08 \leq y \leq 0.15$, the IR-spectra is the superimposed form of $\text{PTB}_{\text{cubic}}$ and $\text{Li}_2\text{W}_2\text{O}_7$ phase [compare in Fig. 22]. For $y > 0.15$, sample the IR-spectra indicate

a structural relation to $\text{Li}_2\text{W}_2\text{O}_7$ which thus imply the formation of $\text{Li}_2\text{W}_{2-x}\text{Mo}_x\text{O}_7$ type composition.

The as measured reflectivity spectra of series 7 are given in Fig 34. The color of the as prepared sample goes from deep blue to blue to gray bluish with increasing molybdenum content. For $y = 0.0$ the spectra show a reflectivity minimum about 15000 cm^{-1} which

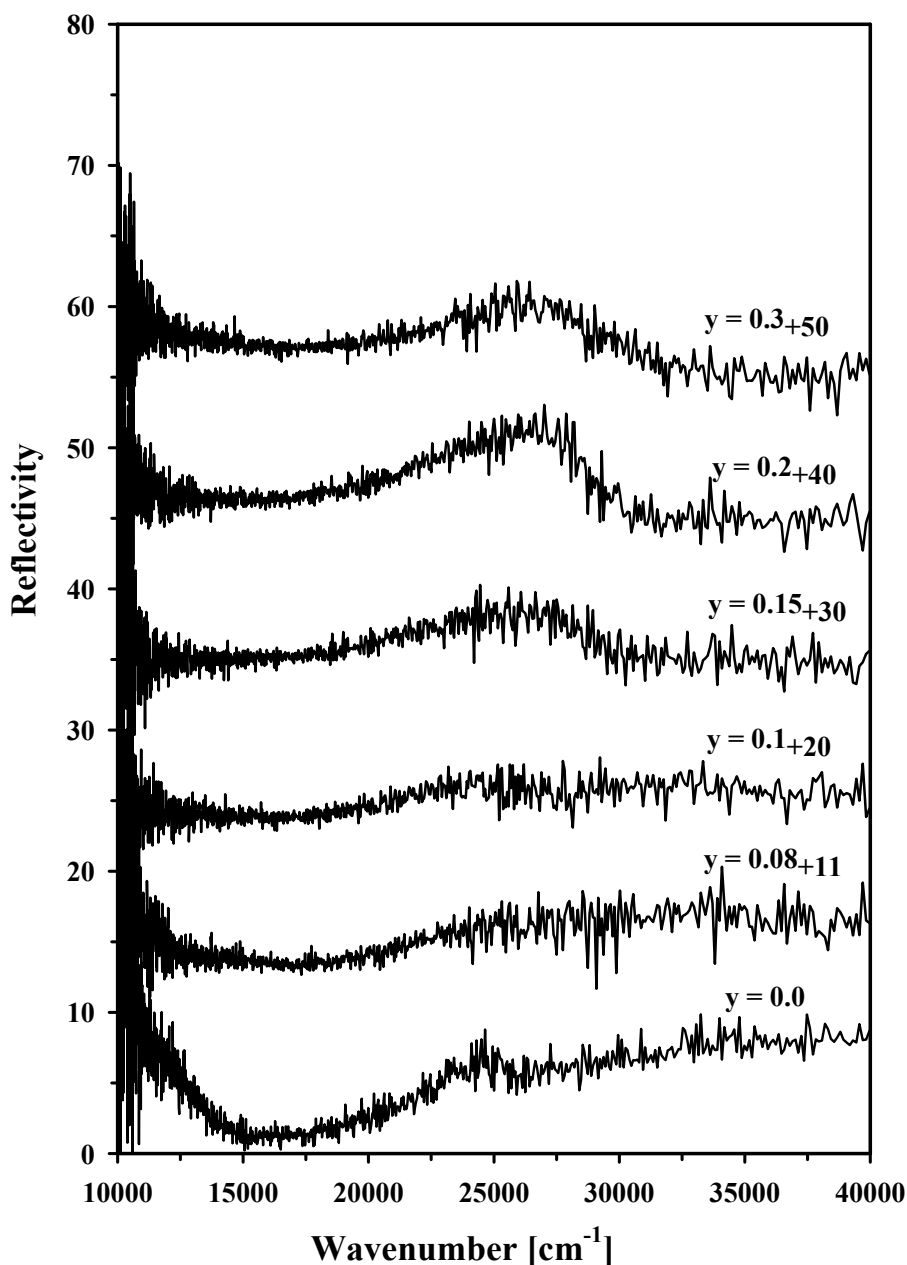


Fig. 34. As measured UV-VIS spectra of $\text{Li}_{0.4}\text{Mo}_y\text{W}_{1-y}\text{O}_3$ ($y = 0.0 - 0.3$) system of series 7 taken immediately after opening the reaction tubes.

disappears with increasing molybdenum content. For $y > 0.1$ the reflection curves above about 25000 cm^{-1} indicate a strong new absorption effect of Li which is due to the $\text{Li}_2\text{W}_{2-x}\text{Mo}_x\text{O}_7$ type phase.

3.5 Characterisation of $\text{Li}_{0.1}\text{Mo}_y\text{W}_{1-y}\text{O}_3$ system where $y = 0.00 - 0.1$

The X-ray diffraction patterns of all the samples of system $\text{Li}_{0.1}\text{Mo}_y\text{W}_{1-y}\text{O}_3$ with $y = 0.00 - 0.1$ collected from Philips diffractometer are given in Fig. 35. For $y = 0.02$ the X-ray patterns

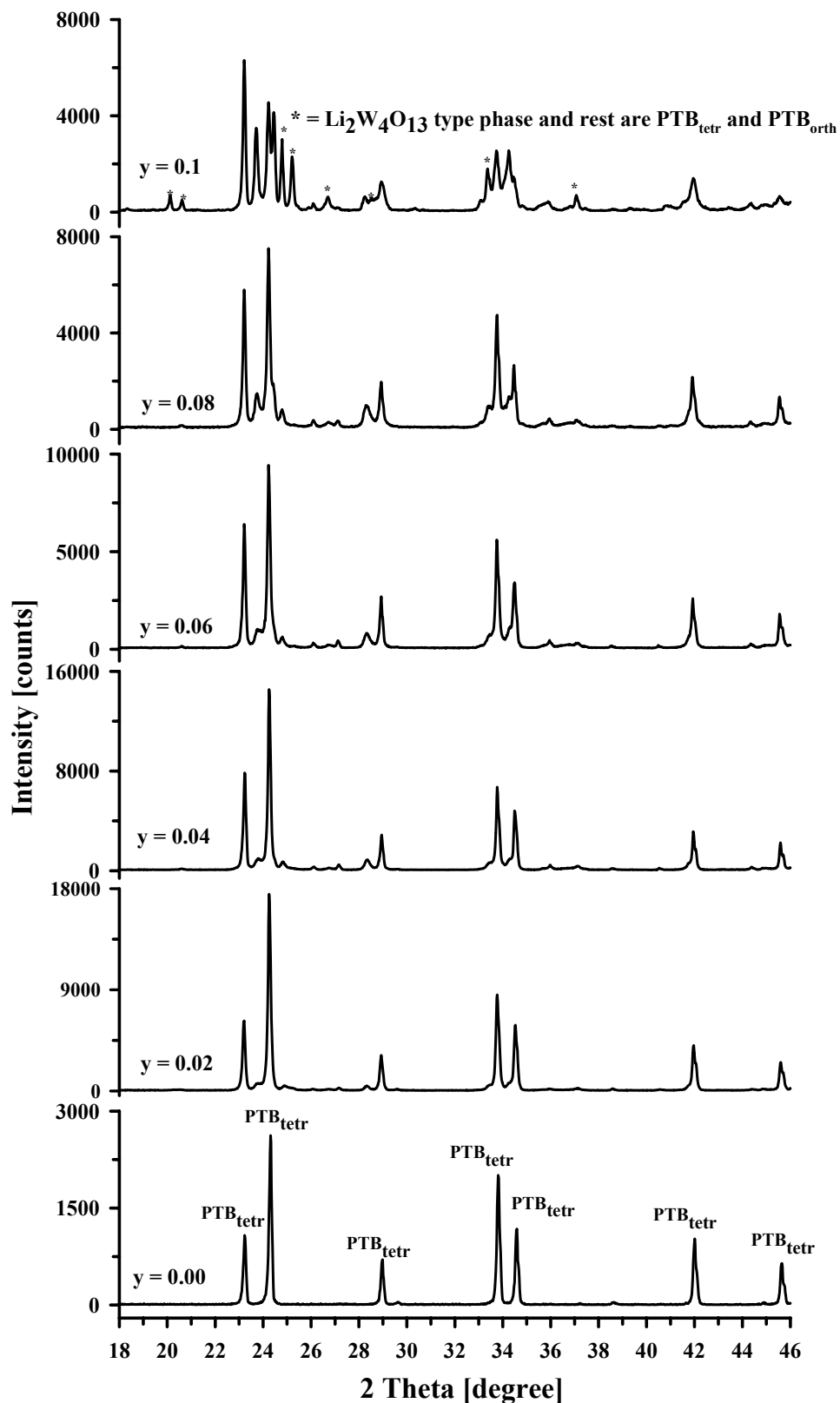


Fig. 35. X-ray powder diffraction patterns of $\text{Li}_{0.1}\text{Mo}_y\text{W}_{1-y}\text{O}_3$ system taken immediately after opening the reaction tubes with $y = 0.0 - 0.1$ as denoted.

can be identified mainly as PTB_{tet} with the peaks 001 at 23.24, 110 at 24.31, 101 at 28.97, 111 at 33.81 and 200 at 34.58 2-theta position. Up to $y = 0.08$ these peaks are present strongly. However, in the presence of very small amount of molybdenum as for example for $y = 0.02$ the sample contains a small amount of PTB_{orth} and $\text{Li}_2\text{W}_4\text{O}_{13}$ phase along with main PTB_{tet} phase as impurity. The intensity of these impure phases increases with increasing molybdenum content. For $y = 0.1$ the X-ray diffraction pattern mainly could identified as PTB_{orth} in presence of a small amount of PTB_{tet} and $\text{Li}_2\text{W}_4\text{O}_{13}$ phase as marked in the diffraction patterns.

The IR absorption spectra between 375 cm^{-1} and 1600 cm^{-1} of the system $\text{Li}_{0.1}\text{Mo}_y\text{W}_{1-y}\text{O}_3$ of series 8 are given in Fig. 36. For $y = 0.02$ the IR-spectra show a typical PTB_{tet} structure with

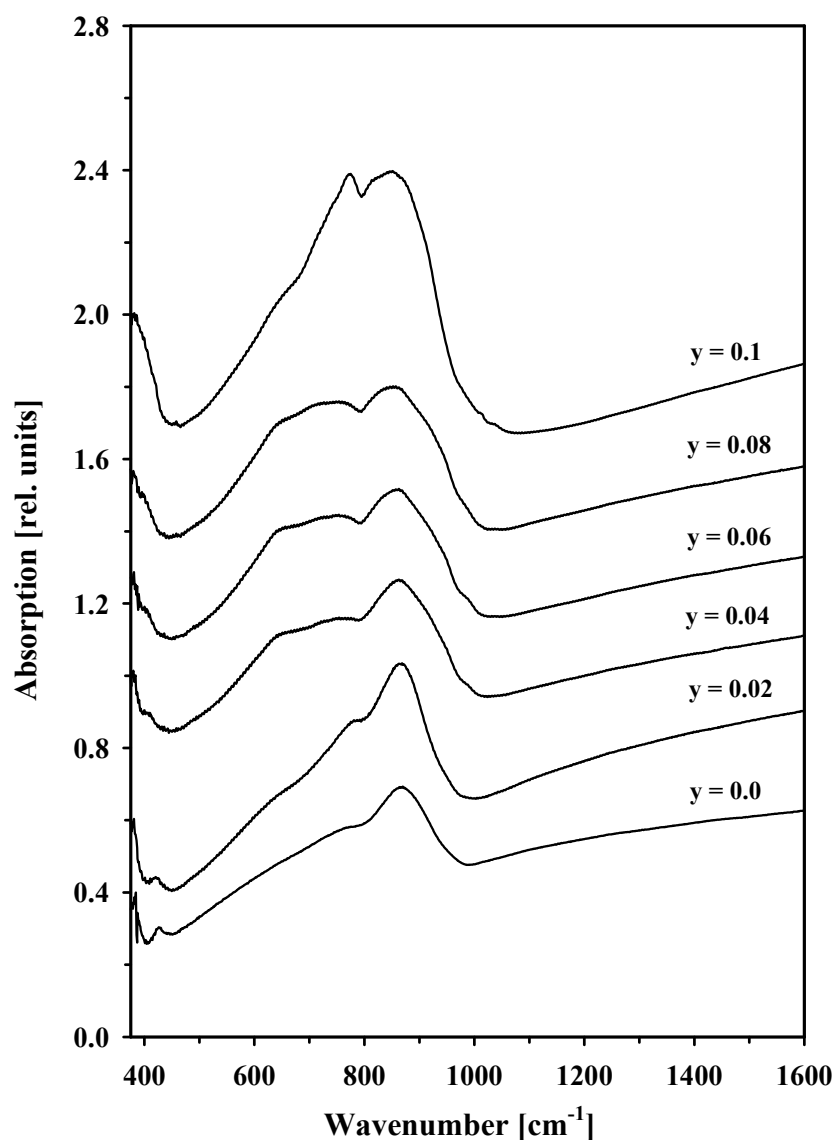


Fig.36. IR absorption spectra (KBr-method) of $\text{Li}_{0.1}\text{Mo}_y\text{W}_{1-y}\text{O}_3$ system as measured immediately after opening the reaction tubes with $y = 0.0 - 0.1$ as denoted.

a peak maximum at about 865 cm^{-1} . The absorption feature at 423 cm^{-1} also can be seen for $y = 0.0, 0.02$ and 0.04 . A further increase of molybdenum concentration leads to an increase of the peak intensity at about 865 cm^{-1} together with a shift of the main peak position towards lower wavenumber. For $y > 0.02$ a shoulder also observed around 650 cm^{-1} and 754 cm^{-1} . However, for $y = 0.1$ the IR-spectra shows two sharp peaks at about 773 cm^{-1} and 848 cm^{-1} position like the orthorhombic form of WO_3 .

3.6 Characterisation of $\text{Na}_{0.6}\text{Mo}_y\text{W}_{1-y}\text{O}_3$ system where $y = 0.00 - 0.25$

The X-ray powder diffraction patterns of all samples of $\text{Na}_{0.6}\text{Mo}_y\text{W}_{1-y}\text{O}_3$ system with $y = 0.00 - 0.2$ of series 9 prepared at 600°C and 700°C are given in Fig. 37 and 38. In Fig. 37 for $y = 0.0$ the sodium bronze is typically identified as $\text{PTB}_{\text{cubic}}$ by the peaks 100 ($2\theta^\circ$ at about 23.30), 110 ($2\theta^\circ$ at about 33.13), 111 ($2\theta^\circ$ at about 40.85) and 200 ($2\theta^\circ$ at about 47.52). For $y = 0.05$ the X-ray pattern can be identified mainly as $\text{PTB}_{\text{cubic}}$ with the peaks as observed for $y = 0.0$ in presence of two weak lines at about 26.05 and 37.05 2θ -position. These 2 weak lines are due to the presence of WO_2 reactant as impurity. However, for $y > 0.1$ along with $\text{PTB}_{\text{cubic}}$ phase and WO_2 impurity some other extra weak lines are also present in the diffraction pattern in different 2θ -position. For example several weak lines are present at about 12.10, 16.13, 18.83, 23.36, 27.09, 27.05, 27.59, 29.99, 34.01 and 35.2 2θ -positions. All of these extra lines were identified as $\text{Na}_2\text{Mo}_2\text{O}_7$ type phase, which is listed in the JCPDS index. With increasing molybdenum content the intensity of these extra lines increases. The structure of $\text{Na}_2\text{Mo}_2\text{O}_7$ is made up of $(\text{Mo}_n\text{O}_{3n+1})^{2-}$ anion chains, and the construction of the chains depends on the value of n . $\text{Na}_2\text{W}_2\text{O}_7$ is isomorphous with $\text{Na}_2\text{Mo}_2\text{O}_7$. In Fig. 38 the X-ray powder patterns of the sample of $\text{Na}_{0.6}\text{Mo}_y\text{W}_{1-y}\text{O}_3$ system, prepared at 700°C show the same behaviour as observed in Fig. 37.

The IR absorption spectra between 375 cm^{-1} and 1500 cm^{-1} as obtained for series 9 are shown in Fig. 39. For $y = 0.0$ the IR-spectra shows the typical $\text{PTB}_{\text{cubic}}$ spectra with very weak phonon signature at about 900 cm^{-1} and 930 cm^{-1} . For $y = 0.05$ and 0.1 the IR-spectra shows the same behaviour as observed for $y = 0.0$. However, $y > 0.1$ the IR-spectra show the many phonon lines due to the presence of $\text{Na}_2\text{Mo}_2\text{O}_7$ phase. Therefore, the spectra of the sample with $y > 0.1$ are the superimposed from of $\text{PTB}_{\text{cubic}}$ phase and $\text{Na}_2\text{Mo}_2\text{O}_7$ phase.

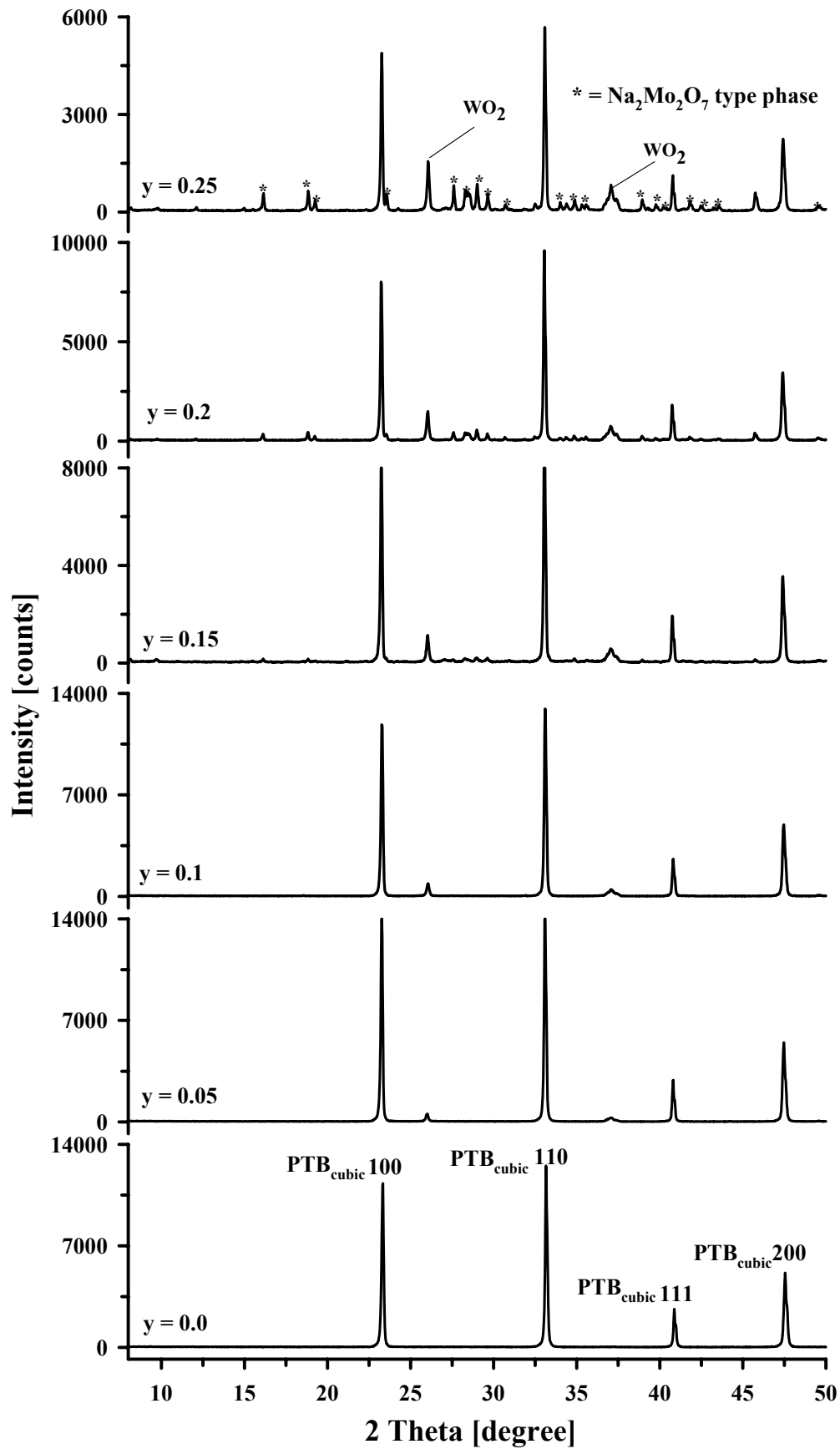


Fig. 37. X-ray powder diffraction patterns of $\text{Na}_{0.6}\text{Mo}_y\text{W}_{1-y}\text{O}_3$ system with $y = 0.0 - 0.25$ as denoted prepared at 600°C .

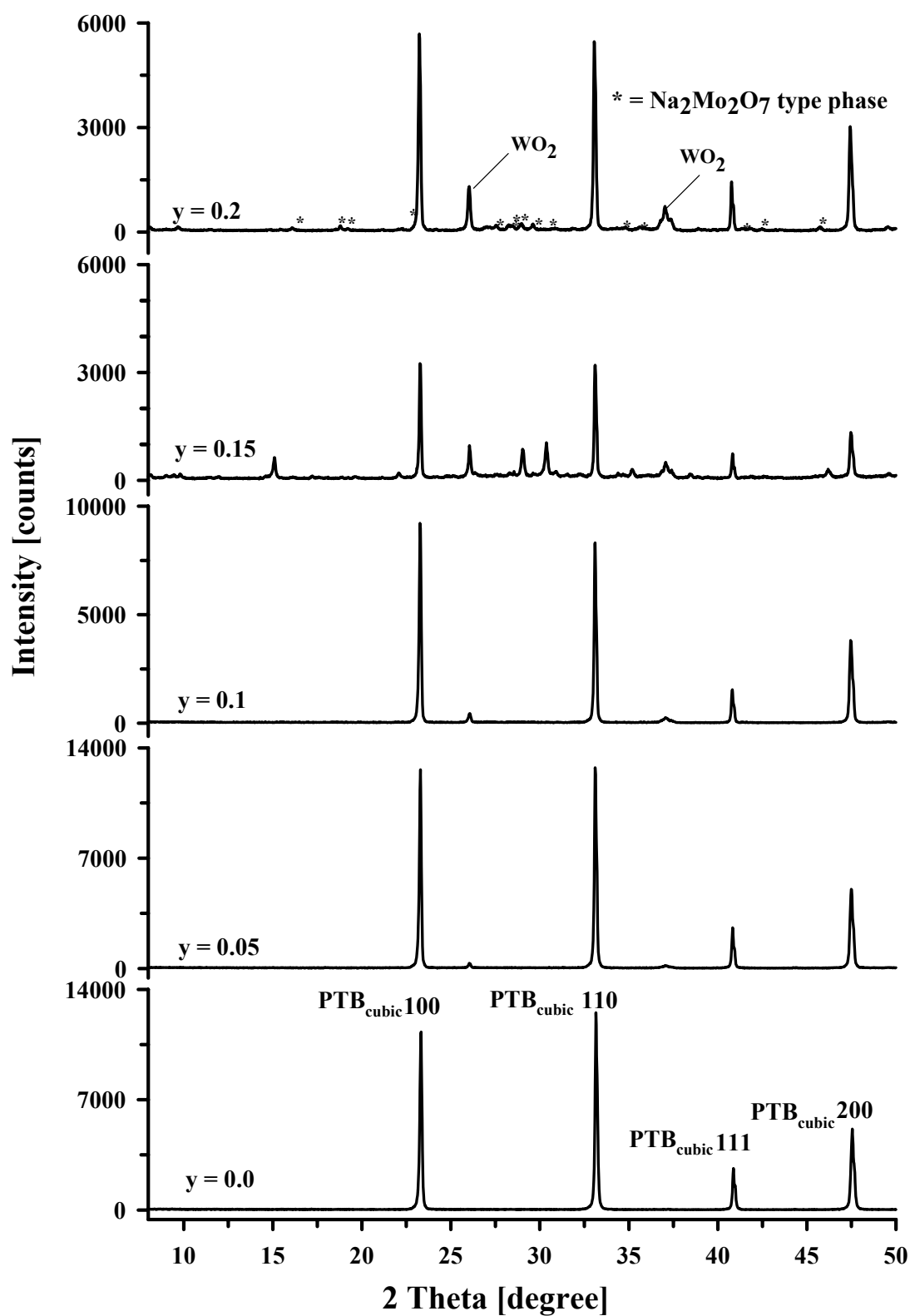


Fig.38. X-ray powder diffraction patterns of $\text{Na}_{0.6}\text{Mo}_y\text{W}_{1-y}\text{O}_3$ system with $y = 0.0 - 0.2$ as denoted prepared at 700°C .

The X-ray and IR results indicate that molybdenum can be doped in the $\text{PTB}_{\text{cubic}} \text{Na}_{0.6}\text{WO}_3$ at 600°C and 700°C up to nominal $y = 0.1$. These results are supported by the TEM/EDX analysis. Most of the samples from $\text{Na}_{0.6}\text{Mo}_y\text{W}_{1-y}\text{O}_3$ series were examined in the SEM and some samples were also examined by TEM microscopes. The shape and size of the crystal

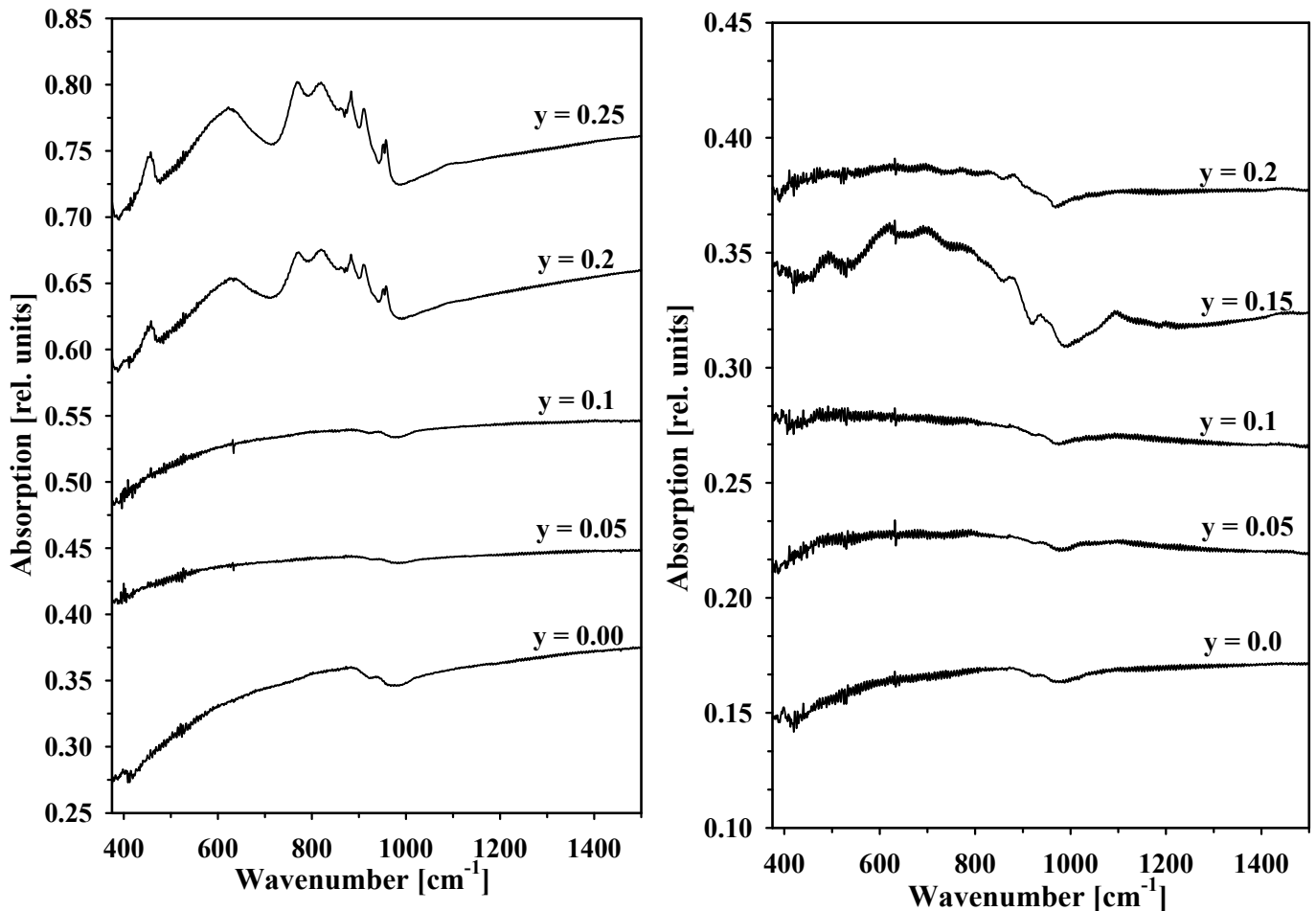
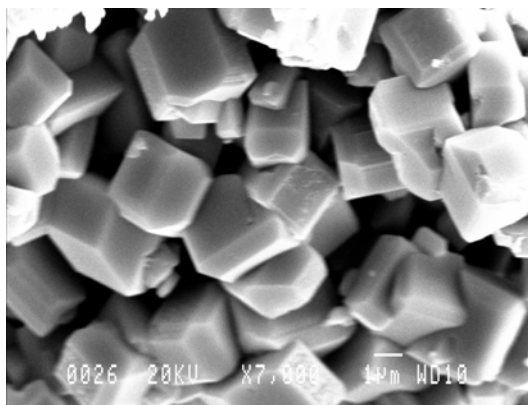
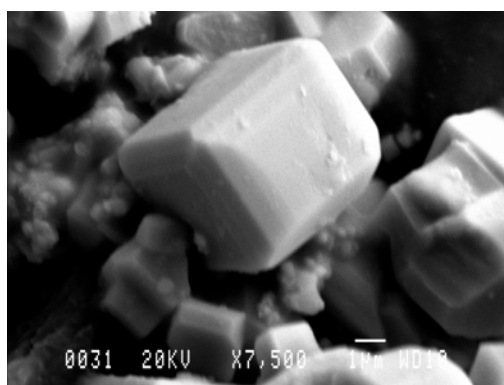
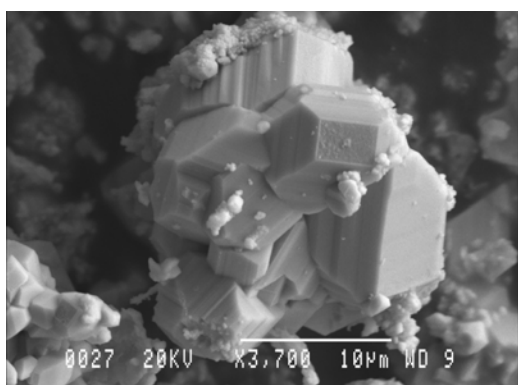


Fig.39. IR absorption spectra (KBr-method) of $\text{Na}_{0.6}\text{Mo}_y\text{W}_{1-y}\text{O}_3$ system with $y = 0.0 - 0.25$ as denoted prepared at 600°C (left) and 700°C (right).

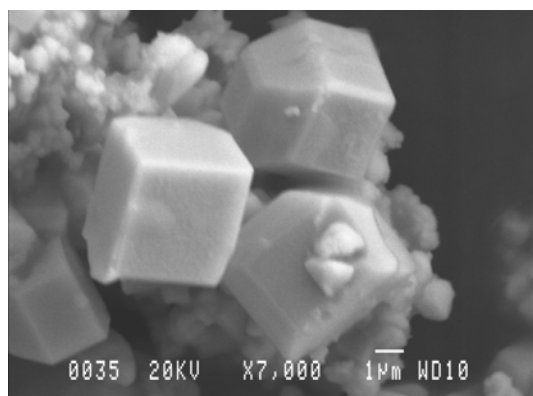
vary considerably in samples with increasing Mo content as shown Fig. 40a and 40b in the SEM images. From SEM image, it can be seen that until $y \leq 0.1$ the cubic shape crystal is present, whereas with $y > 0.1$ some extra solid slab with cubic crystal appear. These results also support the X-ray and IR results. EDX analysis of crystals from each bulk sample in the SEM microscope shows that the average Na content was $x = 0.9$ which is higher than the starting material. However, the EDX analysis of thin crystal fragments in the TEM microscope showed that most of the crystals of the system contain average Na content $x = 0.6 \pm 0.01$ and this is in good agreement with that of the starting composition. The diagram in Fig. 41b shows the TEM/EDX analysis of a nominal $\text{Na}_{0.6}\text{Mo}_{0.2}\text{W}_{0.8}\text{O}_3$ sample which shows the



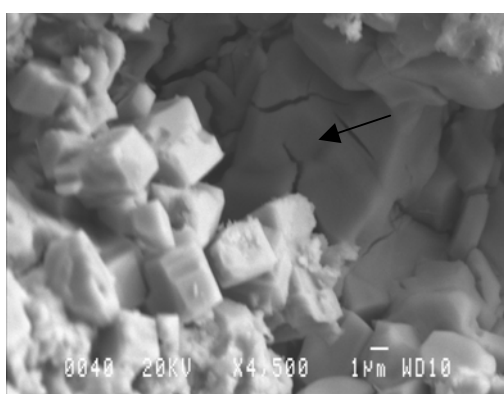
SEM image of nominal Na_{0.6}WO₃ sample showing the cubic crystals.



SEM image of nominal Na_{0.6}Mo_{0.05}W_{0.95}WO₃ sample showing the cubic crystals together with small amount of polycrystalline powder.

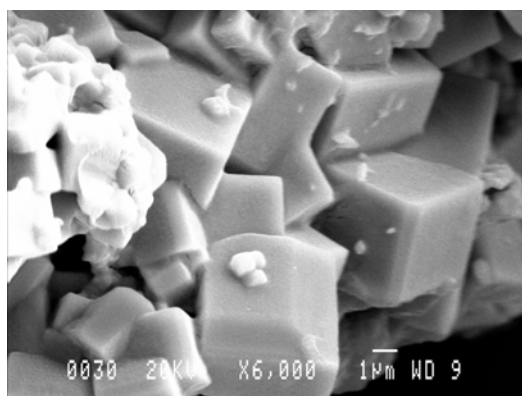


SEM image of nominal Na_{0.6}Mo_{0.1}W_{0.9}WO₃ showing the cubic crystals together with small amount of polycrystalline powder.

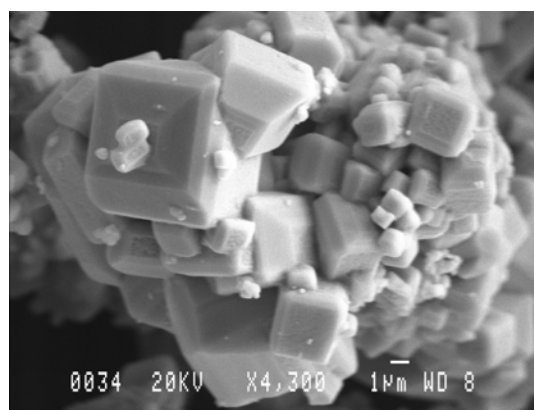
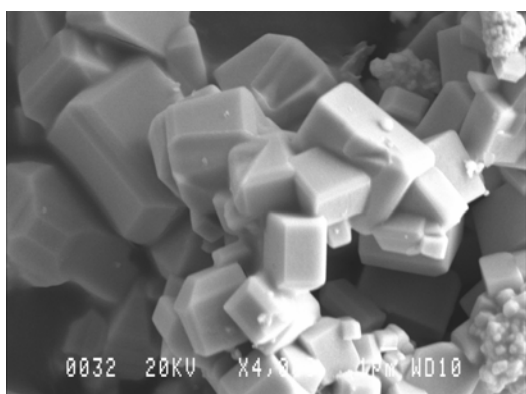


SEM image of nominal Na_{0.6}Mo_{0.15}W_{0.85}WO₃ showing the cubic crystals together with some solid slab of impurity phase (denoted by arrow).

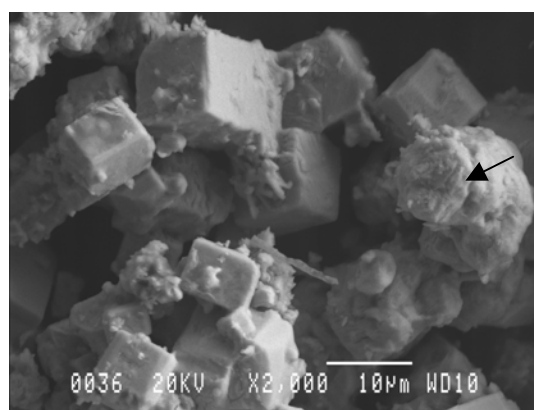
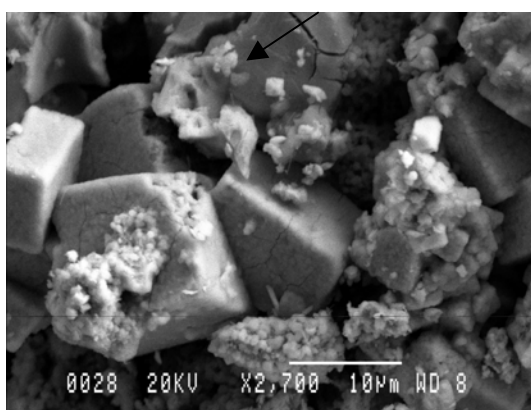
Fig. 40a. Systematic SEM-image of Na_{0.6}Mo_yW_{1-y}O₃ system prepared at 600°C with $y = 0.00 - 0.15$ as denoted, showing that with increasing Mo content the amount of cubic crystals decreases.



SEM image of nominal $\text{Na}_{0.6}\text{WO}_3$ sample showing the cubic crystals.



SEM image of nominal $\text{Na}_{0.6}\text{Mo}_{0.05}\text{W}_{0.95}\text{WO}_3$ (left) and $\text{Na}_{0.6}\text{Mo}_{0.1}\text{W}_{0.9}\text{WO}_3$ (right) sample showing the cubic crystals together with very small amount of polycrystalline powder.



SEM image of nominal $\text{Na}_{0.6}\text{Mo}_{0.15}\text{W}_{0.85}\text{WO}_3$ (left) and $\text{Na}_{0.6}\text{Mo}_{0.2}\text{W}_{0.8}\text{WO}_3$ (right) sample showing the cubic crystals together with polycrystalline powder and small amount of solid of impurity phase (denoted by arrow) .

Fig. 40b. Systematic SEM-image of $\text{Na}_{0.6}\text{Mo}_y\text{W}_{1-y}\text{O}_3$ system with $y = 0.0 - 0.2$ as denoted prepared at 700°C showing that with increasing Mo the amount of cubic crystals decreases.

average Na content about 0.55 and Mo about 0.09. The EDX spectrum of the same sample $\text{Na}_{0.6}\text{Mo}_{0.2}\text{W}_{0.8}\text{O}_3$ showing the presence of Na and Mo as shown in the Fig. 41a.

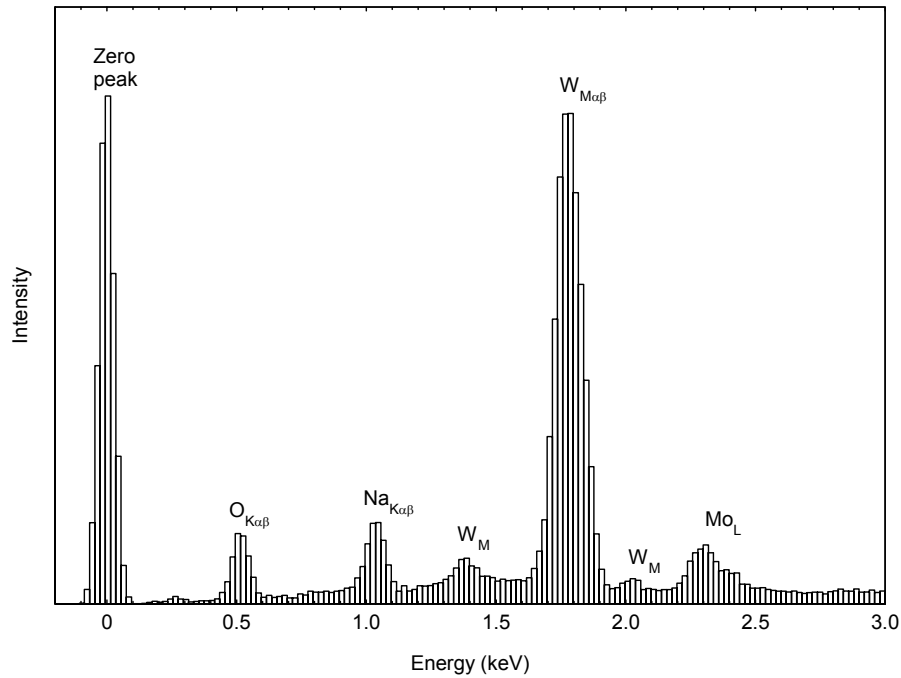


Fig. 41a. Typical EDX spectra of $\text{Na}_{0.6}\text{Mo}_y\text{W}_{1-y}\text{O}_3$ system.

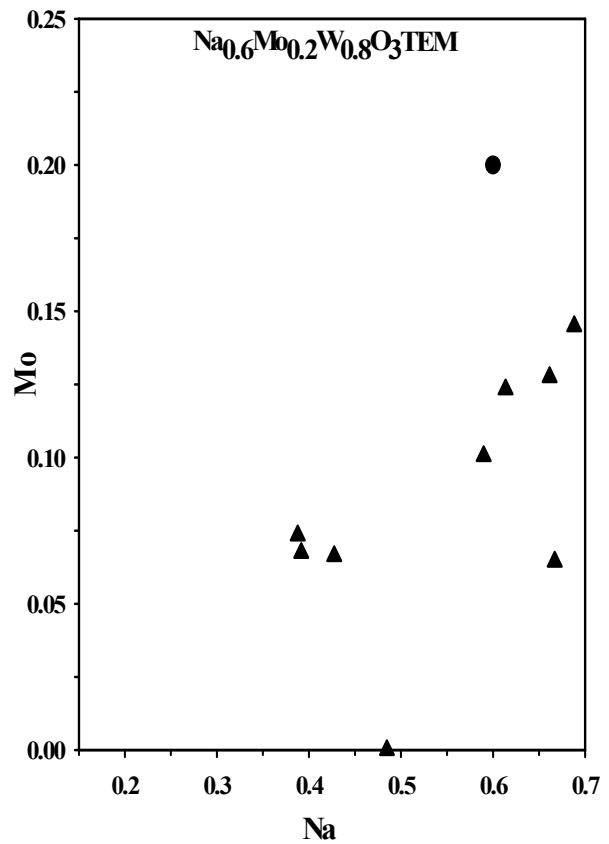
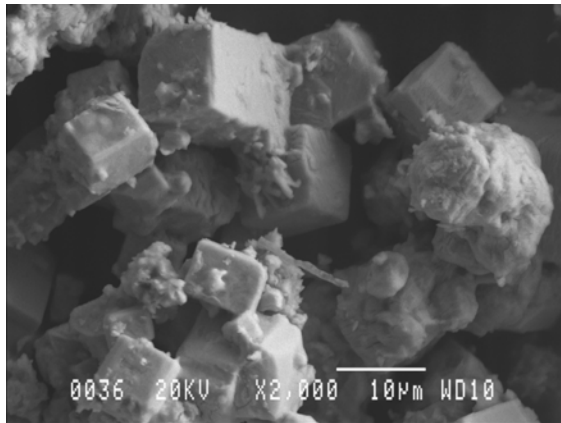


Fig. 41b. SEM-image and plot of TEM/EDX analysis results of nominal $\text{Na}_{0.6}\text{Mo}_{0.2}\text{W}_{0.8}\text{O}_3$ sample (black circle). Each triangle point represent the mean of two or three measurements on the same crystal. The value of the Na and Mo are calculated from the signal intensities as $\text{Na} = \text{Na} / (\text{Mo} + \text{W})$ and $\text{Mo} = \text{Mo} / (\text{Mo} + \text{W})$.

In Fig. 42, the as measured reflectivity spectra of $\text{Na}_{0.6}\text{Mo}_y\text{W}_{1-y}\text{O}_3$ system of series 9 are given. Fig. 42 shows a reflectivity minima at about 17000 cm^{-1} for $y = 0.0$ sample. Up to $y = 0.15$ the sample shows nearly the same reflectivity minimum at the same position as observed for $y = 0.0$. However, for $y > 0.15$ the reflectivity minimum decreases due to the dilution by $\text{Na}_2\text{Mo}_2\text{O}_7$ phase. Same behaviour is observed in the same figure for the samples of $\text{Na}_{0.6}\text{Mo}_y\text{W}_{1-y}\text{O}_3$ prepared at 700°C .

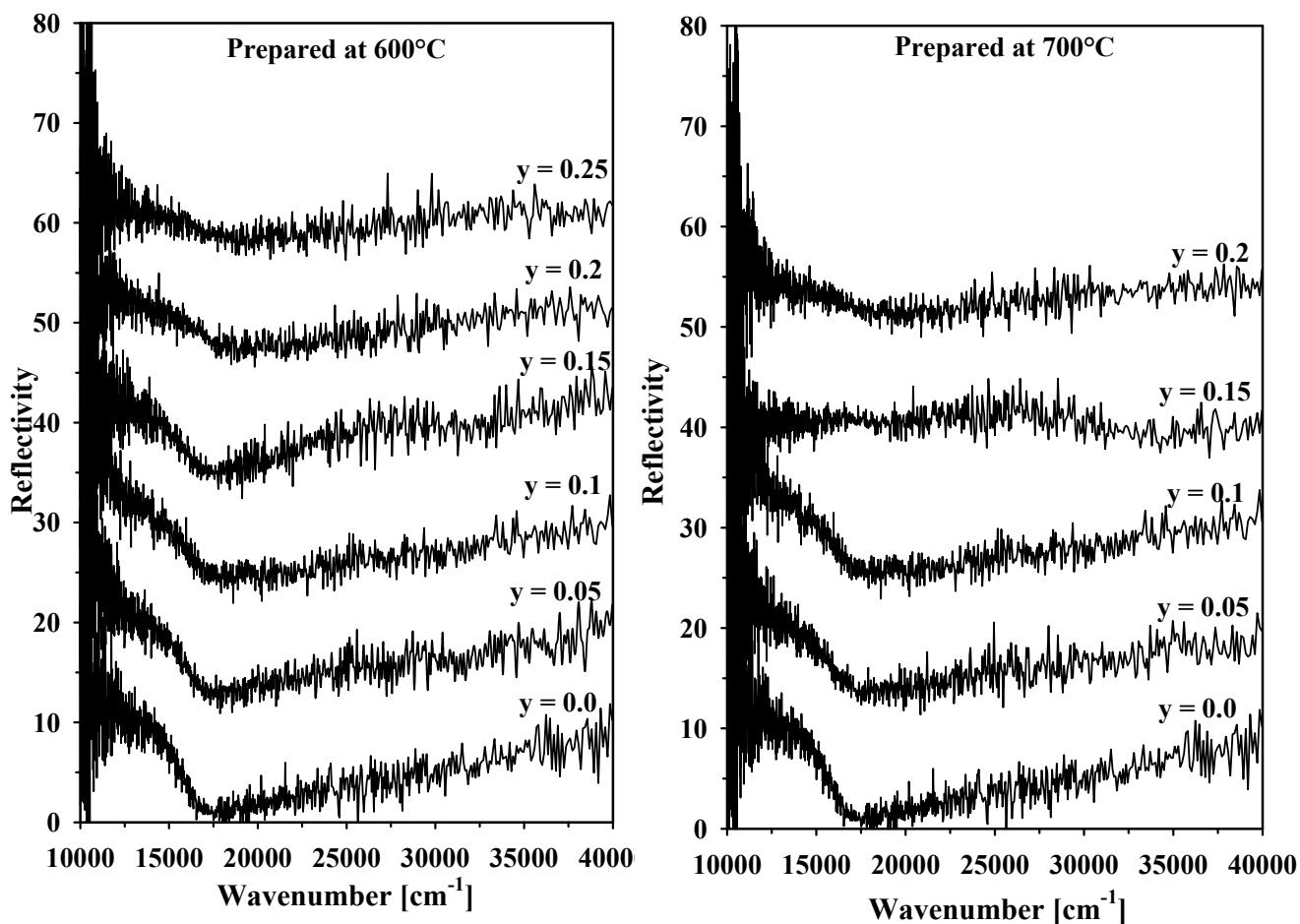


Fig. 42. UV-VIS spectra of $\text{Na}_{0.6}\text{Mo}_y\text{W}_{1-y}\text{O}_3$ ($y = 0.0 - 0.25$) system prepared at 600°C (left) and 700°C (right).

The sample $\text{Na}_{0.6}\text{Mo}_{0.2}\text{W}_{0.8}\text{O}_3$ was also selected for further structural studies by HRTEM method. Fig. 43 shows an well ordered image of a thin crystallite from fragment of $\text{Na}_{0.6}\text{Mo}_{0.2}\text{W}_{0.8}\text{O}_3$ crystalline powder sample with corresponding ED-pattern. However, a small amount of impure phase of $\text{Na}_2\text{Mo}_2\text{O}_7$ and WO_2 are present along with the main $\text{PTB}_{\text{cubic}}$ phase in the sample $\text{Na}_{0.6}\text{Mo}_{0.2}\text{W}_{0.8}\text{O}_3$, Fig. 43 shows only the well ordered HRTEM image of $\text{PTB}_{\text{cubic}}$ part of the sample.

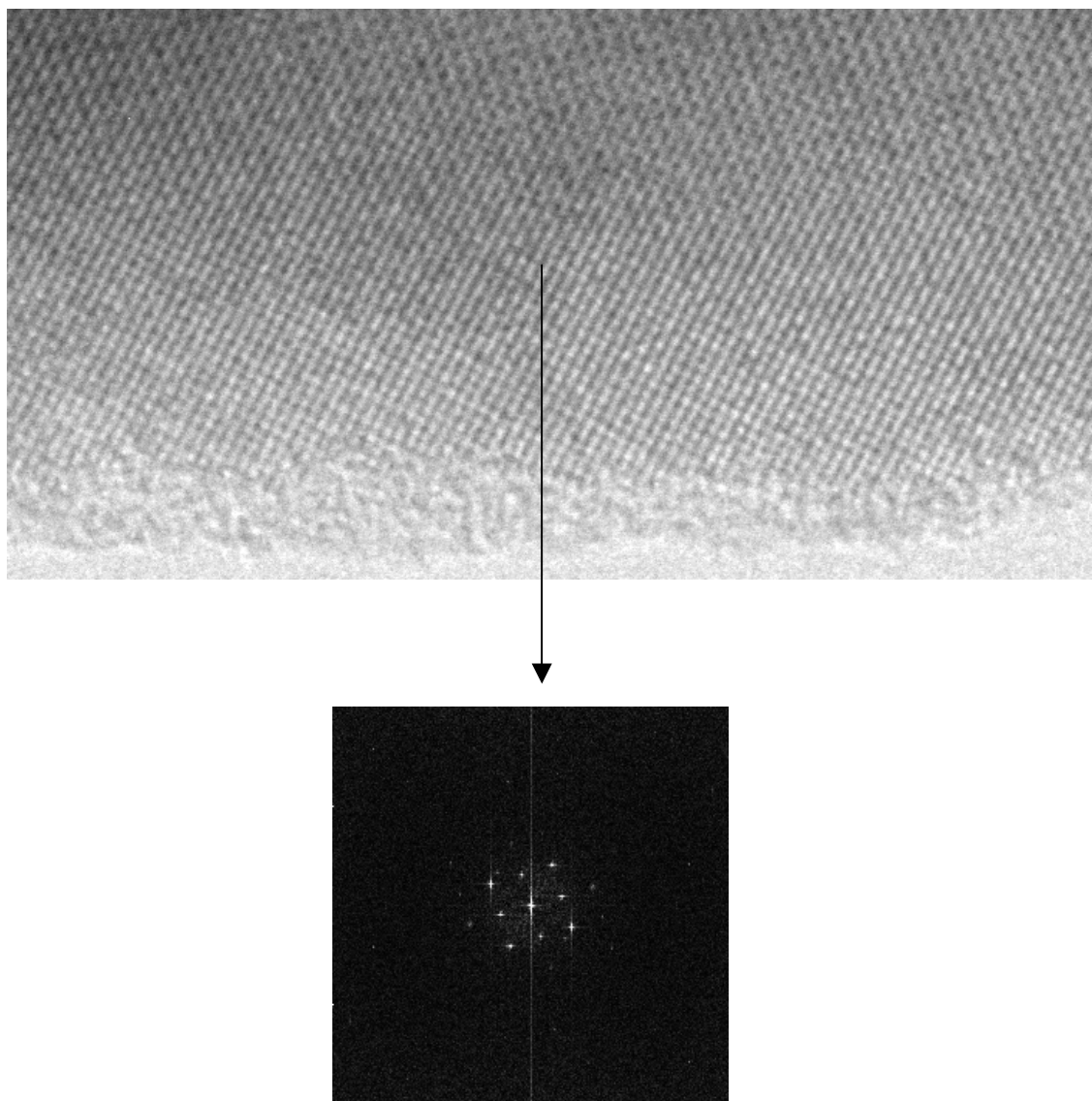


Fig. 43. HRTEM image of a thin crystallite from $\text{Na}_{0.6}\text{Mo}_{0.2}\text{W}_{0.8}\text{O}_3$ powder sample with corresponding DP pattern processed with the CRISP program

3.7 Characterisation of $\text{Cs}_x\text{Nb}_y\text{W}_{1-y}\text{O}_3$ system where $x = 0.25, 0.3$ and $y = 0.00 - 0.2$ and $\text{Rb}_x\text{Nb}_y\text{W}_{1-y}\text{O}_3$ system where $x = 0.3$ and $y = 0.00 - 0.175$

The X-ray powder diffraction patterns (Philips Diffractometer) of $\text{Cs}_{0.25}\text{Nb}_y\text{W}_{1-y}\text{O}_3$ and $\text{Cs}_{0.3}\text{Nb}_y\text{W}_{1-y}\text{O}_3$ system of series 10 are given in Fig. 44 and Fig. 45, respectively. In Fig. 44 the X-ray diffraction pattern of nominal $\text{Cs}_{0.25}\text{WO}_3$ is identified mainly as HTB-I type bronze phase by the peaks 100 ($2\theta^\circ$ at about 13.85), 002 ($2\theta^\circ$ at about 23.53), 110 ($2\theta^\circ$ at about 24.04), 111 ($2\theta^\circ$ at about 26.80), 102 ($2\theta^\circ$ at about 27.38), 200 ($2\theta^\circ$ at about 27.83), 112 ($2\theta^\circ$ at about 33.87) and 202 ($2\theta^\circ$ at about 36.73) in presence of few weak lines of unknown phase at about 24.25, 26.25, 31.15 and 32.62 2-theta position. However, these weak lines of unknown phase in the X-ray diffraction pattern disappear in presence of niobium. For $y = 0.05$ the X-ray pattern can be identified as single phase of HTB-I type bronze phase with the peaks as observed for the sample $\text{Cs}_{0.25}\text{WO}_3$ HTB-I type phase. For $y = 0.1$ and 0.15 samples were identified mainly as HTB-I type bronze phase in presence of some weak lines in different 2-theta position. The intensity of these weak lines increases with increasing niobium content. As for example the sample with $y = 0.2$ shows many weak lines which were indexed as $\text{Cs}_{0.2}\text{Nb}_{0.2}\text{W}_{0.8}\text{O}_3$ HTB-II type oxidized phase [119] with the peaks 002 ($2\theta^\circ$ at about 22.5), 102 ($2\theta^\circ$ at about 26.59), 200 ($2\theta^\circ$ at about 27.94) and 112 ($2\theta^\circ$ at about 33.24).

In Fig. 45 it can be seen that the X-ray powder pattern of nominal $\text{Cs}_{0.3}\text{WO}_3$ shows a pure HTB-I type bronze phase with the peaks 100 ($2\theta^\circ$ at about 13.86), 002 ($2\theta^\circ$ at about 23.49), 110 ($2\theta^\circ$ at about 24.09), 111 ($2\theta^\circ$ at about 26.82), 102 ($2\theta^\circ$ at about 27.35), 200 ($2\theta^\circ$ at about 27.85), 112 ($2\theta^\circ$ at about 33.85) and 202 ($2\theta^\circ$ at about 36.71). For $y = 0.05$ the X-ray pattern also identified as pure HTB-I type bronze phase with the peaks as observed for $y = 0.0$. However, for $y = 0.1$ and 0.15 samples are identified mainly as HTB-I type bronze phase in presence of some weak lines in different 2-theta position. The intensity of these weak lines increases with increasing niobium content. The sample with $y = 0.15$ shows many weak lines at about 2-theta 22.56, 26.51, 28.48, 33.18 and 36.19 positions. Most of these extra weak lines were identified as a $\text{Cs}_{0.2}\text{Nb}_{0.2}\text{W}_{0.8}\text{O}_3$ HTB-II type phase with the peaks 002 ($2\theta^\circ$ at about 22.56), 102 ($2\theta^\circ$ at about 26.51) and 112 ($2\theta^\circ$ at about 33.18). Two very weak reflections at about 28.48 and 29.80 2-theta positions are also observed. These two weak reflections correspond to $\text{Cs}_{0.35}\text{Nb}_{0.35}\text{W}_{0.65}\text{O}_3$ pyrochlore type phase listed [119] in the JCPDS index.

The results of the X-ray powder analysis (Guinier) of all niobium doped cesium tungsten bronzes, $\text{Cs}_x\text{Nb}_y\text{W}_{1-y}\text{O}_3$ of series 10 are given in table 6. Results obtained from Rietveld

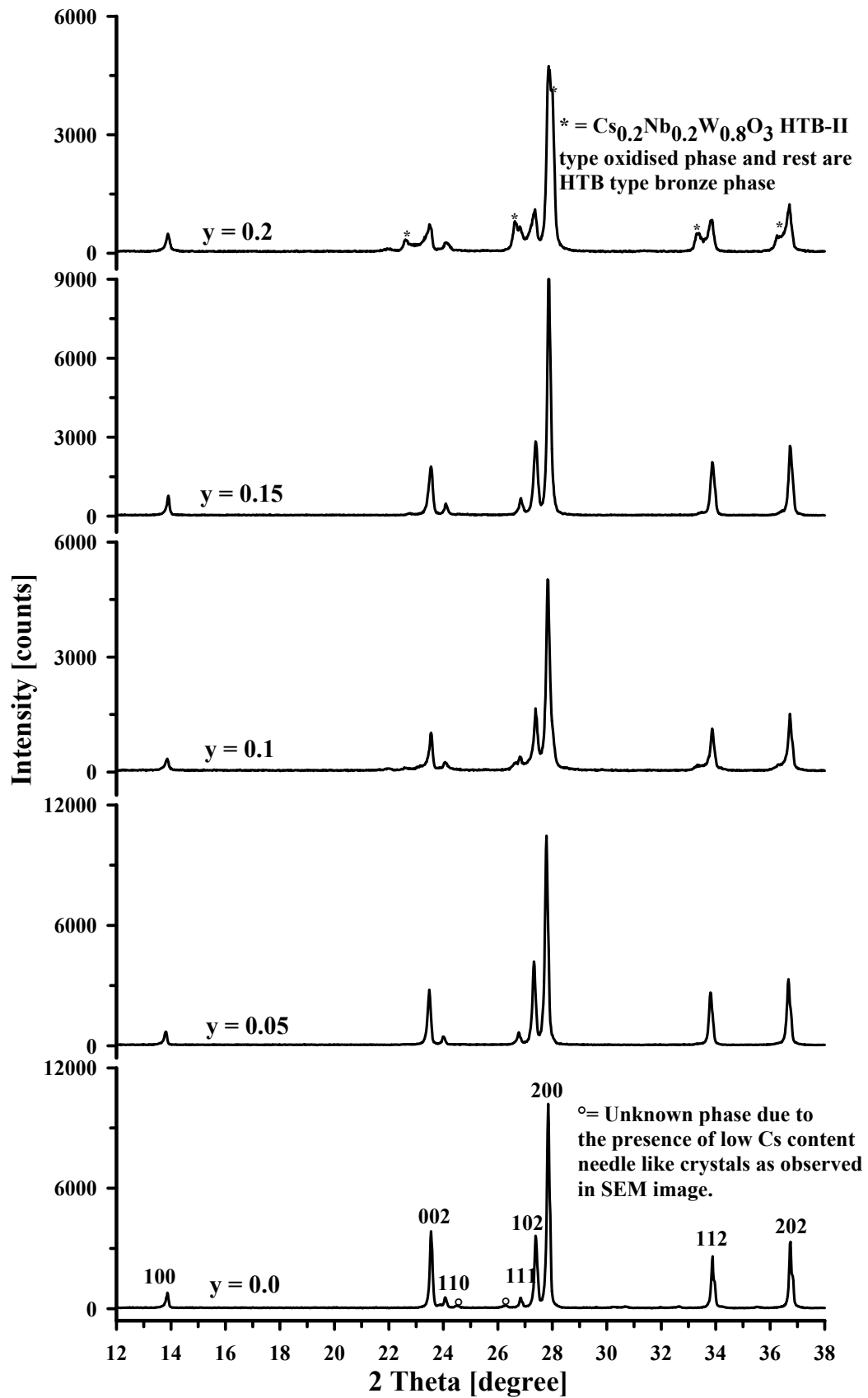


Fig.44. X-ray powder diffraction patterns of $\text{Cs}_{0.25}\text{Nb}_y\text{W}_{1-y}\text{O}_3$ system with $y = 0.0 - 0.2$ as denoted.

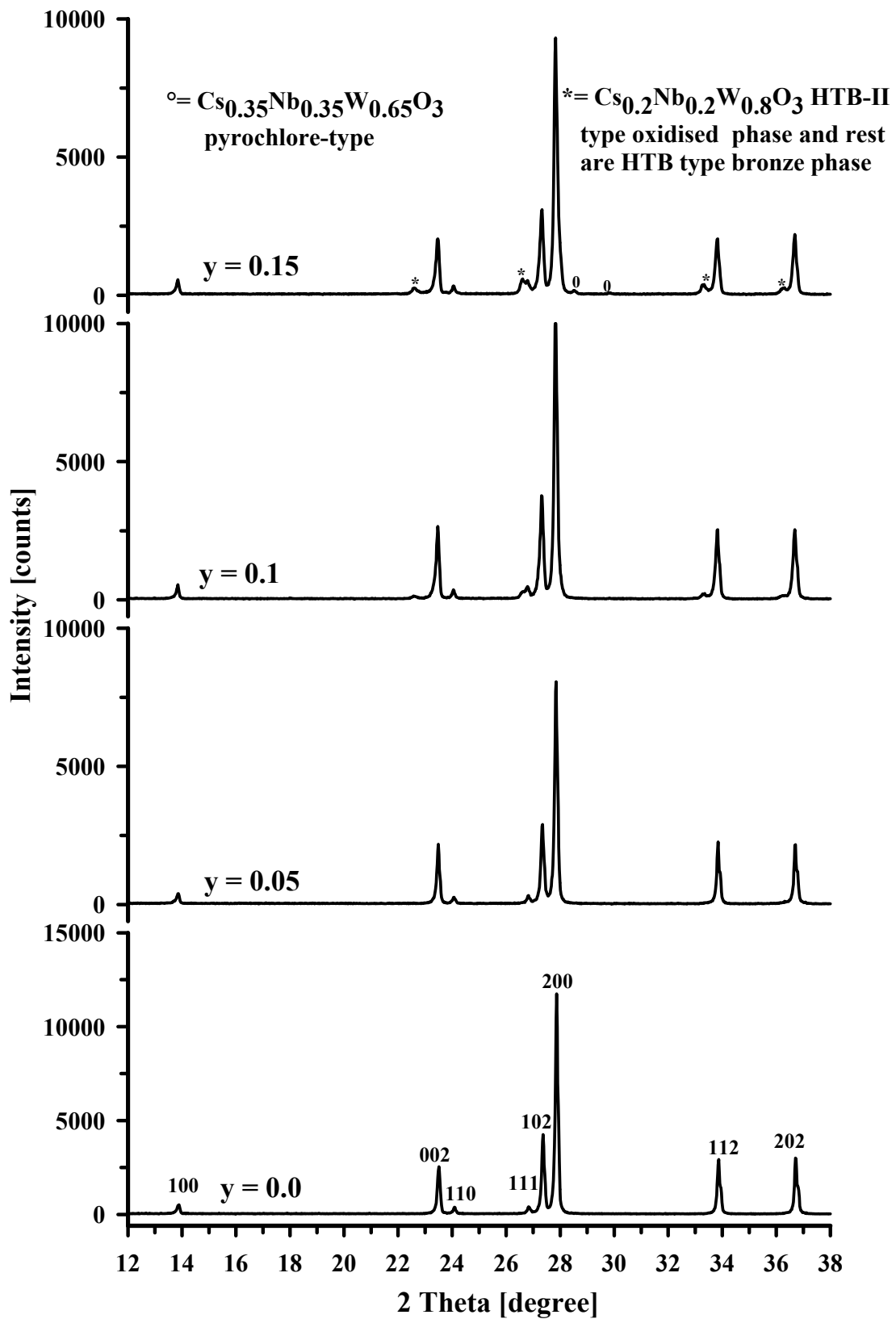


Fig.45. X-ray powder diffraction patterns of $\text{Cs}_{0.3}\text{Nb}_y\text{W}_{1-y}\text{O}_3$ system with $y = 0.0 - 0.15$ as denoted.

refinements of series 10 are also given in table 6. From this table it can be seen that the cell parameters and phase obtained from Guinier method are in good agreement with the results obtained from Rietveld method. Additionally, by the Rietveld method the percentage of the main HTB-I type bronze phase and HTB-II type oxidized phase was calculated as given in table 6. From the Rietveld refinement results it can be seen that when nominal Nb = 0.1 the main HTB type bronze phase is about 95% and the extra phase is about 5%. For nominal Nb = 0.15, the main HTB type phase is about 86% - 88% and the extra phase is about 12% - 14%. For nominal Nb = 0.2, the main HTB type phase is about 64% and the extra phase is about 36%. These refinements were carried out in $P6_3/mcm$ (No. 193) with Cs at (0, 0, 0) position. Alternative refinements are also possible by using $P6_322$ (No. 182) with splitting of Cs atom on $4e$ (0, 0, 0.22) position.

The lattice parameters of the extra HTB- II type [Table 6] oxidized phase significantly differ compared to the typical values of the Cs-HTB type bronze phase. All these X-ray results are supported by SEM and TEM microanalysis. The minimum, maximum and the average value of Cs and Nb according to SEM and TEM microanalysis for each sample are also given in table 6. For an example, the SEM/EDX and TEM/EDX analysis of nominal $Cs_{0.25}WO_3$, shows that the minimum content of x is 0.04 and 0.06 respectively as given in table 6, which are responsible for the unknown weak lines in the X-ray pattern. However, in most cases it can be seen in table 6, that the average value of x and y according to SEM and TEM microanalysis are nearly the same value as starting composition of each sample. A large number of ED pattern has been taken for some sample of series 10. They also confirm the unit cell dimensions obtained from the X-ray study.

The SEM image and the distribution of the SEM/EDX and TEM/EDX analysis made on crystals of $Cs_{0.25}Nb_yW_{1-y}O_3$ ($y = 0.00 - 0.2$) and $Cs_{0.3}Nb_yW_{1-y}O_3$ ($y = 0.00 - 0.15$) systems are given in fig. 46 and 47 in details. The microanalysis of $Cs_{0.25}Nb_yW_{1-y}O_3$ system gives some information about the homogeneity of the samples. A small local variation in Cs and Nb content is observed by ED/EDX method for some crystals of this system. But most of the crystals shows nearly no local variation. The microanalysis results, thus indicate that the fragments from $Cs_{0.25}WO_3$ sample contain some needle like crystal with a low Cs concentration $x = 0.04 - 0.05$, which are therefore, not HTB type [Fig. 46a]. But most of the crystals contain higher amount of Cs corresponding to a HTB type bronze phase with almost

Table 6. X-ray and electron microscopy results of the system $Cs_xNb_yW_{1-y}O_3$
($x = 0.25, 0.3; y = 0.05 - 0.2$)

Starting Composition	Phase observed (Guinier and philips Diffractometer) and Percentage of phase calculated by Rietveld method.	Cell parameters (Å)		EDX analysis			
		Güinier method	Rietveld method	SEM		TEM	
				$X_{min}-X_{max}$, X_{avg}	$Y_{min}-Y_{max}$, Y_{avg}	$X_{min}-X_{max}$, X_{avg}	$Y_{min}-Y_{max}$, Y_{avg}
$Cs_{0.25}WO_3$	HTB-I + 2-3 very weak extra line	a = 7.4163(15) c = 7.5808(12)	a = 7.4216(01) c = 7.5840(01)	0.04 - 0.26, 0.24	-	0.06 - 0.32, 0.24	-
$Cs_{0.25}Nb_{0.05}W_{0.95}O_3$	HTB-I	a = 7.4173(17) c = 7.5821(18)	a = 7.4247(01) c = 7.5885(01)	0.06 - 0.33, 0.22	0.01 - 0.06, 0.04	-	-
$Cs_{0.25}Nb_{0.1}W_{0.9}O_3$	HTB-I (about 95.8 %)	a = 7.4169(20) c = 7.5913(24)	a = 7.4125(14) c = 7.5875(11)	0.06 - 0.26, 0.22	0.02 - 0.14 0.06	0.22 - 0.31, 0.26	0.04 - 0.08, 0.06
	+traces of HTB - II (about 4.2 %)	-	a = 7.3706(84) c = 7.7976(94)				
$Cs_{0.25}Nb_{0.15}W_{0.85}O_3$	HTB-I (about 88.47 %)	a = 7.4124(09) c = 7.5998(19)	a = 7.4031(15) c = 7.6017(11)	0.26 - 0.3, 0.27	0.1 - 0.2, 0.14	0.25 - 0.32, 0.31	0.09 - 0.24, 0.1
	+HTB - II (about 11.53 %)	a = 7.3731(08) c = 7.8960(08)	a = 7.3693(37) c = 7.8187(39)				
$Cs_{0.25}Nb_{0.2}W_{0.8}O_3$	HTB-I (about 64.17%)	a = 7.4155(22) c = 7.6080(32)	a = 7.4044(12) c = 7.6085(10)	-	-	0.29 - 0.36, 0.31	0.08-0.4 0.19
	+ HTB- II (about 35.83%)	-	a = 7.3689(16) c = 7.8460(16)				
$Cs_{0.3}WO_3$	HTB-I	a = 7.4144(20) c = 7.5923(16)	a = 7.4178(01) c = 7.5982(01)	0.29-0.37 0.31	-	0.34 - 0.38 0.36	-
$Cs_{0.3}Nb_{0.05}W_{0.95}O_3$	HTB-I	a = 7.4099(14) c = 7.5849(08)	a = 7.4175(01) c = 7.5982(01)	0.29 - 0.4 0.34	0.04 - 0.1 0.07	-	-
$Cs_{0.3}Nb_{0.1}W_{0.9}O_3$	HTB-I (about 94.8 %)	a = 7.4178(19) c = 7.6043(27)	a = 7.4113(07) c = 7.5979(05)	0.29 - 0.4 0.33	0.03 - 0.18 0.10	-	-
	+ traces of HTB II (about 5.2 %)	-	a = 7.3799(43) c = 7.8699(46)				
$Cs_{0.3}Nb_{0.15}W_{0.85}O_3$	HTB-I (about 86.44%)	a = 7.4221(15) c = 7.5953(17)	a = 7.4144(05) c = 7.5987(04)	0.28 - 0.3 0.30	0.04 - 0.23 0.14	-	-
	+HTB -II (about 13.56%)	a = 7.3804(04) c = 7.8929(02)	a = 7.3770(15) c = 7.8707(15)				

fully occupied hexagonal tunnel sites. However, from X-ray pattern and even from this microanalysis and from SEM image, it can be seen that with increasing Nb content, as for example $Nb \geq 0.1$ this low Cs content needle like crystals disappear [Fig. 46c]. With high Nb content, for example the nominal $Cs_{0.25}Nb_{0.2}W_{0.8}O_3$ sample shows that some crystals contain around $Cs = 0.3$ and $Nb = 0.05 - 0.15$ which belongs to HTB-I type bronze phase, whereas some crystal contain high amount of Cs and Nb, which may be belong to HTB-II type phase. But in most cases, it was not possible to identify the phase separation.

$Cs_{0.25}WO_3$

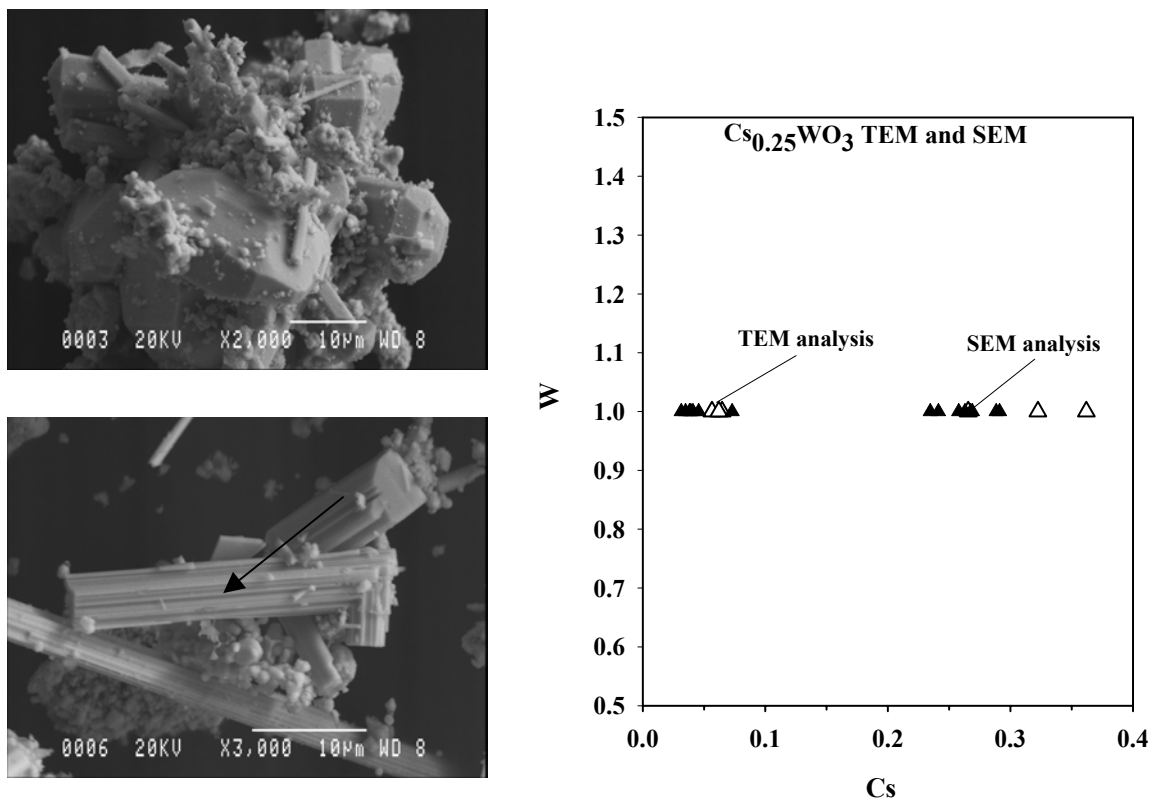


Fig. 46a. SEM image of nominal $Cs_{0.25}WO_3$ sample showing the typical HTB type crystals together with some needle like crystals. Some polycrystalline powder also present. HTB type crystals containing high Cs ($x = 0.23 - 0.34$) whereas the needle crystals containing very low Cs ($x = 0.03 - 0.08$). The TEM/EDX analysis results denoted by open triangle and SEM/EDX analysis results denoted by filled triangle in the same diagram. Each filled triangle point represent the mean of two or three measurements on the same crystal. The value of the Cs is calculated from the signal intensities as $Cs = Cs / W$.

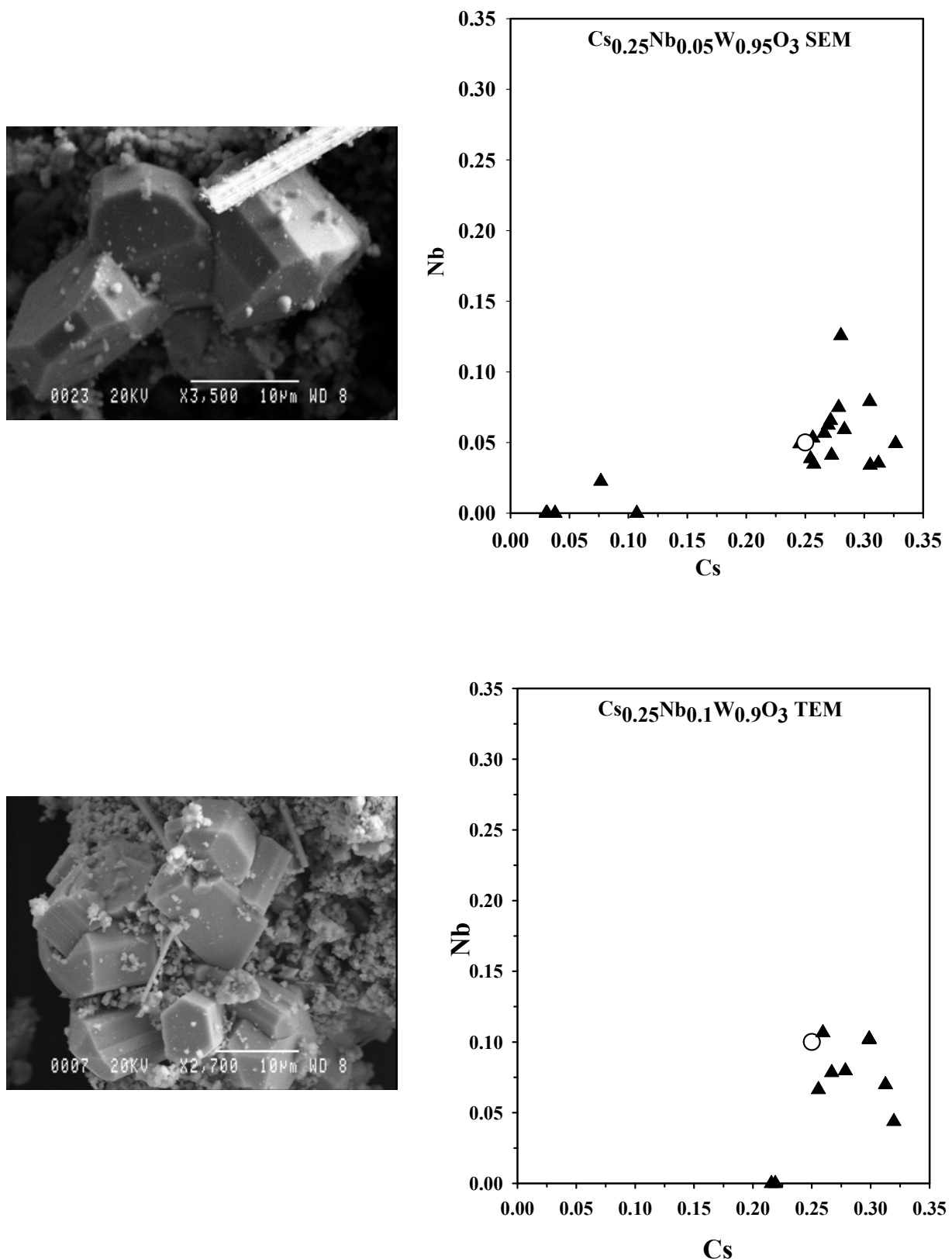


Fig. 46b. SEM image of nominal $\text{Cs}_{0.25}\text{Nb}_{0.05}\text{W}_{0.95}\text{O}_3$ (up) and $\text{Cs}_{0.25}\text{Nb}_{0.1}\text{W}_{0.9}\text{O}_3$ (down) sample showing the typical HTB type crystals together with some needle like crystals. Some polycrystalline powder also present. The HTB like bronze crystals are containing Cs about 0.23 to 0.34 and Nb about 0.0 to 0.15 as shown in the EDX analysis diagram. The nominal composition of $\text{Cs}_{0.25}\text{Nb}_{0.05}\text{W}_{0.95}\text{O}_3$ and $\text{Cs}_{0.25}\text{Nb}_{0.1}\text{W}_{0.9}\text{O}_3$ are shown in the diagram by open circle. Each filled triangle point represent the mean of two or three measurements on the same crystal. The value of the Cs and Nb are calculated from the signal intensities as $\text{Cs} = \text{Cs} / (\text{Nb} + \text{W})$ and $\text{Nb} = \text{Nb} / (\text{Nb} + \text{W})$.

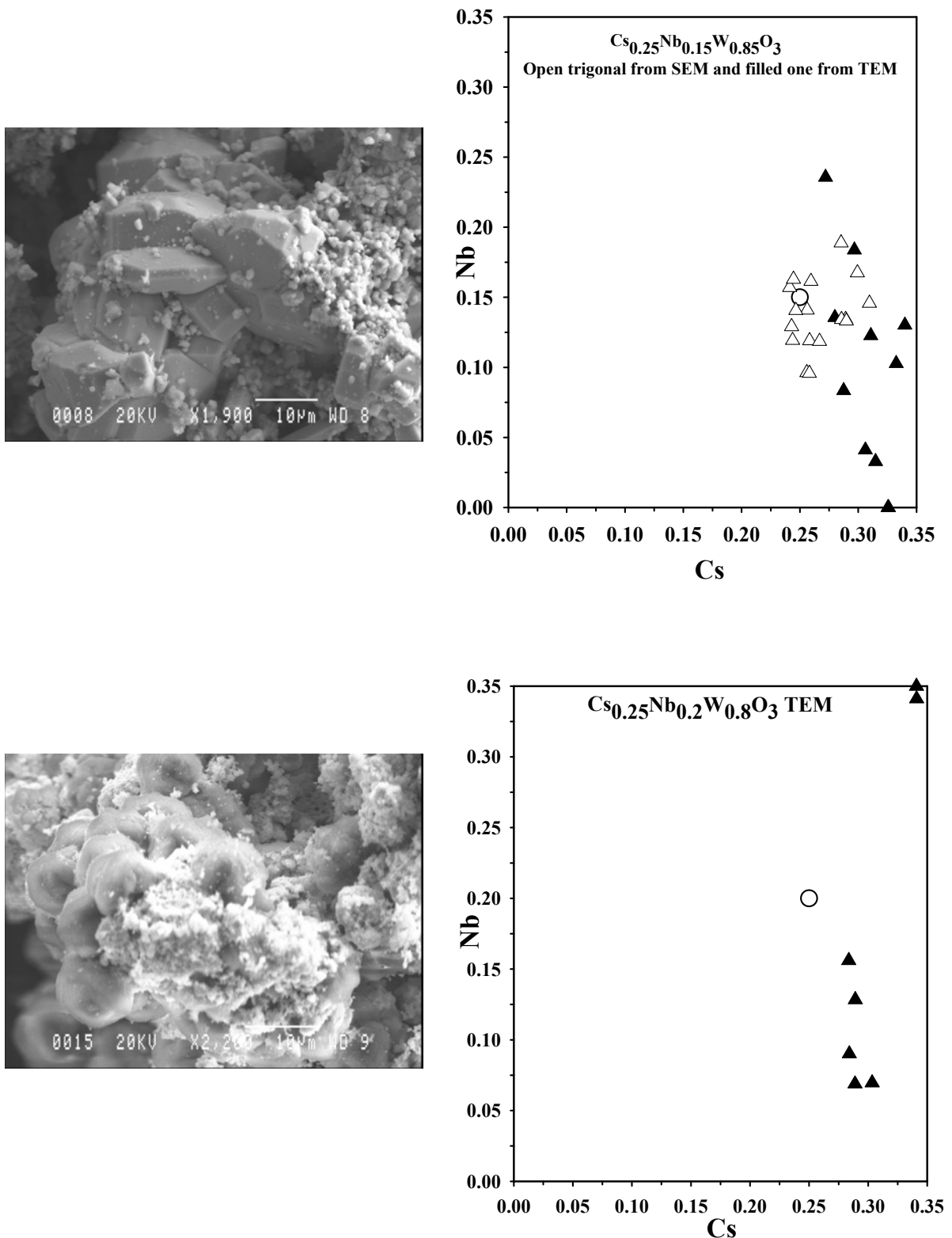
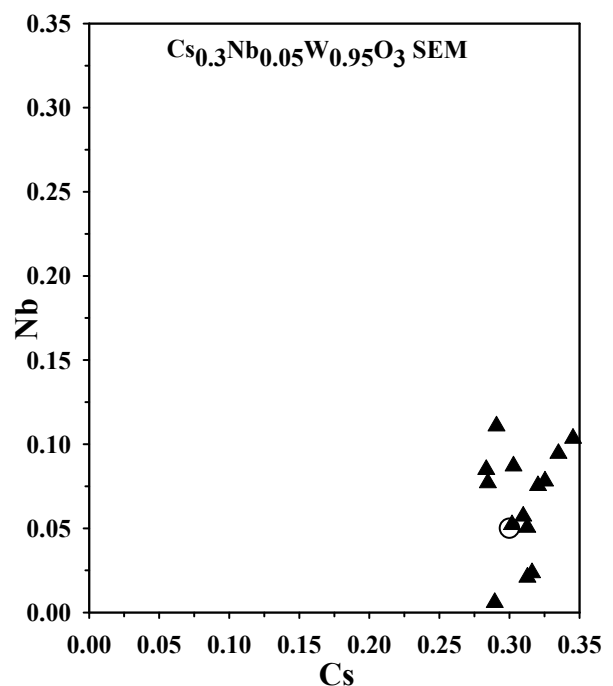
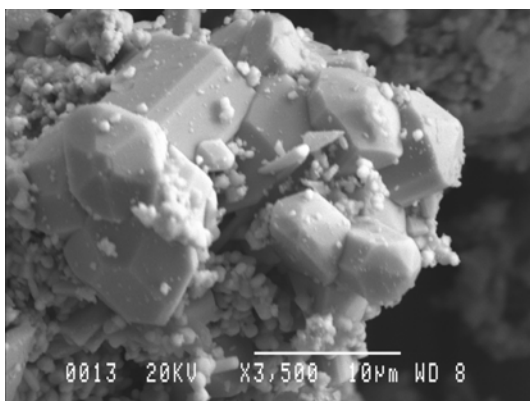
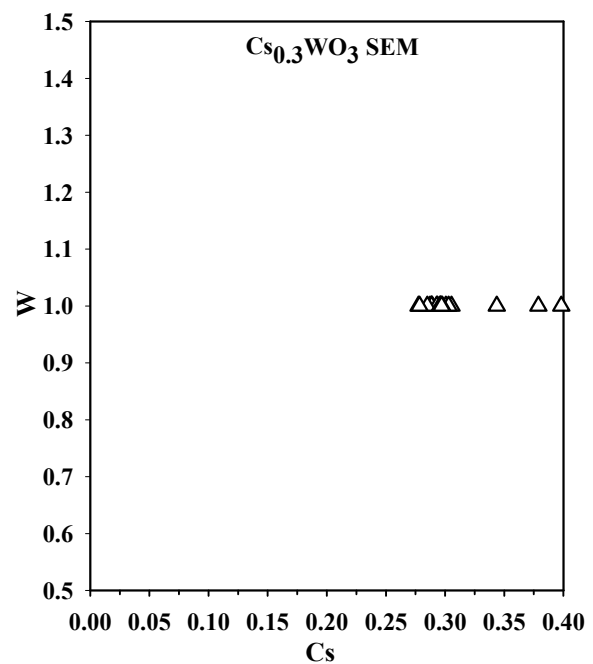
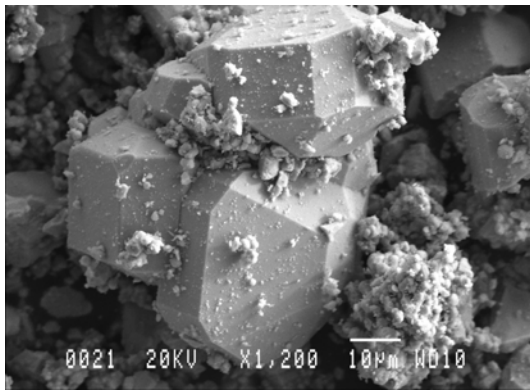


Fig. 46c. SEM image of nominal $\text{Cs}_{0.25}\text{Nb}_{0.15}\text{W}_{0.85}\text{O}_3$ (up) and $\text{Cs}_{0.25}\text{Nb}_{0.2}\text{W}_{0.8}\text{O}_3$ (down) sample showing the typical HTB type crystals together with some polycrystalline powder. The HTB like bronze crystals are containing Cs about 0.23 to 0.34 and Nb about 0.0 to 0.15 as shown in the EDX analysis diagram. The nominal composition of $\text{Cs}_{0.25}\text{Nb}_{0.05}\text{W}_{0.95}\text{O}_3$ and $\text{Cs}_{0.25}\text{Nb}_{0.1}\text{W}_{0.9}\text{O}_3$ are shown in the diagram by open circle. Each filled triangle point represent the mean of two or three measurements on the same crystal. The value of the Cs and Nb are calculated from the signal intensities as $\text{Cs} = \text{Cs} / (\text{Nb} + \text{W})$ and $\text{Nb} = \text{Nb} / (\text{Nb} + \text{W})$.

For $\text{Cs}_{0.3}\text{Nb}_y\text{W}_{1-y}\text{O}_3$ ($y = 0.00 - 0.15$) system it can be seen from the SEM image that some crystals are bigger in size whereas some are small. All these big crystals have the same size and shape containing the same composition as observed on EDX quantitative analysis [Fig. 47]. X-ray powder diffraction and transmission electron microscope (TEM) studies of the sample $\text{Cs}_{0.3}\text{WO}_3$ suggests the fully occupied tunnels for this sample. With high Nb content, for example the nominal $\text{Cs}_{0.3}\text{Nb}_{0.15}\text{W}_{0.8}\text{O}_3$ sample shows that some crystal contain around Cs = 0.3 and Nb = 0.05 – 0.15 which belongs to HTB-I type bronze phase, whereas some crystals contain higher amount of Cs and Nb which could belong to HTB-II type phase. But in most cases it was also not possible to identify the phase separation.



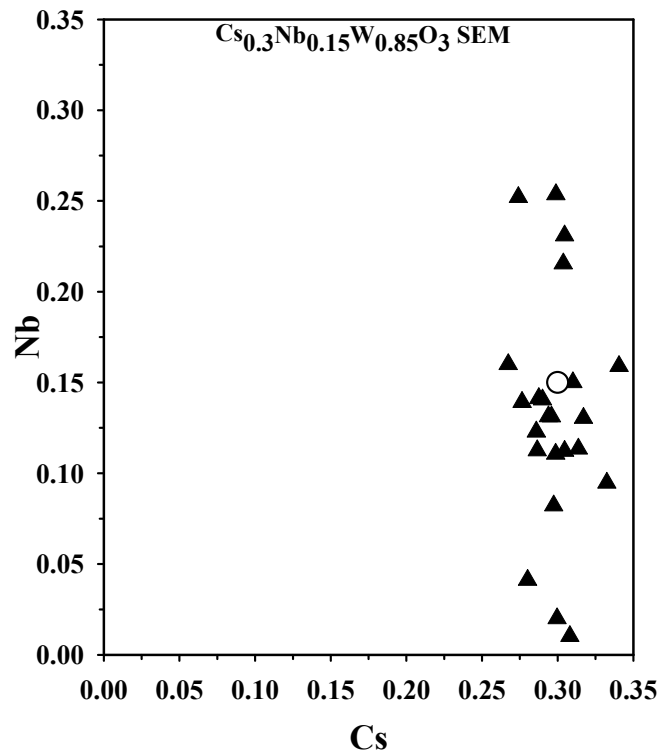
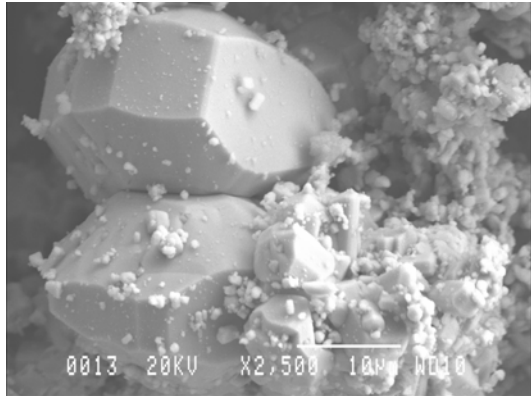
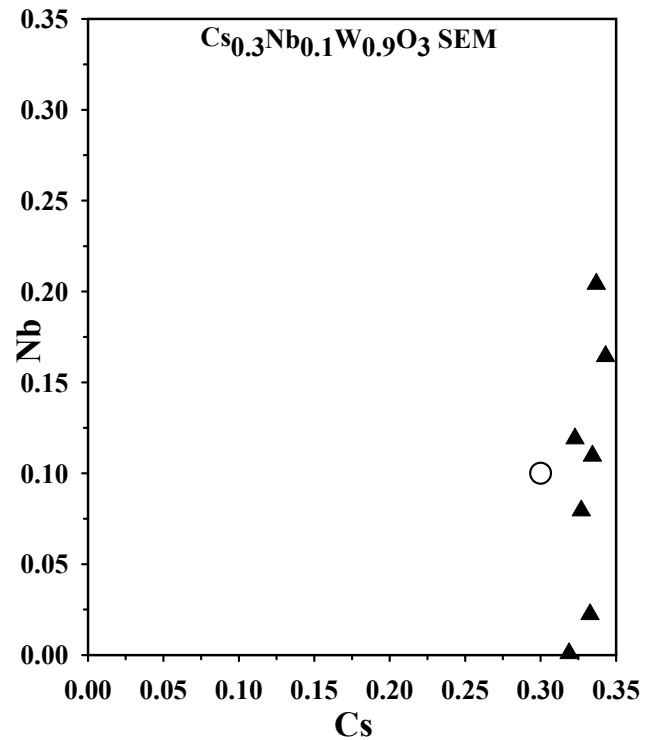
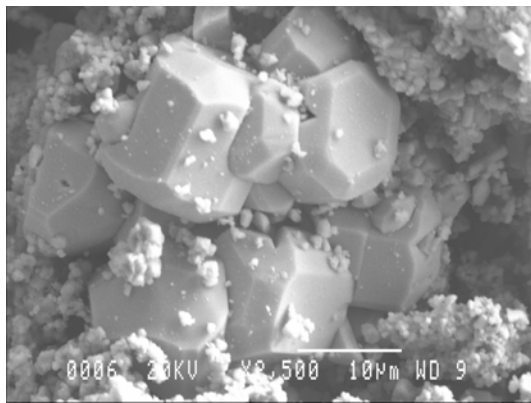


Fig. 47. SEM image of $\text{Cs}_{0.3}\text{Nb}_y\text{W}_{1-y}\text{O}_3$ system with $y = 0.0 - 0.15$ showing the typical HTB type bronze crystals together with some polycrystalline powder. HTB type bronze crystals containing $\text{Cs} = 0.25 - 0.34$ and $\text{Nb} = 0.0 - 0.15$ as shown in the EDX analysis diagram. Crystals with $\text{Nb} \geq 0.15$ are belongs to oxidised HTB-II type phase, which is difficult to see in the SEM image. The nominal composition of the sample of $\text{Cs}_{0.3}\text{Nb}_y\text{W}_{1-y}\text{O}_3$ with $y = 0.0 - 0.15$, denoted by open circle in the diagram. Each triangle point represent the mean of two or three measurements on the same crystal. The value of the Cs and Nb are calculated from the signal intensities as $\text{Cs} = \text{Cs} / (\text{Nb} + \text{W})$ and $\text{Nb} = \text{Nb} / (\text{Nb} + \text{W})$.

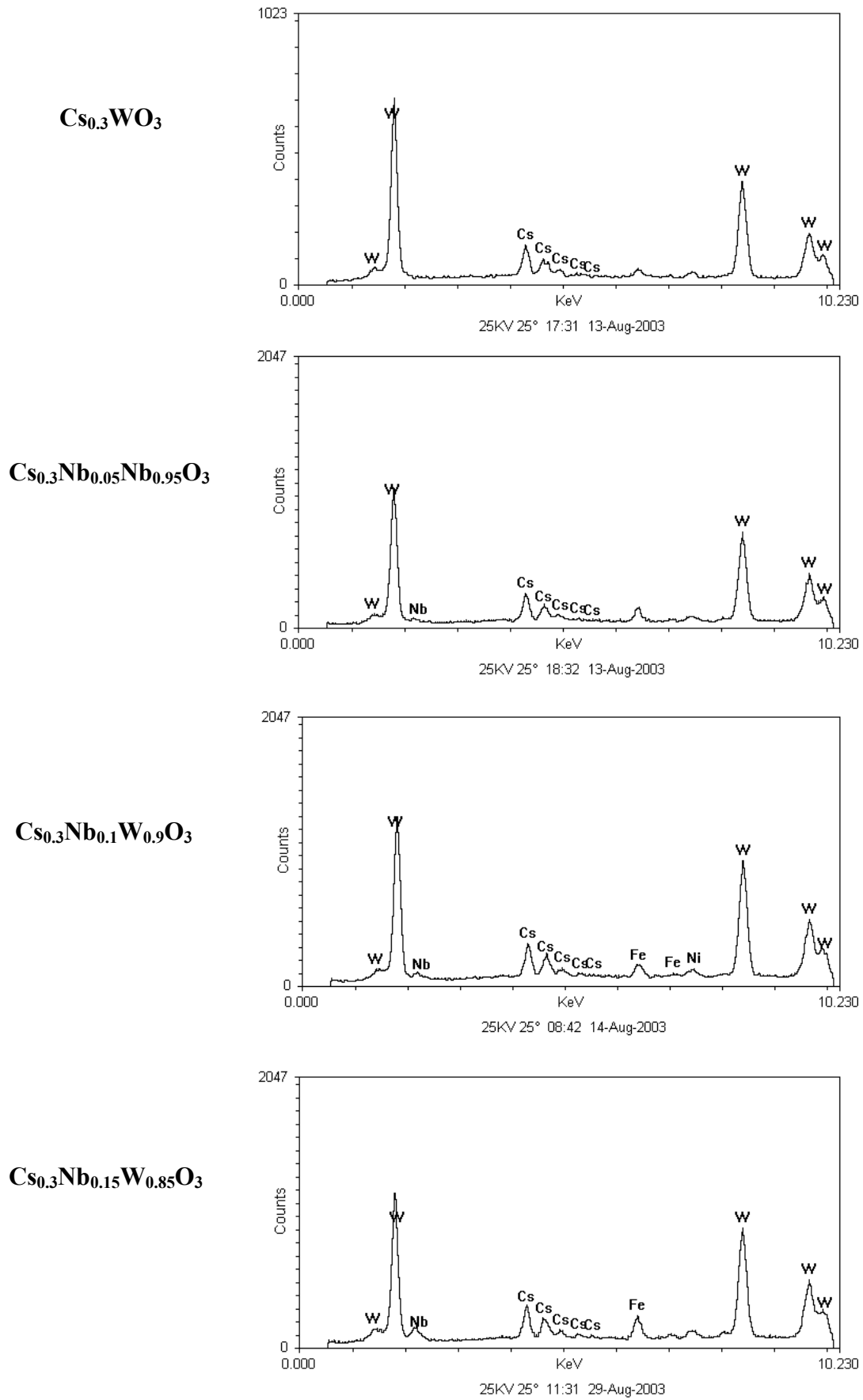


Fig. 48a. Typical EDX spectra of $\text{Cs}_{0.3}\text{Nb}_y\text{W}_{1-y}\text{O}_3$ system with $y = 0.0 - 0.15$.

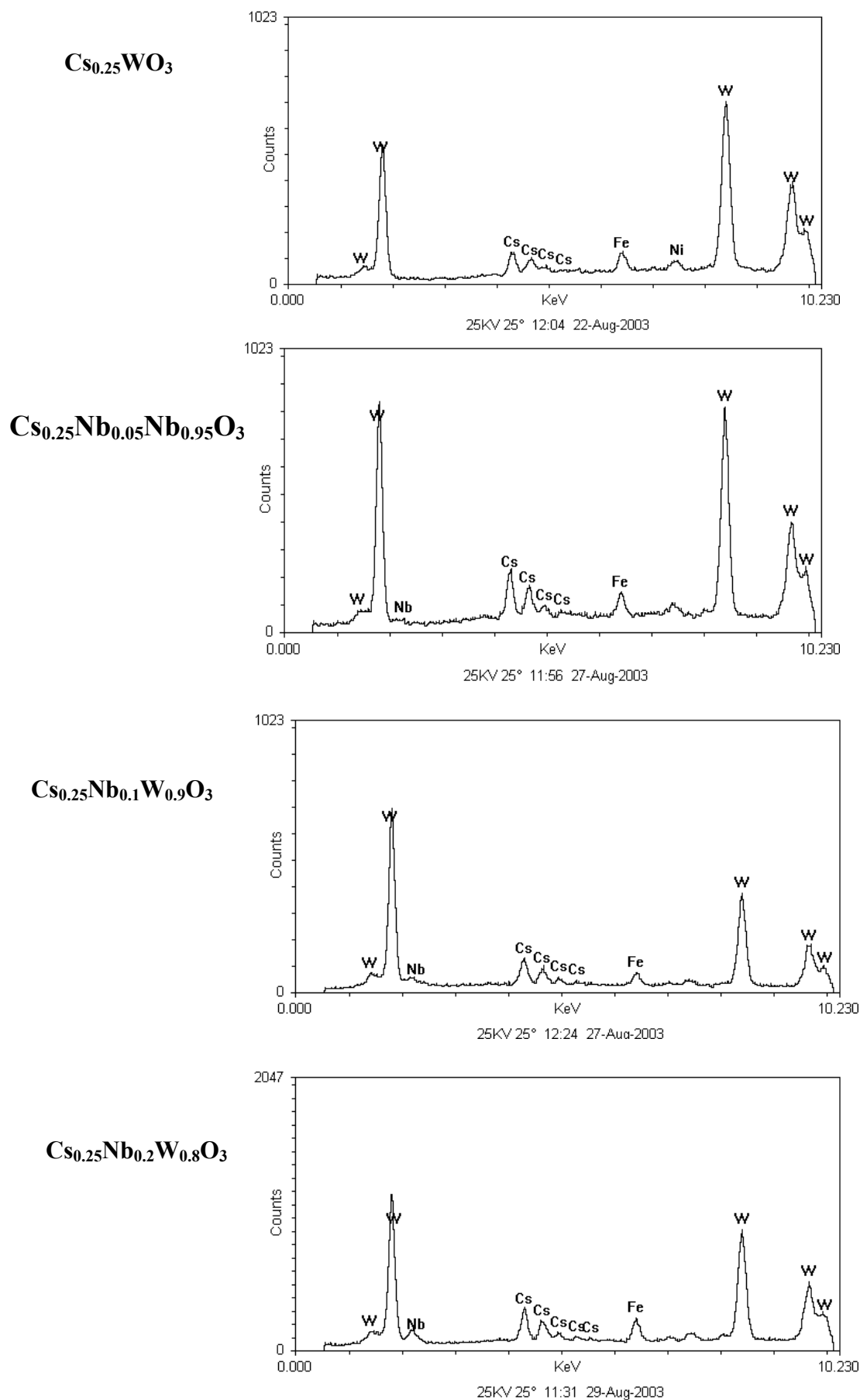


Fig. 48b. Typical EDX spectra of $\text{Cs}_{0.25}\text{Nb}_y\text{W}_{1-y}\text{O}_3$ system with $y = 0.0 - 0.2$.

The combined ED and EDX studies in thin crystal fragments from the samples of different batches in the TEM microscope confirmed that the tungsten bronze of HTB structure types were the dominating phase in the bulk product. The ED pattern taken from the HTB crystals in (001) and (100) orientations did not show any streaking effect of the reflections or any additional superstructure spots. But very few crystals with high niobium content showed streaking effect which may be related to oxidized HTB-II type phase.

Fig. 48a and 48b show the typical EDX spectra of the samples of $\text{Cs}_{0.3}\text{Nb}_y\text{W}_{1-y}\text{O}_3$ and $\text{Cs}_{0.25}\text{Nb}_y\text{W}_{1-y}\text{O}_3$ systems respectively. The presence of small amount of Nb can be seen clearly in the spectra.

The IR-absorption spectra between 375 cm^{-1} and 2000 cm^{-1} as obtained for $\text{Cs}_{0.25}\text{Nb}_y\text{W}_{1-y}\text{O}_3$ and $\text{Cs}_{0.3}\text{Nb}_y\text{W}_{1-y}\text{O}_3$ systems of series 10 are shown in Fig. 49. For $y = 0.0$, the IR-spectra

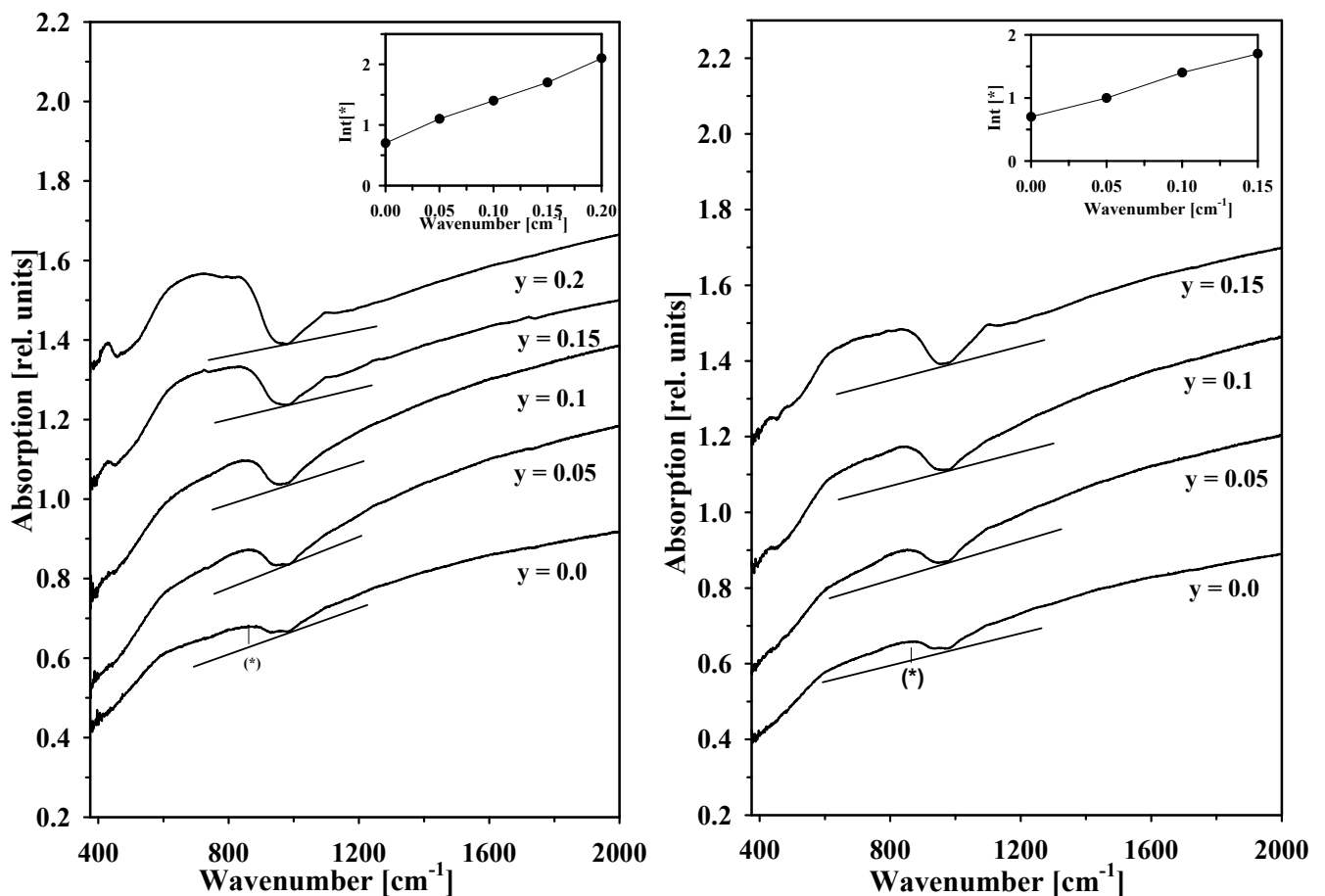


Fig. 49. IR absorption spectra (KBr-method) of $\text{Cs}_{0.25}\text{Nb}_y\text{W}_{1-y}\text{O}_3$ (left) and $\text{Cs}_{0.3}\text{Nb}_y\text{W}_{1-y}\text{O}_3$ (right) system. Spectra are shifted vertically against each other for better comparison. Vertical line marks wavenumber position at which the intensities (int^*) relative to an extrapolated background line as indicated by solid lines were measured. Insert: The dependence of (int^*) on niobium content y .

show only a weak broad phonon absorption band below 1000 cm^{-1} . However, for $y > 0.05$, the intensity of this broad phonon absorption band increases with increasing niobium content. For $y \geq 0.15$, the IR-spectra show a small peak at about 1100 cm^{-1} . The absorption peak can be explained by HTB-II type oxidized phase.

The optical reflectivity of the powder sample of series 10 were measured in the range 4000 cm^{-1} to 22000 cm^{-1} are given in Fig. 50. For $y = 0.0$ the sample show two minima at about 16000 cm^{-1} and 10000 cm^{-1} . This minimum feature in the reflectivity becomes weaker and

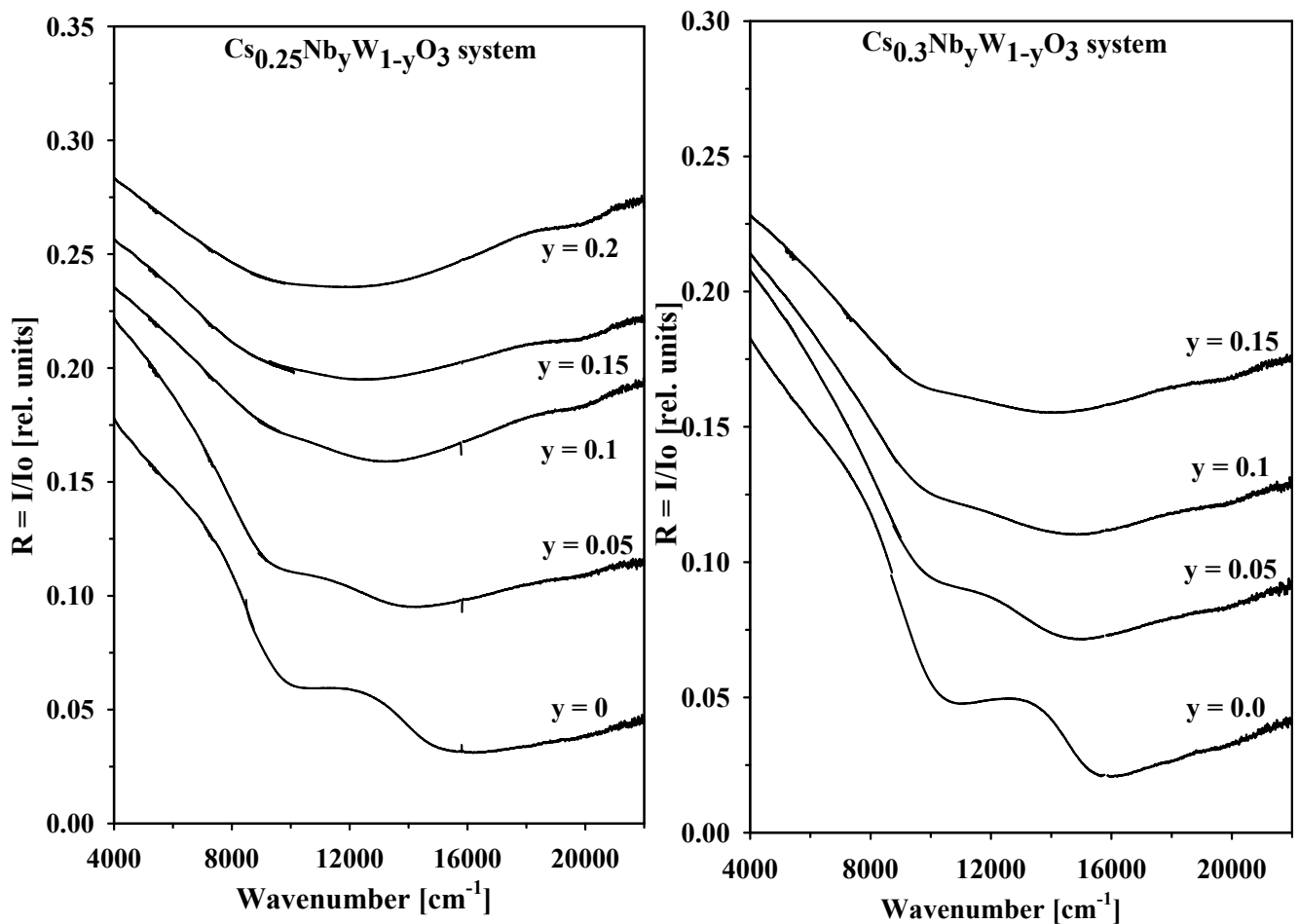


Fig.50. Reflection spectra of powder samples of $\text{Cs}_{0.25}\text{Nb}_y\text{W}_{1-y}\text{O}_3$ (left) and $\text{Cs}_{0.3}\text{Nb}_y\text{W}_{1-y}\text{O}_3$ (right) system with $y = 0.0 - 0.2$ as denoted. Spectra are shifted vertically against each other for better comparison.

shifted to lower wavenumber with increasing niobium content. For $y > 0.1$ the minimum structures become less significant and there is nearly no shift in position because of the dilution by the oxidised phase, whereas for $y < 0.1$ a doping effect could be indicated.

A HRTEM image of a thin crystal of nominal $\text{Cs}_{0.25}\text{Nb}_{0.1}\text{W}_{0.9}\text{O}_3$ projected along $[010]$ is shown in fig. 51. The image shows a misfit layer along b direction which can not be seen in the hexagonal c direction. The corresponding ED pattern was taken from the different part of the image. The ED pattern from the image including the defect part shows the streaking effect whereas, the DP pattern from the other part shows the HTB pattern without any streaking effect.

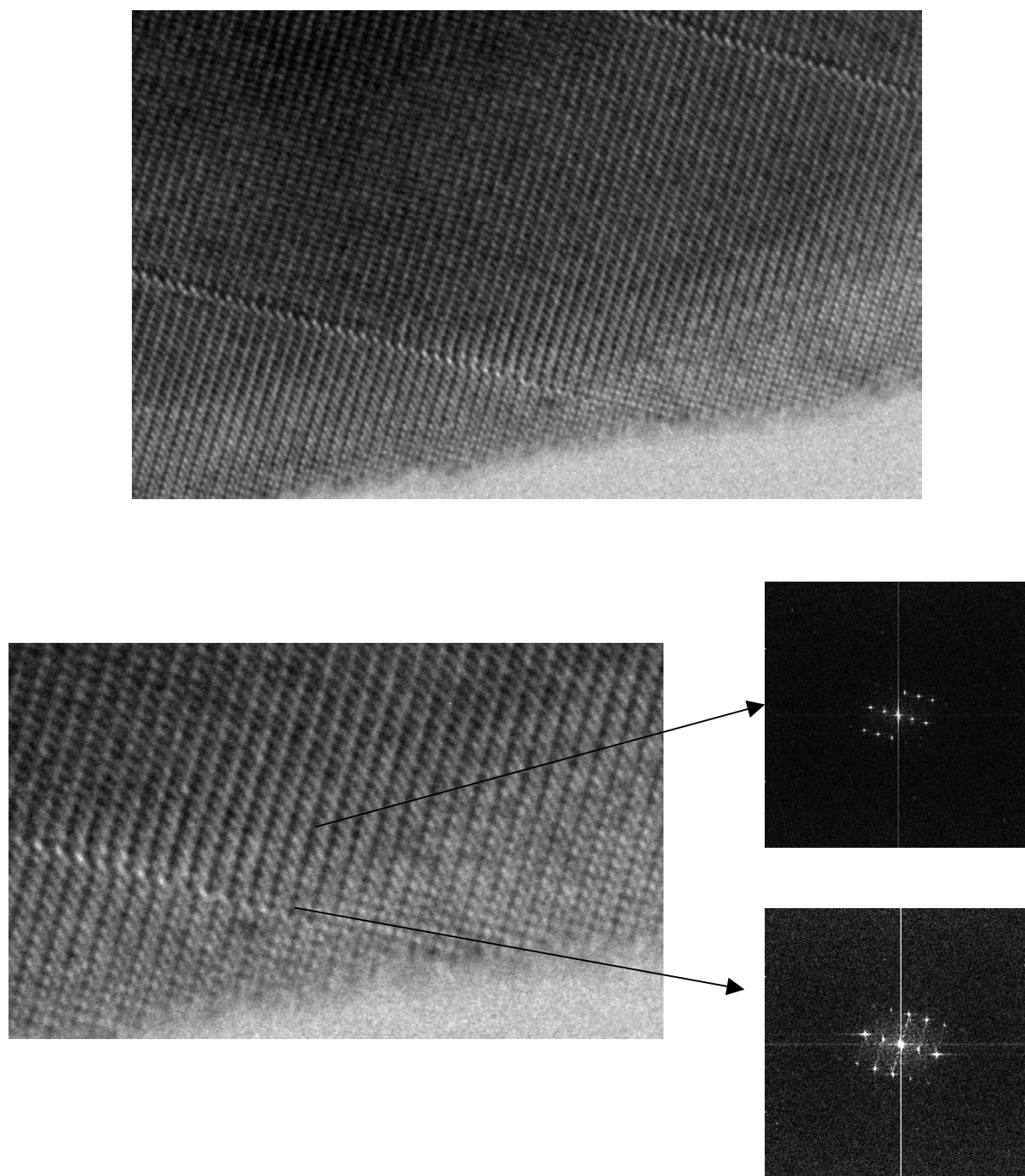


Fig. 51. HRTEM image of a thin crystallite from $\text{Cs}_{0.25}\text{Nb}_{0.1}\text{W}_{0.9}\text{O}_3$ powder sample with corresponding DP patterns processed with the CRISP program projected along $[010]$ axis.

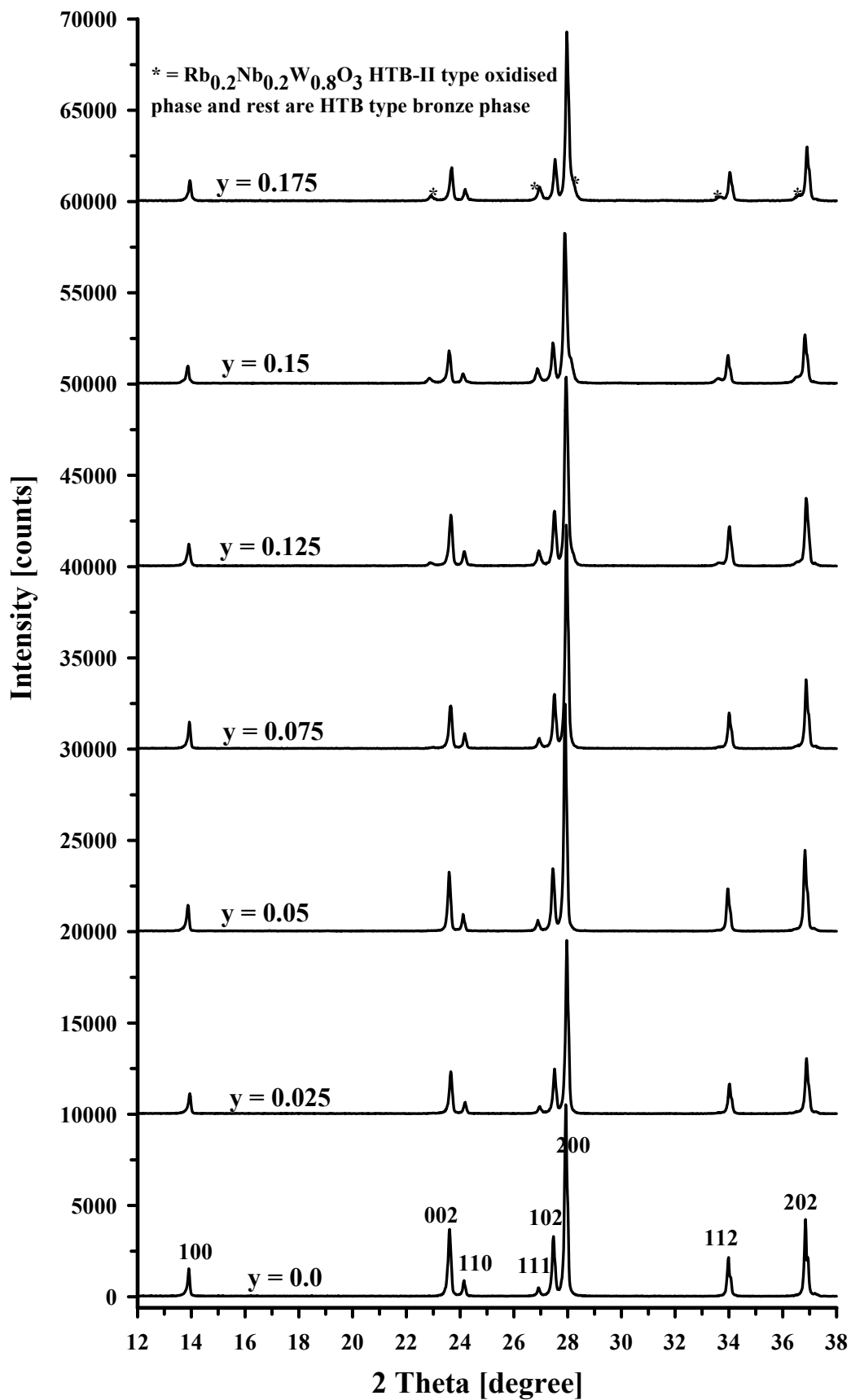


Fig. 52. X-ray powder diffraction patterns of $\text{Rb}_{0.3}\text{Nb}_y\text{W}_{1-y}\text{O}_3$ system with $y = 0.0 - 0.175$ as denoted.

In a previous investigation [110], it was reported that single phase of niobium substituted Rb and K hexagonal tungsten bronzes can be prepared for $x = 0.2$, $y \leq 0.05$; $x = 0.25$, $y \leq 0.125$ and $x = 0.3$, $y \leq 0.15$. Following the observation of $Cs_xNb_yW_{1-y}O_3$ system, in the present study the $Rb_{0.3}Nb_yW_{1-y}O_3$ system was reinvestigated from the same sample as obtained from Hussain et al. [110]. The X-ray powder diffraction patterns (Philips Diffractometer) of system $Rb_{0.3}Nb_yW_{1-y}O_3$ are given in Fig. 52. It can be seen that the X-ray powder diffraction pattern of nominal $Rb_{0.3}WO_3$ shows a pure HTB-I type bronze phase with the peaks 110 (2θ at about 13.85), 002 (2θ at about 23.57), 110 (2θ at about 24.10), 111 (2θ at about 26.87), 102 (2θ at about 27.43), 200 (2θ at about 27.89), 112 (2θ at about 33.95) and 202 (2θ at about 36.82). For samples with $y = 0.025$ and 0.05 , the X-ray patterns are identified as pure HTB-I type bronze phase with the peaks as observed for $y = 0.0$. However, for samples with $y = 0.075$ and 0.125 , the X-ray patterns are mainly identified as HTB-I type bronze phase in presence of some weak lines at about 2θ 22.85 , 33.57 and 36.49 positions. The intensity of these weak lines increases with increasing niobium content. All these extra weak lines were indexed as HTB-II type oxidised phase, with lattice parameters reported for Rb bronzoid phases ($Rb_{0.2}Nb_{0.2}W_{0.8}O_3$) [119]. Results obtained from Rietveld refinements of nominal $Rb_{0.3}Nb_{0.175}W_{0.825}O_3$ sample show that the main HTB-I type bronze phase is about 84% and the non-bronze HTB-II type phase about 16%. This refinements were carried out in $P6_3/mcm$ (No. 193) with Rb at (0, 0, 0) position.

Some samples of $Rb_{0.3}Nb_yW_{1-y}O_3$ system were studied by SEM/EDX microanalysis. Fig. 53 shows the crystal sizes and shapes of the samples with $y = 0.125$, 0.15 and 0.175 in the SEM

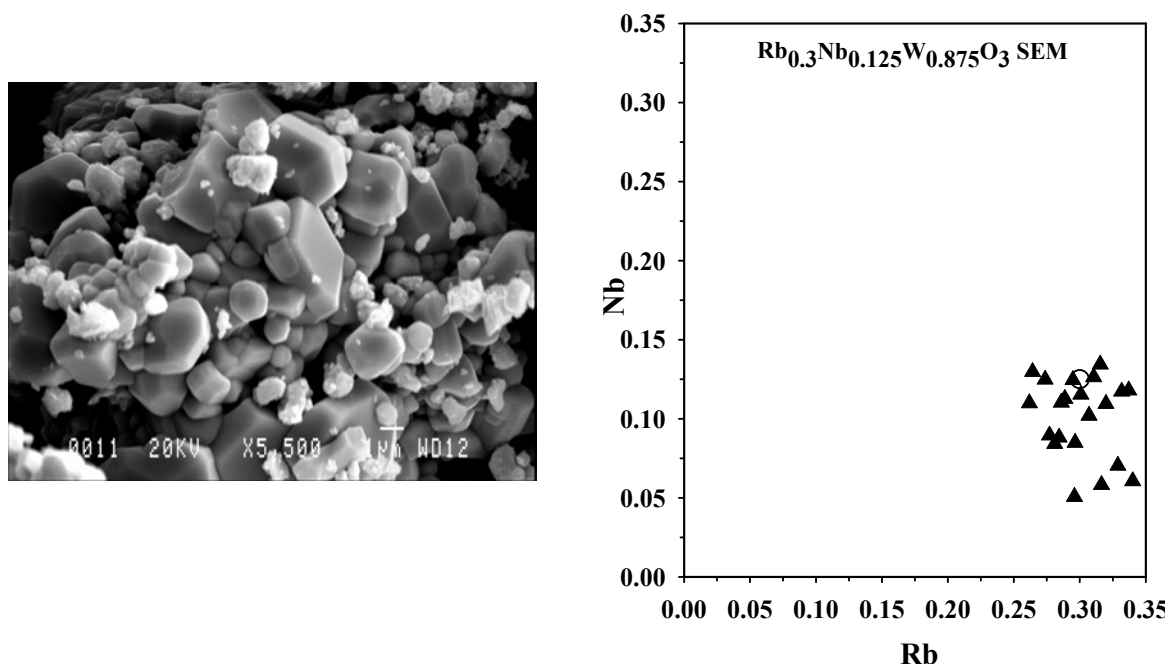


image. The distribution of the SEM/EDX analysis of these crystals are also given in the same figure. The results of these samples consist of crystals with $Rb = 0.29 - 0.37$ and $Nb = 0.06 - 0.11$ which belong to HTB-I type bronze phase. Since the amount of impure HTB-II type

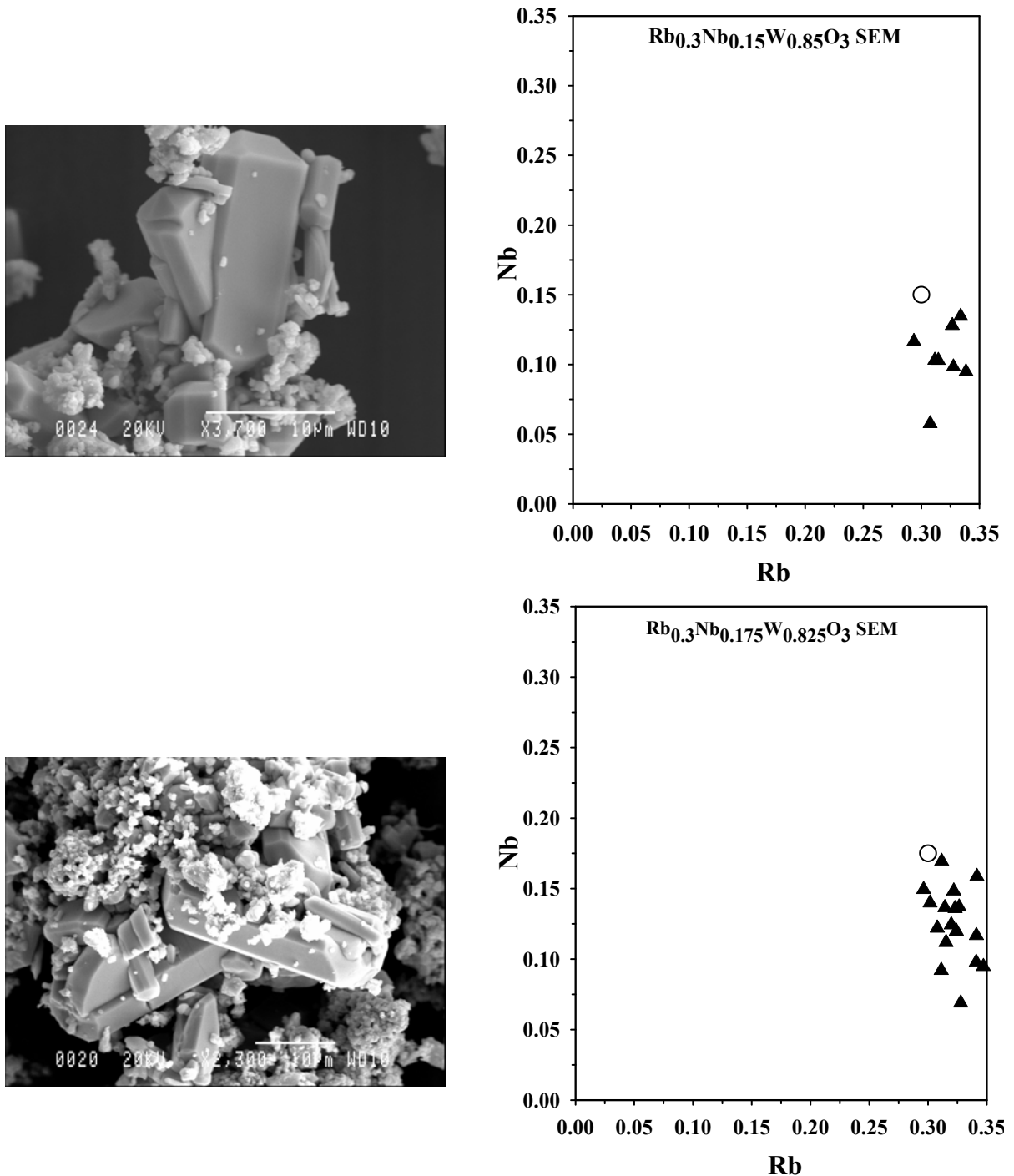


Fig. 53. SEM image of $Rb_{0.3}Nb_yW_{1-y}O_3$ system showing the HTB type crystals together with some polycrystalline powder. The HTB-I type bronze crystals containing Rb about 0.25 – 0.33 and Nb about 0.05 – 0.15 as shown in the SEM/EDX diagram. The nominal composition of $Rb_{0.3}Nb_yW_{1-y}O_3$ ($y = 0.0 - 0.15$) denoted by open circle in the diagram and the value of Rb and Nb are calculated from the signal intensities as $Rb = Rb / (Nb+W)$ and $Nb = Nb / (Nb+W)$. Each triangle point represent the mean of two or three measurements on the same crystal.

phase is very small in amount, it was not possible to detect for this microanalysis. However, like Cs-Nb-W-O system, it is also difficult to identify the phase separation in the system Rb-Nb-W-O.

From all these results it can be observed that Rb and Cs systems show the similar behaviour with increasing niobium content, i.e. with increasing Nb content all these systems go to a mixture of HTB-I bronze type phase and HTB-II type oxidized phase.

4. DISCUSSION

4.1. Li_xWO_3 system

4.1.1 Phase stabilities in the Li_xWO_3 system and relation to the thermally induced WO_3 phase transitions.

The phase diagram of Li_xWO_3 by Réau et al [100] is given in fig. 54. In the same figure the results of the X-ray powder analysis of different samples of lithium tungsten bronzes, Li_xWO_3 of series 1 and series 2 are also given. The results obtained from series 1 closely agree with the results of Réau et al. At low x content Réau et al showed for $x = 0.03$ sample, a pure PTB_{orth} phase whereas series 1 reveals a mixed phase of PTB_{tetr} and PTB_{orth} . Series 2 gives even more different results, because of the difference of the reactant used for series 1 and series 2. Similarly there is a significant difference between the series 2 and Réau et al data, Réau et al showed that the single $\text{PTB}_{\text{cubic}}$ phase in the range $0.26 \leq x \leq 0.5$, whereas series 2 shows the $\text{PTB}_{\text{cubic}}$ phase region for $0.35 < x < 0.55$. In series 2 it is observed that sample with

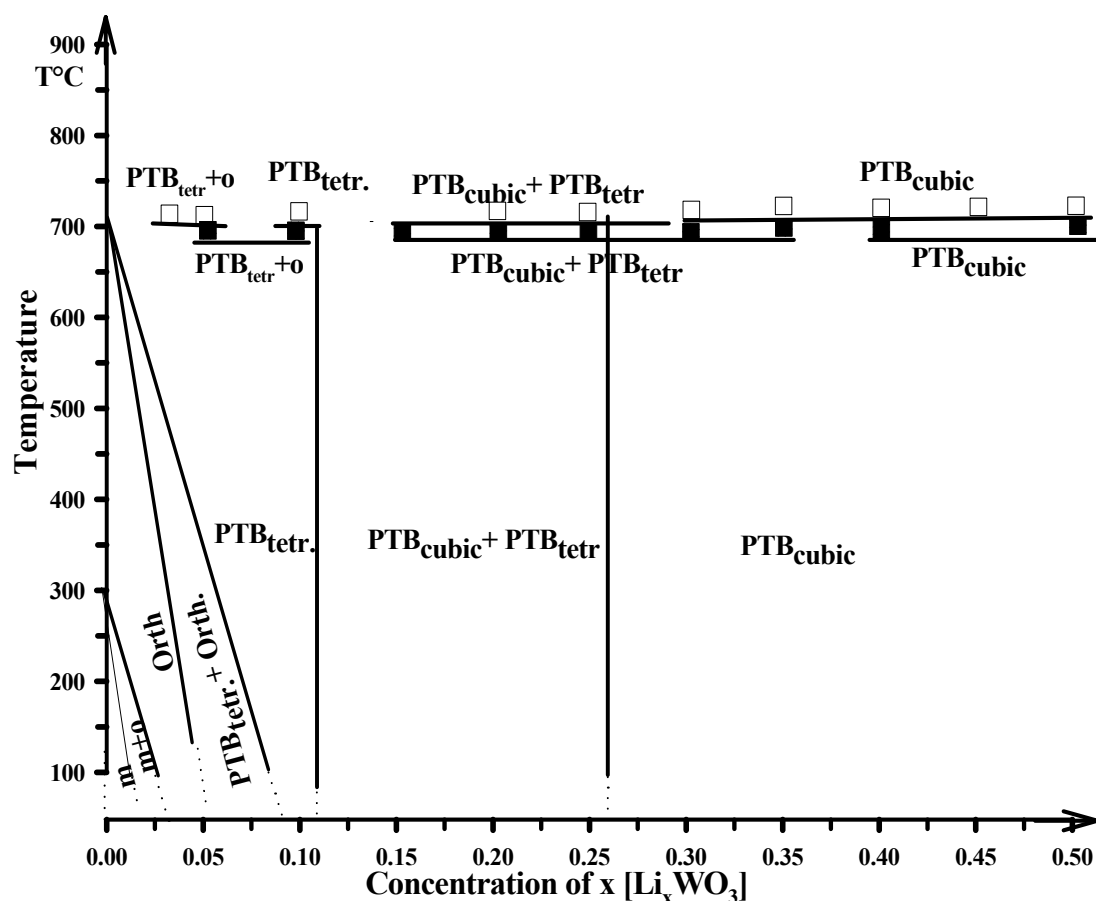


Fig. 54. Phase diagram of the lithium tungsten bronze, Li_xWO_3 , from the data of Réau et al. and the results of the lithium tungsten bronze, Li_xWO_3 ($x = 0.03 - 0.7$) of series 1 (open square) and series 2 (black square) obtained from Guinier powder method.

$x = 0.1$ always gives 2-3 extra lines of PTB_{orth} along with PTB_{tetr} whereas, Reau et al showed only PTB_{tetr} with $x = 0.1$. Samples with $0.15 \leq x \leq 0.35$, in series 2 also show some very weak lines which could not be indexed as any reported phase of tungsten bronzes. During the investigation of series 2 (old reactant) it was found that the commercially available WO_2 was not stoichiometric, containing an excess of oxygen. Therefore, the whole series (series 1) was prepared once again using analytical grade WO_2 . This reproduces the results which is shown in Fig. 54 by open square with an extended homogeneity range of $\text{PTB}_{\text{cubic}}$ phases. Further on with the new reactant in series 1 it is observed that all forms of $\text{PTB}_{\text{cubic}}$ possess a doubling of the unit cell. This observation about the doubling of the unit cell are in good agreement with Wiseman and Dickens [113]. With the old reactant in series 2 the doubling of unit cell could also be identified.

The lattice parameter obtained from Guinier method of series 1 and series 2 and some literature values as given by Réau et al [100] and Mart et al. [114] are plotted in Fig. 55. It is

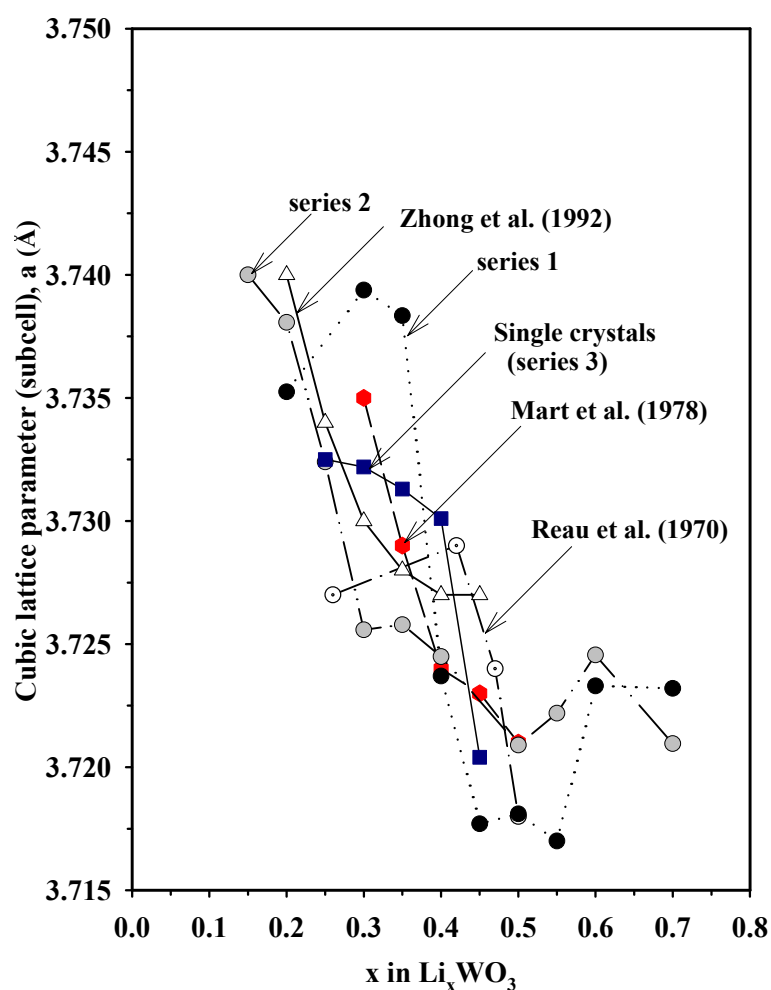


Fig. 55. Lattice parameters versus composition for cubic lithium tungsten bronzes of series 1, series 2 and series 3 together with some literature data.

observed from this figure that the value of the cubic lattice parameter of series 1 and series 2 tend to increase systematically with decreasing x into the two phase region. The same trend has also been observed by in situ measurements during the intercalation in electrolytic cells by Zhong et al. [101] also given in Fig. 55 (here changes in x was calculated from the cathode mass, the constant current and the time of current flow). The results of Réau et al also shows the same trend as shown in Fig. 55 but in different position (Réau et al. prepared the bronzes by the thermal method at 750°C using sealed gold tubes).

The variation of lattice parameter, though small, as a function of x could imply a solid solution type dependence suggesting a homogeneous distribution of Li on the perovskite A sites within the stability field of $0.25 < x < 0.55$. However, this effect is related to a strain induced interaction between the tetragonal and cubic phases where the tetragonal part tends to expand the cubic one.

The IR-absorption spectra of series 1 of Li_xWO_3 , obtained directly after opening the reaction tubes show that the sample with $x = 0.05$ and 0.1 can be explained by orthorhombic and tetragonal lattice of WO_3 respectively. It is also observed that the amount of tetragonal phase becomes gradually smaller with increasing x up to 0.2 . All spectra for samples with $x = 0.25 - 0.5$ closely agree to each other with some low intensity phonon signature at the same position indicating residual tetragonal phase within a cubic matrix.

The absence of any IR phonon absorption in $\text{PTB}_{\text{cubic}}$ can be explained by the free carrier effect with a plasma frequency sufficiently larger than the phonon frequencies. Conclusively the decreasing phonon intensity from single phase tetragonal $\text{Li}_{0.1}\text{WO}_3$ to $\text{Li}_{0.2}\text{WO}_3$ is explained by the upcoming content of $\text{PTB}_{\text{cubic}}$ and thus by an increase in the total carrier concentration. The phonon intensities at peak maximum relative to the minimum absorption intensities are plotted as a function of x [Fig. 56]. There is an overall decrease in phonon absorption intensity of the WO_3 matrix, which is therefore related to the increase in carrier (electron) concentration also below $x = 0.1$. For samples with $x > 0.5$, the IR spectra also show upcoming phonon intensity which is mainly related to Li_2WO_4 .

X-ray powder (Guinier method) and infrared absorption (KBr-method) investigations of single crystal of Li_xWO_3 show a close analogy with the results obtained from powder samples of Li_xWO_3 , which, however, produce crystal powders of submicron sizes. The lattice

parameters obtained from Guinier method of single crystals also given in Fig. 55 shows the same trend as observed for series 1 and series 2. According to single crystal investigation, it is

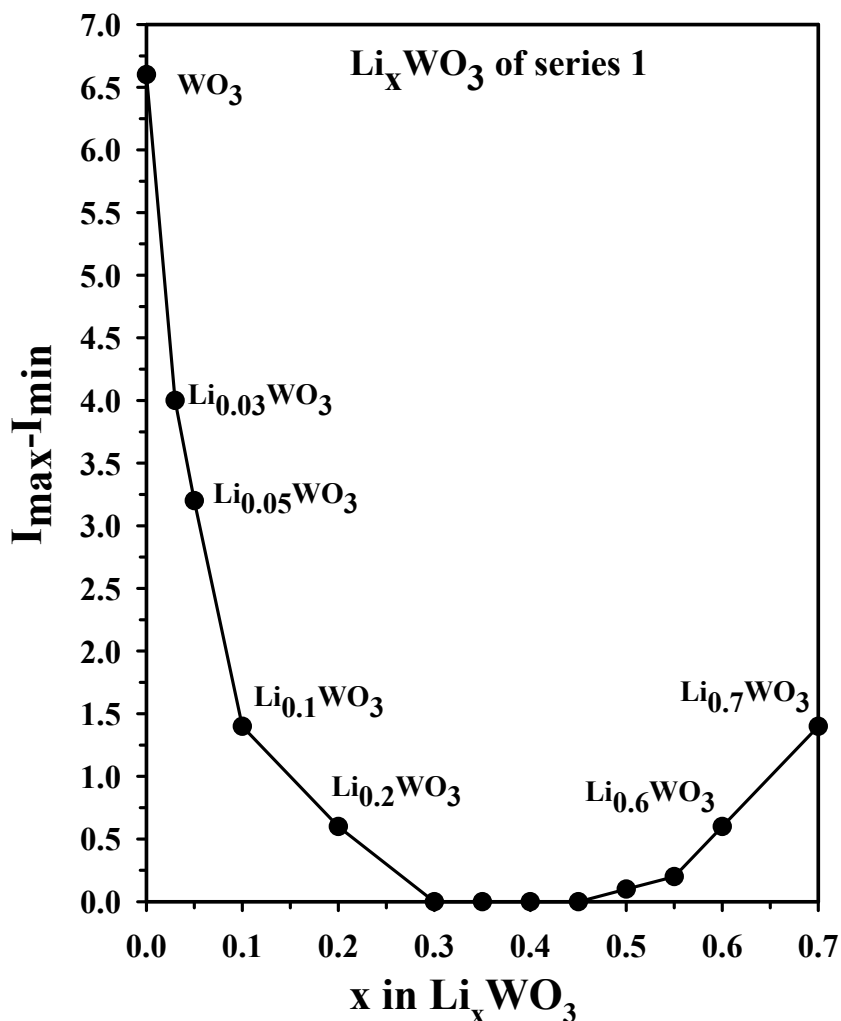


Fig. 56. The phonon intensities at peak maximum relative to the minimum absorption intensities as a function of x in Li_xWO_3 ($x = 0.0 - 0.7$) of series 1.

observed that single phase $\text{PTB}_{\text{cubic}}$ for Li_xWO_3 is obtained with nominal composition of $x = 0.45, 0.4$ and mixed phase of $\text{PTB}_{\text{cubic}}$ and $\text{PTB}_{\text{tetra}}$ for $x = 0.35, 0.3, 0.25$. The $x = 0.1$, sample reveals mixed phases of $\text{PTB}_{\text{tetra}}$ and PTB_{orth} of lower symmetry. These results are in good agreement with the stability field reported by Zhong et al [101] as $0.36 < x < 0.5$ for $\text{PTB}_{\text{cubic}}$ and $0.082 < x < 0.13$ for $\text{PTB}_{\text{tetra}}$ during intercalation. It can be noted that although same reactants were used for the crystal growth (in series 3) and for powder samples (in series 1), the stability field of $\text{PTB}_{\text{cubic}}$ is different. The stability field of $\text{PTB}_{\text{cubic}}$ for the powder samples (in series 1) was observed with $0.3 \leq x \leq 0.5$ where that for single crystals (in series 3) was found with $0.4 \leq x \leq 0.5$. The difference of the stability field of these two series could be related to different preparation conditions revealing a different scale in the formation of exsolution lamellars of Li_xWO_3 .

In Fig. 57 the obtained lattice parameter of the $\text{PTB}_{\text{cubic}}$ phase are plotted together with the refined tetragonal lattice parameter as recalculated by the equation $a_{\text{tetr}} \sim a_{\text{cubic}}^{2^{1/2}}$.

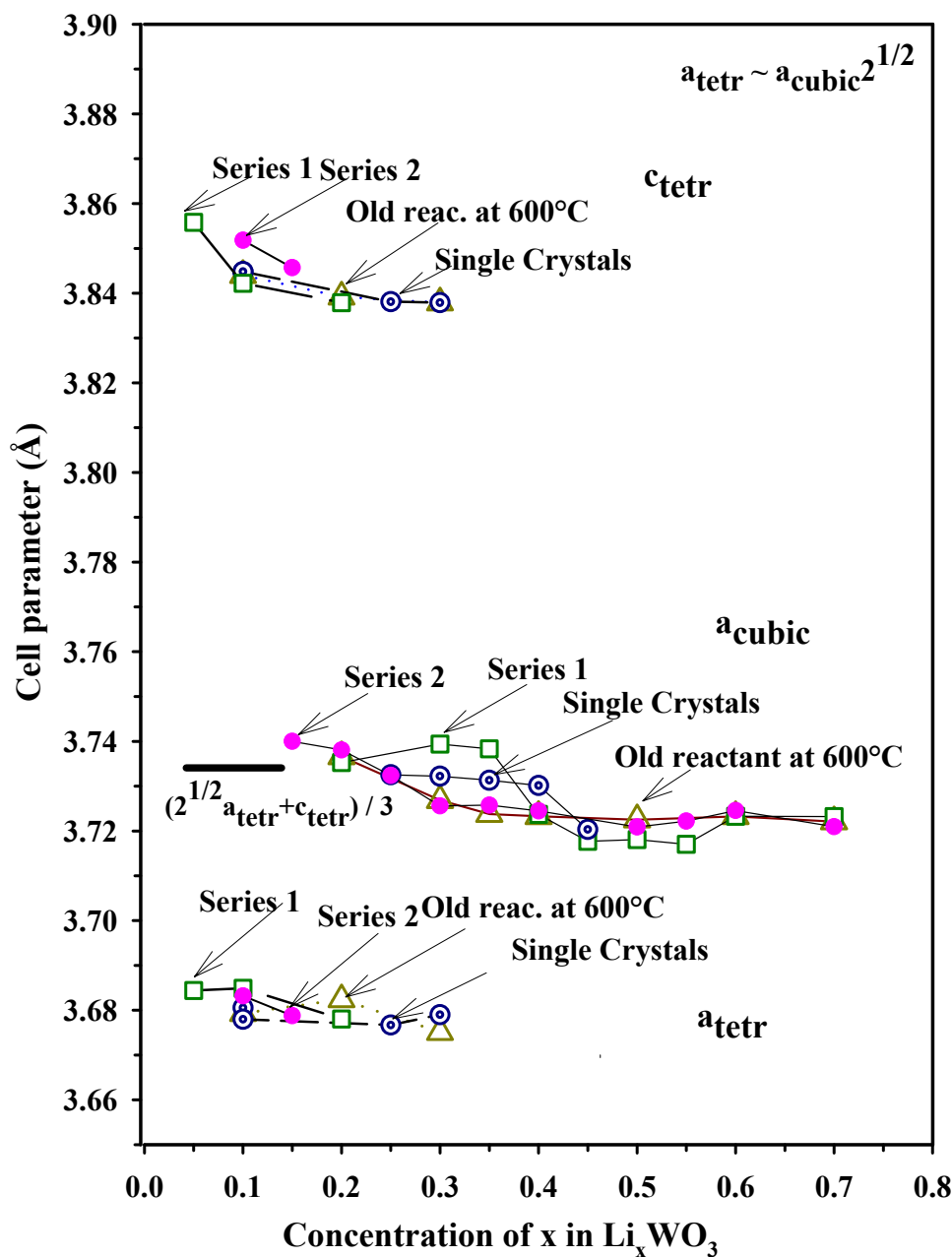
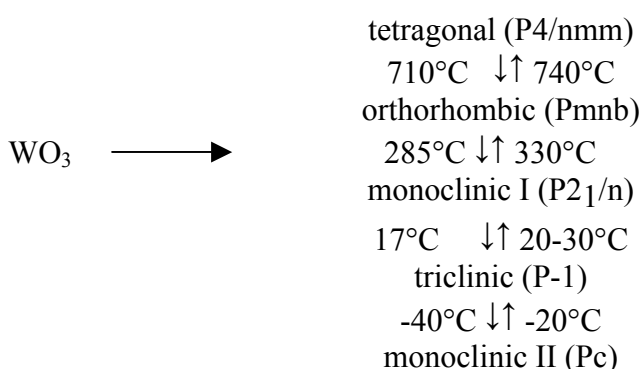


Fig. 57. Lattice parameters versus concentration of x of lithium tungsten bronzes, Li_xWO_3 obtained from different series. The a_{cubic} and c_{tetr} lattice parameters are plotted as obtained from refinement. Whereas, the lattice parameters of a_{tetr} are plotted from the values recalculated by the equation $a_{\text{tetr}} \sim a_{\text{cubic}}^{2^{1/2}}$.

The average of a_{tetr} and c_{tetr} is calculated by the equation $(\sqrt{2}a_{\text{tetr}} + c_{\text{tetr}}) / 3$ which is denoted by a black bar in the fig. 57. From this figure, it can be seen that the a parameter of $\text{PTB}_{\text{cubic}}$ phase with increasing content of PTB_{tetr} in the bulk sample becomes close to this average value. Therefore, this indicates a strong interaction between these related phases.

All data show that with increasing lithium concentration in Li_xWO_3 , the WO_3 host changes to the higher symmetric structure. This is similar in pure WO_3 with increasing temperature. The structure of tungsten trioxide, WO_3 is of a distorted ReO_3 type and shows displasive successive phase transitions. They are stable within well defined temperature ranges and transform into each other reversibly. The structure of ReO_3 is the BO_3 structure in which the A ion of the ABO_3 perovskite crystal is completely missing.

The structure of WO_3 is tetragonal above 740°C . It undergoes the tetragonal–orthorhombic transition (740°C), the orthorhombic–monoclinic transition (330°C), the monoclinic–triclinic transition (17°C) and the triclinic–monoclinic transition (-40°C) as shown below [120, 121].



As the structure of WO_3 in each phase are of a distorted ReO_3 type, it is assumed that WO_3 is cubic with the ideal ReO_3 type in the hypothetical highest temperature phase.

Salje and Viswanathan [116] determined the cell dimensions of WO_3 from -100°C to 900°C by X-ray powder method. They have shown that the lattice constants change very gradually during the monoclinic-orthorhombic transformation, whereas they change abruptly during the monoclinic–triclinic and orthorhombic–tetragonal transformations. In particular, the transition to the tetragonal form is characterized by a large decrease in the volume and in b . They have also shown from the X-ray data that the monoclinic modification undergoes only two transitions, namely, the monoclinic-orthorhombic transition at 480°C and the orthorhombic-tetragonal transition at 740°C . The triclinic first becomes monoclinic at about 200°C with identical lattice constants. Then it behaves just like the monoclinic modification. This important phase transition alters the physical properties considerably and causes a change in the space group.

Salje [122] discusses the different phase transitions on the basis of “critical modes” : a torsional mode, which gives rise to tilt structures and a deformational mode, which induces

deformations of the individual WO_6 octahedra and particularly the off-centre position of the W atoms. Starting from the tetragonal phase of highest symmetry [123], in which, with respect to the cubic reference structure of a, b and c cubic axis with length about 3.7\AA , the W positions are shifted from the octahedral midpoints to form zigzag chains along (110), the transition to the orthorhombic phase at 740°C can be explained by freezing critical modes, which induce a change in the lattice cell, with $a' = a\sqrt{2}$, $b' = b\sqrt{2}$ and $c' = 2c$, the tilt axis being parallel to a. The transition to the monoclinic room temperature phase implies an other torsional mode with tilt axis about c. The structure of the triclinic phase, studied from the data of a single crystal diffractometer is known precisely [124] and has been compared to the monoclinic modification determined by powder neutron diffraction [125]. The comparison shows clearly that the transformation occurs at some of the oxygen positions, involving a tilt of WO_6 octahedra about the b axis, i.e. the third direction, the tilting angle being about 17° . This angle is the critical parameter during the triclinic-monoclinic phase transition, the interatomic distances and angles remaining almost unchanged.

In the present investigation, the temperature dependent IR-spectra (KBr-method) of WO_3 was measured between 25°C to 651°C , the upper temperature limit of the experimental setup here for experimental reasons. The spectral change depending on phase transition of WO_3 with temperature has been observed in this experiment. The tetragonal phase was not seen here up to 650°C , however, the peak shape is almost indicative for the tetragonal phase of WO_3 . The same peak form and peak position is also observed for $\text{Li}_{0.1}\text{WO}_3$, which is PTB_{tet} according to the X-ray investigation. Additionally peak form and peak position are also very similar and indicative for $\text{Li}_{0.05}\text{WO}_3$ and orthorhombic WO_3 , showing that the Li – content has a similar effect on WO_3 as increasing the temperature to the orthorhombic and even the tetragonal modification. Further increase in Li has equal effectivity on the W-O bond lengths in the a and b direction and the zigzag rotations of the octahedra in the c direction disappear. Thus the structure of the WO_3 host finally becomes cubic and the W-O bond length becomes effectively equal in all three directions.

4.1.2 Electronic properties and color of the lithium tungsten bronze, Li_xWO_3 .

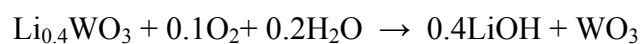
The optical measurement could be a very sensitive analytical method to detect Li exsolution phenomena and structural changes in the system Li_xWO_3 . For nominal composition of $\text{Li}_{0.45}\text{WO}_3$ and $\text{Li}_{0.4}\text{WO}_3$ the crystals appear homogeneous in the microscope. The appearance of a large scale exsolution phenomena into $\text{PTB}_{\text{cubic}}$ and PTB_{tet} is observed directly in the

microscope for $x = 0.35 - 0.25$ samples. But even for the supposed cubic part, submicroscopical exsolution phenomena can be suggested from their reflectivity spectra. This indicates a very limited stability field for $\text{PTB}_{\text{cubic}}$ on x (i.e. $x > 0.4$) or a high tendency to separate into lithium enriched ($\text{PTB}_{\text{cubic}}$) and Li exhausted (PTB_{tetr}) areas. The structural change is produced by ordering of Li in the crystal. During preparation, when the sample is quenched to room temperature within minutes by taking the reaction tubes out of the furnace, the high temperature framework tends to collapse around the interstitial cation. A sufficiently large content of Li may be able to prevent the collapse, while a smaller content of atoms allows the framework to distort, reducing the symmetry. The high mobility of Li might be the reason for the formation of Li enriched $\text{PTB}_{\text{cubic}}$ and Li exhausted PTB_{tetr} during cooling as driven by the distortion of the framework.

All of the reflectivity spectra of $x = 0.45$ crystals, show the same Drude free carrier type isotropic reflectivity. The reflectivity spectra of the crystals from the batches with $x = 0.4$ and 0.35 , all slightly differ indicating a superimposition of an additional spectral contribution in the range of the minimum. This contribution is related to the influence of submicroscopical exsolution of the tetragonal phase, since this effect becomes increasingly significant for crystals from the $x = 0.35$ batch. For these crystals there are brighter lamellars which are separated by sharp interfaces due to the phase separation. The brighter lamellars become more significant in area for crystals from the batches $x = 0.3$ and 0.25 and their optical properties were measured separately. The dark parts show significant deviations from isotropy down from 14000 cm^{-1} extending into the mid infrared. Moreover, a systematic decrease in the NIR reflection indicates an increasing influence from Li-exsolution phenomena on a submicroscopic scale. The bright part of the crystals shows a non-Drude like strong anisotropic behaviour with the appearance of phonon effects in the MIR. It can be noted that the non cubic parts of the crystals possess strong infrared absorption phenomena which are peaked in the range between 2000 cm^{-1} to 8000 cm^{-1} strongly dependent on crystal orientation. The data further imply that any deviation from single phase $\text{PTB}_{\text{cubic}}$ is related with a break down of the Drude free carrier dominated near infrared response. The excitation spectra of PTB_{tetr} and PTB_{orth} phases, may be explained by photon assisted hopping of polarons with a strong anisotropy in their coupling parameters due to the tetragonal / orthorhombic host.

The as measured reflectivity spectra of powder samples of series 1 after recalculating by using the Kubalka Munk formula show that with increasing x in Li_xWO_3 there is a strong increase in intensity of a broad peak between 15000 cm^{-1} and 18000 cm^{-1} for $x = 0.25 - 0.55$ [Fig. 11]. These broad peaks can be explained by the free carrier plasma effect. A shift of the peak to higher wave number with increasing x would imply an increase in carrier concentration. However, although remeasured several times, it was quite difficult from the powder series to see the shifting of the peak as a function of x , i.e with an increase in Li content. On the other hand, the increase in intensity at 16000 cm^{-1} suggests an increase in content of $\text{PTB}_{\text{cubic}}$ phase. In this context it is interesting to note that a clustering into higher and lower Li- contents implies a separation into metallic and nonmetallic domains on a nanometer scale. The absorption peak which is responsible for the dark blue color is due to the so called surface plasmon, as for example, described for nanoparticles of gold and silver in ceramic matrices [126]. It is interesting to note that there is also a broad peak for the samples with $x = 0.2$ and 0.15 at around $15,000\text{ cm}^{-1}$ which could be present also in the sample with $x = 0.25$ as a shoulder in the plasmon peak. In further experiments in the spectral range 2000 cm^{-1} to 15000 cm^{-1} , a peak is observed around 10000 cm^{-1} and 8000 cm^{-1} for the sample with $x = 0.1$ and 0.05 respectively which closely corresponds to the peaks also observed in thin films [106].

Lithium tungsten bronzes, Li_xWO_3 prepared at 600°C , 700°C and 800°C show deep blue colour for $0.3 \leq x \leq 0.6$ and more violet blue for $x = 0.7$ if kept in closed evacuated tubes. The changes in colour can be explained by the high mobility of Li which is attracted by surface oxygen. The IR spectra of the exposed sample shows the presence of OH^- and CO_3^{--} species, which can be explained by the following way- Li_xWO_3 ($x < 0.5$) in atmospheric condition reacts with O_2 and forms Li_2O , which may then react with the atmospheric H_2O and CO_2 and can form $\text{Li}(\text{OH})$ and Li_2CO_3 . These $\text{Li}(\text{OH})$ and Li_2CO_3 can be detected by IR-absorption spectra. The reaction is going on in the following way –



It can be suggested that in all cases Li_xWO_3 for $x < 0.5$ will become Li-free at the surface thus obtaining the monoclinic form of WO_3 at room temperature. From the appearance of the IR absorption characteristics it can be seen that all compositions of Li_xWO_3 for $x < 0.5$ are gradually transferred from the higher symmetry phase to the lower symmetry phase with

increasing exposure time at atmospheric conditions due to a gradual depletion in Li. For compositions $x > 0.5$, a slight increase in the concentration of Li_2WO_4 could occur with increasing exposure time. There is very little change in colour of sample with composition, $\text{Li}_{0.5}\text{WO}_3$, even after 90 days of exposure time. Therefore, it may be concluded that $\text{Li}_{0.5}\text{WO}_3$ is the most stable composition due to a half occupation of Li on the A site in the ABO_3 structure.

After reheated, the exposed samples regain their original color and the IR spectra and x-ray result of the samples indicate the formation of $\text{Li}_2\text{W}_2\text{O}_7$ with main $\text{PTB}_{\text{cubic}}$ phase. The $\text{Li}_2\text{W}_2\text{O}_7$ type phase is may be due to the presence of WO_3 , LiOH and Li_2CO_3 which lead the formation of $\text{Li}_2\text{W}_2\text{O}_7$. Probably a reversible process occurs in part or would occur to 100% in dried and CO_2 free O_2 atmosphere, which could be useful for an electronic device for measurement of oxygen partial pressure. The surface-related properties of the bronzes have been reported earlier in a number of publications. Spitzin and Kaschtanoff [127] stated that the bronze powders (1-20 μm) contain adsorbed water to the extent of about 0.4 wt %, which can be driven off by heating at 200-300°C. Straumanis and Dravnieks [128] observed for sodium tungsten bronzes that, when the sintered bronze is exposed to moist air, the electrical resistivity increases with time, probably owing to the formation of a surface layer at the intergrain boundaries. A preliminary electron-diffraction work of Muldawer [129] indicate that the surface of a $\text{Na}_{0.7}\text{WO}_3$ single crystal immersed in HF and / or exposed to moist air was converted partly to the tetragonal bronzes ($x = 0.1$) and partly to tungsten oxides as it is observed in the present investigation for Li_xWO_3 system. Consadori and Stella [130] observed (for optical reflectivity of Na_xWO_3) that the bronze exposed to air exhibits time-dependent optical–reflectivity spectra, indicative of a film growing on the surface.

4.2 $\text{Li}_{0.4}\text{Nb}_y\text{W}_{1-y}\text{O}_3$ and $\text{Li}_{0.1}\text{Nb}_y\text{W}_{1-y}\text{O}_3$ system

In $\text{Li}_{0.4}\text{Nb}_y\text{W}_{1-y}\text{O}_3$ system there is only a small effect of Nb/W substitution. This system shows that even in presence of small amount of Nb ($y = 0.04$) a trace amount of LiNbWO_6 type phase comes as impurity along with $\text{PTB}_{\text{cubic}}$ phase. The intensity of $\text{PTB}_{\text{cubic}}$ phase reduces and the intensity of LiNbWO_6 trirutile type phase increases with increasing Nb content. For $x = y = 0.4$ the structure shows mainly the LiNbWO_6 trirutile type structure in presence of very small amount of $\text{Nb}_2\text{W}_3\text{O}_{14}$ and LiNb_3O_8 as impurity phase. Y. Xia et al. [131] also found Nb_2WO_8 and LiNb_3O_8 as impurity phase around 2% along with main phase when they worked on in the system $\text{Li}_{1-x}\text{Nb}_{1-x}\text{W}_x\text{O}_3$ ($0 \leq x \leq 0.5$). However, Yamada et al.

[115] reported that single phase of cubic perovskite-type compound was obtained when $y < 0.15$ in the system $\text{Li}_x\text{Nb}_y\text{W}_{1-y}\text{O}_3$ ($x \sim 0.4$, $0 \leq y < 0.15$) prepared by electrolysis of fused salt.

The cubic cell parameter obtained from series 5 and some previous data obtained from old reactants are given in table 3 and also plotted in Fig. 58. The different behaviour on y in the

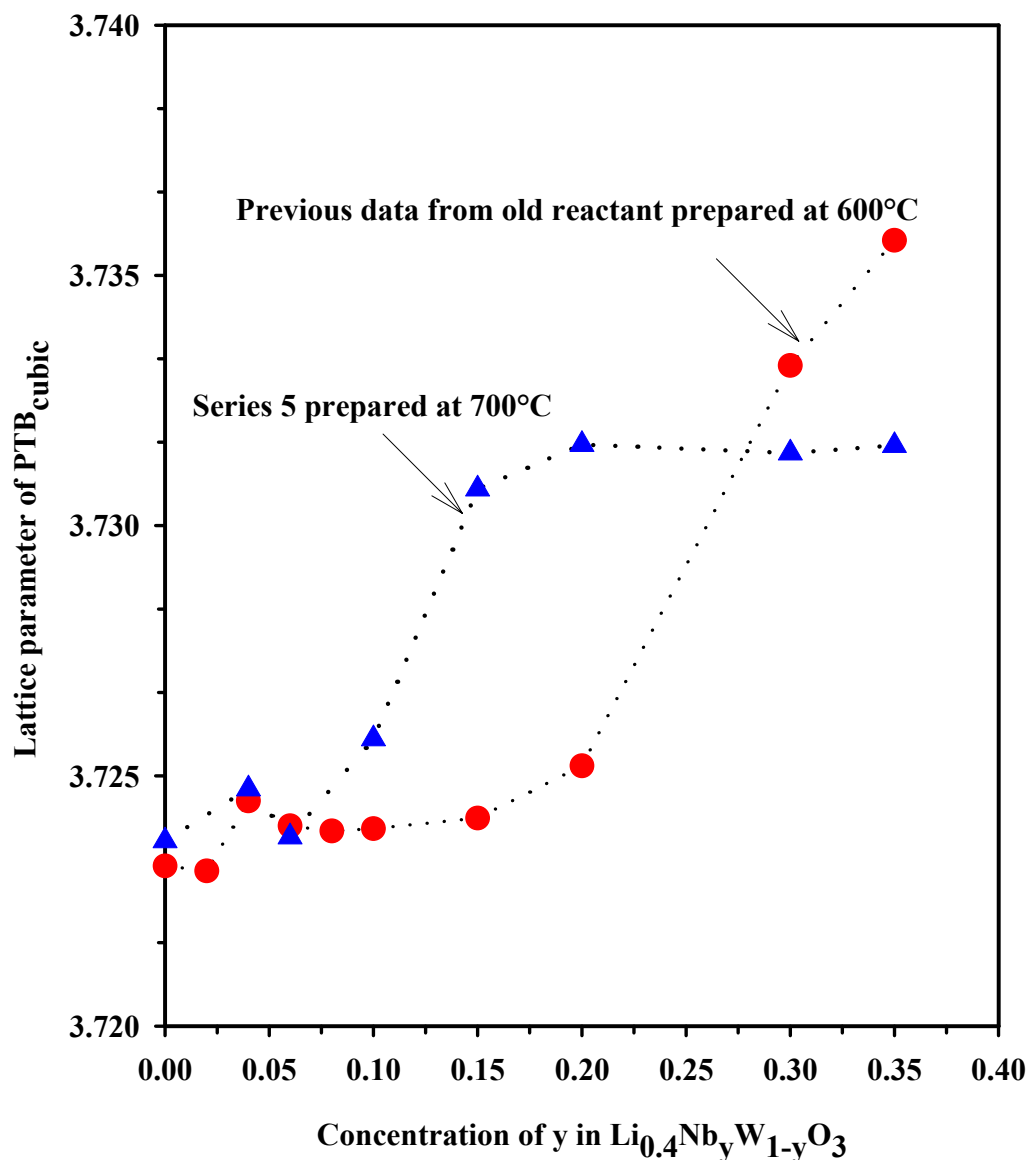


Fig. 58. Lattice parameters versus concentration of y in $\text{Li}_{0.4}\text{Nb}_y\text{W}_{1-y}\text{O}_3$ of series 5 and some previous data of the same system which was prepared from old reactants at 600°C .

cell parameter between series 4 and series 5 as shown in Fig. 58 could be due to different WO_2 reactant used. In Fig. 58 it can be seen that with increasing Nb content the a_{cubic} cell parameter increases. This general trend is very similar to the behaviour which is also observed for decreasing Li content in Li_xWO_3 . Therefore, the cell parameter increasing behaviour

observed in $\text{Li}_{0.4}\text{Nb}_y\text{W}_{1-y}\text{O}_3$ system does not give any evidence of Nb substitution for W in $\text{Li}_{0.4}\text{WO}_3$ PTB_{cubic} phase.

Some hints of the effect of the substitution of tungsten by niobium in $\text{Li}_{0.4}\text{Nb}_y\text{W}_{1-y}\text{O}_3$ system are, however, obtained from the optical spectra [Fig. 26]. The single crystal spectral properties of $\text{Li}_{0.4}\text{WO}_3$ have been explained in terms of a Drude free carrier plasma frequencies which show a minimum at about $14,000\text{ cm}^{-1}$. Similar spectrum is observed with the same minimum for the powder sample of $\text{Li}_{0.4}\text{WO}_3$. The reflectivity of the powder samples of series 5 [Fig. 26] of $\text{Li}_{0.4}\text{Nb}_y\text{W}_{1-y}\text{O}_3$ system shows that the minimum is somewhat shifted to lower wave number with increasing Nb concentration, which has not been observed as a function of Li in Li_xWO_3 . This behaviour can be explained by an effective decrease of the carrier concentration due to the doping with Nb. The EDX analysis results support this explanation by showing the different amount of niobium in different crystals as described in results. From all these experimental results it can be suggested that 5-8 atom % niobium can be doped in the system $\text{Li}_{0.4}\text{Nb}_y\text{W}_{1-y}\text{O}_3$.

At atmospheric condition the PTB_{cubic} phase contribution in system $\text{Li}_{0.4}\text{Nb}_y\text{W}_{1-y}\text{O}_3$ is affected, i.e. gradually transferred to WO_3 type compound. For this reason the oxidised phase becomes more significant with increasing exposure time in atmospheric condition.

For $\text{Li}_{0.1}\text{Nb}_y\text{W}_{1-y}\text{O}_3$ system the main observation is the gradual loss of the tetragonal phase with increasing Nb content and upcoming orthorhombic phase. With increasing Nb, a small amount of Nb_2O_5 and LiNb_3O_8 type phase also observed along with main PTB_{tetr} and PTB_{orth} phase. The reflectivity of the powder sample of series 6 shows that the minimum feature in the reflectivity becomes weaker and shifted to lower wavenumber with increasing niobium content. For the sample with $y \geq 0.08$, the minimum structure becomes less significant and there is nearly no shift in position, which could indicate the effect of the substitution of tungsten by niobium in the system $\text{Li}_{0.1}\text{Nb}_y\text{W}_{1-y}\text{O}_3$ [Fig. 30]. This behaviour can be explained by an effective decrease of the carrier concentration due to the doping with Nb. Therefore, there can be a small effect of substitution in this system. However, the change in properties mostly can be related to a decreasing amount of Li in Li_xWO_3 . There is no clear evidence in this system for a substitution effect.

4.3 $\text{Li}_{0.4}\text{Mo}_y\text{W}_{1-y}\text{O}_3$ and $\text{Li}_{0.1}\text{Mo}_y\text{W}_{1-y}\text{O}_3$ system

In the system $\text{Li}_{0.4}\text{Mo}_y\text{W}_{1-y}\text{O}_3$ the proportion of $\text{PTB}_{\text{cubic}}$ phase reduces with increasing molybdenum content. In presence of small amount of Mo, a $\text{Li}_2\text{W}_2\text{O}_7$ type phase is formed along with $\text{PTB}_{\text{cubic}}$ phase. From the X-ray and IR results it can be suggested that with increasing molybdenum content W is replaced according to $\text{Li}_2\text{W}_2\text{O}_7$ phase, but not at all in Li_xWO_3 phase of $\text{PTB}_{\text{cubic}}$. For sample with $y > 0.15$, the $\text{PTB}_{\text{cubic}}$ phase totally disappeared and $\text{Li}_2\text{W}_2\text{O}_7$ type phase is mainly identified. Variation in the X-ray pattern compared to the $\text{Li}_2\text{W}_2\text{O}_7$ pure phase could indicate the formation of $\text{Li}_2\text{W}_{2-x}\text{Mo}_x\text{O}_7$ of variable composition.

The EDX analysis results support this explanation by showing the different amount of molybdenum and tungsten in different crystals as described in results. The SEM image also supports this observation by showing that sample with $y > 0.15$ has no cubic crystal, only some flake crystals together with polycrystalline powder remain. From EDX analysis results, it can be suggested that may be only about 5% Mo can be doped in $\text{Li}_{0.4}\text{Mo}_y\text{W}_{1-y}\text{O}_3$ system.

Attempts were also made to substitute tungsten by Mo in $\text{PTB}_{\text{tetra}} \text{Li}_{0.1}\text{WO}_3$. From the X-ray powder diffraction pattern, it can be seen that with increasing Mo content the proportion of $\text{PTB}_{\text{tetra}}$ decreases and a phase of orthorhombic symmetry increases in presence of small amount of impure phase of $\text{Li}_2\text{W}_4\text{O}_{13}$. This X-ray result is supported by the IR absorption spectra of the samples. X-ray and IR results show that with increasing Mo content the higher symmetry phase goes to lower symmetry phase as it is observed in $\text{Li}_{0.1}\text{Nb}_y\text{W}_{1-y}\text{O}_3$ system. Only a small effect of substitution can be present in the system $\text{Li}_{0.1}\text{Mo}_y\text{W}_{1-y}\text{O}_3$. However, the change in properties is mostly be related to a decreasing amount of Li in Li_xWO_3 . There is no clear evidence in this system for a substitution effect.

On the basis of the experimental results, it can be concluded that the experimental condition which was used for the synthesis of these systems is unsuccessful for the substitution of tungsten by Nb and Mo in $\text{PTB}_{\text{tetra}} \text{Li}_{0.1}\text{WO}_3$ and $\text{PTB}_{\text{cubic}} \text{Li}_{0.4}\text{WO}_3$ system.

4.4 $\text{Na}_{0.6}\text{Mo}_y\text{W}_{1-y}\text{O}_3$ System

The sodium tungsten bronzes, Na_xWO_3 with $0.35 < x < 0.96$, are typically metallic and had been classified to the ideal perovskite structure as postulated from the cubic sublattice of tungsten in the earlier X-ray study [132]. In the present study, $\text{Na}_{0.6}\text{WO}_3$ was prepared at different temperature (600°C , 700°C and 800°C) to check the structure at first. From the X-

ray powder diffraction pattern all of them were indexed as $\text{PTB}_{\text{cubic}}$. Then an attempt was made to replace the W atom by Mo in $\text{Na}_{0.6}\text{WO}_3$ at 600°C and 700°C and to investigate their properties and structural changes with increasing Mo concentration. From both series, it can be seen that with $y \leq 0.1$ the X – ray pattern shows 3-4 very weak reflections along with $\text{PTB}_{\text{cubic}}$ phase which are identified as WO_2 . However, for $y > 0.1$ an extra phase of $\text{Na}_2\text{Mo}_2\text{O}_7$ is observed along with $\text{PTB}_{\text{cubic}}$ and WO_2 . This is similar as $\text{Li}_2\text{Mo}_2\text{O}_7$ was observed in the system $\text{Li}_{0.4}\text{Mo}_y\text{W}_{1-y}\text{O}_3$. It has been reported [133] that $\text{Na}_2\text{W}_2\text{O}_7$ type phase is formed after oxidation of $\text{Na}_{0.65}\text{WO}_3$ in air at 500°C for 12hr, which is isomorphous [134] with $\text{Na}_2\text{Mo}_2\text{O}_7$ phase.

The IR absorption spectra of the samples with $y \leq 0.1$ of system $\text{Na}_{0.6}\text{Mo}_y\text{W}_{1-y}\text{O}_3$ can be explained as $\text{PTB}_{\text{cubic}}$ phase of Na bronze. The IR spectra of the sample with $y > 0.1$ show the upcoming phonon intensity which is related to $\text{Na}_2\text{Mo}_2\text{O}_7$ type compound. However, the spectra for $y > 0.1$ are the superimposed forms of $\text{PTB}_{\text{cubic}}$ and $\text{Na}_2\text{Mo}_2\text{O}_7$, because according to X-ray $\text{PTB}_{\text{cubic}}$ phase is present strongly along with $\text{Na}_2\text{Mo}_2\text{O}_7$ phase. From SEM image, it can be seen that until $y \leq 0.1$ a cubic shape of the crystals is present, whereas with $y > 0.1$ some extra forms appear. This results support the X-ray and IR results. The EDX analysis of thin crystal fragments in the TEM microscope shows that for most of the crystals of sample $\text{Na}_{0.6}\text{Mo}_{0.2}\text{W}_{0.8}\text{O}_3$ have the average Na content $x = 0.6 \pm 0.01$ and this is in good agreement with that of the starting composition. However, the TEM microanalysis results also show that most of the crystals have Mo content $y = 0.05 - 0.15$.

From all the experimental results, it can be seen that molybdenum substituted $\text{PTB}_{\text{cubic}}$ bronze phase can be prepared up to $y \leq 0.1$ in the system $\text{Na}_{0.6}\text{Mo}_y\text{W}_{1-y}\text{O}_3$.

4.5 $\text{Cs}_x\text{Nb}_y\text{W}_{1-y}\text{O}_3$ and $\text{Rb}_x\text{Nb}_y\text{W}_{1-y}\text{O}_3$ System

Cesium tungsten bronzes, Cs_xWO_3 with $x = 0.19 - 0.33$ had been classified as hexagonal tungsten bronzes [135]. In the present study $\text{Cs}_{0.25}\text{WO}_3$ and $\text{Cs}_{0.3}\text{WO}_3$ were prepared at 800°C . From the X-ray powder diffraction pattern $\text{Cs}_{0.3}\text{WO}_3$ was indexed as pure HTB type bronze phase whereas $\text{Cs}_{0.25}\text{WO}_3$ shows 2-3 very weak extra lines along with HTB phase. An attempt was made to replace the W atom by Nb in $\text{Cs}_{0.25}\text{WO}_3$ and $\text{Cs}_{0.3}\text{WO}_3$ at 800°C and to investigate their properties and structural changes with increasing Nb concentration. From both series it can be seen that with $y \leq 0.1$ the X – ray pattern shows some weak reflections along with HTB type bronze phase which are identified as oxidised HTB-II type phase. HTB-

II type oxidised phase corresponds to Cs bronzoid phases of $\text{Cs}_{0.2}\text{Nb}_{0.2}\text{W}_{0.8}\text{O}_3$ which was reported by Sharma [119]. In $\text{Cs}_{0.3}\text{Nb}_y\text{W}_{1-y}\text{O}_3$ system for $y = 0.15$ sample along with HTB type bronze and HTB-II type oxidised phase, a trace amount of $\text{Cs}_{0.35}\text{Nb}_{0.35}\text{W}_{0.65}\text{O}_3$ pyrochloro-type phase is observed. It was also reported [119] that in the Cs-Nb samples the increase in the alkali content results in the formation of a (defect) pyrochloro-type phase with Cs.

According to TEM microanalysis, sometimes even in the same crystals different Cs and Nb content is obtained. This indicates that there is intergrowth on a submicroscopical scale of different compositions. Some needle like crystals were observed for $\text{Cs}_{0.25}\text{WO}_3$ sample in the SEM image which contain very low Cs as shown in the microanalysis diagram. These needle crystals could be responsible for the weak extra line in the X-ray diffraction pattern of $\text{Cs}_{0.25}\text{WO}_3$ sample. With increasing niobium content, the needle like crystals disappeared. Such a behaviour has been reported recently on Rb_xWO_3 HTB by Brusetti et al. [136]. They have shown that for $x < 0.2$ there are parasitic peaks in the X-ray pattern which correspond to ITB type structures. In this context it is argued that the addition of Nb avoids the formation of ITB. SEM and TEM microanalysis also show the incorporation of Nb as shown in results.

Recently, structure refinements by Rietveld method for samples of nominal composition $\text{Cs}_{0.23}\text{Nb}_{0.09}\text{W}_{0.91}\text{O}_3$ and $\text{Cs}_{0.29}\text{Nb}_{0.1}\text{W}_{0.9}\text{O}_3$ [137] supports the incorporation of niobium on tungsten site which agrees well with nominal composition of the starting materials. The data for structure refinement in Ref. 137 were collected in a STOE STADI P diffractometer in a 0.02 mm capillary tube and then the weak extra reflections other than main HTB type phase in the samples has been ignored. The EDX analysis support the Rietveld refinements in so far as significant Nb contents were detected in samples according to an increase in the Nb signal relative to the W signal.

A large number of ED pattern has been taken for some samples of series 10. They confirm the unit cell dimensions obtained from the X-ray study. A HRTEM image of a thin crystal of nominal $\text{Cs}_{0.25}\text{Nb}_{0.1}\text{W}_{0.9}\text{O}_3$ in (010) projection shows an interruptions of the tunnels in the b direction. For such a defect in the crystal the Cs atom can not move easily and probably for this defect the optical property measurement in the b-direction is difficult.

In a previous investigation [110] it was observed that single phase of niobium substituted Rb and K hexagonal tungsten bronzes can be prepared for $x = 0.2$, $y \leq 0.05$; $x = 0.25$, $y \leq 0.125$

and $x = 0.3$, $y \leq 0.15$. It was also reported [110] that some of the extra lines observed at high niobium due to the presence of WO_3 and some weak lines were not indexed as any reported phase of HTB. However, in the present study by reinvestigation of the system $\text{Rb}_{0.3}\text{Nb}_y\text{W}_{1-y}\text{O}_3$, it is observed that the pure Rb - HTB type phase is only possible when $x = 0.3$ and $y \leq 0.05$. With $y > 0.05$ some very weak extra lines are observed along with main HTB phase as it was observed in $\text{Cs}_{0.3}\text{Nb}_y\text{W}_{1-y}\text{O}_3$ system. All these extra lines were indexed as HTB-II type oxidised phase. This HTB-II type oxidised phase corresponds to $\text{Rb}_{0.2}\text{Nb}_{0.2}\text{W}_{0.8}\text{O}_3$ type HTB phase reported by Sharma [119]. SEM/EDX microanalysis results also supported this X-ray observation by showing about $\text{Rb} = 0.25 - 0.35$ and $\text{Nb} = 0.05 - 0.15$ in the bulk crystals. However, it was difficult to observe the oxidised phase by SEM/EDX analysis probably due to the less amount of sample.

The infrared absorption spectra (KBr-method) within each series of $\text{M}_x\text{W}_{1-y}\text{Nb}_y\text{O}_3$, $M = \text{K}$, Rb (Hussain et al.) and $\text{Cs}_x\text{Nb}_y\text{W}_{1-y}\text{O}_3$ shows a broad phonon absorption band below 1000 cm^{-1} which increases in intensity for $y > 0.05$. Hussain et al. have described that this could indicate a metal to insulator transition due to a disappearance of free carriers and the

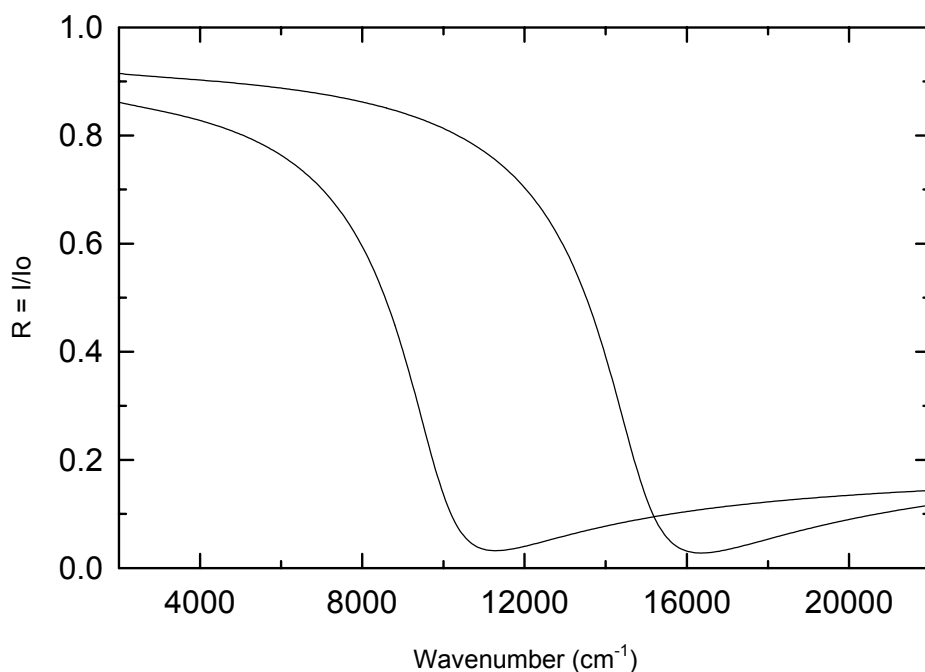


Fig. 59. Reflection spectra of $\text{Cs}_{0.3}\text{WO}_3$ for polarizations parallel (E par. C) and perpendicular (E per. C) to the c-axis using the Drude model

appearance of polarons quasi particles which dominates the near infrared response instead. The spectral feature of the phonon absorption band closely agrees with spectra obtained by

Maczka et al. [138] for the fully oxidized compositions with $y = x$ in these systems. The observation of the additional HTB-signature in the X-ray diffraction pattern indicates, therefore, a gradual increase of the contribution of $M_xNb_yW_{1-y}O_3$ with $x = y$ with increasing y . There are also some evidences in optical reflectivity spectra of $Cs_xNb_yW_{1-y}O_3$ powder samples for the effect of Nb/W substitution in reduced HTB system. The optical reflectivity of the powder sample of $Cs_{0.3}WO_3$ shows two minima at about 16000 cm^{-1} and 10000 cm^{-1} [Fig. 50]. This is explained by two different Drude free carrier plasma frequencies for polarizations perpendicular and parallel to the hexagonal axis as calculated from single crystal spectra [Fig. 59]. A qualitatively similar spectrum is observed for $Cs_xNb_yW_{1-y}O_3$ ($x = 0.25, 0.3; 0 \leq y \leq 0.2$) system [Fig. 50] with the plasma frequencies shifted to lower values. The minimum feature in the reflectivity becomes weaker and shifted to lower value with increasing niobium concentration. For $y > 0.1$ the minimum structures become less significant and there is nearly no shift in position. A similar observation has been observed for $Rb_xNb_yW_{1-y}O_3$ system. The shift up to a certain y can be explained by the decreasing concentration of formally W^{5+} states as $M_xNb_y^{5+}W_{x-y}^{5+}W_{1-x}^{6+}O_3$. However, this can be an effect of oxidized HTB-II type phase. With increasing Nb content the HTB bronze type phase can be diluted by the oxidized HTB-II type phase.

ACKNOWLEDGEMENTS

Foremost, I would like to express my sincere gratitude to my supervisor PD Dr. C. H. Rüscher, Institute of Mineralogy, University of Hannover, Germany, for his continuous interest and valuable guidance through this work which have been a great source of encouragement. I am grateful to him for his kind help during my stay here.

My heartfelt thanks to Professor J. –Ch. Buhl, Institute of Mineralogy, University of Hannover, Germany, for introducing me to the electron microscopy and for his whole-hearted guidelines.

I have the great pleasure to express my sincere gratefulness to Professor Margareta Sundberg, Department of Chemistry, University of Stockholm, Sweden for allowing me to work in her laboratory for three months and for her excellent guidance and valuable advice during my stay in Stockholm.

I am also deeply indebted to professor Altaf Hussain, Department of Chemistry, University of Dhaka, who introduced me to the field of Tungsten Bronzes. His kind cooperation, encouragement and valuable advice have helped me to perform my research work smoothly.

I am thankful to Professor Robert Glaum, Department of chemistry, University of Bonn, Germany, for giving me the opportunity to work in his laboratory and for arranging everything for my stay in Bonn.

My heartfelt thanks to PD Dr. Thorsten M. Gesing, Institute of Mineralogy, University of Hannover, Germany, for his kind help about Rietveld method and computer problem.

I would also like to thank Professor S. H. Rahman, Institute of Mineralogy, University of Hannover, Germany, for his kind help in electron microscopy.

My heartfelt thanks to Professor Lars Kihlburg for nice discussion about my work. I am also grateful to Dr. Kjell Janson who helped me lot for scanning microscopy during my stay in Stockholm.

I would like to thank all of my friends especially Dr. Andrea Hartman, Jasmin Miltz, Nada Salman, Olaf Bode, Mazharul Islam, Jenny Liersch, Murat Erdogan and also to all my friends in my dormitory and in the department who always make my life joyful.

I would also like to thank my loving parents and my brother and sister for their constant encouragement and support in carrying out this research work and to stay alone without them.

Finally, I would like to thank the Land Niedersachsen for allowing me for the ‘‘Lichtenberg Stipendium’’ which have made possible my studies in Germany and also to the Humboldt foundation for financial support to the project

REFERENCES

- [01] T. Ekström and R. J. D. Tilley, *Chem. Scripta* 16, 1 (1980)
- [02] E. Salje, *Acta Cryst. B* 33, 574 (1977)
- [03] B. Gerand, G. Nowogrocki, J. Guenot and M. Figlarz., *J. solid State Chem.* 29, 429 (1979)
- [04] C. G. Granqvist, *Handbook of Inorganic Electrochromic Materials* (Elsevier, Amsterdam, 1995)
- [05] P. M. S. Monk, R. J. Mortimer, and D. R. Rosseinsky, *Electrochromism: Fundamentals and applications* (VCH Verlagsgesellschaft, Weinheim, 1995)
- [06] A. Aird, M. C. Domeneghetti, F. Mazzi, V. Tazzoli and E K H Salje, *J. Phys. Condens. Matter* 10, L569 (1998)
- [07] A. Aird and E K H Salje, *J. Phys. Condens. Matter* 10, L377 (1998)
- [08] A. Shengelaya, S. Reich, Y. Tsabba and K. A. Müller, *Eur. Phys. J. B* 12, 13 (1999)
- [09] F. Wöhler, *Ann. Chim. Phys.* 2, 43, 29 (1823).
- [10] A. Laurent., *Ann. Chim. Phys.* 267, 215 (1838)
- [11] L. A. Hallopeau, *Ann. Chim. Phys.* 7, 19, 92 (1900)
- [12] G. von Knorre and *J. Prakt. Chem.* 2, 27, 49 (1838)
- [13] G. von Knorre and E. Schäfer, *Ber.* 35, 3407 (1902)
- [14] E. Schäfer, *Z. anorg. Allgem. Chem.* 38, 142 (1903)
- [15] O. Brunner, *Diss. Zürich* (1903)
- [16] G. Hägg, *Z. Phys. Chem.* B29, 192 (1935)
- [17] A. Magnéli and B. Blomberg, *Acta chem. Scand.* 5, 372 (1951).
- [18] Hägg and A. Magnéli, *Rev. Pure Appl. Chem. (Australia)* 4, 235 (1954)
- [19] M. J. Sienko, *Adv. Chem. Ser.* 39, 224 (1963)
- [20] H. R. Shanks, P. H. Sidles, and G. C. Danielson, *Adv. Chem. Ser.* 39, 237 (1963).
- [21] A. S. Ribnick, B. Post, and E. Banks, *Adv. Chem. Ser.* 39, 246 (1963)
- [22] A. D. Wadsley, "inorganic Non-Stoichiometric Compounds", *Non-stoichiometric Compounds*, L. Mandelcorn, Ed., Academic Press, New York, Chapter 3 (1964)

- [23] P. G. Dickens and M. S. Whittingham, *Quart. Rev. Chem. Soc.* 22, 30 (1968)
- [24] F. S. Galasso, Pergamon Press, Oxford, England (1969)
- [25] P. Hagenmuller, *Les Bronzes Oxygénés*, *Progress in Solid State Chemistry*, H. Reiss, Ed., Pergamon Press, Oxford, 5, 71 (1971)
- [26] D. J. M. Bevan and P. Hagenmuller, *Nonstoichiometric compounds: Tungsten Bronzes, Vanadium Bronzes and Related Compounds*, Pergamon Press, New York (1975)
- [27] F. R. Gamble and T. H. Geballe, *Inclusion compounds*, "Treatise on Solid State Chemistry, Vol. 3, Crystalline and noncrystalline Solids, N. B. Hannay, Ed., Chapt. 2, Plenum Press, New York (1976).
- [28] M. M. Dobson, J. L. Hutchison, R. J. D. Tilley and K. A. Watts, *J. Solid State Chem.*, 71, 47 (1987)
- [29] Ph. Labbe, *key Engineering Materials* 68, 293 (1992)
- [30] R. Sabatier and G. Baud, *J. Inorg. Nucl. Chem.* 34, 873 (1972)
- [31] L. Kihlberg and R. Sharma, *J. Microsc. Spectrosc. Electron.* 7, 387 (1982)
- [32] A. Magnéli, 12th European Crystallographic meeting, Moscow (1989)
- [33] L. Kihlberg, *solid State Chem. Proc. 2nd Europ. Conf.*, Veldhoven, The Netherlands 143 (1982)
- [34] D. R. Wanlass and M. J. Sienko, *J. Solid State Chem.* 12, 362 (1975)
- [35] D. B. Šepa, A. Damjanovic, and J. O'M. Bockris, *Electrochim. Acta* 12, 746 (1967)
- [36] D. B. Šepa, D. S. Ovcin, and M. V. Vojnovic, *J. Electrochem. Soc.* 119, 1285 (1972)
- [37] D. B. Šepa, M. V. Vojnovic, D. S. Ovcin and N. D. Pavlović, *Electroanal. Chem. Interfacial Electrochem.* 51, 99 (1974)
- [38] M. V. Vojnović and D. B. Šepa, *J. Chem. Phys.* 51, 5344 (1969)
- [39] M. V. Vojnović and D. B. Šepa, and D. S. Ovcin, *Croat. Chem. Acta* 44, 89 (1972)
- [40] M. A. Wechter, H. R. Shanks, G. carter, G. H. Ebert, R. Guglielmino, and A. F. Voigt, *Anal. Chem.* 44, 850 (1972)
- [41] M. A. Wechter, P. B. Hahn, G. M. Ebert, P. R. Montoya, and A. F. Voigt, *anal. Chem.* 45, 1267 (1973)
- [42] J. Vondrak and J. Balej, *electrochem. Acta* 18, 1017 (1973)
- [43] J. Vondrak and J. Balej, *Electrochem. Acta* 20, 283 (1975)

-
- [44] J. -P. Randin, A. K. Vijh, and A. B. Chughtai, *J. Electrochem. Soc.* 120, 1174 (1973)
- [45] J. -P. Randin, *J. electrochem. Soc.* 120, 378 (1973)
- [46] J. -P. Randin, *Electrochim. Acta* 19, 87 (1974a)
- [47] J. -P. Randin, *Can. J. chem.* 52, 2542 (1974c)
- [48] J. -P. Randin and A. K. Vijh, *Electrochem. Acta* 20, 37 (1975)
- [49] M. Amjad and D. Pletcher, *J. Electroanal. Chem. Interfacial Electrochem.* 59, 61 (1975)
- [50] P. G. Dickens, *Adv. Chem. Ser.* 163, 165 (1977)
- [51] P. B. Hahn, M. A. Wechter, D. C. Johnson, and A. F. Voigt, *Anal. Chem.* 45, 1016 (1973)
- [52] F. T. Jones, *Diss. Abstr.* 21, 1390 (1960)
- [53] J. H. Fishman, J. F. Henry, and S. Tessore, *Electrochem. Acta* 14, 1314 (1969)
- [54] J. McHardy and J. O'M Bockvis, *J. Electrochem. Soc.* 120, 53 (1973)
- [55] J. O'M. Bockris and J. Mettardy, *J. Electrochem. Soc.* 120, 61 (1973)
- [56] S. S. Moody and D. Taylor, *J. Chem. Soc. Faraday Trans.* 73, 289 (1973)
- [57] A. J. Appleby and C. Van Druenen, *J. Electrochem.* 123, 200 (1976).
- [58] J. -P. Randin, *J. Electrochem. Soc.* 121, 1029 (1974d)
- [59] J. -P. Randin, *J. Electrochem. Soc.* 122, 742 (1975)
- [60] M. F. Weber and H. R. Shanks, *National Bureau of standards Special Publication* 455 (1976)
- [61] B. Broyde, *J. Catalysis* 10, 13 (1968)
- [62] L. W. Niedrach and H. I. Zeliger, *J. Electrochem. Soc.* 116, 152 (1969)
- [63] R. D. Armstrong, A. F. Donglas, and D. E. Williams, *Energy Convers.* 11, 7 (1971)
- [64] A. Magneli, *Nova Acta Regiae Soc. Sci. Upsaliensis* 14, 4 (1950)
- [65] A. Hussain, *Chem. Commun. Univ. Stockholm* No.2, 1 (1978)
- [66] A. Magneli, *Acta Chem. Scand* 5, 670 (1951)
- [67] A. Magneli, *Nova Acta Regiae Societatis Scientiarum Upsaliensis*, 14, 1 (1949)

- [68] M. E. Straumains and S. S. Hsu, *J. Am. Chem. Soc.* 72, 4027 (1950)
- [69] A. Magnelie, *Arkiv Kemi* 1, 213, 269 (1949)
- [70] L. Kihlborg and A. Klug, *Chem. Scr.* 3, 207 (1973)
- [71] F. Takusagawa and R. A. Jacobsson, *J. Solid State Chem.* 18, 163 (1976)
- [72] A. Magneli, *Acta Chem. Scand.* 7, 315 (1953)
- [73] N. D. Zakharov, Z. Liliental-Weber, V. P. Filonenko, I. P. Zibrov and M. Sundberg, *Mater. Res. Bull.* 31, 373 (1996)
- [74] L. E. Conroy and T. Yokokawa, *Inorg. Chem.* 4, 994 (1965)
- [75] R. Pape, G. Gauthier and P. Hagenmuller, *C. R. Hebd. Seanc. Acad. Sci. Ser. C266*, 803 (1968)
- [76] C. Cros, R. Feurer, M. Pouchard and P. Hagenmuller, *Mat. Res. Bull.* 10, 383 (1975)
- [77] B. Gerand, G. Nowogrocki, J. Guenot and M. Figlarz *J. Solid state Chem.* 29, 429 (1979)
- [78] M. Figlarz and B. Gerand, *Proc. 9th Intern. Symp. Reactivity of Solids, Cracow* 660 (1980)
- [79] K. H. Cheng, A. J. Jacobson and M. S. Whittingham, *Solid State Ionics* 5, 355 (1981)
- [80] A. Hussain and L. Kihlborg, *Acta Crystallogr.* A32, 551 (1976)
- [81] A. Hussain, R. Gruehn and C. H. Rüscher, *journal of Alloys and compounds* 246, 51 (1997)
- [82] T. A. Bither, J. L. Gillson and H. S. Young, *Inorganic Chemistry Vol. 5*, 9, 1559 (1966)
- [83] M. Figlarz: *Prog. Solid state Chem.*, 19, 1 (1989)
- [84] P. V. Kletsov, L. Yu kharchenko and R. F. Klevtsova, *Dokl. Akad. Nauk. SSSR.* 176 3, 575 (1967)
- [85] K. P. Reis, A. Ramanan and M. S. Whittingham, *J. Solid State Chem.* 96, 31 (1992)
- [86] T. E. Gier, D. C. Pease, A. W. Sleight and T. A. Bither: *Inog. Chem.* 7, 1646 (1968)
- [87] R. Fuchs, *J. Chem. Phys.* 42, 3781 (1965)
- [88] P. A. Lightsey, *Phys. Rev. B8*, 3586 (1973)
- [89] A. T. Fromhold, Jr., and A. Narath, *Phys. Rev.* 136, A487 (1964)

-
- [90] J. G. Roper and H. B. Knowles, *Phys. Lett.* 38A, 477 (1972)
- [91] I. Webman, J. Jortner and M. H. Cohen, *Phys. Rev.* B13, 713 (1976)
- [92] D. P. Tunstall, *Phys. Rev.* B14, 4735 (1976)
- [93] R. S. Crandall and B. W. Faughnan, *Phys. Rev.* B16, 1750 (1977)
- [94] B. R. Weinberger, *Phys. Rev.* B17, 566 (1978)
- [95] B. W. Brown, and E. Banks, *J. Am. Chem. Soc.* 76, 963 (1954)
- [96] D. W. Lynch, R. Rosei, J. H. Weaver and C. G. Olson, *J. solid State Chem.* 8, 242 (1973)
- [97] P. Camagni and A. Manara, *Phys. Rev.* B15, 4623 (1977a)
- [98] P. Camagni and A. Manara, *Nuovo Cimento Soc. Ital. Fis.* B 39B, 417 (1977b)
- [99] A. Hjelm, C. G. Granqvist and J. M. Wills, *Physical Review B* 54, 4, 2436 (1996)
- [100] J. M. Reau, C. Fouassier, G. Le Flem, J. Y. Barraval, J. P. Doumère and P. Hagemüller, *Revue de Chimie minerale*, t. 7, 975 (1970)
- [101] Q. Zhong, J. R. Dahn, and K. Colbow, *Physical Review B* 46, No. 4, 2554 (1992)
- [102] G. Hoppmann, E. Salje, *Phys. Stat. Sol A* 37, K 187 (1976)
- [103] O. Schirmer and E. Salje, *Solid State Commun.* 33, 333 (1980)
- O. Schirmer and E. Salje, *J. phys. C: Solid State Phys.* 13, L1067 (1981)
- [104] E. Salje, B. Güttler, *Philos. Mag.* B50, 607 (1984)
- [105] E. K. H. Salje, *Polarons and Bipolarons in high - T_c superconductors and related materials*, eds. Salje et al., Cambridge University Press, 110 (1995)
- [106] Z. Hussain, *Applied Optics*, 41, 31, 6708 (2002)
- [107] J. F. Owen, K. J. Teegarden and H. R. Shanks, *Physical review* B18, 8, 3827 (1978)
- [108] A. A. Likalter, *Physica B* 315, 252 (2002)
- [109] Y. Inaguma, C. Liqun, M. Itoh, T. Nakamura, T. Uchida, H. Ikuta and M. Wakihara, *Solid State Commun.*, 86, 689 (1993)
- [110] A. Hussain, A. Ul-Monir, M. M. Murshed and C. H. Rüscher, *Z. Anorg. Allg. Chem.* 628, 416 (2002)

- [111] Th. M. Gesing, personal communication, program Korgui and Asin, MS-Dos version based on VAX source code from M. Möller, Ph.D thesis, University of Dortmund (1983)
- [112] K. R. Dey, M. Phil thesis, University of Dhaka, Bangladesh (2001)
- [113] P. J. Wiseman and P. G. Dickens, *Journal of solid state chemistry*, 17, 91 (1976)
- [114] P. L. Mart and N. J. Clark, *Mat. Res. Bull.* 13, 1199 (1978)
- [115] H. Yamada, M. Hibino and T. Kudo, *Journal of the Ceramic society of Japan*, 109, 3, 278 (2001)
- [116] E. Salje and K. Viswanathan, *Acta Cryst.* A31, 356 (1975)
- [117] C. H. Rüscher, Th. M. Gesing, K. R. Dey, A. Hussain, *Z. krist. Suppl.* No 18, 184 (2001)
- [118] K. R. Dey, M. Sc. thesis, University of Dhaka, Bangladesh (1997)
- [119] R. Sharma, *Mat. Res. Bull.* 20, 1373 (1985)
- [120] J. Wyart, and M. Foex, *C. R. Acad. Sci. Paris*, 233, 2459 (1951)
- [121] S. Tanisaki, *J. Phys. Soc. Japan*, 15, 566 (1960b)
- [122] E. Salje, *Acta Cryst.*, A31, 360 (1975)
- [123] K. L. Kehl, R. G. Hay and D. Wahl, *J. Appl. Phys.* 23, 212 (1952)
- [124] R. Diehl, G. Brandt and E. Salje, *Acta Cryst.*, B34, 1105 (1978)
- [125] B. O. Loopstra and H. M. Rietveld, *Acta Cryst.*, B25, 1420 (1969)
- [126] C. H. Rüscher, D. Speer. *Ceramic Forum International (Ber. DKG)*, No. 6, 1 (2001)
- [127] L. Spitzin and Z. Kaschtanoff, *Anal. Chem.* 75, 440 (1928)
- [128] E. Straumanis and A. Dravnieks, *J. Am. Chem. Soc.* 71, 683 (1949)
- [129] L. Muldower, *Electron Diffraction in Surfaces of Sodium Tungsten Bronzes*; Department of physics, Temple University (1962)
- [130] F. Consadori and A. Stella, *Lett. Nuovo Cimento* 3, 600 (1970)
- [131] Y. Xia, N. Machida, X. Wu, C. Lakeman, L. Wüllen, F. Lange, C. Levi, H. Eckert and S. Anderson, *J. Phys. Chem. B*, 101, 9180 (1997)
- [132] W. F. deJONG, *Z. Krist.* 81, 314 (1932).
- [133] F. H. Potter and R. G. Egdell, *J. Mater. Chem.* 4(10), 1647 (1994)

-
- [134] K. Okada, H. Morikawa, F. Marumo and S. Iwai, *Acta Cryst.* B31, 1451 (1975)
- [135] A. Hussain, *Acta Chem. Scand.* A32, 479 (1978)
- [136] R. Brusetti, P. Bordet and J. Marcus, *journal of solid state chemistry* 172, 148 (2003)
- [137] K. R. Dey, Th. M. Gesing, C. H. Rüscher and A. Hussain, *Z. Kristallogr. NCS* 217 (2002)
- [138] M. Maczka, J. Hanuza and A. Waskowska, *J. Raman Spectrosc.* 34, 432 (2003)